frontiers | Research Topics

Advances of imaging techniques in identifying malignancy in thyroid nodules

Edited by
Emerita Andres Barrenechea and Hendra Zufry

Published in
Frontiers in Endocrinology

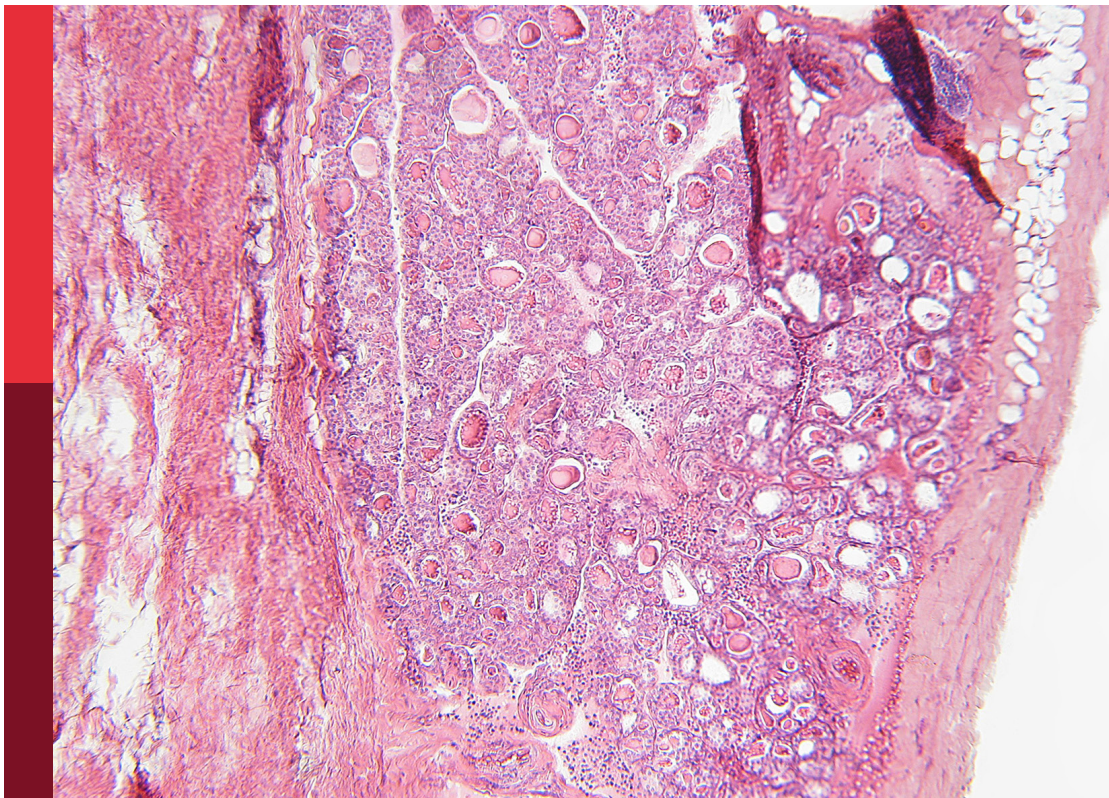

ISSN 1664-8714
ISBN 978-2-8325-2297-4
DOI 10.3389/978-2-8325-2297-4

About Frontiers

Frontiers is more than just an open access publisher of scholarly articles: it is a pioneering approach to the world of academia, radically improving the way scholarly research is managed. The grand vision of Frontiers is a world where all people have an equal opportunity to seek, share and generate knowledge. Frontiers provides immediate and permanent online open access to all its publications, but this alone is not enough to realize our grand goals.

Frontiers journal series

The Frontiers journal series is a multi-tier and interdisciplinary set of open-access, online journals, promising a paradigm shift from the current review, selection and dissemination processes in academic publishing. All Frontiers journals are driven by researchers for researchers; therefore, they constitute a service to the scholarly community. At the same time, the *Frontiers journal series* operates on a revolutionary invention, the tiered publishing system, initially addressing specific communities of scholars, and gradually climbing up to broader public understanding, thus serving the interests of the lay society, too.

Dedication to quality

Each Frontiers article is a landmark of the highest quality, thanks to genuinely collaborative interactions between authors and review editors, who include some of the world's best academicians. Research must be certified by peers before entering a stream of knowledge that may eventually reach the public - and shape society; therefore, Frontiers only applies the most rigorous and unbiased reviews. Frontiers revolutionizes research publishing by freely delivering the most outstanding research, evaluated with no bias from both the academic and social point of view. By applying the most advanced information technologies, Frontiers is catapulting scholarly publishing into a new generation.

What are Frontiers Research Topics?

Frontiers Research Topics are very popular trademarks of the *Frontiers journals series*: they are collections of at least ten articles, all centered on a particular subject. With their unique mix of varied contributions from Original Research to Review Articles, Frontiers Research Topics unify the most influential researchers, the latest key findings and historical advances in a hot research area.

Find out more on how to host your own Frontiers Research Topic or contribute to one as an author by contacting the Frontiers editorial office: frontiersin.org/about/contact

Advances of imaging techniques in identifying malignancy in thyroid nodules

Topic editors
Emerita Andres Barrenechea — Veterans Memorial Medical Center, North Avenue Quezon city, Philippines
Hendra Zufry — Syiah Kuala University, Indonesia

Topic coordinator
Aisyah Elliyanti — Andalas University, Indonesia

Citation
Barrenechea, E. A., Zufry, H., eds. (2023). *Advances of imaging techniques in identifying malignancy in thyroid nodules*. Lausanne: Frontiers Media SA.
doi: 10.3389/978-2-8325-2297-4

The authors declare that the research was conducted in the absence of any commercial or financial relationships that could be construed as a potential conflict of interest

Table of contents

frontiers | Frontiers in Endocrinology

TYPE Editorial
PUBLISHED 14 April 2023
DOI 10.3389/fendo.2023.1188250

OPEN ACCESS

EDITED AND REVIEWED BY
Terry Francis Davies,
Icahn School of Medicine at Mount Sinai,
United States

*CORRESPONDENCE
Hendra Zufry
hendra_zufry@unsyiah.ac.id

SPECIALTY SECTION
This article was submitted to
Thyroid Endocrinology,
a section of the journal
Frontiers in Endocrinology

RECEIVED 17 March 2023
ACCEPTED 03 April 2023
PUBLISHED 14 April 2023

CITATION
Zufry H, Barrenechea EA and Elliyanti A
(2023) Editorial: Advances of imaging
techniques in identifying malignancy in
thyroid nodules.
Front. Endocrinol. 14:1188250.
doi: 10.3389/fendo.2023.1188250

Editorial: Advances of imaging techniques in identifying malignancy in thyroid nodules

Hendra Zufry[1,2]*, Emerita Andres Barrenechea[3,4] and Aisyah Elliyanti[5]

[1]Division of Endocrinology, Metabolism, and Diabetes, Thyroid Center, Department of Internal Medicine, School of Medicine, Universitas Syiah Kuala/Dr. Zainoel Abidin General Teaching Hospital, Banda Aceh, Indonesia, [2]Innovation and Research Center of Endocrinology, School of Medicine, Universitas Syiah Kuala, Banda Aceh, Indonesia, [3]Department of Nuclear Medicine and Research, Veterans Memorial Medical Center, Quezon City, Philippines, [4]Department of Nuclear Medicine and PET, St. Luke's Medical Center, Quezon City, Philippines, [5]Nuclear Medicine Division of Radiology Department, Faculty of Medicine, Universitas Andalas/Dr. M. Djamil Hospital, Padang, Indonesia

KEYWORDS

thyroid nodules, artificial intelligence, deep learning, advanced thyroid imaging, real-world evidence, TIRADS

Editorial on the Research Topic
Advances of imaging techniques in identifying malignancy in thyroid nodules

The management of thyroid nodules (TNs) has gained attention due to its increasingly high incidence rate (1). It was estimated that over 586,000 people were diagnosed with TNs in 2020 (2). TNs have been identified more frequently in recent years due to increased sensitivity in imaging techniques (3). TNs patients are diagnosed by history taking and physical examination, ultrasonography, Thyroid -stimulating hormone (TSH) serum measurement, fine needle aspiration, and scintigraphy (4). Most TNs proved benign; however, 7 to 15% of TNs are malignant, causing mortality if not treated properly (5, 6). Hence, diagnostic tools are most necessary to differentiate benign and malignant TNs to provide optimal treatment.

We invited researchers worldwide to address advanced imaging techniques to differentiate TNs and innovations in thyroid imaging approaches for therapy. We received diverse and insightful nine manuscripts involving 68 authors from various backgrounds. The Research Topic was divided into three areas of research: 1) Artificial intelligence prediction models compared to real-world evidence; 2) Advanced ultrasonography from grey-scale to contrast-enhanced ultrasonography; and 3) Ultrasonography (US) characterization for TNs and lymph node metastasis. This research aimed to assess the malignancy risk, identify poor prognostic factors, and determine the optimal management plan for patients.

The US is an operator-dependent technique, and the imaging results' interpretation is affected by the radiologists' experience (5). To reduce a variation of US interpretations between operators, recent studies have investigated the role of a deep-learning prediction model to assess thyroid nodule malignancy risk and metastatic lymph nodes. Zhang et al. invented a deep learning prediction model for diagnosing papillary thyroid carcinoma (PTC) malignancy that incorporated many variables – demographic, serological, ultrasound, and biopsy data of 2,029 patients. The study reported an excellent predictive ability to differentiate between benign and malignant PTC. Furthermore, Chang et al. developed a deep learning model integrated with clinical and ultrasound factors to predict

central lymph node metastasis (CLNM) in PTC by using the dataset of 3,359 CLNM patients, and the study may have superior clinical predictive tools compared to other deep learning-based models.

Even though the deep learning prediction model has promising predictive capabilities, the US remains the conservative diagnostic modality of TNs malignancy, especially in areas with limited healthcare facilities (5). Feng et al. explored the effectiveness of ultrasound grayscale ratio (UGSR) to differentiate benign and malignant TNs in patients with Hashimoto's thyroiditis (HT). The UGSR showed an excellent diagnostic result to determine TNs malignancy in HT patients. Wang et al. studied the US to detect partially cystic thyroid nodules (PCTNs). The study described US characteristic features for malignant and benign PCTNs with reliable diagnostic ability. Chen et al. examined the role of contrast-enhanced ultrasonography (CEUS) to differentiate mummified TNs from other malignant TNs. However, a large-scale population with a multicenter prospective study is needed to verify the specificity and sensitivity of the CEUS findings.

The US features a high prediction tool for malignant TNs (1). Thyroid Imaging Reporting and Data System (TIRADS) provides US prediction tools for TNs malignancy – the most popular are ACR-TIRADS, EU-TIRADS, and K-TIRADS. A study by Chen et al. compared malignancy risk stratification of TNs for C-TIRADS, K-TIRADS, and ACR-TIRADS. Results showed that C-TIRADS has outstanding performance in the malignancy risk stratifications by optimized cut-off value compared with other TIRADS. Another interesting study was provided by Zhou et al. and Yao et al., where both studies support each other. Zhou et al. evaluated the sonographic characteristics and risk factors of CLNM in 2,376 patients. Although the US reported excellent sensitivity and specificity, Yao et al. suggested that a combination of US and CT-Scan showed better results in diagnosing CLNM rather than the US alone. Moreover, Liu et al. determined the optimal imaging time after Iodine $^{-131}$ treatment; imaging sensitivity on day three detected residual thyroid tissue and on day seven and day ten detected cervical lymph nodes and lung metastases.

These findings highlight how advanced imaging techniques provide a more expansive view of TNs diagnosis. Although the artificial intelligence prediction model had better accuracy than the conventional ones, it may be limited to developing countries. We encourage more accessibility with exact accuracy tools such as a web-based deep learning model, which will be clinically applicable in iodine-deficit regions – mainly in developing countries. Nevertheless, we are confident that all selected studies on this Research Topic bring essential and enduring contributions to differentiate thyroid nodule malignancy.

Author contributions

HZ: conceptualizing, writing the original draft, writing–review, and editing. EB: writing–review, and editing. AE: writing–review, and editing. All authors approved the submitted version.

Acknowledgments

We would like to express our gratitude to all the authors who proposed their work and to all the researchers who reviewed the submission to this Research Topic.

Conflict of interest

The authors declare that the research was conducted in the absence of any commercial or financial relationships that could be construed as a potential conflict of interest.

Publisher's note

References

1. Ha EJ, Chung SR, Na DG, Ahn HS, Chung J, Lee JY, et al. Korean Thyroid imaging reporting and data system and imaging-based management of thyroid nodules: Korean society of thyroid radiology consensus statement and recommendations. *Korean J Radiol* (2021) 22(12):2094. doi: 10.3348/kjr.2021.0713

2. Siegel RL, Miller KD, Fuchs HE, Jemal A. Cancer statistics. *CA Cancer J Clin* (2022) 72(1):7–33. doi: 10.3322/caac.21708

3. Mu C, Ming X, Tian Y, Liu Y, Yao M, Ni Y, et al. Mapping global epidemiology of thyroid nodules among general population: a systematic review and meta-analysis. *Front Oncol* (2022) 12. doi: 10.3389/fonc.2022.1029926

4. Tamhane S, Gharib H. Thyroid nodule update on diagnosis and management. *Clin Diabetes Endocrinol* (2016) 2(1):17. doi: 10.1186/s40842-016-0035-7

5. Lee JY, Baek JH, Ha EJ, Sung JY, Shin JH, Kim Jh, et al. Imaging guidelines for thyroid nodules and differentiated thyroid cancer: Korean society of thyroid radiology. *Korean J Radiol* (2020) 22(5):840. doi: 10.3348/kjr.2020.0578

6. Lin JK, Sakoda LC, Darbinian J, Socarras M, Chiao W, Calixto N, et al. Risk of mortality between untreated and treated papillary thyroid cancer: a matched cohort analysis. *Ann Otol Rhinol Laryngol* (2020) 129(3):265–72. doi: 10.1177/0003489419885403

frontiers in Endocrinology

ORIGINAL RESEARCH
published: 18 March 2022
doi: 10.3389/fendo.2022.850698

Value of Contrast-Enhanced Ultrasound in Mummified Thyroid Nodules

Sijie Chen[1,2†], Kui Tang[1,2†], Yi Gong[3], Fei Ye[3], Liyan Liao[4], Xiaodu Li[1,2], Qi Zhang[1,2], Yan Xu[1,2], Rongsen Zhang[1,2] and Chengcheng Niu[1,2]*

[1] Department of Ultrasound Diagnosis, The Second Xiangya Hospital, Central South University, Changsha, China, [2] Research Center of Ultrasonography, The Second Xiangya Hospital, Central South University, Changsha, China, [3] Department of Thyroid Surgery, The Second Xiangya Hospital, Central South University, Changsha, China, [4] Department of Pathology, The Second Xiangya Hospital, Central South University, Changsha, China

Mummified thyroid nodules (MTNs) are rarely reported and are usually misdiagnosed as malignant nodules. This article first reviewed the contrast-enhanced ultrasound (CEUS) enhancement features of 218 MTNs and classified them into three (A, B, C) patterns. The A pattern MTNs show linear hypo-enhancement, the B pattern MTNs show heterogeneous hypo-enhancement, and the C pattern MTNs show no enhancement in thyroid nodules. The A and C pattern enhancements of MTNs demonstrated a high specificity compared with the enhancement of previously reported typical papillary thyroid carcinomas (PTCs). To further study the B pattern MTNs, 24 B pattern MTNs and 42 PTCs were enrolled in this study, and CEUS parameters for each nodule were evaluated. Univariate analysis indicated that compared with PTCs, the B pattern MTNs more frequently exhibited heterogeneous hypo-enhancement and clear margins after clearance ($p < 0.05$). A multivariate analysis revealed that heterogeneous hypo-enhancement and clear margins after clearance were independent characteristics related to the B pattern MTNs for differentiating them from PTCs ($p < 0.05$). Thus, preoperative CEUS may provide more important information for distinguishing MTNs from malignant thyroid nodules to avoid surgical excisions or unnecessary fine-needle aspiration (FNA).

Keywords: contrast-enhanced ultrasound (CEUS), mummified thyroid nodules (MTNs), papillary thyroid carcinomas (PTCs), thyroid ultrasonography, fine-needle aspiration (FNA)

OPEN ACCESS

Edited by:
Hendra Zufry,
Syiah Kuala University, Indonesia

Reviewed by:
Ilker Sengul,
Giresun University, Turkey
Giovanni Docimo,
University of Campania Luigi Vanvitelli, Italy

***Correspondence:**
Chengcheng Niu
niuchengcheng@csu.edu.cn

[†]These authors have contributed equally to this work

Specialty section:
This article was submitted to Thyroid Endocrinology, a section of the journal Frontiers in Endocrinology

Received: *08 January 2022*
Accepted: *14 February 2022*
Published: *18 March 2022*

Citation:
Chen S, Tang K, Gong Y, Ye F, Liao L, Li X, Zhang Q, Xu Y, Zhang R and Niu C (2022) Value of Contrast-Enhanced Ultrasound in Mummified Thyroid Nodules. Front. Endocrinol. 13:850698. doi: 10.3389/fendo.2022.850698

INTRODUCTION

High-frequency ultrasound (US) is an important imaging modality for detecting thyroid nodules and differentiating malignant thyroid nodules from benign thyroid nodules (1–4). However, some previously proven benign thyroid nodules may spontaneously shrink in size and show morphologic changes of suspicious malignancy on US examinations spontaneously over time or result from thyroid nodule fine-needle aspiration biopsy (FNAB), percutaneous ethanol injection, or radiofrequency ablation (5–8). These changes include strong hypoechogenicity, solid components, irregular margins and microcalcifications. These features are collectively referred to

as the thyroid nodule mummification process, and the thyroid nodules are called mummified thyroid nodules (MTNs) (5, 9).

According to the Thyroid Imaging Reporting and Data System (TI-RADS), five US suspicious features were applied to categorize the thyroid nodules, whereas the MTNs usually have more than two suspicious features and are classified as TIRADS scores 4b to 5 (9). Thus, some patients with MTNs undergo fine-needle aspiration (FNA) or even surgery, which results in the potential for over-management (10).

Contrast-enhanced ultrasound (CEUS) could provide improved characterization of dynamic microvessel perfusion in the differential diagnosis of focal thyroid nodules compared with color Doppler US, which could help to differentiate malignant thyroid nodules from benign thyroid nodules (9, 11–13). However, MTNs with the same conventional US appearance may have different CEUS features according to our current study. In this study, we first reviewed the CEUS enhancement features of 218 MTNs and classified them into three (A, B, C) patterns. A pattern with linear hypo-enhancement and C pattern with no enhancement could easily diagnose MTNs combined with a previous clinical history (14). However, the B pattern with heterogeneous hypo-enhancement was very similar to the enhancement of typical papillary thyroid carcinomas (PTCs), which is necessary to identify PTCs from malignant thyroid nodules, especially in the absence of clinical history. The purpose of our study was to highlight the different CEUS features of MTNs that should help to differentiate benign collapsed thyroid nodules from malignant thyroid nodules.

MATERIALS AND METHODS

Patients

The study was approved by the Ethical Committee of the Second Xiangya Hospital of Central South University in China and was performed in accordance with the Declaration of Helsinki for human studies. The requirement of informed consent from human subjects is occasionally waived by IRBs for protocols that include a retrospective review of images acquired for clinical diagnostic purposes. From November 2016 to November 2021, 469 patients with 469 suspicious MTNs who received conventional US and CEUS examinations were retrospectively enrolled in this case-control study. The inclusion criteria were as follows: (1) patients with thyroid nodules were suspected to be malignant according to conventional US; (2) nodules have a clinical history with no suspicious features; and (3) nodules were confirmed as benign by pathology after surgery or by FNAB. Among them, 251 patients with no follow-up US examinations or further FNAs were excluded. Finally, 218 patients with 218 MTNs were included in this study. Then, the MTNs were classified into 3 patterns according to the different CEUS enhancement types.

As a control group, 236 patients with 236 malignant thyroid nodules who received conventional US and CEUS examinations from July 2020 to January 2021 were recruited in this study with the inclusion criteria: (1) patients with thyroid nodules confirmed as PTCs by pathological examination after surgery; (2) suspicious nodules for malignancy in conventional US; (3) all nodule sizes in the control group were less than 15 mm, which is consistent with that noted in the study group; and (4) hypo-enhancement of nodules, which is consistent with that noted in the study group. Four patients with 4 thyroid nodules were excluded because they had different types of thyroid cancers: 3 follicular and 1 medullary thyroid cancers. A total of 127 patients with 127 thyroid nodules were excluded due to a nodule size greater than 15 mm, and 63 patients with 63 thyroid nodules were excluded due to hyper- or iso-enhancement. Finally, 42 patients with 42 PTC nodules were included in this study.

Conventional US

A Siemens Acuson S3000 US scanner (Mountain View, CA, USA) was used for conventional US and CEUS. The equipped 9L4 and 18L6 linear array transducers were used for conventional US, and the 9L4 for CEUS. All selected thyroid nodules were evaluated by conventional US and classified according to the Kwak TI-RADS (4). Five US suspicious features (solid component, marked hypo- or hypo-echogenicity, irregular margins, taller-than-wide shape, and microcalcifications) were applied to categorize the thyroid nodules as TI-RADS category 3 (no suspicious US features), 4a (1 suspicious US feature), 4b (2 suspicious US features), 4c (3 or 4 suspicious US features), and 5 (5 suspicious US features).

CEUS and Analysis

CEUS performed technology and the ultrasound contrast agents were the same as our previous studies (9, 11–13). The CEUS videos were acquired and time-intensity curves (TICs) of the thyroid within selected regions of interest (ROIs) were analyzed according to our previous study (11). We simply divided the CEUS time into two phases: the early enhancement phase (from the microbubbles entering the nodule until reaching the peak intensity) and the late enhancement phase (the microbubbles in the nodule begin to fade away until they disappear). After comparison with the surrounding thyroid parenchymal enhancement, the contrast enhancement features were classified as follows: enhancement type (no enhancement, linear enhancement, which means marked hypo-enhancement, homogeneous hypo-enhancement or heterogeneous hypo-enhancement), arrival time (the time of microbubbles arriving at the nodule compared with the thyroid parenchymal tissue), peak intensity (PI, expressed as a percentage), and area under the curve (AUC, expressed in percentage by seconds). The PI and AUC of the nodules are reported as indices by the ratio of the ROI of the nodules to the ROI of the thyroid parenchymal tissue according to our previous studies (11, 12).

Reference Standard

FNA Bethesda cytology (BC) diagnoses were divided into six categories according to the Bethesda System (1). For PTCs, the histopathological results after surgery were used as the reference standard. For MTNs, the FNA results classified as BC 2 within at least 6 months of the follow-up US were used as the reference standard in addition to the histopathologic results after surgery.

Statistical Analysis

SPSS version 21.0 software (SPSS, Chicago, IL, USA) was used for statistical analysis. Continuous data are presented as mean and standard deviation and were compared by the independent t-test. Categorical data are presented as percentages and were analyzed by the Chi-square test. Binary logistic regression was used to assess significant CEUS features and their independent association with MTNs. P <0.05 means the difference has statistical significance.

RESULTS

A total of 218 patients with MTNs were included in the analysis. Twelve (5.5%) patients underwent total thyroidectomy for PTC on the other lobe, and the MTNs were demonstrated to be nodular goiter by paraffin section examination. Fifteen (6.9%) patients who underwent partial thyroidectomy for cytopathologic examination disclosed atypia of unknown significance by ultrasound guided FNA and requests for surgery from patients, and the nodules were benign, as confirmed by histopathology. The remaining 191 (87.6%) patients underwent FNA. In total, 176 lesions were proven to be benign and 15 were considered inadequate specimens at the initial FNA and underwent repeat FNA. All nodules were consistent with benign thyroid nodule collapse changes (**Table 1**).

According to the TI-RADS diagnostic classification by Kwak et al. (4), the US performances of the MTNs were classified (**Table 1**). In this study, all MTNs had at least 2 suspicious US features: a solid component and hypoechogenicity or marked hypoechogenicity. Thus, 28 (12.9%) patients were classified as TI-RADS category 4b, 142 (65.1%) patients as TI-RADS category 4c, and 48 (22.0%) patients as TI-RADS category 5.

According to the CEUS enhancement types, the MTNs were classified into 3 patterns (A, B, C patterns) (**Figure 1**). The A pattern enhancement of MTNs shows a linear perfusion of microbubbles (marked hypo-enhancement) with a clear margin compared with surrounding enhanced thyroid parenchymal tissue in the early enhancement phase, and the microbubbles faded away with a clear margin in the late enhancement phase (**Figure 2**). The B pattern enhancement of MTNs shows heterogeneous hypo-enhancement of microbubbles perfusion with a blurred margin compared with surrounding enhanced thyroid parenchymal tissue in the early enhancement phase, and the microbubbles faded away with a clear margin in the late enhancement phase (**Figure 3**). The C pattern enhancement of MTNs shows no microbubbles (no enhancement) entering the thyroid nodules, which has a clear margin compared with surrounding enhanced thyroid parenchymal tissue in both the early and late enhancement phases (**Figure 4**). The A and C pattern enhancements of MTNs demonstrated a high specificity compared with the enhancement of previously reported typical PTCs, and linear enhancement and no enhancement were almost never shown in the enhancement of PTCs. However, the B pattern enhancement of MTNs exhibited heterogeneous hypo-enhancement, which was also shown in most PTCs. Therefore, more CEUS features of the B pattern MTNs require further study to differentiate them from PTCs.

In this study, 149 patients with 149 A pattern MTNs, 24 patients with 24 B pattern MTNs and 45 patients with 45 C pattern MTNs were included in the analysis. To further study the B pattern MTNs, 42 patients with 42 PTCs were also included in the control group. The mean diameter of the B pattern MTNs was 8.46 ± 3.05 mm and ranged from 4 to 15 mm. The mean diameter of the PTCs was 7.62 ± 3.02 mm and ranged from 4 to 15 mm. The diameters of the nodules were not significantly different between the two groups (p >0.05, **Table 2**). The CEUS features of the B pattern MTNs and PTCs are summarized in **Table 2**. For both the B pattern MTN and PTC groups, all nodules showed hypo-enhancement, PI index <1 and AUC index <1, and no differences were noted between the two groups. Regarding the enhancement type, 23 (95.8%) nodules exhibited heterogeneous hypo-enhancement and only 1 (4.2%) nodule showed homogeneous hypo-enhancement in the B pattern MTNs, indicating that the microbubbles in most of the nodules were unevenly distributed. However, 29 (69.0%) nodules exhibited homogeneous hypo-enhancement and 13 (31.0%) nodules showed heterogeneous hypo-enhancement in the PTC groups, indicating that the microbubbles in most of the nodules were evenly distributed. A significant difference was noted between the two groups (p <0.05). Regarding arrival time, 23 (95.8%) nodules showed late arrival time in the B pattern MTNs, whereas 37 (88.1%) nodules showed late arrival time in the PTC group. These findings demonstrated that the microbubbles arriving at the nodules were later than those of the thyroid parenchymal tissue in most of the nodules in both groups, and no significant difference was noted between the groups (p >0.05). Regarding the margin after clearance, 20 (83.8%) nodules exhibited a clear margin after the microbubbles faded away, and only 4 (16.7%) nodules showed blurred margins after the microbubbles faded away in the B pattern MTNs. These finding indicates that the microbubbles vanished quickly in the whole nodule and left a clear margin with

TABLE 1 | Diagnostic Performance of the MTNs by the Kwak TI-RADS.

TI-RADS score	Number of malignant US features	MTNs (n = 218)	Pathologic method	
			Surgery (n = 27)	FNA (n = 191)
4b	2	28	0	28
4c	3–4	142	22	120
5	5	48	5	43

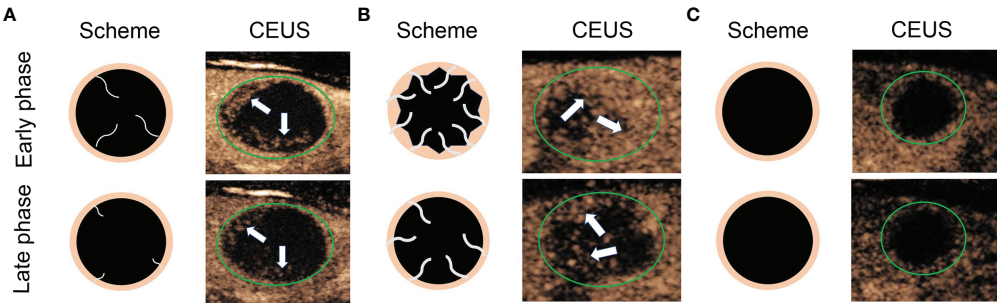

FIGURE 1 | Diagram shows different CEUS enhancement patterns of mummified thyroid nodules. **(A)** Early phase of CEUS shows a linear perfusion of microbubbles with a clear margin compared with surrounding enhanced thyroid parenchymal tissue, and the late phase of CEUS shows the microbubbles faded away with a clear margin. **(B)** Early phase of CEUS shows a heterogeneous hypo-enhancement of microbubbles perfusion with a blurred margin compared with surrounding enhanced thyroid parenchymal tissue, and the late phase of CEUS shows the microbubbles faded away with a clear margin. **(C)** Both early phase and late phase of CEUS show no microbubbles enter the thyroid nodules, which has a clear margin compared with surrounding enhanced thyroid parenchymal tissue. The green circles indicate the margin of the thyroid nodules, the white arrows indicate the microbubbles perfusion in the thyroid nodules.

the thyroid parenchymal tissue. However, 39 (92.9%) nodules exhibited blurred margins after the microbubbles faded away and 3 (7.1%) nodules showed clear margins after the microbubbles faded away in the PTC groups, indicating that the microbubbles had a small dose retention in the nodules without an obvious disappearance in the late phase. A significant difference was noted between the two groups (p <0.05). Thus, the univariate analysis indicated that compared with the PTC nodules, the B pattern MTNs more frequently exhibited heterogeneous hypo-enhancement and clear margins after clearance (p <0.05).

A binary logistic regression analysis was performed for two statistically significant CEUS variables (p <0.05). The results indicated that heterogeneous hypo-enhancement (B = 2.655, odds ratio [OR] = 14.225, 95% confidence interval [CI] = 1.383–146.265, p = 0.026) and clear margin after clearance (B = 3.264, OR = 26.167, 95% CI = 4.771–143.512, p = 0.000) were independent characteristics related to the B pattern MTNs for their differentiation from PTC nodules (**Table 3**).

DISCUSSION

Benign thyroid nodules may display morphologic changes with suspicious malignant US features over time, and the progression of benign thyroid nodule necrosis, desiccation, and subsequent collapse is called thyroid nodule mummification (5). Previous studies have shown that the typical MTNs have US imaging features, such as solid components, marked hypoechogenicity, punctate echogenic foci, double black-and-white peripheral halos and posterior shadowing (9). Comparison with previous images showing thyroid nodule shrinkage over time is useful for reaching the correct final diagnosis (5, 9, 15). Thus, some patients with MTNs could effectively avoid any unnecessary FNA or even surgical procedures, which maybe cause more severe complications (16–18).

In this study, according to the Kwak TI-RADS classification, at least 2 suspicious US features (solid component and hypo-echogenicity) were shown in all MTNs, so their classifications were at least a TI-RADS score of 4b. Of the 218 MTNs, 28 nodules had a TI-RADS score of 4b, 142 nodules had a TI-RADS score of 4c, and 48 nodules had a TI-RADS score of 5. Of 218 patients, 27 patients underwent total thyroidectomy or underwent total thyroidectomy, and 191 patients underwent FNA. However, if the patients have no clear clinical history, such as previous cystic or predominantly cystic thyroid nodules, this collapsed nodule with a high TI-RADS classification in grayscale US may have to undergo unnecessary FNA or even surgery.

CEUS exhibits significant value in the diagnosis of collapsing benign cystic or predominantly cystic thyroid nodules, especially combined with clinical history. No enhancement or scant punctate-linear enhancement in the whole or most areas of the nodules exhibits good specificity for MTNs (14). In this study, 218 patients with 218 MTNs were included and classified into 3 patterns (A, B, C) according to the different CEUS enhancement types. The A pattern CEUS of MTNs shows a linear perfusion of microbubbles with a clear margin compared with surrounding thyroid parenchymal tissue, which was consistent with the scant punctate-linear enhancement mode for the whole or most of the regions of the nodules (14). These nodules usually displayed fibrous tissue hyperplasia, cholesterol crystallization, foam tissue cells and lymphocyte infiltration in histopathology. The C pattern CEUS of MTNs shows no microbubbles entering the thyroid nodules, which have a clear margin compared with surrounding enhanced thyroid parenchymal tissue in both the early and late enhancement phases. This finding was consistent with no enhancement in previously reported studies (9, 14). The A and C pattern enhancements of MTNs demonstrated high specificity compared with the enhancement of previously reported typical PTCs, and linear enhancement and no enhancement were almost never noted in the enhancement of PTCs (14). However, the B pattern CEUS of MTNs shows heterogeneous hypo-enhancement of microbubbles perfusion with a blurred margin compared with surrounding enhanced thyroid parenchymal tissue in the early enhancement phase, and

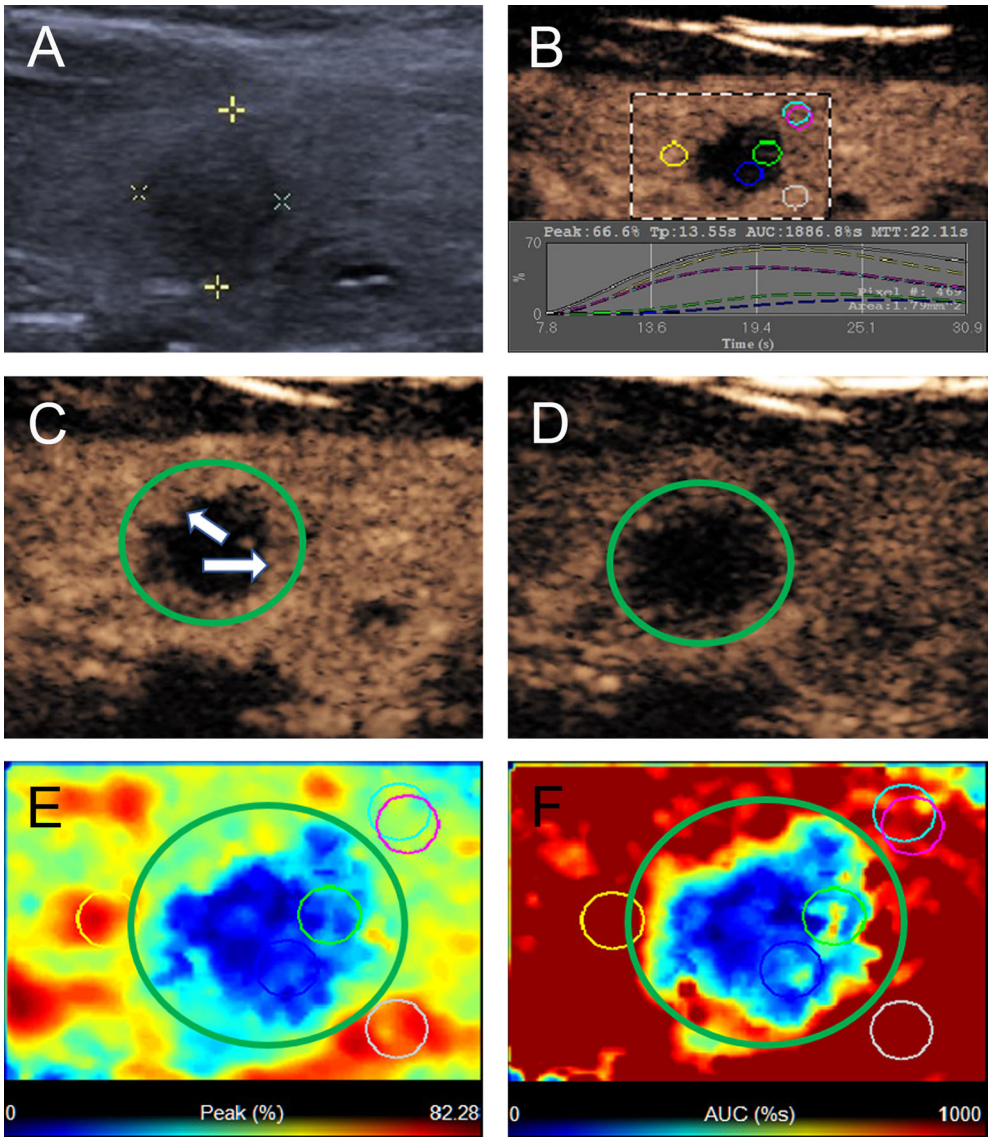

FIGURE 2 | A 40-year-old woman with A pattern mummified thyroid nodule proven by FNAB. **(A)** Nodule showed solid component, hypoechogenicity, ill-defined margin and taller than wide shape (TI-RADS 4c). **(B)** Time-intensity curve showed the CEUS parameters of this nodule compared with peripheral thyroid parenchyma. **(C)** The early phase of CEUS showed a linear enhancement (white arrows) in the whole nodule (green circle). **(D)** The late phase of CEUS showed the microbubbles in the nodule fade away with a clear margin compared with peripheral thyroid parenchyma. **(E)** Parametric color map showed the values of peak for the nodule was totally deep blue compared with the surrounding yellow color of thyroid parenchyma, indicated the peak intensity of the nodule was markedly lower than peripheral thyroid parenchyma. **(F)** Parametric color map showed that the AUC for the nodule was totally deep blue with a little linear yellow on the peripheral of the nodule, indicated AUC of the nodule was obviously lower than peripheral thyroid parenchyma.

this hypo-enhancement mode is highly similar to the enhancement mode of PTCs (19, 20). In this study, heterogeneous hypo-enhancement occurred more frequently in the B pattern MTNs than in PTCs. In the late enhancement phase, the microbubbles faded away with a clear margin, which was an independent feature for MTNs compared with PTCs. This finding indicates that the microvessels of the MTNs were less abundant than those of PTCs and were typically distributed on the peripheral part of the nodule. This type of MTN will further collapse and lacks vasculature on the follow-up US examination over time in our current study. However, these findings have not been systematically reported to date. Therefore, familiarity with the CEUS features of these different enhancement modes suggests that MTNs may be helpful in reducing repeated FNA or unnecessary surgery.

This study had several limitations. First, most of the final diagnoses for MTN result used FNA with at least 6 months of follow-up US as the reference standard, which may lead to false

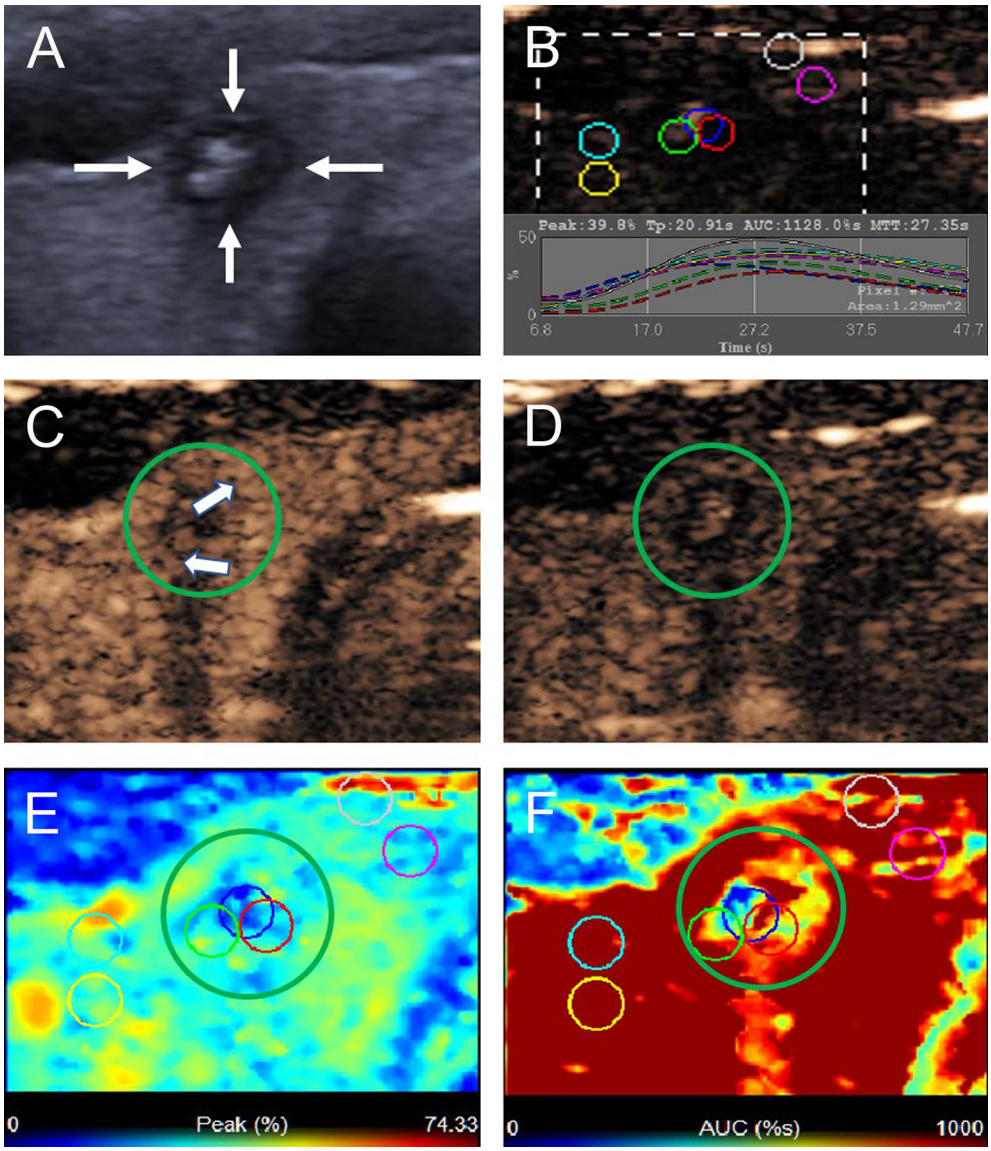

FIGURE 3 | A 22-year-old woman with the B pattern mummified thyroid nodule proven by FNAB. **(A)** Nodule showed solid component, hypoechogenicity, ill-defined margin, taller than wide shape and microcalcification (TI-RADS 5). **(B)** Time-intensity curve showed the CEUS parameters of this nodule compared with peripheral thyroid parenchyma. **(C)** The early phase of CEUS showed a heterogeneous hypo-enhancement (white arrows) in the whole nodule (green circle). **(D)** The late phase of CEUS showed the microbubbles in the nodule fade away with a clear margin compared with peripheral thyroid parenchyma. **(E)** Parametric color map showed the values of peak for the nodule was uneven deep blue and blue, compared with the surrounding yellow and blue color of thyroid parenchyma, indicated the peak intensity of the nodule was lower than peripheral thyroid parenchyma. **(F)** Parametric color map showed that the AUC for the nodule was uneven deep blue and yellow color, compared with the surrounding red color of thyroid parenchyma, indicated AUC of the nodule was lower than peripheral thyroid parenchyma.

negatives. Second, unavoidable selection bias may exist because the patients with suspicious US features of malignancy might not undergo surgery or further examination. Third, the control group of PTCs was chosen with a size less than 15 mm and hypo-enhancement for in line with the study group, which may cause unavoidable selection bias and inaccurate evaluation of the effect for CEUS features. Thus, a large-scale study with a multicenter prospective design is needed to clarify our data and provide the specificity and sensitivity of the reported CEUS findings.

CONCLUSION

In conclusion, we first reviewed the CEUS enhancement features of 218 MTNs and classified them into three (A, B, C) patterns. The A pattern MTNs show linear hypo-enhancement with only scant microbubbles entering the thyroid nodule. The B pattern MTNs show heterogeneous hypo-enhancement and a small amount of microbubbles perfusion with uneven distribution in the thyroid nodule. The C pattern MTNs show no enhancement

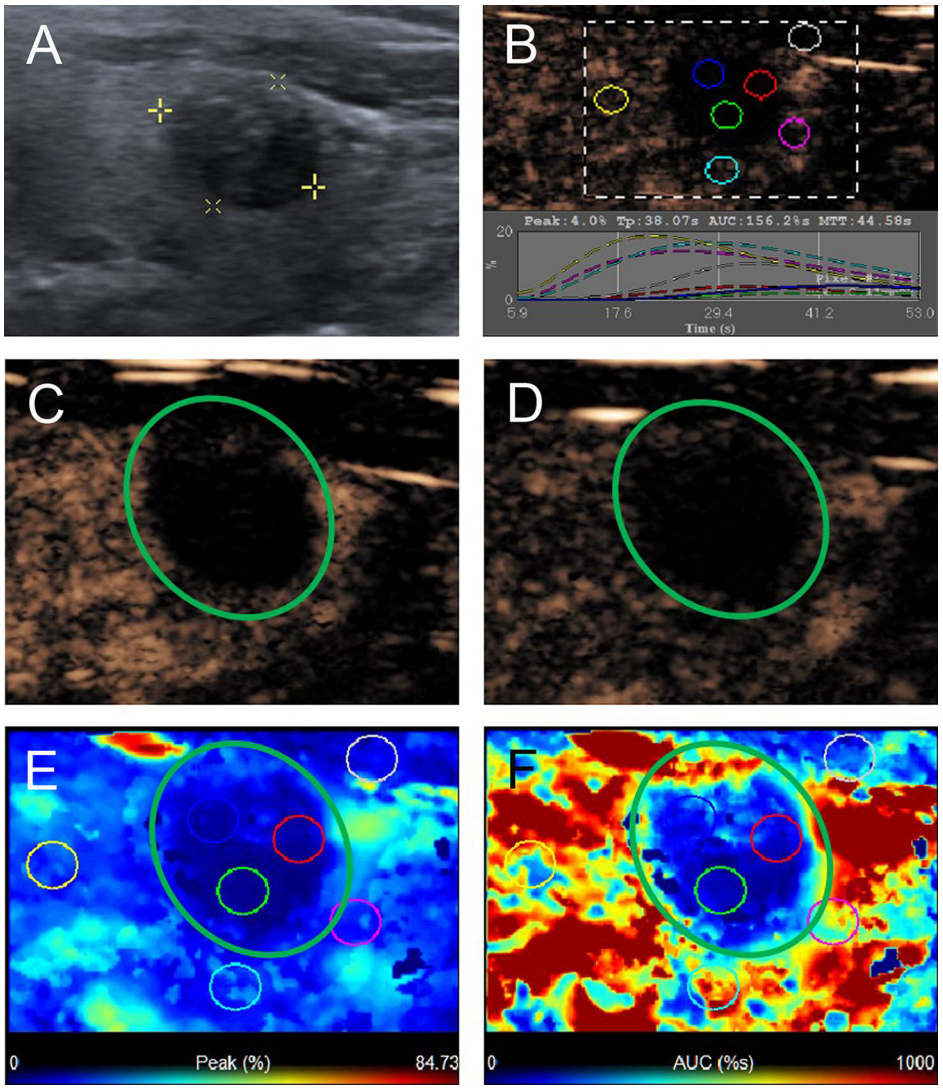

FIGURE 4 | A 58-year-old man with C pattern mummified thyroid nodule proven by FNAB. **(A)** Nodule showed solid component and hypoechogenicity (TI-RADS 4b). **(B)** Time-intensity curve showed the CEUS parameters of this nodule compared with peripheral thyroid parenchyma. **(C)** The early phase and **(D)** the late phase of CEUS showed no microbubbles enter the nodule (green circle). **(E)** Parametric color map showed the values of peak for the nodule was completely deep blue, indicated the peak intensity of the nodule was markedly lower than peripheral thyroid parenchyma. **(F)** Parametric color map showed that the AUC for the nodule was totally deep blue compared with the surrounding red color of thyroid parenchyma, indicated AUC of the nodule was obviously lower than peripheral thyroid parenchyma.

TABLE 2 | CEUS Characteristics of the B pattern MTNs and PTCs.

Characteristics	MTNs (n = 24)	PTCs (n = 42)	*p*
Size (mm)	8.46 ± 3.05	7.62 ± 3.02	0.683
Enhancement type			0.000*
Homogeneous hypo-enhancement	1 (4.2)	29 (69.0)	
Heterogeneous hypo-enhancement	23 (95.8)	13 (31.0)	
Arrival time			0.404
Early	1 (4.2)	5 (11.9)	
Late	23 (95.8)	37 (88.1)	
Margin after clearance			0.000*
Clear	20 (83.3)	3 (7.1)	
Blurred	4 (16.7)	39 (92.9)	

**p <0.05 was considered a significant difference.*

TABLE 3 | Multivariate logistic regression analysis of CEUS characteristics related to the B pattern MTNs distinguishing from PTCs.

Characteristics	Partial regressioncoefficient, β	Odds ratio	95% Confidence interval	*P*-Value
Heterogeneous hypo-enhancement	2.655	14.225	1.383–146.265	0.026*
Clear margin after clearance	3.264	26.167	4.771–143.512	0.000*

*$p < 0.05$ was considered a significant difference.

and have no microbubbles in the thyroid nodules. In addition, compared with PTCs, heterogeneous hypo-enhancement and clear margins after clearance were independent characteristics related to the B pattern MTNs for their differentiation from PTCs ($p < 0.05$). Therefore, preoperative CEUS characteristics may provide more important information for distinguishing MTNs from malignant thyroid nodules to avoid surgical excisions or unnecessary FNAs.

DATA AVAILABILITY STATEMENT

The raw data supporting the conclusions of this article will be made available by the authors, without undue reservation.

ETHICS STATEMENT

The studies involving human participants were reviewed and approved by the Ethical Committee of the Second Xiangya Hospital of Central South University in China. The patients/participants provided their written informed consent to participate in this study. Written informed consent was obtained from the individual(s) for the publication of any potentially identifiable images or data included in this article.

AUTHOR CONTRIBUTIONS

CN contributed to the conception and design of the work. SC and KT participated to data analysis and manuscript writing. YG, FY, LL, XL, QZ, YX, and RZ participated to data collection and follow-up of patients. All authors listed have made a substantial, direct, and intellectual contribution to the work and approved it for publication.

FUNDING

This project was funded by the National Natural Science Foundation of China (81974267) and the Science and Technology Innovation Program of Hunan Province (2021RC3033).

REFERENCES

1. Haugen BR, Alexander EK, Bible KC, Doherty GM, Mandel SJ, Nikiforov YE, et al. 2015 American Thyroid Association Management Guidelines for Adult Patients With Thyroid Nodules and Differentiated Thyroid Cancer: The American Thyroid Association Guidelines Task Force on Thyroid Nodules and Differentiated Thyroid Cancer. *Thyroid* (2016) 26(1):1–133. doi: 10.1089/thy.2015.0020
2. Tessler FN, Middleton WD, Grant EG, Hoang JK, Berland LL, Teefey SA, et al. ACR Thyroid Imaging, Reporting and Data System (TI-RADS): White Paper of the ACR TI-RADS Committee. *J Am Coll Radiol* (2017) 14(5):587–95. doi: 10.1016/j.jacr.2017.01.046
3. Moon WJ, Jung SL, Lee JH, Na DG, Baek JH, Lee YH, et al. Benign and Malignant Thyroid Nodules: US Differentiation - Multicenter Retrospective Study. *Radiology* (2008) 247(3):762–70. doi: 10.1148/radiol.2473070944
4. Kwak JY, Han KH, Yoon JH, Moon HJ, Son EJ, Park SH, et al. Thyroid Imaging Reporting and Data System for US Features of Nodules: A Step in Establishing Better Stratification of Cancer Risk. *Radiology* (2011) 260 (3):892–9. doi: 10.1148/radiol.11110206
5. Lacout A, Chevenet C, Marcy PY. Mummified Thyroid Syndrome. *AJR Am J Roentgenol* (2016) 206(4):837–45. doi: 10.2214/AJR.15.15267
6. Koo JH, Shin JH, Han BK, Ko EY, Kang SS. Cystic Thyroid Nodules After Aspiration Mimicking Malignancy: Sonographic Characteristics. *J Ultrasound Med* (2010) 29(10):1415–21. doi: 10.7863/jum.2010.29.10.1415
7. Ma S, Zhou P, Wu X, Tian S, Zhao Y. Detection of the Single-Session Complete Ablation Rate by Contrast-Enhanced Ultrasound During Ultrasound-Guided Laser Ablation for Benign Thyroid Nodules: A Prospective Study. *BioMed Res Int* (2016) 2016:9565364. doi: 10.1155/2016/9565364
8. Park NH, Kim DW, Park HJ, Lee EJ, Park JS, Park SI, et al. Thyroid Cysts Treated With Ethanol Ablation can Mimic Malignancy During Sonographic Follow-Up. *J Clin Ultrasound* (2011) 39(8):441–6. doi: 10.1002/jcu.20861
9. Peng Q, Niu C, Zhang Q, Zhang M, Chen S, Peng Q. Mummified Thyroid Nodules: Conventional and Contrast-Enhanced Ultrasound Features. *J Ultrasound Med* (2019) 38(2):441–52. doi: 10.1002/jum.14712
10. Tan XQ, Qian L, Wang Y. Distinguishing Mummified Thyroid Nodules From Malignant Thyroid Nodules. *Med Ultrason* (2019) 21(3):251–6. doi: 10.11152/mu-1894
11. Peng Q, Niu C, Zhang M, Chen S. Sonographic Characteristics of Papillary Thyroid Carcinoma With Coexistent Hashimoto's Thyroiditis: Conventional Ultrasound, Acoustic Radiation Force Impulse Imaging and Contrast-Enhanced Ultrasound. *Ultrasound Med Biol* (2019) 45(2):471–80. doi: 10.1016/j.ultrasmedbio.2018.10.020
12. Zhang Q, Liao L, Peng Q, Tang K, Xu Y, Zhang R, et al. Value of Contrast-Enhanced Ultrasound in Differentiating Clinically Atypical Subacute Thyroiditis From Papillary Thyroid Carcinomas. *Ultrasound Med Biol* (2021) 47(12):3384–92. doi: 10.1016/j.ultrasmedbio.2021.09.001
13. Fang F, Gong Y, Liao L, Ye F, Zuo Z, Qi Z, et al. Value of Contrast-Enhanced Ultrasound in Partially Cystic Papillary Thyroid Carcinomas. *Front Endocrinol (Lausanne)* (2021) 12:783670. doi: 10.3389/fendo.2021.783670
14. Zhou J, Yin L, Wei X, Zhang S, Song Y, Luo B, et al. 2020 Chinese Guidelines for Ultrasound Malignancy Risk Stratification of Thyroid Nodules: The C-TIRADS. *Endocrine* (2020) 70(2):256–79. doi: 10.1007/s12020-020-02441-y.
15. Tan TSE, Sanamandra SK. Mummified Thyroid Nodule: A Diagnostic and Management Conundrum. *BMJ Case Rep* (2021) 14(5):e242238. doi: 10.1136/bcr-2021-242238
16. Conzo G, Docimo G, Ruggiero R, Napolitano S, Palazzo A, Gambardella C, et al. Surgical Treatment of Papillary Thyroid Carcinoma Without Lymph Nodal Involvement. *G Chir* (2012) 33(10):339–42.

17. Conzo G, Calo PG, Gambardella C, Tartaglia E, Mauriello C, Della Pietra C, et al. Controversies in the Surgical Management of Thyroid Follicular Neoplasms. Retrospective Analysis of 721 Patients. *Int J Surg* (2014) 12 (Suppl 1):S29–34. doi: 10.1016/j.ijsu.2014.05.013
18. Gambardella C, Patrone R, Di Capua F, Offi C, Mauriello C, Clarizia G, et al. The Role of Prophylactic Central Compartment Lymph Node Dissection in Elderly Patients With Differentiated Thyroid Cancer: A Multicentric Study. *BMC Surg* (2019) 18(Suppl 1):110. doi: 10.1186/s12893-018-0433-0
19. Zhang Y, Zhou P, Tian SM, Zhao YF, Li JL, Li L. Usefulness of Combined Use of Contrast-Enhanced Ultrasound and TI-RADS Classification for the Differentiation of Benign From Malignant Lesions of Thyroid Nodules. *Eur Radiol* (2017) 27(4):1527–36. doi: 10.1007/s00330-016-4508-y
20. Chen S, Niu C, Peng Q, Tang K. Sonographic Characteristics of Papillary Thyroid Carcinoma With Coexistent Hashimoto's Thyroiditis in the Preoperative Prediction of Central Lymph Node Metastasis. *Front Endocrinol (Lausanne)* (2021) 12:556851. doi: 10.3389/fendo.2021.556851

Conflict of Interest: The authors declare that the research was conducted in the absence of any commercial or financial relationships that could be construed as a potential conflict of interest.

frontiers | Frontiers in Endocrinology

ORIGINAL RESEARCH
published: 16 May 2022
doi: 10.3389/fendo.2022.861070

Analysis of Differential Diagnosis of Benign and Malignant Partially Cystic Thyroid Nodules Based on Ultrasound Characterization With a TIRADS Grade-4a or Higher Nodules

Chen-Yi Wang[1,2,3], *Yang Li*[1,2], *Meng-Meng Zhang*[1,2], *Zhi-Long Yu*[1,2], *Zi-Zhen Wu*[1,2], *Chen Li*[1,2], *Dong-Chen Zhang*[1,2], *Ying-Jiang Ye*[1,2], *Shan Wang*[1,2*] and *Ke-Wei Jiang*[1,2*]

[1] *Department of Gastroenterological Surgery, Peking University People's Hospital, Beijing, China,* [2] *Laboratory of Surgical Oncology, Beijing Key Laboratory of Colorectal Cancer Diagnosis and Treatment Research, Peking University People's Hospital, Beijing, China,* [3] *Thyroid Surgery Department, The First Affiliated Hospital of Zhengzhou University, Zhengzhou, China*

OPEN ACCESS

Edited by:
Emerita Andres Barrenechea, Veterans Memorial Medical Center, Philippines

Reviewed by:
Giovanni Docimo, University of Campania Luigi Vanvitelli, Italy
Serena Ippolito, ASL Napoli 1 Centro, Italy

***Correspondence:**
Shan Wang
shanwang60@sina.com
Kewei Jiang
jiangkewei@pkuph.edu.cn

Specialty section:
This article was submitted to Thyroid Endocrinology, a section of the journal Frontiers in Endocrinology

Received: *24 January 2022*
Accepted: *29 March 2022*
Published: *16 May 2022*

Citation:
Wang C-Y, Li Y, Zhang M-M, Yu Z-L, Wu Z-Z, Li C, Zhang D-C, Ye Y-J, Wang S and Jiang K-W (2022) Analysis of Differential Diagnosis of Benign and Malignant Partially Cystic Thyroid Nodules Based on Ultrasound Characterization With a TIRADS Grade-4a or Higher Nodules. Front. Endocrinol. 13:861070. doi: 10.3389/fendo.2022.861070

Partially cystic thyroid nodules (PCTNs) are a kind of thyroid nodule with both solid and cystic components, and are usually misdiagnosed as benign nodules. The objective of this study was to determine the ultrasound (US) characterizations with a TIRADS Grade-4a or higher partially cystic thyroid nodules (PCTNs) which are associated with being malignant or benign. In this study, 133 PCTNs with a TIRADS Grade-4a or higher were enrolled; 83 were malignant and 50 were benign. TI-RADS classification can detect malignant PCTNs, and its sensitivity, specificity, positive predictive value, negative predictive value, and accuracy are 39.8%, 96.0%, 94.3%, 49.0%, and 60.9%, respectively. Univariate analyses revealed that nodule shape, margin, and structure were related to PCTNs' being benign and malignant, among which nodules taller-than-wide, with an irregular shape, non-smooth margin, eccentric sharp angle, or edge sharp angle were significantly associated with malignancy while ovoid to round nodules, smooth margins, multiple separation, and eccentric obtuse angle structures were significantly associated with a benign nature. For the solid part of PCTNs, its free margin, echo, and calcification are related to benign and malignant PCTNs. Among them, the free margin of the solid part is non-smooth, hypoechoic, and microcalcification, which are related to malignant PCTNs, while the free margin of the solid part is smooth, isoechoic, macrocalcification, non-calcification and are related to benign PCTNs. Calcification of solid part and free margin are important factors for predicting malignant PCTNs. In addition, nodules' composition, blood flow signal, and other factors had nothing to do with PCTNs' being benign or malignant. In the multivariate Logistic regression analysis, solid part calcification (OR: 17.28; 95%CI:

5.14~58.08) and free margin (OR: 3.18; 95%CI: 1.01~10.00) were revealed to be the strongest independent predictors for malignancy(P<0.05). Our study indicated that understanding the ultrasound characteristics of malignant PCTNs, to avoid misdiagnosed PCTNs patients, is important to make a precise diagnosis and prognosis of PCTNs.

Keywords: thyroid neoplasms, thyroid nodule, ultrasonography, factor analysis, statistical, partially cystic thyroid nodules

INTRODUCTION

Partially cystic thyroid nodules (PCTNs) are a kind of thyroid nodule with both solid and cystic components, accounting for approximately 20.9% of thyroid nodules (1). Since most PCTNs are potentially benign lesions induced by degeneration, such as nodular hyperplasia, the management of partially cystic thyroid nodules is often underrated. However, PCTNs still have a 3.3% to 17.6% rate of malignancy, and the incidence of malignancy is not related to the proportion of cystic components (2). Therefore, it is of great importance to identify sonographic features that distinguish malignant PCTNs in clinical practice.

Fine-needle aspiration biopsy (FNAB) is a reliable and cost-efficient method to evaluate thyroid nodules, with an overall accuracy of 98% and a false-negative rate below 5%. Current guidelines in China only consider the size (1.0-1.5 cm) as a criterion for FNAB, regardless of the cystic portion (3). Similar guidelines from the American Thyroid Association consider a size ≥1 cm (in nodules with high suspicion), 1.5–2.0 cm (in nodules with any suspicious US features), or 2.0 cm (in nodules without any suspicious US features) as the threshold size (4). However, its reliability in cystic thyroid is not clear. In cystic thyroid malignancy, performing a diagnostic FNAB is challenging due to the lack of cellularity in cystic areas, presence of nuclear debris, and histiocyte/macrophages (5), which frequently lead to misdiagnosis of a benign cystic nodule.

Thyroid ultrasonography(US) is an essential diagnostic technique for assessing the malignancy risk of thyroid nodules (6, 7), but there are few studies on the ultrasound characteristics of PCTNs diagnosis and prediction, and previous studies showed that the number of malignant samples was too little, and the benign control group lacked postoperative pathological results. Shi et al. (8) reported that a taller-than-wide shape, eccentric configuration, non-smooth margin, hypoechogenicity, microcalcification, and spiculated or microlobulated margin were significantly associated with PCTNs malignancy. According to Kim et al. (9), eccentric configuration with an acute angle and microcalcifications can significantly increase the risk of malignancy. With PCTNs, it is difficult to distinguish between benign and malignant in clinical practice, and it is easy to misdiagnose as a benign condition. Hence, the aim of the present study was to investigate the benign and malignant ultrasound characteristics of PCTNs in order to help clinicians make accurate treatment choices. The results are reported below.

1 MATERIALS AND METHODS

1.1 Patients

The study was approved by the Ethical Committee of the First Affiliated Hospital of Zhengzhou University in China and was performed in accordance with the Declaration of Helsinki for human studies. The requirement of informed consent from human subjects is sometimes waived by institutional review boards (IRBs) for protocols that include a retrospective review of images acquired for clinical diagnostic purposes. From January 2016 to January 2020, 133 PCTNs patients who underwent thyroidectomy surgery were retrospectively enrolled in this case-control study. The inclusion criteria were: 1) patients with mixed echoic thyroid nodules that were confirmed by our central ultrasound examination before surgery; 2) no invasive procedure such as thyroid surgery or FNA was previously performed; and 3) all PCTNs were suspicious for malignancy (preoperative TIRADS grade 4a and above) and underwent surgical resection. In addition, the exclusion criteria were as follows: 1) without PCTNs pathologic examinations after surgery and 2) the color Doppler report was not checked by the chief physician. Finally, 133 PCTNs patients were included in this study; there were 59 males and 74 females, ranging in age from 9 to 71 years old, with an average age of 46.32 ± 12.27 years. The longest diameter of the nodules is 9 to 48mm. According to Chinese Thyroid Imaging Reporting and Data System (C-TIRADS) (3), 98 patients were classified into score 4a (1 point, 2-10% malignancy rate), seven patients were classified into score 4b (2 points, 10-50% malignancy rate), 0 patients were classified into score 4c (3-4 points, 50-90% malignancy rate), and 28 patients were classified into score 5 (5 points, >90% malignancy rate). We defined score 4a as suspected malignant, and score 4b or higher was defined as malignant.

83 patients with postoperative pathological findings confirmed to be malignant were included in the malignant PCTNs group, and were made up of 80 papillary thyroid carcinomas and three follicular thyroid carcinomas. The remaining 50 patients with benign PCTNs were included in the case-control group, and included 44 cases of nodular goiter, four cases of Hashimoto's thyroiditis, and two cases of thyroid adenoma.

1.2 Methods

1.2.1 Equipment

Images were acquired using a Toshiba Aplio® XG ultrasound scanner (Toshiba, Japan) connected to an 8-14 MHz linear transducer (PLT 1202S probe). Patients took the supine

position to fully expose the neck. Ultrasonography was performed by two attending physicians in the same medical group with more than 8 years of experience in thyroid ultrasonography (>2000 cases/year), and the results were checked by one chief physician who had 24 years of experience in thyroid ultrasonography (>4000 cases/year) to prevent any artificial bias and ensure optimized image quality. The depth, gain, and focus of scanning were adjusted according to physical status after locating the thyroid nodules, and then clear 2D images were displayed and stored. Then, color Doppler ultrasound was applied to inspect the thyroid nodules and surrounding tissues, so as to determine the blood flow inside the foci and the surrounding tissues. The range was set to 9.8 cm/s, the frame rate was 8 frames/s, the color gain was 50 dB, and the filter was 6.

1.2.2 Image Analysis

US images in our study were retrospectively evaluated by two experienced physicians (each with more than 8 years of experience in thyroid ultrasonography) who were blinded to the other imaging results and clinical as well as histopathological data. Two physicians performed the following US finding for each entire nodule: size (the longest diameter), internal content (predominantly solid vs. predominant cystic), shape (ovoid to round vs. irregular vs. taller-than-wide), margin (smooth vs. non-smooth), and structure (eccentric acute angle, edge acute angle, eccentric obtuse angle, multiple separation). The internal solid portion inspection includes: free margin(smooth vs. non-smooth), echo (hypoechoic, isoechoic, and hyperechoic), calcification (microcalcification, macrocalcification, none), and blood flow signal level (0, 1, 2, 3). The ultrasound results report uses the 2020 Chinese thyroid nodule ultrasound malignant tumor risk stratification guideline C-TIRADS recommended term (3): hyperechoic refers to the echogenicity is higher than that of the surrounding thyroid parenchyma, hypoechoic means the echogenicity is similar to that of the surrounding thyroid parenchyma, isoechoic refers to the echogenicity that is similar to that of the surrounding thyroid parenchyma. Predominately solid means solid components accounted for more than 50% of the nodules (**Figure 1**). Predominately cystic refers to solid components that accounted for <50% of the nodules (**Figure 2**). Spongiform refers to multiple tiny cystic spaces that occupy the entire nodules without aggregated solid tissues; multiple separation is defined as the inner solid portion bordered by the

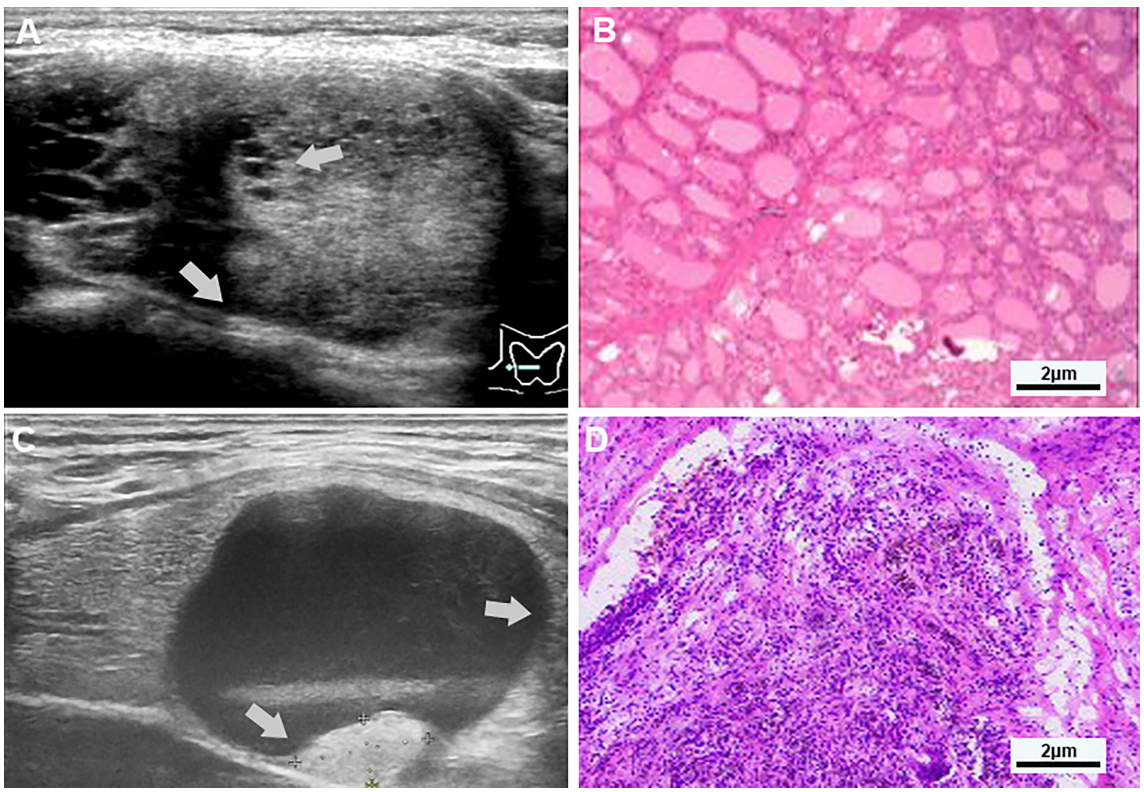

FIGURE 1 | **(A, B)** Examples of typical ultrasonographic and pathological sections of multiple separation partially cystic thyroid nodules. Transverse section of a cystic-solid nodule of the thyroid, mainly solid, with smooth and irregular margins, and an acute angle between the multiple-separated and fused solid components and the nodule wall (indicated by gray-white arrows), for the hypoechoic, the free edge is non-smooth, and the pathology confirmed nodular goiter. **(C, D)** Examples of typical ultrasonographic and pathological sections of predominant cystic partially cystic thyroid nodules. Longitudinal section of a cystic-solid nodule of the thyroid, mainly cystic, with smooth, oval nodule margins, and an obtuse angle between the solid part attached to the posterior wall and the nodule wall (indicated by the gray-white arrow), For isoechoic, the free edge is smooth, and the pathology confirmed nodular goiter with cystic degeneration, close to the thyroid membrane.

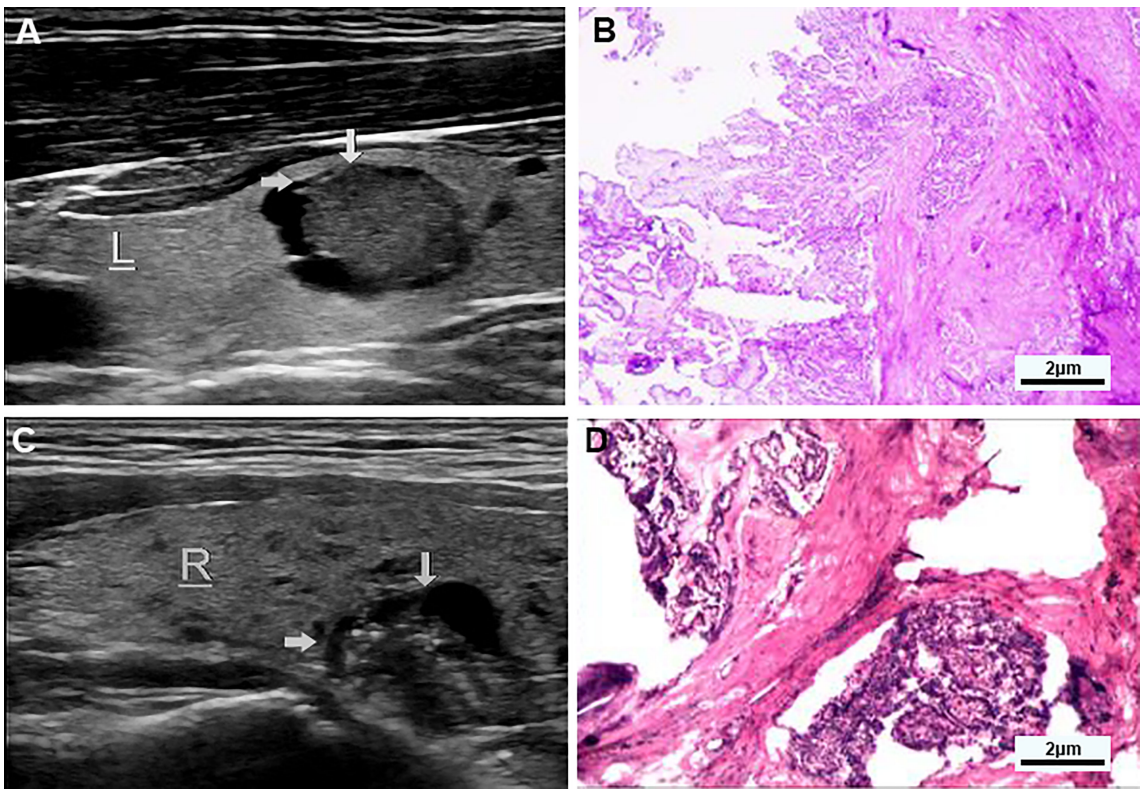

FIGURE 2 | **(A, B)** Examples of typical ultrasonographic and pathological sections of predominant solid partially cystic thyroid nodules. Longitudinal section of a cystic-solid nodule of the thyroid, mainly solid, with smooth and irregular margins, and an acute angle between the solid part of the anterior wall and the nodule wall (indicated by the gray arrow). It is hypoechoic, and the free edge is not smooth. TI-RADS grade 5 and the pathology confirmed papillary thyroid carcinoma, invading surrounding tissues. **(C, D)** Examples of typical ultrasonographic and pathological sections of macrocalcification cystic thyroid nodules. Longitudinal section of a cystic-solid nodule of the thyroid gland, mainly cystic, with smooth and irregular borders, and an acute angle between the solid part attached to the posterior wall and the nodule wall (indicated by the gray arrow) has multiple strong echogenic light spots, which are isoechoic, and the free edge is not smooth, and the pathology confirmed papillary thyroid carcinoma.

interface between the cystic and solid components (**Figure 1**); microcalcifications are defined as punctate echogenic foci of less than about 1 mm with or without shadowing; macrocalcifications are defined as the echogenic foci that are larger than 1 mm, usually accompanied by posterior shadowing (**Figure 2**). The class of blood flow signal was graded according to the Adler semi-quantitative method: grade 0, no blood flow; grade 1, little blood flow; grade 2, moderate blood flow; grade 3, abundant blood flow.

1.3 Statistical Methods

All analyses were conducted using SPSS version 24.0 (IBM SPSS Statistics for Macintosh, Version 24.0). Normally distributed enumeration data were expressed as cases and percentages (%), measurement data were expressed as mean ± standard deviation ($\bar{x} \pm s$), continuous variables were compared by t-test, and categorical variables were compared by $\chi 2$ test. The multivariate analysis was performed by binary logistic regression analysis. Because nodule sizes were distributed non-normally, the Mann-Whitney U test was chosen. Statistical significance was established at $P<0.05$.

2 RESULTS

According to the C-TIRADS (3) in the 2020 Chinese Thyroid Nodules Ultrasound Malignancy Risk Stratification Guidelines, there were 98 grade 4a nodules, seven grade 4b nodules, and 28 grade 5 nodules in this study. 98 cases were considered suspected malignant(TI-RADS 4a), and 35 cases were considered malignant (TI-RADS 4b or higher). According to preoperative ultrasound and postoperative pathological results, 33 true positive, 48 true negative, two false positive, and 50 false-negative(n=133) were detected, and the sensitivity, specificity, positive predictive value, negative predictive value, and accuracy were respectively 39.8% (33/83), 96.0% (48/50), 94.3% (33/35), 49.0% (48/98), and 60.9% (81/133).

Univariate analyses of US features of 133 PCTNs with TIRADS grade-4a or higher were summarized in **Table 1**. According to the postoperative pathological results, the prevalence of malignant PCTNs was 83 of 133(62.4%) and the prevalence of benign PCTNs was 50 of 133(37.6%). There was no significant gender difference between benign and malignant

TABLE 1 | Basic characteristics of the patients.

Essential information	Malignancy (n = 83)	Benign condition (n =50)	t/χ^2	P
Gender (%)			0.43	0.51
Male	35 (42.2%)	24 (48.0%)		
Female	48 (57.8%)	26 (52.0%)		
Age (year, Mean ± SD)	44.14 ± 11.59	49.92 ± 12.62	-2.64	0.01
TI-RADS grade (%)			20.70	<0.01
4a	50 (60.2%)	48 (96.0%)		
4b	7 (8.4%)	0 (0.0%)		
5	26 (31.3%)	2 (4.0%)		

PCTNs patients. The average age of malignant PCTNs patients was smaller than that of benign PCTNs patients [(44.14 ± 11.59) years vs. (49.92 ± 12.62) years]. The TI-RADS grade of malignant PCTNs patients was higher than that of benign PCTNs patients. The difference was statistically significant (P<0.01, t=20.70).

Ultrasound features of PCTNs found that nodule shape, margin, and structure were associated with benign and malignant PCTNs, among which taller-than-wide, irregular shape, non-smooth margin, and structure with eccentric/edge acute angle were significantly associated with malignant PCTNs, but ovoid to round shape, smooth margin, eccentric obtuse angle, and multiple separation structures were associated with benign PCTNs. For the solid part of PCTNs, the free edge, echo, and calcification of PCTNs are related to benign and malignant PCTNs. The free edge of the solid part being non-smooth, hypoechoic, and microcalcification are related to malignant PCTNs, while the free edge of solid part being smooth and isoechoic, macrocalcification, and non-calcification are related to benign PCTNs. The above results were statistically significant (P < 0.01) (**Table 2**). In addition, we found that nodule composition (P=0.83) and blood flow signal (P=0.20) were not associated with benign or malignant PCTNs.

Multivariate Logistic regression analysis showed (**Table 3**) solid partial calcification (OR: 17.28; 95%CI: 5.14-58.08) and free margin (OR: 3.18; 95%CI: 1.01-10.00) were the predictors of malignant PCTNs (all P<0.05). Among them, microcalcification and non-smooth free margin were important factors for predicting malignant PCTNs, and the risk of microcalcification in ultrasound signs was the most significant, which was 17.28 (P<0.05) times higher than that of macrocalcification and non-calcification.

TABLE 2 | Ultrasound characteristics of the partial cystic nodules of the thyroid gland.

Ultrasonic feature	Pathological results		χ^2	P
	Malignancy (n = 83)	Benign (n = 50)		
Composition (%)			0.49	0.83
Predominant cystic	4 (4.8%)	2 (4.0%)		
Predominant solid	79 (95.2%)	48 (96.0%)		
Shape (%)			15.76	<0.01
Ovoid to round	24 (28.9%)	32 (64.0%)		
Irregular	55 (66.3%)	18 (36.0%)		
Taller-than-wide	4 (4.8%)	0 (0.0%)		
Margin (%)			18.38	<0.01
Smooth	33 (39.8%)	39 (78.0%)		
Non-smooth	50 (60.2%)	11 (22.0%)		
Structure (%)			7.50	<0.01
Eccentric sharp angle	69 (83.1%)	36 (72.0%)		
Edge sharp Angle	8 (9.6%)	2 (4.0%)		
Multiple separation	6 (7.2%)	8 (16.0%)		
Eccentric obtuse angle	0 (0.0%)	4 (8.0%)		
Free margin (%)			12.96	<0.01
Smooth	18 (21.7%)	26 (52.0%)		
Non-smooth	65 (78.3%)	24 (48.0%)		
Echo (%)			10.43	<0.01
Isoechoic	0 (0.0%)	6 (12.0%)		
Hypoechoic	83 (100%)	44 (88.0%)		
Calcification (%)			43.85	<0.01
Non-calcification	6 (7.2%)	24 (48.0%)		
Macrocalcification	75 (90.4%)	18 (36.0%)		
Macrocalcification	2 (2.4%)	8 (16.0%)		
Blood flow signal (%)			0.95	0.20
0	3 (3.6%)	0 (0.0%)		
1	27 (32.5%)	12 (24.0%)		
2	34 (41.0%)	28 (56.0%)		
3	19 (22.9%)	10 (20.0%)		

3 DISCUSSION

TI-RADS is thyroid imaging reporting and data system for ultrasonography, mainly to classify the benign and malignant degree of thyroid nodules. Among them, the malignancy of TI-RADS 4a may be about 2-10%, TI-RADS 4b is up to 10-50%, TI-RADS 4c is 50-90% and TI-RADS 5 is >90% (3). PCTNs are easily misdiagnosed, especially for inexperienced radiologists, as their typical US characteristics differ from solid nodules, so the clinical management of PCTNs remains a challenge. In our study, the sensitivity of TI-RADS for PCTNs was 39.8% and the specificity was 96.0%, which was slightly different from the sensitivity of 72.7% and the specificity of 98.0% in similar studies (9). PCTNs whose ultrasound features are between benign and malignant are more difficult to differentiate. Compared with other related studies of solid thyroid nodules (10), the sensitivity and specificity of TI-RADS for differentiating benign and malignant thyroid nodules were 91.67% and 52.8%. Therefore, compared with solid nodules, PCTNs have a lower sensitivity and higher specificity for ultrasound diagnosis.

According to the analysis of the results of ultrasound images in this study, the solid component in some cystic nodules with eccentric sharp angle, edge sharp angle, non-smooth free edge, nodule hypoechoic, or microcalcification was associated with malignant PCTNs (P<0.01). A related report found that, compared with benign nodular goiters, PCTNs more frequently presented with calcification, hypoechogenicity of the solid part, hypoenhancement, heterogeneous enhancement, centrifugal perfusion, peak intensity index <1, time to peak index ≥1, and area under the curve index <1 on preoperative US and CEUS (11). A recent review included eight studies with a total of 2,004 PCTNs. Seven features were considered to be associated with malignancy. High specificity (>0.9) was found in nodules with a taller-than-wide shape, those that were spiculated/microlobulated or with an ill-defined margin, those with microcalcification, and a non-smooth rim. Among US features, eccentric configuration, microcalcification, and

TABLE 3 | Results of Logistic regression analysis of the ultrasound characteristics of partial cystic thyroid nodules.

Factor	β	SE	Wald	OR	95%CI	P
Free edge (smooth vs non-smooth)	1.16	0.59	3.92	3.18	1.01~10.00	0.05
Calcification (non-calcification & macrocalcification vs microcalcification)	2.85	0.62	21.22	17.28	5.14~58.08	<0.01

marked or mild hypoechogenicity were more reliable in predicting malignancy (AUC: 0.9592, 0.8504, and 0.8092, respectively) (2). We also found that the nodules that were ovoid to round, with a smooth free margin in solid parts, isoechoic, macrocalcification, and non-calcification were also associated with benign PCTNs (P<0.01).

A domestic study in 2014 showed that the free margin of the solid part of PCTNs was divided into two groups: smooth and non-smooth. In this study, our findings are consistent with the above conclusions. We can explain this phenomenon by the fact that the tumor growth is heterogeneous, invasive, migratory, and has no complete capsule formation.

In most TI-RADS grading systems, the proportion of solid parts in the nodule and the blood flow signal are used as independent predictors in the risk assessment of thyroid nodules (12). However, the present study found no statistical difference between PCTNs with predominantly cystic and predominantly solid PCTNs in benign and malignant nodules, nor with the blood flow signal level. Therefore, we should not ignore nodules with predominantly cystic components and low blood flow signal grades.

Multivariate Logistic regression analysis showed that PCTNs solid part calcification and free margin were important factors for predicting malignant PCTNs, of which the non-smooth free margin and microcalcification in the solid part were poor factors for predicting malignant PCTNs, showing the key to predicting benign and malignant PCTNs. It is the observation of the general shape of the nodule(free margin) and the calcification of the solid part.

A suspicious FNAB is the most common indication for thyroidectomy. However, its reliability in large nodules is not clear. Osman described a lower sensitivity (55.5-71.4%) and higher false-negative rate (6.7-9.7%) in nodules larger than 4 cm, and only 17.3% patients were detected as having cancer (13, 14); meanwhile, PCTNs lack of cellularity in cystic areas, presence of nuclear debris, and histiocyte/macrophages (5) frequently lead to misdiagnosis of a cystic benign nodule. In the thyroid nodules we included in our study, all had cystic components, and the average diameter of the nodules was 3.2cm, therefore, compared with solid small nodules, the reference value of FNAB before surgery was relatively low. Published research (15) reported 119 patients with PCTNs who underwent thyroidectomy after FNA; 21 were malignant, yielding a 17.6% malignancy rate, and their team therefore recommended FNA for all PCTNs, however, the malignancy rate among PCTNs may have been overestimated due to selection bias for the enrolled patients. So, we consider the limitations of FNAB should be taken into consideration when making treatment decisions in PTCNs or nodules larger than 4 cm in size.

Not all surgeons are equally experienced in performing thyroid surgery. Studies have shown that surgeons who perform a large number of thyroidectomies each year have fewer complications than those who perform fewer operations. Such data do not mean that low-volume surgeons should not perform these operations. However, before undertaking a difficult operation, the surgeon should consider whether that patient might be better served by referral to a specialized institution for care. Meanwhile, in solitary small low-risk PTCNs, hemithyroidectomy, thanks to its lower complication rates, is still the safest standard of care, avoiding unnecessary morbidity (16).

This study has some limitations. First, the retrospective assessment of static ultrasound images of PCTNs in this study was less accurate than prospective dynamic ultrasound images. Secondly, the number of benign cases in this study is small, as patients are usually recommended surgical treatment when the TI-RADS grade is 4 or above in the ultrasound diagnosis. For nodules below grade 4, ultrasound follow-up or ultrasound-guided fine-needle aspiration is often recommended. Since this study did not use all PCTNs as candidates and only selected patients with surgical and pathological results, selection bias is inevitable for patients with only ultrasound results or puncture results. In addition, no hyperechoic nodules were found in this study, which may be a characteristic feature of benign PCTNs nodules.

4 CONCLUSION

TI-RADS can detect malignant PCTNs, and its sensitivity, specificity, positive predictive value, negative predictive value, and accuracy rate are 39.8%, 96.0%, 94.3%, 49.0%, and 60.9%, respectively. For PCTNs, nodule shape, margin, and structure were associated with benign and malignant PCTNs (P < 0.01). Among them, nodules taller-than-wide, with an irregular shape, non-smooth margin, eccentric sharp angle, and edge sharp angle were associated with malignant PCTNs, while ovoid to round nodules, smooth margins, multiple separation, and eccentric obtuse angle structures were associated with benign PCTNs. For the solid part of PCTNs, its free margin, echo, and calcification were related to benign and malignant PCTNs. Among them, the free margin of the solid part being non-smooth, hypoechoic, and microcalcification are related to malignant PCTNs, while the free margin of the solid part being smooth, isoechoic, macrocalcification, and non-calcification are related to benign PCTNs. The calcification of solid part and free margin are important factors for predicting malignant PCTNs. In addition, nodules with predominant cystic components and low blood flow signal levels cannot be ignored

in clinical diagnosis and treatment. These findings are helpful for clinicians to more accurately identify benign and malignant PCTNs, avoid missing diagnosis and misdiagnosis of PCTNs patients, and are crucial for the clinical treatment and prognosis of PCTNs.

DATA AVAILABILITY STATEMENT

The raw data supporting the conclusions of this article will be made available by the authors, without undue reservation.

ETHICS STATEMENT

The studies involving human participants were reviewed and approved by the Ethics Review Committee of First Affiliated Hospital of Zhengzhou University. Written informed consent from the participants' legal guardian/next of kin was not required to participate in this study in accordance with the national legislation and the institutional requirements.

AUTHOR CONTRIBUTIONS

CW, YY, SW and KJ designed the study. CW, DZ and CL collected the clinical data, ultrasonography images and histopathological/cytopathology results. YL and MZ performed the statistical analysis. CW, ZY and ZW drafted and revised the manuscript. All authors contributed to the article and approved the submitted version.

FUNDING

This study was supported by the National Nature Science Foundation of China (No. 81871962), National Scientific Center Project (No. 62088101) and the Industry-University-Research Innovation Fund in Ministry of Education of the People's Republic of China (No.2018A01013).

ACKNOWLEDGMENTS

We wish to thank the timely help given by Cheng L in analyzing the ultrasound features of thyroid nodules.

REFERENCES

1. Gyu ND, Ji-Hoon K, Sik KD, Jin KS. Thyroid Nodules With Minimal Cystic Changes Have a Low Risk of Malignancy. *Ultrasonography (Seoul Korea)* (2016) 35(2):153–8. doi: 10.14366/usg.15070
2. Shi X, Liu R, Gao L, Xia Y, Jiang Y. Diagnostic Value of Sonographic Features in Distinguishing Malignant Partially Cystic Thyroid Nodules: A Systematic Review and Meta-Analysis. *Front Endocrinol (Lausanne)* (2021) 12:624409. doi: 10.3389/fendo.2021.624409
3. JianQiao Z. 2020 Chinese Guidelines for Ultrasound Malignancy Risk Stratification of Thyroid Nodules: The C-TIRADS. *Endocrine* (2020) 70 (2):256–79. doi: 10.1007/s12020-020-02441-y
4. Haugen BR, Alexander EK, Bible KC, Doherty GM, Mandel SJ, Nikiforov YE, et al. 2015 American Thyroid Association Management Guidelines for Adult Patients With Thyroid Nodules and Differentiated Thyroid Cancer: The American Thyroid Association Guidelines Task Force on Thyroid Nodules and Differentiated Thyroid Cancer. *Thyroid* (2016) 26:1–133. doi: 10.1089/thy.2015.0020
5. Mokhtari M, Kumar PV, Hayati K. Fine-Needle Aspiration Study of Cystic Papillary Thyroid Carcinoma: Rare Cytological Findings. *J Cytol* (2016) 33:120–4. doi: 10.4103/0970-9371.188046
6. Zhao HN, Liu JY, Lin QZ, He YS, Luo HH, Peng YL, et al. Partially Cystic Thyroid Cancer on Conventional and Elastographic Ultrasound: A Retrospective Study and a Machine Learning-Assisted System. *Ann Transl Med* (2020) 8:495. doi: 10.21037/atm.2020.03.211
7. Chiofalo MG, Signoriello S, Fulciniti F, Avenia N, Ristagno S, Lombardi CP, et al. Predictivity of Clinical, Laboratory and Imaging Findings in Diagnostic Definition of Palpable Thyroid Nodules. A Multicenter Prospective Study. *Endocrine* (2018) 61:43–50. doi: 10.1007/s12020-018-1577-5
8. Shi YZ, Jin Y, Zheng L. Partially Cystic Thyroid Nodules on Ultrasound: The Associated Factors for Malignancy. *Clin Hemorheol Microcirc* (2020) 74:373–81. doi: 10.3233/CH-190582
9. Kim DW, Lee EJ, In HS, Kim SJ. Sonographic Differentiation of Partially Cystic Thyroid Nodules: A Prospective Study. *AJNR Am J Neuroradiol* (2010) 31:1961–6. doi: 10.3174/ajnr.A2204
10. Shayganfar A, Hashemi P, Esfahani MM, Ghanei AM, Moghadam NA, Ebrahimian S. Prediction of Thyroid Nodule Malignancy Using Thyroid Imaging Reporting and Data System (TIRADS) and Nodule Size. *Clin Imaging* (2020) 60:222–7. doi: 10.1016/j.clinimag.2019.10.004
11. Fang F, Gong Y, Liao L, Ye F, Zuo Z, Qi Z, et al. Value of Contrast-Enhanced Ultrasound in Partially Cystic Papillary Thyroid Carcinomas. *Front Endocrinol (Lausanne)* (2021) 12:783670. doi: 10.3389/fendo.2021.783670
12. Adam MA, Goffredo P, Youngwirth L, Scheri RP, Roman SA, Sosa JA. Same Thyroid Cancer, Different National Practice Guidelines: When Discordant American Thyroid Association and National Comprehensive Cancer Network Surgery Recommendations are Associated With Compromised Patient Outcome. *Surgery* (2016) 159:41–50. doi: 10.1016/j.surg.2015.04.056
13. Bozbıyık O, Öztürk Ş, Ünver M, Erol V, Bayol Ü, Aydın C. Reliability of Fine Needle Aspiration Biopsy in Large Thyroid Nodules. *Turk J Surg* (2017) 33:10–3. doi: 10.5152/UCD.2017.3329
14. Godazandeh G, Kashi Z, Zargarnataj S, Fazli M, Ebadi R, Kerdabadi EH. Evaluation the Relationship Between Thyroid Nodule Size With Malignancy and Accuracy of Fine Needle Aspiration Biopsy (FNAB). *Acta Inform Med* (2016) 24:347–50. doi: 10.5455/aim.2016.24.347-350
15. Bellantone R, Lombardi CP, Raffaelli M, Traini E, De Crea C, Rossi ED, et al. Management of Cystic or Predominantly Cystic Thyroid Nodules: The Role of Ultrasound-Guided Fine-Needle Aspiration Biopsy. *Thyroid* (2004) 14:43–7. doi: 10.1089/105072504322783830
16. Conzo G, Calò PG, Gambardella C, Tartaglia E, Mauriello C, Della Pietra C, et al. Controversies in the Surgical Management of Thyroid Follicular Neoplasms. Retrospective Analysis of 721 Patients. *Int J Surg* (2014) 12 Suppl 1:S29–34. doi: 10.1016/j.ijsu.2014.05.013

Conflict of Interest: The authors declare that the research was conducted in the absence of any commercial or financial relationships that could be construed as a potential conflict of interest.

Publisher's Note: All claims expressed in this article are solely those of the authors and do not necessarily represent those of their affiliated organizations, or those of the publisher, the editors and the reviewers. Any product that may be evaluated in this article, or claim that may be made by its manufacturer, is not guaranteed or endorsed by the publisher.

frontiers | Frontiers in Endocrinology

ORIGINAL RESEARCH
published: 09 June 2022
doi: 10.3389/fendo.2022.865911

Real-World Evidence on the Sensitivity of Preoperative Ultrasound in Evaluating Central Lymph Node Metastasis of Papillary Thyroid Carcinoma

Fan Yao[1,2,3†], *Zhongyuan Yang*[1,2,3†], *Yixuan Li*[1,2,3†], *Weichao Chen*[1,2,3], *Tong Wu*[1,2,3], *Jin Peng*[1,2,3], *Zan Jiao*[1,2,3] *and Ankui Yang*[1,2,3*]

[1] Department of Head and Neck, Sun Yat-sen University Cancer Center (SYSUCC), Guangzhou, China, [2] State Key Laboratory of Oncology in South China, Sun Yat-sen University Cancer Center (SYSUCC), Guanghzou, China, [3] Collaborative Innovation Center for Cancer Medicine, Sun Yat-Sen University Cancer Center, Guangzhou, China

OPEN ACCESS

Edited by:
Hendra Zufry,
Syiah Kuala University, Indonesia

Reviewed by:
Erivelto Martinho Volpi,
Centro de Referência no Ensino do Diagnóstico por Imagem (CETRUS), Brazil
Yu Heng,
Fudan University, China

***Correspondence:**
Ankui Yang
yangak@sysucc.org.cn

†These authors have contributed equally to this work and share first authorship

Specialty section:
This article was submitted to Thyroid Endocrinology, a section of the journal Frontiers in Endocrinology

Received: 30 January 2022
Accepted: 20 April 2022
Published: 09 June 2022

Citation:
Yao F, Yang Z, Li Y, Chen W , Wu T, Peng J, Jiao Z and Yang A (2022) Real-World Evidence on the Sensitivity of Preoperative Ultrasound in Evaluating Central Lymph Node Metastasis of Papillary Thyroid Carcinoma. Front. Endocrinol. 13:865911. doi: 10.3389/fendo.2022.865911

Introduction: Guidelines for prophylactic dissection in clinical central negative node (cN0) of papillary thyroid carcinoma vary among different countries due to the uncertainty on the benefit of dissection. The Chinese guidelines recommend prophylactic central compartment lymph node dissection (pCLND) under professional technology. Preoperative ultrasound (US) evaluation of central lymph node determines the surgical strategy used. Sensitivity differs significantly when US is conducted by different physicians even in diverse hospitals. In this study, the aim was to explore why the Chinese guidelines were different from the America Thyroid Association (ATA) guidelines through the real-world evidence on the preoperative diagnosis of cN0.

Methods: Preoperative US and surgical pathology data for 1,015 patients with PTC attending 13 Grade-A tertiary hospitals in 2017 were collected. A retrospective analysis using US assessment of CLNM was the conducted to explore the benefits of this approach in China. US physicians in our hospital were trained on scanning the thyroid gland and its regional lymph nodes in normalization. Data of 1,776 patients were collected under the same condition from 2012 to 2017, whose ultrasonography was performed by diverse physicians and doctors. Further, data of 339 patients evaluated by the same sonographer and operated by the same surgical team was collected between 2015 and 2017. In this set of data, US combined CT versus US alone was compared. Patients were grouped into metastasis group and non-metastasis group based on postoperative pathological diagnosis of CLNM. Diagnostic efficacy of US was evaluated.

Results: A total of 925 patients who underwent preoperative ultrasonography in central lymph node, including 825 cases who underwent thyroidectomy and central lymph node dissection were included in this study. The sensitivity of ultrasonography in detecting CLNM was 23.18%, with occult metastasis rate of 40.8%. Data for 1,776 patients comprising paired ultrasonic report and pathological report were collected in our hospital,

whose physicians underwent standardized training. The sensitivity was 37.58%. Furthermore, specialized evaluation showed high sensitivity in US/CT (84.58%) than US (58.21%) alone.

Conclusion: Although the sensitivity of US could be enhanced by standardized training and combination with CT, the prevalence of low sensitivity of US in real-world multicenter data and the high occult metastasis rate indicated that the Chinese guidelines were based on the current conditions.

Keywords: papillary thyroid carcinmona, central lymph mode metastasis, real-world data, sensitivity, ultrasound

INTRODUCTION

Incidence of thyroid carcinoma has significantly increased in the past few decades and is ranked fifth most common cancer type in females worldwide (1). In China, a 20% increase in thyroid carcinoma has been reported yearly (2). Papillary thyroid carcinoma (PTC) is the most common histological subtype accounting for approximately 80% of thyroid carcinoma cases (3). PTC is characterized by regional lymph node metastasis (LNM) at early stages. Most patients with PTC present with cervical LNM at the time of diagnosis (4). Central lymph node (CLN) is characterized by high rates of metastasis with CLN metastasis (CLNM) rate ranging from 20% to 90% (4).

The central compartment lymph node dissection (CCND) is recommended for diagnosis of clinical CLNM (cN1a) patients. However, guidelines on prophylactic central compartment lymph node dissection (pCLND) in patients with PTC with clinical negative node (cN0) vary among different countries due to varying reports on benefits associated with pCLND (5–12). This is attributed to lack of reliable large-scale prospective study due to the favorable prognosis of PTC. According to the ATA guidelines, patients with clinical central negative node (cN0) with low risk level are not recommended to perform pCLND (13). In China, the consensus proposed that pCLND should only be performed in low-risk patients in the case of effective preservation of parathyroid and recurrent laryngeal nerve (14, 15). This gave us curiosity to figuring out how the differences between the two guidelines came about. We tried to discuss it from the diagnosis of cN0, which determines the surgical strategy preoperatively. In addition, CLN occult metastasis rate of patients with cN0 could be as high as 84.3% (16), which changed tumor stage and postoperative management.

ATA recommended preoperative ultrasound (US) as the preferred evaluation method for thyroid nodules and cervical lymph nodes of thyroid malignance (13). Although preoperative US is highly effective in diagnosis of lateral lymph node metastasis (LLNM) with a sensitivity of 64%–93.8%, sensitivity of CLNM diagnosis is relatively low (10%–63%) and differs significantly in diverse centers (5–12). Preoperative evaluation of CLNM determines the surgical strategy; therefore, high sensitivity and accuracy of US should be ensured. Experience of sonographers, subjectivity, and messy US report format may all contribute to low sensitivity. In this study, we investigated the status of preoperative US in evaluating CLNM from 13 Grade-A tertiary hospitals in China and that in our single center. The findings of this study provide real-world evidence to help understanding how the ATA guidelines and the Chinese guidelines differ in management of cN0.

MATERIALS AND METHODS

Ethics Statement

The studies involving human participants were reviewed and approved by the Ethics Committee of Sun Yat-sen University Cancer Center. All participants were informed of the purpose and risks of the study before signing written informed consents.

Patients

Every 50–100 consecutive patients in 2017 with a diagnosis of papillary thyroid carcinoma from 13 Grade-A tertiary hospitals in China were enrolled in this study. Hospitals included in this study are located in different districts in China. Preoperative ultrasonography reports and pathology reports that were unmatched were removed and a total of 1,015 patients were enrolled in the study. Among the participants, 226 were male and 789 were female patients with a median age of 43.1 years (range from 9 to 76 years). Out of the 1,015 patients, 825 cases underwent CLN dissection confirmed by postoperative pathology.

A total of 1,776 cases with CLND in Sun Yat-sen University Cancer Center from 2012–2017 were collected, whose ultrasonography was performed by diverse physicians and doctors. In addition, a set of published data comprising 339 patients who were evaluated by the same sonographers and radiologists and operated by the same surgical team from June 2015 to December 2017 was retrieved. These data were referred as specialized evaluation, including US combined with CT. Specialized evaluation diminished the impact caused by subjective differences between different examiners and surgeons.

Lymph Node Diagnostic Criteria

All materials were analyzed following guidelines from written reports of ultrasonography and postoperative pathology. Patients who underwent CLN dissection were grouped into metastasis group and non-metastasis group based on postoperative pathological diagnosis of CLNM. The diagnosis criteria was based on the fact that US report detected typical CLNM characteristics including focal hyperecho, microcalcification,

peripheral blood flow signals, and round lymph nodes. For CT, CLNM would be diagnosed when one of the following features come up: gross calcification, uneven enhancement, short diameter greater than 5 mm, and focal cystic degeneration.

Statistical Analyses

All statistical analyses were performed using SPSS software (version 23.0; IBM Corp, USA). The ratio of the cases that US reported as CLN to the cases that US did evaluation on CLN was referred as the detection rate. Sensitivity, specificity, accuracy, positive predictive value (PPV), and negative predictive value (NPV) of US and US/CT for estimating CLNM were analyzed using postoperative report as the golden standard. Weighted Youden index was used to estimate the diagnostic value of US and US/CT in screening suspicious CLNM. The formula of Jω was 2 (ω × sensitivity + (1 − ω) × specificity) − 1 ($0 \leq \omega \leq 1$) (17).

RESULTS

Current Condition in China

Data collected were collected from 1,015 patients attending 13 Grade-A tertiary hospitals in China (**Table 1**). A total of 925 patients underwent preoperative ultrasonography on CLN, whereas 825 patients underwent CLN dissection. In addition, 202 cases underwent lateral lymph node dissection synchronously. The participants comprised 226 male and 789 female patients with a median age of 43.1 years (range from 9 to 76 years).

Only one center out of the 13 Grade-A tertiary hospitals showed low assessment on CLN (20.8%), whereas other hospitals performed CLN evaluation on most cases (71.4%–100.0%) (**Table 1**). Notably, four hospitals performed CLN evaluation on all patients.

The sensitivity, specificity, accuracy, PPV, and NPV of US were 23.18%, 97.05%, 62.67%, 87.25%, and 59.2% (**Table 3**).

Surgical strategies determined by preoperative US varied from hospital to hospital. Ten hospitals performed prophylactic CLN dissection (pCLND) regardless of detection of CLNM using US. Hospital A, K, and L did not carry out pCLND if US report showed no CLNM. In addition, these hospitals did not perform CLND even when US reports showed CLNM in a few cases. CLNM rate was 46.5% (28.3%–70.7%), whereas the LLNM rate was 13.9% (0.0%–29.3%) (**Table 1**). Hospitals with higher CLNM rate showed higher LLNM and higher detection rate such as hospital F and L. For those without CLNM, the occult metastasis was generally high (25.5%–57.7%) (**Table 1**).

These findings show differences in evaluation level of ultrasonography among different hospitals. Sensitivity and diagnostic value of preoperative were low and varied greatly. In addition, surgical strategies guided by ultrasonography for CLND differed among hospitals. These factors contributed to the high rate of missed CLNM.

TABLE 1 | The basic situation of preoperative US evaluation in13 Grade-A tertiary hospitals among China.

Hospitals	Cases	LN-Evaluated	US-diagnosed CLNM (Strict Criteria)	CLND	No CLND with CLNM (Strict Criteria)	Pathological CLNM	Pathological CLNM With LLNM	CLND with No US-Diagnosed CLNM	Occult CLNM
Hospital A	100	100 (100.0%)	2 (2.0%)	56	1	19	0	55	18 (32.7%)
Hospital B	67	67 (100.0%)	0 (0%)	67	0	29	19	67	29 (43.3%)
Hospital C	79	67 (84.8%)	0 (0%)	77	0	34	14	77	34 (44.2%)
Hospital D	72	53 (73.6%)	1 (1.4%)	70	0	35	7	69	34 (49.3%)
Hospital E	99	92 (92.9%)	4 (4.0%)	99	0	28	5	94	24 (25.5%)
Hospital F	106	105 (99.1%)	35 (33.0%)	102	0	59	25	61	25 (41.0%)
Hospital G	50	50 (100.0%)	2 (4.0%)	50	0	20	5	44	15 (34.1%)
Hospital H	21	15 (71.4%)	0 (0%)	18	0	6	0	18	6 (33.3%)
Hospital I	74	73 (98.6%)	8 (10.8%)	74	0	40	9	64	31 (48.4%)
Hospital J	97	97 (99.0%)	15 (15.3%)	96	1	47	11	79	31 (39.2%)
Hospital K	99	97 (98.0%)	1 (1.0%)	24	0	15	2	18	10 (55.6%)
Hospital L	98	98 (100.0%)	15 (15.3%)	41	3	29	12	26	15 (57.7%)
Hospital M	53	11 (20.8%)	0 (0%)	51	0	23	6	51	23 (45.1%)
Total	1,015	925 (91.1%)	83 (8.2%)	825	5	384	115	723	295 (40.8%)

Standardization of US Improves Sensitivity of US

Experience and subjectivity of sonographers affects the sensitivity of US. In our hospital, US physicians underwent unified training on thyroid and its regional lymph nodes. The training included scanning of CLN based on subregions to prevent omission, extending the scanning range by adopting flexible methods such as longitudinal scanning with probe on areas that are difficult to detect. Furthermore, they were required to use a normalized US report format to minimize subjectivity of sonographers.

A total of 1,776 cases were reported (**Table 2**). The sensitivity was higher than the Multicenter Evaluation (37.58% vs. 23.18%) (**Table 3**). In addition, the specificity, accuracy, PPV, and NPV of US were 91.94%, 61.88%, 85.22%, and 54.36%, respectively (**Table 3**).

Despite that the standardized training might reduce the difference caused by subjectivity, lack of experience on determination of CLNM and differences in diverse surgical teams also had effect on the sensitivity of US. Therefore, 339 patients evaluated by the same sonographers and radiologists and operated by our surgical team between June 2015 and December 2017 were recruited in the study. In addition, the diagnostic value of US combined with CT (US/CT) was also evaluated for these patients.

CLNM rate was similar to the standardized training (59.29% vs. 55.29%) (**Table 2**). Sensitivity, specificity, accuracy, PPV and NPV of US alone were 58.21%, 86.23%, 69.62%, 86.01%, and 58.62%, respectively (**Table 3**). Sensitivity, specificity, accuracy, PPV, and NPV of US/CT were 84.58%, 71.01%, 79.06%, 80.95%, and 75.97%, respectively (**Table 3**).

Increased sensitivity is important for success of surgeries. Therefore, the weighted Youden Index (Jω) was calculated with setting ω as 0.6 to estimate the diagnostic value of US in CLNM sensitivity. Jω of Multicenter Evaluation was 0.06, and data from our hospital could be increased to 0.19. Besides, Jω of US/CT was higher compared with that for US alone (0.58 vs. 0.39) (**Table 3**).

DISCUSSION

CLNM rate in patients with PTC is approximately 90%, whereas occult metastasis rate ranges between 30% and 84% (16). Studies report contradicting results about CLND associated with PTC, mainly the appropriate timing for performing pCLND in patients with cN0. The ATA guidelines provide limited information on pCLND. These guidelines recommend that surgery on pCLND should be performed for high-risk patients such as T3–T4 stages and extrathyroidal extension (ETE) and pCLND should not be performed on low-risk patients like patients with T1–T2 stages (13). Guidelines in most countries are similar to the ATA guidelines (11, 12). On the contrary, the Japanese Society of Thyroid Surgeons/Japanese Association of Endocrine Surgeons recommends routine pCLND to reduce severe complications of surgery after recurrence, which is possibly related to low rates of radioactive iodine (RAI) treatment in Japan (10). Although these guidelines have some differences, decision-making should be balanced between risks and benefit based on experience of the surgeons.

The pros and cons of pCLND have not been fully explored. This is mainly because most studies on pCLND are retrospective studies with poor evidence. Previous studies report that pCLND reduces recurrence rate and improves survival rate in patients with high occult CLNM (18). Hospitals who perform

TABLE 2 | The basic situation of preoperative US evaluation in our single medical center.

		Cases	LN-Evaluated	US-Diagnosed CLNM	CLND	Pathological CLNM	Pathological CLNM with LLNM
Standardized Training[a]		1,776	1,776 (100.0%)	433 (24.4%)	1,776	982 (55.29%)	392
Specialized Evaluation[b]	US	339	339 (100.0%)	136 (40.1%)	339	201 (59.29%)	/
	CT/US	339	339 (100.0%)	210 (61.9%)	339	201 (59.29%)	/

[a]*Standardized training was performed by different physicians and surgeons.*
[b]*Specialized evaluation was performed by the same group of physicians and surgeons.*

TABLE 3 | The diagnostic value of preoperative US in CLNM.

			Pathological Diagnosis		Sensitivity (%)	Specificity (%)	Accuracy (%)	PPV (%)	NPV (%)	Jω (ω = 0.6)
		Ultrasonic Diagnosis	CLN positive	CLN negative						
Multicenter Evaluation	Multicenter	CLN positive	89	13	23.18%	97.05%	62.67%	87.25%	59.20%	0.05456
		CLN negative	295	428						
Standardized Training[a]		CLN positive	369	64	37.58%	91.94%	61.88%	85.22%	54.36%	0.18568
		CLN negative	613	730						
Specialized Evaluation[b]	US	CLN positive	117	19	58.21%	86.23%	69.62%	86.03%	58.62%	0.38836
		CLN negative	84	119						
	US/CT	CLN positive	170	40	84.58%	71.01%	79.06%	80.95%	75.97%	0.58304
		CLN negative	31	98						

[a]*Standardized training was performed by different physicians and surgeons.*
[b]*Specialized evaluation was performed by the same group of physicians and surgeons.*

prophylactic dissection of cN0 report that the rate of occult metastasis of lymph nodes is high in the central area. Preventive dissection reduces recurrence rate and improves survival rate of patients (18). However, hospitals that do not carry out preventive dissection avoid the procedure to minimize postoperative complications and believe that there is no scientific evidence on the role of pCLND in improving survival of patients (19). Papillary thyroid carcinoma is associated with advanced prognosis, and the longer follow-up time hinders observation of the outcome of preventive dissection. A few studies have report the 10-year OS of patients with pCLND, with significant variation in results (18–20). Most included patients who underwent pCLND also received radioactive I131 therapy (RAI) when they found lymph node metastasis after surgery, thus explaining these differences (18). The average dose of RAI was higher compared with those who did not undergo pCLND, and these patients had strict control standards in TSH suppression treatment. RAI and TSH suppression treatments partially substitute pCLND. Several studies report that patients with pCLND have a higher rate of temporary hypocalcemia and temporary recurrent laryngeal nerve injury. However, no significant difference in incidence of permanent hypoparathyroidism and permanent recurrent laryngeal nerve injury (21). In addition, previous studies did not consider development and changes of treatment strategies and differences in the level of experience of surgeons and have shorter follow-up time, and only few multicenter studies have been carried out. Notably, conducting a large-scale prospective study is challenging. ATA predicted that a prospective multicenter randomized controlled study of pCLND would take 7 years with approximately 5,840 patients, and it would 20 million dollars (22). Recently, Ahn et al. published a prospective randomized controlled trial to assess the efficacy of pCLND. The results found that although patients with pCLND showed higher CLNM rate, there was no difference between the local recurrence and postoperative complications, which made them think that patients with cN0 may not need pCLND (23). The study provides strong evidence for the absence of pCLND in patients with cN0, but we still need to consider that a 50-month follow-up face may not fully predict the long-term risk pf PTC, whose 10-year OS could be as high as 90% after a follow-up of 50 months or so.

The Chinese guideline for differentiated thyroid carcinoma recommends that pCLND in low-risk patients should only be performed under the technical guarantee of effective preservation of parathyroid and recurrent laryngeal nerve (14). In this multicenter study, some hospitals performed pCLND routinely, whereas others did not carry out routine pCLND (**Table 1**). These triggered our curiosity about the differences between ATA and Chinese guidelines in pCLND.

ATA guidelines indicate that US is the first-choice diagnostic approach for thyroid and its regional lymph nodes. US evaluation on CLNM affects the diagnosis of cN0 and surgical strategy. However, it is associated with low sensitivity ranging between 10% and 63%, when used for CLNM, due to the narrow area of the CLNs. The tumor is located deeper and lymph nodes in this area are small, thus affecting detection of microcalcification and cystic degeneration. In addition, it is difficult to display the color flow for the effect of air in the trachea and esophagus next to the lymph nodes. Despite these limitations, preoperative color Doppler US is the preferred assessment method in many hospitals across our country due to its ease of operation, lack of requirement of radiation, and ease of judgment between benign and malignant nodes. Surgeons mainly rely on preoperative US reports to assist in formulation of surgical strategies. Therefore, this study explored the current status of preoperative US evaluation in multicenters across China. Besides, we shared the US evaluation on CLNM at a single-center level. Those real-world evidence helped to figure out if the Chinese guideline was more suitable for the CLN management in China.

The findings of this study show an overall sensitivity of a multicenter is low. In our multicenter study, most hospitals would assess the lymph nodes in the central neck and report them in the US report, except that Hospital M had a lower assessment rate of 20.8% (11/52). However, the diagnosis rate of CLNM in the central area varied significantly. In Hospital K, although 98% patients underwent detection of lymph nodes, the diagnosis rate of malignant lymph nodes was 7% (7/97). Only 24% (24/99) of patients in Hospital K underwent CLND guided by preoperative US. The postoperative CLNM rate was 62.5% (15/24) and the occult metastasis rate was as high as 55.6% (10/18). Hospital F reported highest diagnosis rate of 38.7% (41/105), but it still reported a high occult metastasis rate (41%, 25/61). This difference can be attributed to the location of CLN, making it difficult to assess the features of typical metastatic CLNs. This challenge then results in failure to distinguish benign and malignant nodes. Most hospitals performed CLND for patients with cN0 evaluated by preoperative US, whereas a few hospitals routinely performed CLND with or without cN0. In addition, the overall occult metastasis rate was 40.8% (295/723). These results indicate that US evaluation on CLNM has poor accuracy rates in the real world, which brings high occult metastasis.

US examination is highly subjective, and experience of inspectors affects accuracy of preoperative US. Standardization of preoperative US evaluation in CLN can be improved by normalizing US report format, recording lymph node in detail, replacing subjective judgments by objective factors and conducting professional training to minimize individual differences. We observed that the US report format in the 13 hospitals was uneven, and the description of thyroid and lymph nodes was not complete and objective. Therefore, we investigated the data from our medical center, whose US physicians underwent unified training on thyroid and its regional lymph nodes and the normalized US report format. The result showed that the US on CLNM was a little more sensitive, but it was not high enough (**Table 3**). It is known that lacking of experience and difference in diverse surgical groups may hinder identification of typical CLNM. Further, a specialized evaluation was carried out by the same physicians and surgeries were performed by our surgical team. The sensitivity of CLNM significantly increased compared with those for the standardized training, which was

performed by diverse groups of sonographers and surgeons. Combination of multiple preoperative methods can improve sensitivity of CLNM through advances in detection techniques (5, 24). Suh et al. reported that the sensitivity of CLNM was 38% when using US alone, whereas the sensitivity of CLNM after combining US and CT examination was 57% (25). CT and US are highly used in routine examination; therefore, we compared the sensitivity of combined US and CT with the sensitivity of US alone for specialized evaluation. Combination of the two approaches significantly increased the sensitivity of CLNM. In addition, there are several approaches to improve the sensitivity of CLNM. Artificial intelligence is widely used in medical field, mainly in medical imaging (26). AI can independently learn and identify various data in images to provide objective evaluation and minimize errors caused by subjectivity of physicians. Therefore, it is an important tool for improving medical imaging. Li et al. analyzed US imaging data of thyroid cancer by deep convolutional neural networks and reported similar sensitivity and better specificity compared with experienced radiologists in identification of malignant thyroid nodules (27). Lee et al. reported that CT combined with a computer-aided diagnosis system (CADS) based on deep learning accurately evaluates the features of cervical lymph nodes in thyroid cancer (28).

Our study shows that the accuracy of preoperative US in diagnosis of cN0 significantly varied among different hospitals in the country, which made the management of CLN different. Consistent with many reports, US/CT improved sensitivity of CLNM significantly in our medical center. However, considering that there are so many hospitals across China, whose level is uneven, and the large population, US is a more convenient, economical, and widely used tool. We tried to provide the real-world evidence on the sensitivity of US and share our single-center experience on improving sensitivity. The 13 hospitals in our study were located in different regions of China, and they all had good reputations in their respective regions. Even these excellent hospitals showed low sensitivity, we might discover why the Chinese guidelines shared diverse opinion on pCLND. It did take the diagnostic difficulty of cN0 into account.

Our study had a few limitations. First, although this was a multicenter study, it used retrospective analysis and the sample size was small. Second, the formats of US reports were not uniform and standardized, causing differences in detection of lymph nodes. Third, hospitals that were included in the multicenter study were Grade-A tertiary hospitals. The status for preoperative US in junior hospitals was not evaluated; thus, in the findings of this study, it does not reflect challenges in CLNM evaluation in these hospitals.

CONCLUSION

The sensitivity of preoperative US for the diagnosis of CLNM are low and significantly vary among different hospitals, and sensitivity can be increased through standardized training and specialized evaluation. A combination of multiple examinations such as US/CT can improve preoperative evaluation. These findings reflect the real-world management of CLN in China. Considering the poor sensitivity of US, the Chinese guidelines in the treatment of cN0 were in line with reality.

DATA AVAILABILITY STATEMENT

The original contributions presented in the study are included in the article/**Supplementary Material**. Further inquiries can be directed to the corresponding author/s.

ETHICS STATEMENT

The studies involving human participants were reviewed and approved by Ethics Committee of Sun Yat-sen University Cancer Center. Written informed consent to participate in this study was provided by the participants' legal guardian/next of kin.

AUTHOR CONTRIBUTIONS

All authors listed have made a substantial, direct, and intellectual contribution to the work, and approved it for publication.

SUPPLEMENTARY MATERIAL

The Supplementary Material for this article can be found online at: https://www.frontiersin.org/articles/10.3389/fendo.2022.865911/full#supplementary-material

REFERENCES

1. Sung H, Ferlay J, Siegel RL, Laversanne M, Soerjomataram I, Jemal A, et al. Global Cancer Statistics 2020: GLOBOCAN Estimates of Incidence and Mortality Worldwide for 36 Cancers in 185 Countries. *CA Cancer J Clin* (2021) 71(3):209–49. doi: 10.3322/caac.21660
2. Chen W, Zheng R, Baade PD, Zhang S, Zeng H, Bray F, et al. Cancer Statistics in China, 2015. *CA Cancer J Clin* (2016) 66(2):115–32. doi: 10.3322/caac.21338
3. Shaha A. Patterns of Nodal and Distant Metastasis Based on Histologic Varieties in Differentiated Carcinoma of the Thyroid. *Am J Surg* (1996) 172 (6):692–4. doi: 10.1016/S0002-9610(96)00310-8
4. White ML, Gauger PG, Doherty GM. Central Lymph Node Dissection in Differentiated Thyroid Cancer. *World J Surg* (2007) 31(5):895–904. doi: 10.1007/s00268-006-0907-6
5. Kim E, Park JS, Son KR, Kim JH, Jeon SJ, Na DG. Preoperative Diagnosis of Cervical Metastatic Lymph Nodes in Papillary Thyroid Carcinoma: Comparison of Ultrasound, Computed Tomography, and Combined Ultrasound With Computed Tomography. *Thyroid* (2008) 18(4):411–8. doi: 10.1089/thy.2007.0269
6. Hwang HS, Orloff LA. Efficacy of Preoperative Neck Ultrasound in the Detection of Cervical Lymph Node Metastasis From Thyroid Cancer. *Laryngoscope* (2011) 121(3):487–91. doi: 10.1002/lary.21227

7. Jung JH, Kim CY, Son SH, Kim DH, Jeong SY, Lee SW, et al. Preoperative Prediction of Cervical Lymph Node Metastasis Using Primary Tumor SUVmax on 18F-FDG PET/CT in Patients With Papillary Thyroid Carcinoma. *PLoS One* (2015) 10(12):e0144152. doi: 10.1371/journal.pone.0144152
8. Morita S, Mizoguchi K, Suzuki M, Lizuka K. The Accuracy Of18[F]-Fluoro-2-Deoxy-D-Glucose-Positron Emission Tomography/Computed Tomography, Ultrasonography, and Enhanced Computed Tomography Alone in the Preoperative Diagnosis of Cervical Lymph Node Metastasis in Patients With Papillary Thyroid Carcinoma. *World J Surg* (2010) 34(11):2564–9. doi: 10.1007/s00268-010-0733-8
9. Kim SK, Woo JW, Park I, Lee JH, Choe JH, Kim JH, et al. Computed Tomography-Detected Central Lymph Node Metastasis in Ultrasonography Node-Negative Papillary Thyroid Carcinoma: Is It Really Significant? *Ann Surg Oncol* (2017) 24(2):442–9. doi: 10.1245/s10434-016-5552-1
10. Takami H, Ito Y, Okamoto T, Yoshida A. Therapeutic Strategy for Differentiated Thyroid Carcinoma in Japan Based on a Newly Established Guideline Managed by Japanese Society of Thyroid Surgeons and Japanese Association of Endocrine Surgeons. *World J Surg* (2011) 35(1):111–21. doi: 10.1007/s00268-010-0832-6
11. Sancho JJ, Lennard TWJ, Paunovic I, Triponez F, Sitges-Serra A. Prophylactic Central Neck Disection in Papillary Thyroid Cancer: A Consensus Report of the European Society of Endocrine Surgeons (ESES). *Langenbeck\"s Arch Surg* (2014) 399(2):155–63. doi: 10.1007/s00423-013-1152-8
12. Gonçalves Filho João, Zafereo Mark E, Ahmad Faisal I, Nixon Iain J, Shaha Ashok R, Vander Poorten V, et al. Decision Making for the Central Compartment in Differentiated Thyroid Cancer. *Eur J Surg Oncol* (2018) 44(11):1671–8. doi: 10.1016/j.ejso.2018.08.005
13. Haugen BR, Alexander EK, Bible KC, Doherty GM, Mandel SJ, Nikiforov YE, et al. 2015 American Thyroid Association Management Guidelines for Adult Patients With Thyroid Nodules and Differentiated Thyroid Cancer: The American Thyroid Association Guidelines Task Force on Thyroid Nodules and Differentiated Thyroid Cancer. *Thyroid* (2016) 26(1):1–133. doi: 10.1089/thy.2015.0020
14. Chinese Society of Endocrinology, Chinese Society of Surgery endocrinology team, Chinese Anti-cancer Association Head and Neck Tumor Professional Committeeand and Chinese Society of NuclearMedicine. Clinical Management Guidelines for Thyroid Nodules and Differentiated Thyroid Carcinoma. *Chin J Nucl Med Mol Imaging* (2013) 33(2):96–115. doi: 10.3760/cma.j.issn.1000-6699.2012.10.002
15. Chinese Anti-Cancer Association Thyroid Cancer Professional Committee. Chinese Expert Consensus on the Diagnosis and Treatment of Papillary Thyroid Microcarcinoma (2016 Edition). *Chin J Clin Oncol* (2016) 43(10):405–11. doi: 10.3969/j.issn.1000-8179.2016.10.001
16. Chen Q, Wei T, Wang XL, Li ZH, Du ZH, Zhu JQ. The Total Number of Prelaryngeal and Pretracheal Lymph Node Metastases: Is It a Reliable Predictor of Contralateral Central Lymph Node Metastasis in Papillary Thyroid Carcinoma? *J Surg Res* (2017) 214:162–7. doi: 10.1016/j.jss.2015.02.056
17. Li DL, Shen F, Yin Y, Peng JX, Chen PY. Weighted Youden Index and its Two-Independent-Sample Comparison Based on Weighted Sensitivity and Specificity. *Chin Med J (Engl)* (2013) 126(6):1150–4. doi: 10.3760/cma.j.issn.0366-6999.20123102
18. Barczyński M, Konturek A, Stopa M, Nowak W. Prophylactic Central Neck Dissection for Papillary Thyroid Cancer. *Br J Surg* (2013) 100(3):1115–5. doi: doi: 10.1002/bjs.8985
19. Moreno MA, Edeiken-Monroe BS, Siegel ER, Sherman SI, Clyman GL. In Papillary Thyroid Cancer, Preoperative Central Neck Ultrasound Detects Only Macroscopic Surgical Disease, But Negative Findings Predict Excellent Long-Term Regional Control and Survival. *Thyroid Off J Am Thyroid Assoc* (2012) 22(4):347. doi: 10.1089/thy.2011.0121
20. Viola D, Materazzi G, Valerio L, Molinaro E, Agate L, Faviana P, et al. Prophylactic Central Compartment Lymph Node Dissection in Papillary Thyroid Carcinoma: Clinical Implications Derived From the First Prospective Randomized Controlled Single Institution Study. *J Clin Endocrinol Metab* (2015) 100(4):1316–24. doi: 10.1210/jc.2014-3825
21. Zhao WJ, Han L, Zhou YM, Dai WY, Zhu JQ. Evaluating the Effectiveness of Prophylactic Central Neck Dissection With Total Thyroidectomy for Cn0 Papillary Thyroid Carcinoma: An Update Meta-Analysis. *Eur J Surg Oncol* (2017) 43(11):1989. doi: 10.1016/j.ejso.2017.07.008
22. Carling T, Carty SE, Ciarleglio MM, Cooper DS, Doherty GM, Kim LT, et al. American Thyroid Association (ATA) - Design and Feasibility of a Prospective Randomized. *Thyroid* (2012) 22(3):237. doi: 10.1089/thy.2011.0317
23. Ahn JH, Kwak JH, Yoon SG, Yi JW, Yu HW, Kwon H, et al. A Prospective Randomized Controlled Trial to Assess the Efficacy and Safety of Prophylactic Central Compartment Lymph Node Dissection in Papillary Thyroid Carcinoma. *Surgery* (2022) 171(1):182–9. doi: 10.1016/j.surg.2021.03.071
24. Xu JM, Xu XH, Xu HX, Zhang YF, Guo LH, Liu LN, et al. Prediction of Cervical Lymph Node Metastasis in Patients With Papillary Thyroid Cancer Using Combined Conventional Ultrasound, Strain Elastography, and Acoustic Radiation Force Impulse (ARFI) Elastography. *Eur Radiol* (2016) 26(8):2611–22. doi: 10.1007/s00330-015-4088-2
25. Suh CH, Baek JH, Choi YJ, Lee JH, et al. Performance of CT in the Preoperative Diagnosis of Cervical Lymph Node Metastasis in Patients With Papillary Thyroid Cancer: A Systematic Review and Meta-Analysis. *AJNR Am J Neuroradiol* (2017) 38(1):154–61. doi: 10.3174/ajnr.A4967
26. Bi WL, Hosny A, Schabath MB, Giger ML, Birbak NJ, Mehrtsh A, et al. Artificial Intelligence in Cancer Imaging: Clinical Challenges and Applications. *CA Cancer J Clin* (2019) 69(2): 127–157. doi: 10.3322/caac.21552
27. Li X, Zhang S, Zhang Q, Wei X, Pan Y, Zhao J, et al. Diagnosis of Thyroid Cancer Using Deep Convolutional Neural Network Models Applied to Sonographic Images: A Retrospective, Multicohort, Diagnostic Study. *Lancet Oncol* (2019) 20(2):193–201. doi: 10.1016/S1470-2045(18)30762-9
28. Lee JH, Ha EJ, Kim JH. Application of Deep Learning to the Diagnosis of Cervical Lymph Node Metastasis From Thyroid Cancer With CT. *Eur Radiol* (2019) 29(10):5452–7. doi: 10.1007/s00330-019-06098-8

Conflict of Interest: The authors declare that the research was conducted in the absence of any commercial or financial relationships that could be construed as a potential conflict of interest.

frontiers | Frontiers in Endocrinology

ORIGINAL RESEARCH
published: 17 June 2022
doi: 10.3389/fendo.2022.899575

Validating and Comparing C-TIRADS, K-TIRADS and ACR-TIRADS in Stratifying the Malignancy Risk of Thyroid Nodules

Qingfang Chen, Mingnan Lin and Size Wu *

Department of Ultrasound, The First Affiliated Hospital of Hainan Medical University, Haikou, China

The thyroid imaging reporting and data system (TIRADS) was proposed by experts for optimal ultrasound evaluation of malignancy risk of thyroid focal lesions. There are several versions of TIRADS, some of them have been validated sufficiently, and the others have not been well assessed. In this study, a recently launched Chinese version of TIRADS (C-TIRADS) for malignancy risk stratification of thyroid nodules was validated, and the performance was compared to that of the Korean TIRADS (K-TIRADS) and American College of Radiology(ACR) TIRADS (ACR-TIRADS). Archives of 2177 patients who had undergone thyroid ultrasound examination, coarse needle tissue biopsy and/or surgery were reviewed, and 1978 patients with 1982 thyroid nodules were assessed according to the three TIRADSs. The histopathology was taken as the golden standard. The results showed the 1982 thyroid nodules were consisted of 1306 benign nodules and 676 malignant nodules. The malignancy risk accounted for 1.09%, 2.14%, 10.34%, 49.28%, 88.19% and 85.29% of the total nodules that were categorised as C-TIRADS 2, 3, 4A, 4B, 4C and 5, respectively; 0.00%, 1.64%, 2.87%,18.71% and 82.22% of the total nodules that were categorised as ACR-TIRADS 1, 2, 3, 4 and 5, respectively; 0.85%, 3.27%, 24.27% and 80.96% of the total nodules that were categorised as K-TIRADS 2, 3, 4 and 5, respectively. The correlation between the category of TIRADS and percentile of malignancy was 0.94 in the C-TIRADS, 1.00 in the ACR-TIRADS, and 1.00 in the K-TIRADS, respectively. The highest values of accuracy(AUC) *of* ROC curves *of* C-TIRADS 4B, K-TIRADS 5 and ACR-TIRADS 5 were taken as the cut-off values for risk stratification, respectively. The sensitivity, specificity, positive and negative predictive values and AUC by C-TIRADS 4B, K-TIRADS 5 and ACR-TIRADS 5 for malignancy risk stratification of thyroid nodules were 90.83%, 84.23%, 74.88% and 94.66% and 0.88, respectively; 83.58%, 89.82%, 80.95%, 91.36% and 0.87, respectively; and 85.50%, 90.35%, 82.10%, 92.33% and 0.88, respectively (P>0.05 for all). We concluded that the C-TIRADS has excellent performance in the malignancy risk stratification of thyroid nodules by the optimized cut-off value, which is comparable to that in K-TIRADS and ACR-TIRADS.

Keywords: thyroid nodule, malignancy, ultrasound, thyroid imaging reporting and data system (TIRADS), C-TIRADS, K-TIRADS, ACR-TIRADS

OPEN ACCESS

Edited by:
Emerita Andres Barrenechea, Veterans Memorial Medical Center, North Avenue Quezon city, Philippines

Reviewed by:
Lingyu Bao, National Institutes of Health (NIH), United States
Kui Tang, Second Xiangya Hospital, Central South University, China

***Correspondence:**
Size Wu
wsz074@aliyun.com
orcid.org/0000-0002-1086-764X

Specialty section:
This article was submitted to Thyroid Endocrinology, a section of the journal Frontiers in Endocrinology

Received: *18 March 2022*
Accepted: *05 May 2022*
Published: *17 June 2022*

Citation:
Chen Q, Lin M and Wu S (2022) Validating and Comparing C-TIRADS, K-TIRADS and ACR-TIRADS in Stratifying the Malignancy Risk of Thyroid Nodules. Front. Endocrinol. 13:899575. doi: 10.3389/fendo.2022.899575

INTRODUCTION

Thyroid nodules are common in adults, and they have a prevalence of 19%–68%, depending on the population investigated (1–5). This includes a malignancy rate between 6.7% and 15% (1, 4, 5). Thyroid nodules may be benign, borderline or malignant lesions, and the prevalence of benign nodules are much more common than malignant nodules (1). Timely detection and accurate diagnosis of thyroid nodules are significant for the clinical management of the patients. However, many patients with malignant nodules have no unique clinical manifestations or laboratory abnormalities before distant metastasis. This makes it difficult to differentiate malignant nodules from benign nodules (1, 6–9).

Color Doppler ultrasound (US) is the imaging modality most frequently used to evaluate thyroid nodules. It has an excellent performance in detecting nodules, but its ability to serve as a basis for stratifying the malignancy risk must be improved (6–9). To improve the efficiency of US diagnosis, Horvath et al. established the first thyroid imaging reporting and data system (TIRADS) based on the US features of thyroid nodules in 2009, and as of 2020, there are eight versions of TIRADS in the world (9). The reasons for multiple TIRADSs are that each one has some advantages. However, they also have limitations, such as the similarities and discordance in terminology and standards in describing and defining the US features of thyroid nodules when different researchers establish their classification systems. The TIRADSs have different aims, so no one system has been widely acknowledged and used, and the effort to validate them remains hot (6–16). The latest version of TIRADS is the Chinese version of TIRADS (C-TIRADS), released in 2020 by The Superficial Organ and Vascular Ultrasound Group of the Society of Ultrasound in Medicine of Chinese Medical Association (9).

There are different categorisation schemes for the different versions of TIRADS. Taking as an example, the ACR-TIRADS recommended by the American College of Radiology(ACR), scoring involves 23 US features with different weightings (8). The categorising schemes of the Korean TIRADS (K-TIRADS) recommended by The Korean Society of Thyroid Radiology and Korean Society of Radiology and C-TIRADS involve fewer US features than that of the ACR-TIRADS, and C-TIRADS uses six dominant US features that are highly suggestive of malignancy or benignity (7, 9). Because the scoring scheme of ACR-TIRADS is based on many US features, it has the strength of being systematic and comprehensive, but it is not easy to apply. If a simpler scheme can be found to be effective, that would be an improvement. Whether a simpler scheme of the C-TIRADS compromises or increases its ability to stratify malignancy risk has not been investigated. The aim of this study was to validate the C-TIRADS and compare the performance of the three TIRADSs for malignancy risk stratification of thyroid nodules.

SUBJECTS AND METHODS

Study Population

A total of 2177 patients who had undergone US thyroid examination, coarse needle biopsy and/or surgery in the First Affiliated Hospital of Hainan Medical University between January 2015 and December 2021 were selected as potential research subjects, and their data were retrospectively reviewed. The inclusion criteria were patients with eligible qualified US images of their thyroid nodule(s) and with histopathological results. The exclusion criteria were US images of thyroid nodules that were of inferior quality or had image numbers that could not display the nodular features fully, or the histopathology of the thyroid nodule was undetermined. A coalescence of nodules was counted as one nodule. If a patient had more than thyroid nodules, the nodule with features suggestive of malignancy or a representative nodule of benign nodules was enrolled. (Four patients had malignant nodules in both lobes of the thyroid.) Finally, 1978 patients with 1982 thyroid nodules were included, and 199 patients with 202 thyroid nodules were excluded.

Key Points of Assessment by C-TIRADS

According to the C-TIRADS, the assessment of a thyroid and thyroid nodule involves features of nodular composition (architecture), echogenicity, shape (orientation), margin, and echogenic foci (9). The scoring scheme is based on evaluating sonographic features on the basis of different points. One point is added for features that suggest the malignancy risk, and one point is subtracted for features that suggest benignity. The details are as follows. One point is added for each feature of solid composition, that is markedly hypoechoic; taller than wide (A/T≥1); any one or more of the features of ill-defined, irregular, lobulated, and extrathyroidal extension margin; and punctate hyperechogenicity (suspicious calcification). One point is subtracted for feature of hyperechoic foci with a comet-tail artifact. If there are more than one hyperechoic patterns in a nodule, only the feature with highest value is included. The C-TIRADS has eight categories established according to the total value of the thyroid or thyroid nodule. The categories range from a nodule-free thyroid to a benign nodule, a nodule of highly suspicious malignancy, and a malignant nodule confirmed by histology. A nodule-free thyroid is categorised as TIRADS 1; a nodule with a value of -1 is categorised as TIRADS 2; a nodule with a value of 0 is categorised as TIRADS 3; a nodule with a value of 1 is categorised as TIRADS 4A; a nodule with a value of 2 is categorised as TIRADS 4B; a nodule with a value of 3 or 4 is categorised as TIRADS 4C; a nodule with a value of 5 is categorised as TIRADS 5; a nodule with a malignancy confirmed by histopathology is categorised as TIRADS 6; and a simple cystic nodule or a spongy nodule is categorised as TIRADS 2. Sonographic features for scoring are as follows: solid composition = +1, markedly hypoechoic = +1, taller than wide (A/T≥1) = +1, any one or more of the features of ill-defined, irregular, lobulated, and extrathyroidal extension margin = +1, hyperechoic foci with a comet-tail artifact = -1, and punctate hyperechoic foci (suspicious calcification) = +1. If there are more than one hyperechoic patterns in a nodule, only the highest scored is included.

Key Points of Thyroid Nodular Assessment by the K-TI-RADS (2016)

The K-TIRADS rates the malignancy risk with reference to three suspicious US features: microcalcification, a shape that is taller

than wide and a spiculated or microlobulated margin, and other US features of nodular composition and echogenicity (7). K-TIRADS 5 indicates high suspicion of malignancy when there is solid hypoechoic composition with any of the three US features. K-TIRADS 4 indicates intermediate suspicion of malignancy: (1) Solid hypoechoic composition without any of the three US features; (2) Partial cystic composition with any of three US features; (3) Solid iso/hyperechoic composition with any of three US features. K-TIRADS 3 indicates low suspicion of malignancy: (1) Partially cystic composition without any US feature; (2) Solid iso/hyperechoic composition without any US feature. K-TIRADS 2 indicates the nodule is benign: (1) Spongiform; (2) Partial cystic composition with comet-tail artifact; (3) Pure cyst. K-TIRADS 1 indicates no nodule.

Key Points of Thyroid Nodular Assessment by the ACR TI-RADS (2017)

According to the ACR-TIRADS, the assessment of a thyroid nodule involves a comprehensive evaluation of its composition, echogenicity, shape (orientation) (8). In the scoring scheme, each sonographic feature is awarded from 0 to 3 points, and higher points indicate greater degrees of suspicious malignancy. The ACR-TIRADS categories were established according to the total score of a thyroid nodule, and there are five categories from benign to highly suspicious malignancy. A thyroid nodule with total score of 0, 2, 3, 4-6, and 7 and more is categorised as TIRADS 1, 2, 3, 4, and 5, respectively. Points are awarded for nodular composition (architecture) with these qualities: Cystic = 0, spongy = 0, mixed solid-cystic with dominant cystic = 1, solid = 2 and dominant solid or indeterminate = 2. Scores based on internal echogenicity are: Anechoic = 0, isoechoic = 1, hyperechoic = 1, indeterminate = 1, hypoechoic = 2, markedly hypoechoic = 3. Points awarded for shape (orientation) are: No point for wider than tall (A/T<1), and 3 points for taller than wide (A/T≥1). Points awarded for margin are: Smooth = 0, ill-defined = 0, irregular = 2, lobulated = 2, extrathyroidal extension = 3. Scores awarded for echogenic foci: none = 0, hyperechoic with comet-tail artifact = 0, macrocalcifications = 1, peripheral or rim hyperechoic = 2 and punctate hyperechoic = 3.

The thyroid nodule categorization was performed with reference to the C-TIRADS, K-TIRADS and ACR-TIRADS, the categorization was determined by two physicians with two and 16 years of experience in thyroid US through reviewing the US images in consensus, and they were blind to the histopathological results. Histopathological result was used as a reference to determine whether a thyroid nodule was benign or malignant. The histopathological study was made according to the criteria of the World Health Organization (17). US features of some thyroid nodules, scoring schemes and categorizations using three TIRADSs were illustrated on **Figures 1**–**5**.

Acquisition of Sonographies of the Thyroid Nodules

All patients with thyroid nodular lesions before surgery underwent thyroid US examination, using a linear array transducer with a frequency of 5-14 MHz and different US systems (Siemens Acuson S2000; Mindray DC 8 & 7; Aloka Prosound α-7 & α-10; Phillips EPIQ5 and GE Logiq E9). During the examination, the US systems were adjusted to small parts mode (thyroid gland); the patient took a supine position on a table without a pillow, with the neck fully exposed. The thyroid was scanned by different sections to detect any lesion. If a thyroid nodule was found, its location, shape, orientation(parallel or nonparallel), margin, border, size, architecture(composition) and internal echogenicity, posterior features, vascularity, and relation to abutting tissue were identified and scrutinized. Status of cervical lymph node was noted, with attention to the presence of punctate hyperechoic foci and calcification. The representative images were saved in Picture Archiving and Communications Systems (PACS).

Statistical Analysis

Quantitative data with a normal distribution were expressed as mean and standard deviation (M ± SD), quantitative data that did not show a normal distribution and qualitative data were expressed as median (interquartile range, IQR) and percentile. The consistencies between C-TIRADS and K-TIRADS and ACR-TIRADS were studied, and the levels of malignancy risk stratification corresponding to each TIRADS were evaluated. The number of thyroid nodules and percentage of malignant nodules categorised as C-TIRADS 2, 3, 4A, 4B, 4C and 5, ACR-TIRADS 1, 2, 3, 4 and 5, and K-TIRADS 2, 3, 4 and 5 were calculated; and the correlation between the category and percentage of malignancy was determined, respectively. An independent samples T test was used to test quantitative data with a normal distribution. Qualitative data were analysed by a nonparametric test or a Chi-square test. The receiver operating characteristic (ROC) curve was drawn, the area under the (AUC) curve was obtained to evaluate the performances of the three TIRADSs for malignancy risk stratification, and the sensitivity, specificity, positive predictive value (PPV), and negative predictive value (NPV) were calculated. The highest value of accuracy (AUC) *of* ROC curve *of* each TIRADS was taken as the best threshold for malignancy risk stratification. Medcalc statistical software version 15.2.2 (Medcalc software BVBA, Ostend, Belgium) was used for statistical analyse, and $P < 0.05$ was considered a significant difference.

RESULTS

Among the 1978 patients with 1982 thyroid nodules, there were 1306 benign nodules and 676 malignant nodules, and the demographic and ultrasound features of the patients with thyroid nodules are summarised in **Table 1**. Papillary carcinoma made up 97.48% of the total malignant nodules, and hyperplastic nodules made up 91.19% of the total benign nodules. Details of the distribution of pathologies of the thyroid nodules are listed in **Table 2**. The malignancy risk made up 1.09%, 2.14%, 10.34%, 49.28%, 88.19% and 85.29% of the total nodules that were categorised as C-TIRADS 2, 3, 4A, 4B, 4C and 5, respectively; 0.00%, 1.64%, 2.87%,18.71% and 82.22% of the total nodules that were categorised as ACR-TIRADS 1, 2, 3, 4 and

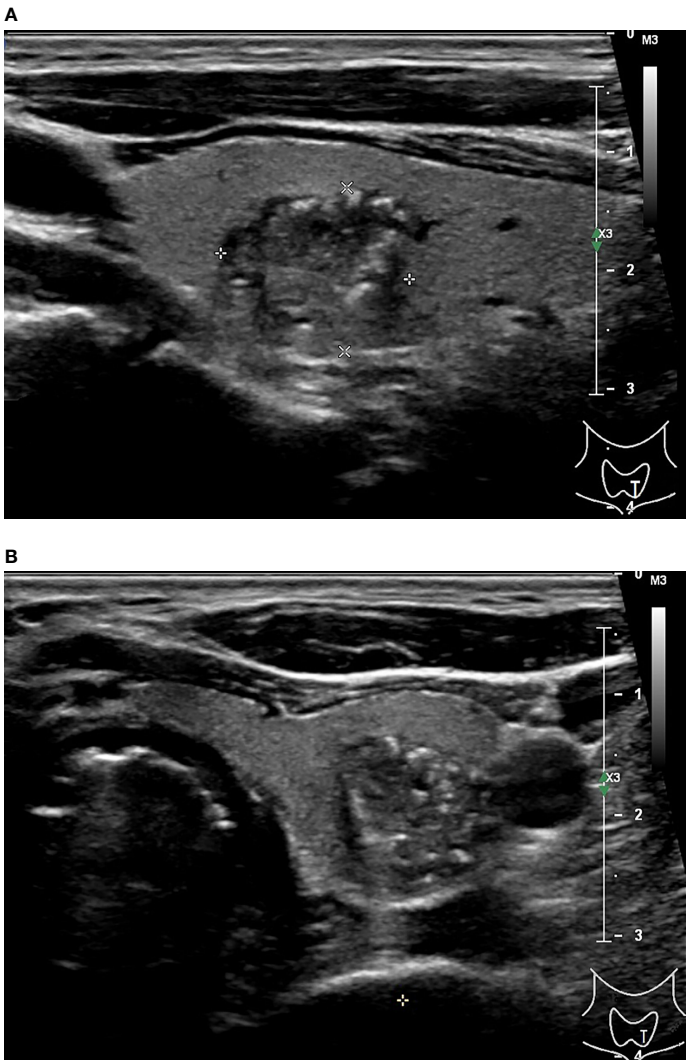

FIGURE 1 | 48-year-old man with thyroid papillary carcinoma. Sonographies of longitudinal scanning **(A)** and axial scanning **(B)** axial scanning show the nodule locates at the left lobe of the thyroid, characterized by 16.1 mm×13.8 mm×13.3mm in size, solid composition, irregular shape, A<T orientation in longitudinal view and A>T orientation in axial view, spiculated margin, heterogeneous iso/hypoechoic, with several punctate hyperechoic foci, and absence of posterior acoustic effect. C-TIRADS 5, K-TIRADS 5, ACR-TIRADS 5. Histopathology confirmed it is a papillary carcinoma.

5, respectively;and 0.85%, 3.27%, 24.27% and 80.96% of the total nodules that were categorised as K-TIRADS 2, 3, 4 and 5, respectively. The correlation between the category of TIRADS and percentage of malignancy was 0.94 in the C-TIRADS, 1.00 in the ACR-TIRADS, and 1.00 in the K-TIRADS, respectively; as summarised in **Table 3**. The highest values of accuracy (AUC) *of* ROC curves *of* C-TIRADS 4B, K-TIRADS 5 and ACR-TIRADS 5 were taken as the optimised cut-off values (thresholds) for malignancy risk stratification, respectively. Using the optimised category of C-TIRADS 4B as the cut-off, 614 nodules were confirmed true positive (malignant lesions), 206 nodules were confirmed false positive (benign lesions), 1100 nodules were confirmed true negative (benign lesions), and 62 nodules were confirmed false negative (malignant lesions). Taking the optimised category of K-TIRADS 5 as the cut-off, 565 nodules were true positive (malignant lesions); 133 nodules were false positive (benign lesions); 1173 nodules were true negative (benign lesions); and 111 nodules were false negative (malignant lesions). Taking the optimised category of ACR-TIRADS 5 as the cut-off, 578 nodules were true positive (malignant lesions), 126 nodules were false positive (benign lesions), 1180 nodules were true negative (benign lesions), and 98 nodules were false negative (malignant lesions). The sensitivity, specificity, PPV, NPV and AUC by C-TIRADS 4B, K-TIRADS 5 and ACR-TIRADS 5 for malignancy risk stratification of thyroid nodules were 90.83%, 84.23%, 74.88%, 94.66% and 0.88; 83.58%, 89.82%, 80.95%, 91.36% and 0.87; and 85.50%, 90.35%, 82.10%, 92.33% and 0.88, respectively. There

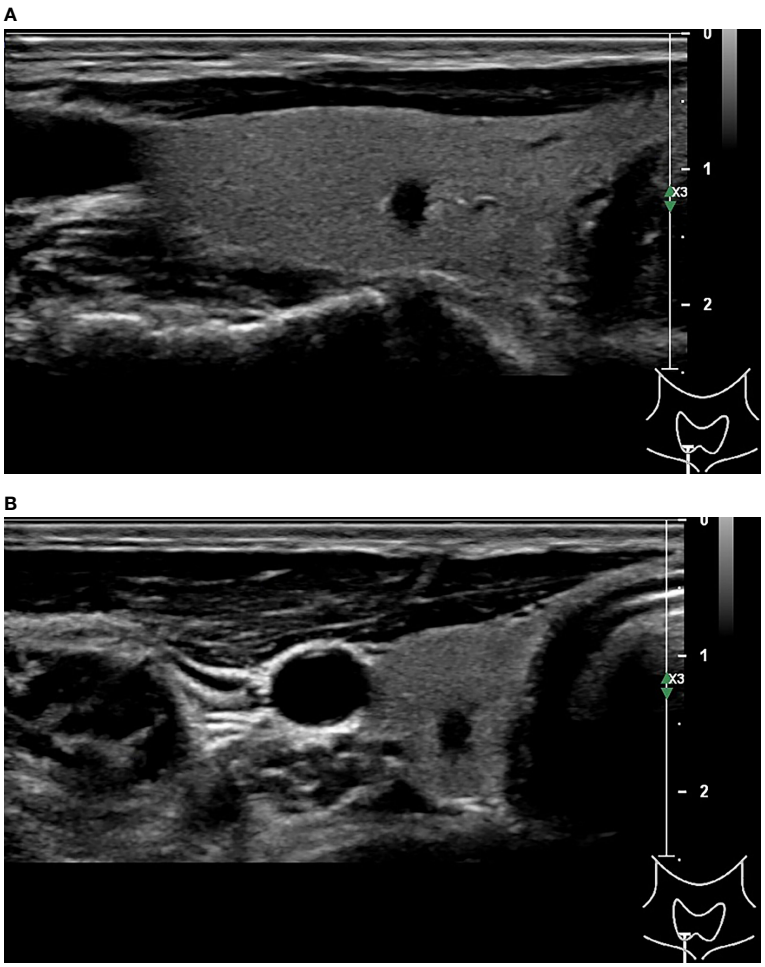

FIGURE 2 | 51-year-old man with thyroid papillary carcinoma. Sonographies of longitudinal scanning **(A)** and axial scanning **(B)** show the nodule locates at the right lobe of the thyroid, characterized by 4.9mm×3.3mm×3.5mm in size, solid composition, irregular shape, A>T orientation, markedly hypoechoic, well-defined margin, and absence of posterior acoustic effect. C-TIRADS 4C, K-TIRADS 5, ACR-TIRADS 5. Histopathology confirmed it is a papillary carcinoma.

was no significant difference between them when comparing AUCs between any two of them (P>0.05 for all). These are summarised in **Table 4** and **Figure 6**. There was significant difference in the comparison between any two of the C-TIRADS 4C, 4B, and 4A for AUC (all P<0.001).

DISCUSSION

Our study showed that the C-TIRADS has high clinical significance for stratifying the malignancy risk of thyroid nodules, and the AUC with a cut-off of C-TIRADS 4B is 0.88. Which is a little higher than that of K-TIRADS 5, equal to that of ACR-TIRADS 5, and higher than that 0.83 of C-TIRADS 4C, 0.52 of C-TIRADS 5, and 0.75 of C-TIRADS 4A. With C-TIRADS 4B as the stratification threshold, the sensitivity and specificity in the stratification of malignant thyroid nodules were 90.83% and 84.23%, respectively, which are similar to the results from K-TIRADS 5 and ACR-TIRADS 5. AUC of C-TIRADS 5 in our study is much lower than the AUCs of C-TIRADS 5, K-TIRADS 5 and ACR-TIRADS 5 in the study by Zhou et al. (18), and the AUC of C-TIRADS 4B in our study is a little higher than the AUCs of K-TIRADS 5 and ACR-TIRADS 5 in the study by Zhou et al. (18). The AUC of ACR-TIRADS 5 in this study is 0.88, which is higher than those in the previous studies of accuracy of 0.52 and AUC of 0.835 and 0.864 (19–21).

In our study, the NPV was 94.66% when using the C-RADS 4B as the optimal cut-off, which was higher than that of the K-TIRADS (91.36%) and ACR-TIRADS 5 (92.23%) at their optimal cut-off; and was a little lower than the result of 96.4% reported by Zhou et al. (18). It suggests that using C-RADS 4B as cut-off may spare more unuseful fine needle aspiration(FNA) or coarse needle biopsy.

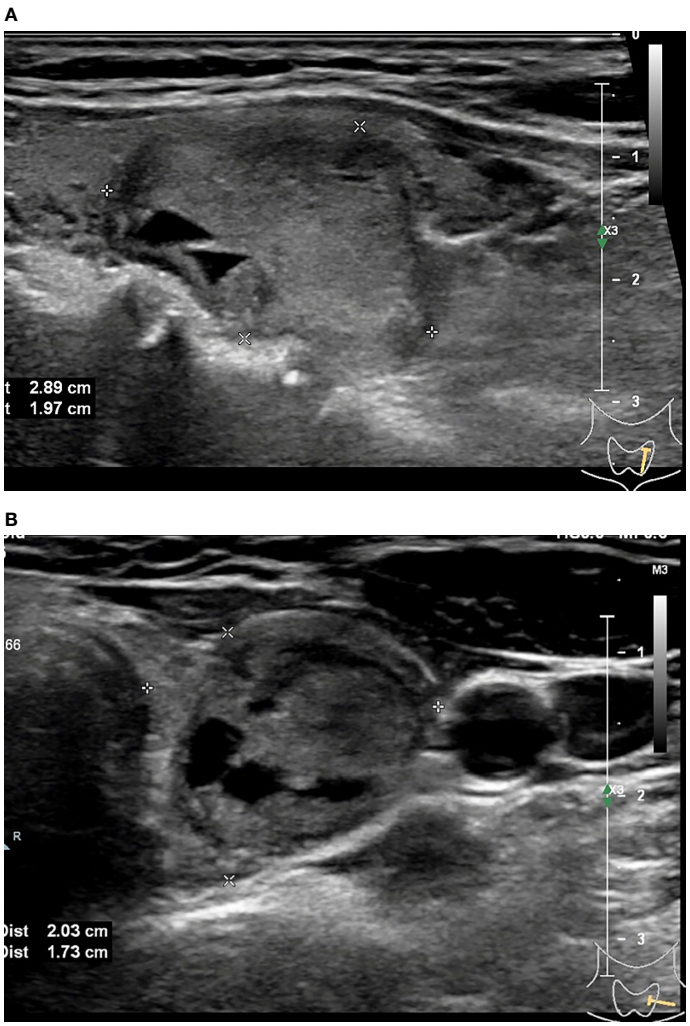

FIGURE 3 | 45-year-old woman with thyroid papillary carcinoma. Sonographies of longitudinal scanning **(A)** and axial scanning **(B)** show the nodule locates at the left lobe of the thyroid, characterized by 28.9mm×19.7mm×19mm in size, mixed solid-cystic composition, irregular shape, A<T orientation, hypoechoic and anechoic, discernible margin, and slight posterior acoustic enhancement. C-TIRADS 3, K-TIRADS 3, ACR-TIRADS 4. Histopathology confirmed it is a papillary carcinoma.

The C-TIRADS has several advantages: First, it is aimed at stratifying the malignancy risk, and clinical management is determined by a clinician with reference to other information. The malignancy risk in C-TIRADS 5 is over 90%, which are substantial higher than those of K-TIRADS (over 60%) and ACR-TIRADS(over 20%). The orientation of ACR-TIRADS is used to stratify the malignancy risk and FNA and/or follow-up, and management should wait for the results of FNA. Second, the US features for stratifying the malignancy risk adopted for the C-TIRADS may be more scientific, since these features have been optimised and evaluated by building a multivariate logistic regression model with forward stepwise selection and significant US features were included in the final logistic regression analysis (18). This was done instead of scoring every US feature based expert opinion. Third, the three TIRADSs have almost the same interpretations of US features, but the schemes are different. The scoring scheme of C-TIRADS is simpler and clearer (8, 9). For example, fine punctate microcalcification is given a value of 1 in the C-TIRADS, awarded 3 points in the ACR-TIRADS, and set as an important indicator of highly suggestive malignancy in the K-TIRADS. The hyperechoic foci with comet-tail artifact are counted as -1 in C-TIRADS, awarded 0 point in ACR-TIRADS, and regarded as an indicator suggestive of benign nodule. The scoring scheme of ACR-TIRADS involves 23 US features with different weighting of scores that suggest malignancy; the scheme of K-TIRADS involves three marked US features highly suspicious of malignancy and twenty or so other US features, without awarding a score. The scoring scheme of C-TIRADS involves counting six US features that are highly suggestive of malignancy or benignity. Other features are

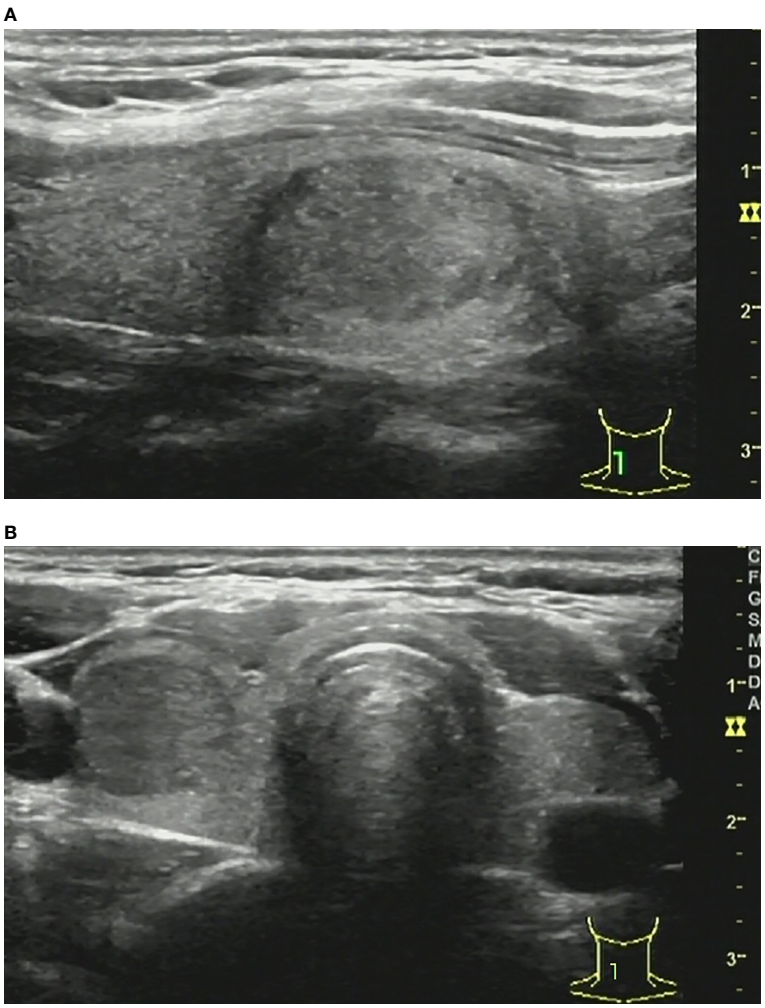

FIGURE 4 | 33-year-old woman with thyroid hyperplasia. Sonographies of longitudinal scanning **(A)** and axial scanning **(B)** show the nodule locates at the right lobe of the thyroid, characterized by 19.46mm×11.97mm×9.74mm in size, solid composition, elliptical shape, A<T orientation, almost isoechoic, well-defined margin, and absence of posterior acoustic effect. C-TIRADS 4A, K-TIRADS 3, ACR-TIRADS 3. Histopathology confirmed it is a thyroid hyperplasia.

precluded. Fourth, the C-TIRADS can spare radiologist time for cumulating scores, and it has more clinical practicability.

The C-TIRADS also has some weaknesses: First, all thyroid nodules with solid composition are counted as 1 in the C-TIRADS, which will lead to many benign nodules with scores of 1 or more, be categorised as C-TIRADS 4A or 4B, and increase the false negative effect. Second, a very (markedly) hypoechoic feature has 1 counting value suggestive of malignancy in the C-TIRADS. However, many malignant nodules do not present markedly hypoechoic feature. For example, Zhou et al. reported it was 27.79% (157/565) (9), but it made up of only 13.9% (94/676) in our study. This offsets the total score of a nodule and leads to an increase in the rate of false negatives. Third, the hypoechoic feature that occurs more frequently in malignant nodules has not been recruited for counting and categorising in the C-TIRADS. It made up of 59.82% (338/565) in the study by Zhou et al. (9) and 77.81% (526/676) in our study. This offsets the total score of a nodule and leads to an increase in the rate of false negatives. Fourth, the C-TIRADS has six categories, four of which are based on the data provided by the Chinese Artificial Intelligence Alliance for Thyroid and Breast Ultrasound, and the other two are otherwise, which may affect the soundness and robustness of the C-TIRADS (9).

According to the C-TIRADS guidelines, the malignancy risk of C-TIRADS 5, 4C, 4B, 4A, 3, 2, 1 were over 90%, over 50% and equal or fewer than 90%, over 10% and equal or fewer than 50%, over 2% and equal or fewer than 10%, fewer than 2%, 0% and 0%, with high consistency and limited deviation (9). Our results for C-TIRADS category 5, 4C, 4B, 4A, 3 and 2 (absence of thyroid nodules for category 1 and 6) were 85.29%, 88.19%, 49.28%, 10.34%, 2.14% and1.09%; the correlation between the category

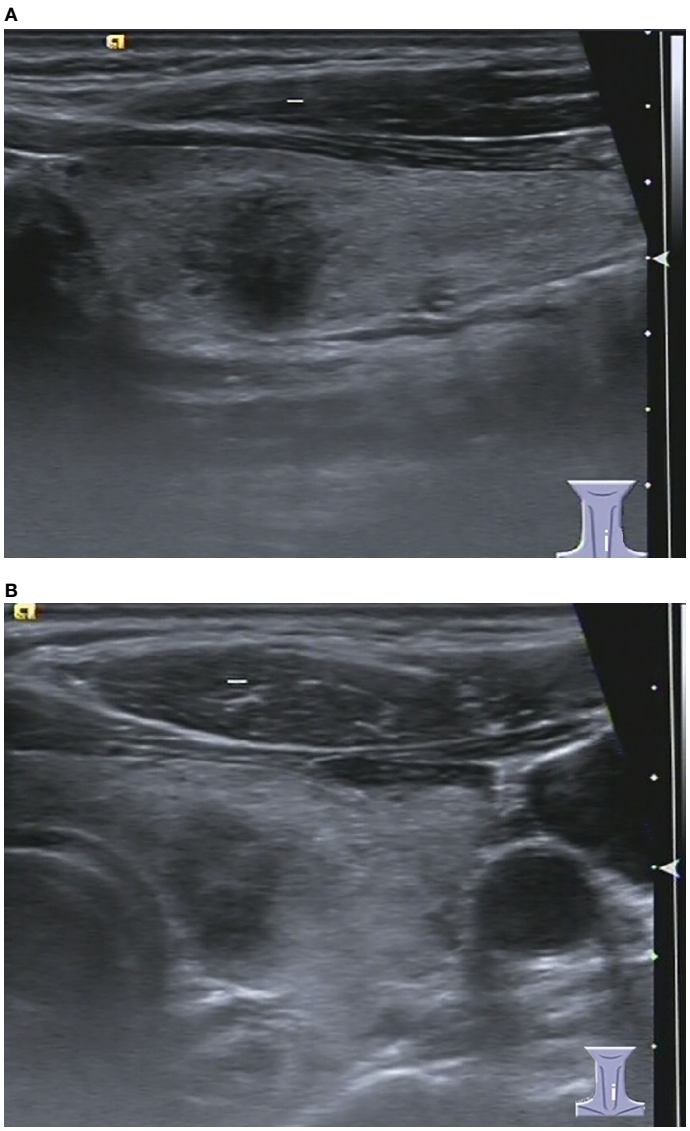

FIGURE 5 | 37-year-old woman with chronic lymphocytic thyroiditis. Sonographies of longitudinal scanning **(A)** and axial scanning **(B)** show the nodule locates at the left lobe of the thyroid, characterized by 9.8mm×9.2mm×9.4mm in size, solid composition, irregular shape, A>T orientation, hypoechoic, ill-defined margin, and absence of posterior acoustic effect. C-TIRADS 4C, K-TIRADS 5, ACR-TIRADS 5. Histopathology confirmed it is a chronic lymphocytic thyroiditis.

and malignancy risk was 0.94; and AUCs of C-TIRADS 5, 4C, 4B and 4A were 0.52, 0.83, 0.88 and 0.75, respectively. These indicate the correlation was excellent, but the AUC was inconsistency and great deviation compared to the Chinese guidelines, especially the C-TIRADS 5. The reasons may be that many malignant nodules do not present some US features that are suggestive of malignant nodules, while substantial weight is placed just on these features, including extra-thyroid extension margin, marked hypoechogenicity and taller-than-wide shape, and these lead to a lower total score, so the nodules cannot be categorised as C-TIRADS 5.

According to the Korea's recommendations, the malignancy risk of K-TIRADS 5, 4, 3, 2, 1 were over 60%, over 15% and equal or less than 60%, over 3% and equal or less than 15%, less than 3%, and 0 (7). Our results of K-TIRADS 5, 4, 3 and 2 (absence of thyroid nodules for 1 category) were 80.96%, 24.27%, 3.27%, and 0.85%; the correlation between the category and malignancy risk was 1.00; and AUCs of K-TIRADS 5 and 4 were 0.87 and 0.83, respectively. The correlation was perfect, but the AUC was not consistent with the recommendations. This means that many thyroid nodules with K-TIRADS 4 and 5 have a higher malignancy risk than the ranges stated in the recommendations,

TABLE 1 | Demographic and ultrasound features of the patients with thyroid nodules.

Characteristics	Benign nodules (n=1306)	Malignant nodules (n=676)	*P value*
Age (year)			<0.0001
Mean	46.41 ± 12.65	43.93 ± 11.93	
Range	7-75	7-82	
Sex			0.5211
Male (n,%)	291 (22.28)	160 (23.67)	
Female (n,%)	1015 (77.72)	516 (76.33)	
Size (mm)			<0.0001
Mean	21.34 ± 11.66	11.71 ± 8.47	
Range	(2-79)	(2-73)	
Distribution of sizes			<0.0001
<10mm (n,%)	131 (10.03)	287 (42.46)	
≥10mm (n,%)	1175 (89.97)	389 (57.54)	
Number			
Single (n,%)	312 (23.89)	162 (23.96)	0.9852
Multiple (n,%)	994 (76.11)	514 (76.04)	
Composition			<0.0001
Cystic/spongiform (n,%)	39 (2.99)	0 (0.00)	
Mixed cystic and solid (n,%)	635 (48.62)	23 (3.40)	
Solid (n,%)	632 (48.39)	653 (96.60)	
Echogenicity			<0.0001
Anechoic (n,%)	32 (2.45)	0 (0.00)	
Iso/hyperechoic (n,%)	604 (46.25)	56 (8.28%)	
Hypoechoic (n,%)	648 (49.62)	526 (77.81%)	
Markedly hypoechoic (n,%)	22 (1.68)	94 (13.91%)	
Shape			<0.0001
Wider-than-tall (n,%)	1262 (96.63)	355 (52.51)	
Taller-than-wide (n,%)	44 (3.37)	321 (47.49)	
Margin			<0.0001
Smooth/ill-defined (n,%)	1246 (95.41)	319 (47.19)	
Lobulated/irregular (n,%)	58 (4.44)	308 (45.56)	
Extrathyroid extension (n,%)	2 (0.15)	49 (7.25)	
Echogenic foci			<0.0001
None or large comet-tail artifacts (n,%)	1055 (80.78)	160 (23.66)	
Macrocalcifications (n,%)	90 (6.89)	25 (3.70)	
Peripheral calcifications (n,%)	22 (1.69)	7 (1.04)	
Punctate echogenic foci (n,%)	139 (10.64)	484 (71.60)	

TABLE 2 | Distribution of pathologies of the thyroid nodules.

Pathology		Number (%)
Benign nodule	Hyperplastic nodules	1191 (91.19)
	Follicular adenoma	49 (3.75)
	Hürthle-cell adenoma	14 (1.07)
	Chronic lymphocytic thyroiditis	41 (3.14)
	Toxic nodular goiter	3 (0.23)
	Granulomatous thyroiditis	8 (0.62)
	Total	1306 (100.00)
Malignant nodule	Papillary carcinoma	659 (97.48)
	Medullary carcinoma	9 (1.33)
	Follicular carcinoma	6 (0.89)
	Anaplastic carcinoma	2 (0.30)
	Total	676 (100.00)

and the K-TIRADS has higher predictive ability than its original data.

The main aim of the ACR-TIRADS category was to determine recommendations for FNA and follow-up, with a low threshold of malignancy risk estimated at 2% or less for ACR-TIRADS 1 to greater than 20% for ACR-TIRADS 5. In our study, the malignancy risk of ACR-TIRADS 5, 4, 3, 2, 1 category was 82.22%, 18.71%, 2.87%, 1.64% and 0.00%; the correlation between the category and malignancy risk was 1.00; and the AUC of 0.88 was high. The correlation was perfect, but the AUC was not consistent with the recommendations. This means that many thyroid nodules with ACR-TIRADS 5 have much higher than 20% malignancy risk, as reported by other studies (18–22).

Previous study has shown that there was wide variability in the description of some US features, while interobserver agreement among different TIRADSs was substantial to almost perfect (23). In our study, the best thresholds for assessing malignant thyroid nodules by the C-TIRADS, K-TIRADS and ACR-TIRADS were C-TIRADS 4B, K-TIRADS 5 and ACR-TIRADS 5, respectively. The reason that C-TIRADS 4B performed better than C-TIRADS 4C and 5 may be that some malignant nodules do not present sufficient US features to indicate malignancy and some benign nodules present more US features, suggesting malignancy. This leads to inappropriate scoring and poorer diagnostic performance. Similar phenomena have occurred in other studies. For example, Basha et al. found

TABLE 3 | Distributions of benign and malignant nodules in different categories of TIRADSs and correlations.

TIRADS	Benigndistribution (n)	Malignantdistribution (n)	Sum and percentile (n,%)	Malignancy risk (%)	Coefficient of malignancy risk and TIRADS
C-TIRADS					0.943
2	90	1	91 (4.59)	1.09	
3	594	13	607 (30.61)	2.14	
4A	416	48	464 (23.41)	10.34	
4B	141	137	278 (14.03)	49.28	
4C	60	448	508 (25.63)	88.19	
5	5	29	34 (1.72)	85.29	
Total	1306	676	1982 (100)		
ACR-TIRADS					1.00
1	34	0	34 (1.72)	0.00	
2	300	5	305 (15.39)	1.64	
3	508	15	523 (26.39)	2.87	
4	339	78	417 (21.04)	18.71	
5	125	578	703 (35.47)	82.22	
Total	1306	676	1982 (100)		
K-TIRADS					1.00
2	116	1	117 (5.90)	0.85	
3	798	27	825 (41.67)	3.27	
4	259	83	342 (17.26)	24.27	
5	133	565	698 (35.22)	80.96	
Total	1306	676	1982 (100)		

TABLE 4 | Diagnostic performances of three TI-RADSs by different cut-off of category.

Cut-off of category	Sensitivity (%,n)	Specificity (%,n)	PPV (%,n)	NPV (%,n)	AUC
C-TIRADS 4A	97.93 (662/676)	52.37 (684/1306)	51.56 (662/1284)	97.99 (684/698)	0.75
	[96.55-98.86]	[49.62-55.11]	[48.78-54.32]	[96.66-98.90]	[0.73-0.77]
C-TIRADS 4B	90.83 (614/676)	84.23 (1100/1306)	74.88 (614/820)	94.66 (1100/1162)	0.88
C-TIRADS 4C	[88.40-92.90]	[82.13-86.16]	[71.76-77.81]	[93.21-95.89]	[0.86-0.89]
C-TIRADS 5	70.86 (479/676)	95.02 (1241/1306)	88.05 (479/544)	86.30 (1241/1438)	0.83
K-TIRADS 4	[67.27-74.26]	[93.71-96.14]	[85.03-90.66]	[84.41-88.04]	[0.81-0.84]
	4.73 (32/676)	99.62 (1301/1306)	86.49 (32/37)	66.89 (1301/1945)	0.52
	[3.26-6.62]	[99.11-99.88]	[71.23-95.46]	[64.75-68.98]	[0.50-0.54]
	95.86 (648/676)	69.98 (914/1306)	62.31 (648/1040)	97.03 (914/942)	0.83
	[94.07-97.23]	[67.42-72.46]	[59.28-65.26]	[95.73-98.02]	[0.81-0.85]
K-TIRADS 5	83.58 (56/676)	89.82 (1173/1306)	80.95 (565/698)	91.36 (1173/1284)	0.87
	[80.57-86.29]	[88.05-91.40]	[77.83-83.79]	[89.68-92.84]	[0.85-0.88]
ACR-TIRADS 4	97.04 (656/676)	64.62 (844/1306)	58.68 (656/1118)	97.69 (844/864)	0.81
	[95.47-98.18]	[61.96-67.22]	[55.73-61.58]	[96.45-98.58]	[0.79-0.82]
ACR-TIRADS 5	85.50 (578/676)	90.35 (1180/1306)	82.10 (578/704)	92.33 (1180/1287)	0.88
	[82.62-88.07]	[88.62-91.90]	[79.07-84.87]	[90.73-93.73]	[0.86-0.89]

C-TIRADS, The Superficial Organ and Vascular Ultrasound Group of the Society of Ultrasound in Medicine of Chinese Medical Association version of thyroid imaging, reporting and data system; K-TIRADS, The Korean Thyroid Imaging Reporting and Data System by The Korean Society of Thyroid Radiology; ACR-TIRADS, American College of Radiology version of thyroid imaging, reporting and data system; PPV, Positive predictive value; NPV, Negative predictive value; AUC, Area under the ROC curve; Variables in parentheses are numbers; Variables in brackets are 95% confidential intervals.

that in their multi-centre prospective study on the validity of ACR-TIRADS based 948 thyroid nodules, the best cut-off value for predicting malignant thyroid nodules was > ACR-TIRADS 3, other than ACR-TIRADS 5 (24).

In our study, the C-TIRADS 4B, K-TI-RADS 5 and ACR-TIRADS 5 showed good sensitivity and specificity in risk stratification of thyroid nodules. This means that they are better at differentiating malignant thyroid nodules from benign ones. This suggests that the three TIRADSs for thyroid nodules are beneficial for patients and radiologists. Because the thyroid cancer is an indolent tumor, the progress is usully slow, so for a lower malignancy risk thyroid nodule, it's not so urgent to perform FNA or a biopsy, and follow-up may be an alternative. These were supported by Grani et al. that patients with presumably benign thyroid nodules assessed by TIRADS can be safely followed with less intensive protocols (25). The C-TIRADS 5 presented excellent specificity, at 99.62%. This means that if a thyroid nodule presents C-TIRADS 5, there is little probability that it is benign. However, a sensitivity of 4.73% handicaps its power in malignancy risk stratification. The ACR-TIRADS and K-TI-RADS have been validated by many studies, but the C-TIRADS 2020 version is a recently launched system (18–27).

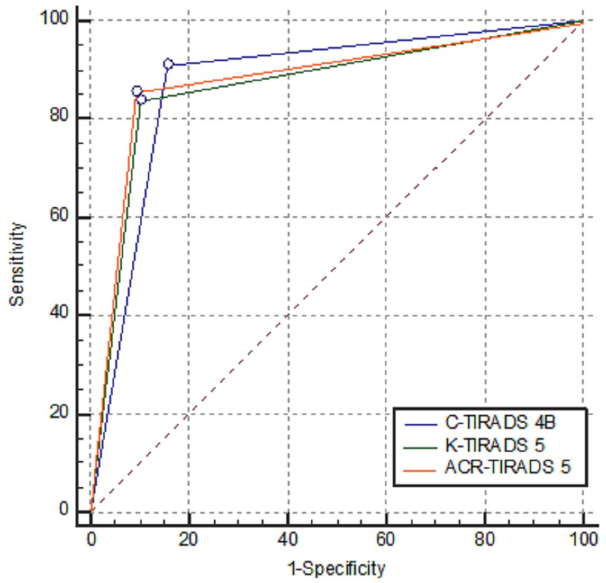

FIGURE 6 | Comparisons of AUCs of C-TIRADS 4B, K-TIRADS 5 and ACR-TIRADS 5. There was no significant difference between each pair of them (*Z* value was 1.402, 0.306 and 1.004, respectively; and *P* value was 0.1610, 0.7593 and 0.3155, respectively).

Prospectively, because the three investigated TIRADSs had not considered the locations of the thyroid nodules, cervical lymph nodes, epidemic factors, contrast-enhanced US features, US elastography, artificial intelligence, and so on. Some experts have suggested adding one or more of these variables to extend and augment these systems and to improve their risk stratification efficiency (14, 28–32). Wang, et al. reported that contrast-enhanced US combining with conventional US in differentiating ACR TI-RADS category 4 and 5 nodules with non-hypovascular may improve the malignancy risk stratification of non-hypovascular thyroid nodules (28). Celletti et al. found that adding strain elastosonography of Strain Ratio to K-TIRADS assessment can significantly increase its sensitivity and negative predictive value (30). A study by Wildman-Tobriner et al. showed that an artificial intelligence-optimized ACR-TIRADS can slightly improve its specificity and maintain sensitivity. Additionally, it simplifies US feature assignments, which may improve ease of use (32).

This study has some limitations: (1) The surgery and histopathological results are used as the gold standard, instead of combining surgery and FNA cytology, which cannot fully include benign lesions, and may inevitably induce selection bias. (2) The absence of assessment of interobserver agreement for the US images acquisition of the thyroid nodules by different operators and different US systems, which may affect the homogeneicity of the images. (3) In this study, the malignant nodules are mainly papillary carcinoma (97.48%), while the benign nodules are hyperplastic nodules (91.19%), and the pathological types are relatively narrow. Therefore, in the future, more study should be done to evaluate the risk stratification efficiency for medullary carcinoma, follicular carcinoma and anaplastic carcinoma.

The strengths of this study are that (1) It is a relative new study for the validation of the latest released C-TIRADS; (2) The sample is large; (3) The pathological natures of the thyroid nodules had been confirmed by histopathology, thyroid nodules with FNA cytology only were excluded, so the final diagnosis of the thyroid nodules was reliable and sound; (4) The validation of C-TIRADS was compared with the widely validated ACR-TIRADS and K-TIRADS, and the results and conclusion are sufficiently informative. The weaknesses of this study are that (1) The sample was rendered from a single medical centre, and (2) The study design was retrospective, which may have potential of causing bias for the study.

In summary, the C-TIRADS has outstanding performance in the malignancy risk stratification of thyroid nodules by the optimised cut-off value, which is comparable to that in K-TIRADS and ACR-TIRADS.

DATA AVAILABILITY STATEMENT

The original contributions presented in the study are included in the article/supplementary material. Further inquiries can be directed to the corresponding author.

ETHICS STATEMENT

The studies involving human participants were reviewed and approved by The Ethics Committee of The First Affiliated Hospital of Hainan Medical University. Informed consent was obtained from all patients for the use of US images and related information for the purpose of teaching and scientific research during the examination.

AUTHOR CONTRIBUTIONS

(1) Contributor SW: Concepts, design, data acquisition and analysis, statistical analysis, manuscript preparation, and guarantor. (2) Contributor QC: Data acquisition and analysis, and statistical analysis. (3) Contributor ML: Data acquisition and analysis, and manuscript preparation. All authors: Final approval of the version to be published; and agreement to be accountable for all aspects of the work in ensuring that questions related to the accuracy or integrity of any part of the work are appropriately investigated and resolved.

FUNDING

This study was financially supported by grant from the National Natural Science Foundation of China (grant no. 81560290).

REFERENCES

1. Haugen BR, Alexander EK, Bible KC, et al. 2015 American Thyroid Association Management Guidelines for Adult Patients With Thyroid Nodules and Differentiated Thyroid Cancer: The American Thyroid Association Guidelines Task Force on Thyroid Nodules and Differentiated Thyroid Cancer. *Thyroid* (2016) 26:1–133. doi: 10.1089/thy.2015.0020
2. Moon JH, Hyun MK, Lee JY, et al. Prevalence of Thyroid Nodules and Their Associated Clinical Parameters: A Large-Scale, Multicenter-Based Health Checkup Study. *Korean J Intern Med* (2018) 33:753–62. doi: 10.3904/kjim.2015.273
3. Jiang H, Tian Y, Yan W, et al. The Prevalence of Thyroid Nodules and an Analysis of Related Lifestyle Factors in Beijing Communities. *Int J Environ Res Public Health* (2016) 13:442. doi: 10.3390/ijerph13040442
4. Morris LG, Tuttle RM, Davies L. Changing Trends in the Incidence of Thyroid Cancer in the United States. *JAMA Otolaryngol Head Neck Surg* (2016) 142:709–11. doi: 10.1001/jamaoto.2016.0230
5. Kitahara CM, Sosa JA. The Changing Incidence of Thyroid Cancer. *Nat Rev Endocrinol* (2016) 12:646–53. doi: 10.1038/nrendo.2016.110
6. Kwak JY, Han KH, Yoon JH, et al. Thyroid Imaging Reporting and Data System for US Features of Nodules: A Step in Establishing Better Stratification of Cancer Risk. *Radiology* (2011) 260:892–9. doi: 10.1148/radiol.11110206
7. Shin JH, Baek JH, Chung JKorean Society of Thyroid Radiology (KSThR) and Korean Society of Radiology. Ultrasonography Diagnosis and Imaging-Based Management of Thyroid Nodules: Revised Korean Society of Thyroid Radiology Consensus Statement and Recommendations. *Korean J Radiol* (2016) 17:370–95. doi: 10.3348/kjr.2016.17.3.370
8. Tessler FN, Middleton WD, Grant EG, et al. ACR Thyroid Imaging, Reporting and Data System (TI-RADS): White Paper of the ACR TI-RADS Committee. *J Am Coll Radiol* (2017) 14:587–95. doi: 10.1016/j.jacr.2017.01.046
9. Zhou J, Yin L, Wei XSuperficial Organ and Vascular Ultrasound Group of the Society of Ultrasound in Medicine of the Chinese Medical Association; Chinese Artificial Intelligence Alliance for Thyroid and Breast Ultrasound. 2020 Chinese Guidelines for Ultrasound Malignancy Risk Stratification of Thyroid Nodules: The C-TIRADS. *Endocrine* (2020) 70:256–79. doi: 10.1007/s12020-020-02441-y
10. Horvath E, Majlis S, Rossi R, et al. An Ultrasonogram Reporting System for Thyroid Nodules Stratifying Cancer Risk for Clinical Management. *J Clin Endocrinol Metab* (2009) 94:1748–51. doi: 10.1210/jc.2008-1724
11. Fradin JM. ACR TI-RADS: An Advance in the Management of Thyroid Nodules or Pandora's Box of Surveillance? *J Clin Ultrasound* (2020) 48:3–6. doi: 10.1002/jcu.22772
12. Ha SM, Baek JH, Choi YJ, et al. Malignancy Risk of Initially Benign Thyroid Nodules: Validation With Various Thyroid Imaging Reporting and Data System Guidelines. *Eur Radiol* (2019) 29:133–40. doi: 10.1007/s00330-018-5566-0
13. Ha EJ, Na DG, Moon WJ, Lee YH, Choi N. Diagnostic Performance of Ultrasound-Based Risk-Stratification Systems for Thyroid Nodules: Comparison of the 2015 American Thyroid Association Guidelines With the 2016 Korean Thyroid Association/Korean Society of Thyroid Radiology and 2017 American College of Radiology Guidelines. *Thyroid* (2018) 28:1532–7. doi: 10.1089/thy.2018.0094
14. Hoang JK, Middleton WD, Tessler FN. Update on ACR TI-RADS: Successes, Challenges, and Future Directions, From the AJR Special Series on Radiology Reporting and Data Systems. *AJR Am J Roentgenol* (2021) 216:570–8. doi: 10.2214/AJR.20.24608
15. Xu T, Wu Y, Wu RX, et al. Validation and Comparison of Three Newly-Released Thyroid Imaging Reporting and Data Systems for Cancer Risk Determination. *Endocrine* (2019) 64:299–307. doi: 10.1007/s12020-018-1817-8
16. Yoon SJ, Na DG, Gwon HY, et al. Similarities and Differences Between Thyroid Imaging Reporting and Data Systems. *AJR Am J Roentgenol* (2019) 213:W76–84. doi: 10.2214/AJR.18.20510
17. Cameselle-Teijeiro JM, Sobrinho-Simões M. New WHO Classification of Thyroid Tumors: A Pragmatic Categorization of Thyroid Gland Neoplasms. *Endocrinol Diabetes Nutr* (2018) 65:133–5. doi: 10.1016/j.endien.2017.11.019
18. Zhou J, Song Y, Zhan WSuperficial Organ and Vascular Ultrasound Group of the Society of Ultrasound in Medicine of Chinese Medical Association and Chinese Artificial Intelligence Alliance for Thyroid and Breast Ultrasound. Thyroid Imaging Reporting and Data System (TIRADS) for Ultrasound Features of Nodules: Multicentric Retrospective Study in China. *Endocrine* (2021) 72:157–70. doi: 10.1007/s12020-020-02442-x
19. Hoang JK, Middleton WD, Farjat AE, et al. Reduction in Thyroid Nodule Biopsies and Improved Accuracy With American College of Radiology Thyroid Imaging Reporting and Data System. *Radiology* (2018) 287:185–93. doi: 10.1148/radiol.2018172572
20. Magri F, Chytiris S, Croce L, et al. Performance of the ACR TI-RADS and EU TI-RADS Scoring Systems in the Diagnostic Work-Up of Thyroid Nodules in a Real-Life Series Using Histology as Reference Standard. *Eur J Endocrinol* (2020) 183:521–8. doi: 10.1530/EJE-20-0682
21. Peng JY, Pan FS, Wang W, et al. Malignancy Risk Stratification and FNA Recommendations for Thyroid Nodules: A Comparison of ACR TI-RADS, AACE/ACE/AME and ATA Guidelines. *Am J Otolaryngol* (2020) 41:102625. doi: 10.1016/j.amjoto.2020.102625
22. Ha EJ, Na DG, Baek JH, et al. US Fine-Needle Aspiration Biopsy for Thyroid Malignancy: Diagnostic Performance of Seven Society Guidelines Applied to 2000 Thyroid Nodules. *Radiology* (2018) 287:893–900. doi: 10.1148/radiol.2018171074
23. Grani G, Lamartina L, Cantisani V, Maranghi M, Lucia P, Durante C. Interobserver Agreement of Various Thyroid Imaging Reporting and Data Systems. *Endocr Connect* (2018) 7:1–7. doi: 10.1530/EC-17-0336
24. Basha MAA, Alnaggar AA, Refaat R, et al. The Validity and Reproducibility of the Thyroid Imaging Reporting and Data System (TI-RADS) in Categorization of Thyroid Nodules: Multicentre Prospective Study. *Eur J Radiol* (2019) 117:184–92. doi: 10.1016/j.ejrad.2019.06.015
25. Grani G, Lamartina L, Biffoni M, et al. Sonographically Estimated Risks of Malignancy for Thyroid Nodules Computed With Five Standard Classification Systems: Changes Over Time and Their Relation to Malignancy. *Thyroid* (2018) 28:1190–7. doi: 10.1089/thy.2018.0178
26. Jin ZQ, Yu HZ, Mo CJ, Su RQ. Clinical Study of the Prediction of Malignancy in Thyroid Nodules: Modified Score Versus 2017 American College of Radiology's Thyroid Imaging Reporting and Data System Ultrasound Lexicon. *Ultrasound Med Biol* (2019) 45:1627–37. doi: 10.1016/j.ultrasmedbio.2019.03.014
27. Zhu H, Yang Y, Wu S, et al. Diagnostic Performance of US-Based FNAB Criteria of the 2020 Chinese Guideline for Malignant Thyroid Nodules: Comparison With the 2017 American College of Radiology Guideline, the 2015 American Thyroid Association Guideline, and the 2016 Korean Thyroid Association Guideline. *Quant Imaging Med Surg* (2021) 11:3604–18. doi: 10.21037/qims-20-1365
28. Wang Y, Dong T, Nie F, et al. Contrast-Enhanced Ultrasound in the Differential Diagnosis and Risk Stratification of ACR TI-RADS Category 4 and 5 Thyroid Nodules With Non-Hypovascular. *Front Oncol* (2021) 11:662273. doi: 10.3389/fonc.2021.662273
29. Yang JR, Song Y, Xue SS, et al. Suggested Amendment of TI-RADS Classification of Thyroid Nodules by Shear Wave Elastography. *Acta Radiol* (2020) 61:1026–33. doi: 10.1177/0284185119889567
30. Celletti I, Fresilli D, De Vito C, et al. TIRADS, SRE and SWE in INDETERMINATE Thyroid Nodule Characterization: Which has Better Diagnostic Performance? *Radiol Med* (2021) 126:1189–200. doi: 10.1007/s11547-021-01349-5
31. Li X, Hou XJ, Du LY, et al. Virtual Touch Tissue Imaging and Quantification (VTIQ) Combined With the American College of Radiology Thyroid Imaging Reporting and Data System (ACR TI-RADS) for Malignancy Risk Stratification of Thyroid Nodules. *Clin Hemorheol Microcirc* (2019) 72:279–91. doi: 10.3233/CH-180477
32. Wildman-Tobriner B, Buda M, Hoang JK, et al. Using Artificial Intelligence to Revise ACR TI-RADS Risk Stratification of Thyroid Nodules: Diagnostic Accuracy and Utility. *Radiology* (2019) 292:112–9. doi: 10.1148/radiol.2019182128

Conflict of Interest: The authors declare that the research was conducted in the absence of any commercial or financial relationships that could be construed as a potential conflict of interest.

this article, or claim that may be made by its manufacturer, is not guaranteed or endorsed by the publisher.

frontiers | Frontiers in Endocrinology

TYPE Original Research
PUBLISHED 12 August 2022
DOI 10.3389/fendo.2022.949847

OPEN ACCESS

EDITED BY
Emerita Andres Barrenechea,
Veterans Memorial Medical Center,
Philippines

REVIEWED BY
Jihong Wang,
University of Texas MD Anderson Cancer Center, United States
Wenlong Wang,
National Clinical Research Center for Geriatric Disorders, Central South University, China
Man Lu,
Sichuan Cancer Hospital, China
Zhongqian Hu,
Southeast University, China
Weiwei Zhan,
Shanghai Jiaotong University School of Medicine, China
Xu Hui'Xiong,
Fudan University, China
Zubang Zhou,
Gansu Provincial Hospital, China
Fenglin Dong,
The First Affiliated Hospital of Soochow University, China

*CORRESPONDENCE
Dong Xu
xudong@zjcc.org.cn
Zhijiang Han
hzj1022@zju.edu.cn

†These authors have contributed equally to this work and share first authorship

SPECIALTY SECTION
This article was submitted to Thyroid Endocrinology, a section of the journal Frontiers in Endocrinology

RECEIVED 21 May 2022
ACCEPTED 19 July 2022
PUBLISHED 12 August 2022

CITATION
Feng N, Wei P, Kong X, Xu J, Yao J, Cheng F, Ou D, Wang L, Xu D and Han Z (2022) The value of ultrasound grayscale ratio in the diagnosis of papillary thyroid microcarcinomas and benign micronodules in patients with Hashimoto's thyroiditis: A two-center controlled study.
Front. Endocrinol. 13:949847.
doi: 10.3389/fendo.2022.949847

The value of ultrasound grayscale ratio in the diagnosis of papillary thyroid microcarcinomas and benign micronodules in patients with Hashimoto's thyroiditis: A two-center controlled study

Na Feng[1,2†], Peiying Wei[3†], Xiangkai Kong[1,2†], Jingjing Xu[4], Jincao Yao[1,2,5,6], Fang Cheng[1,2], Di Ou[1,2], Liping Wang[1,2], Dong Xu[1,2,5,6*] and Zhijiang Han[3*]

[1]Department of Ultrasound, The Cancer Hospital of the University of Chinese Academy of Sciences (Zhejiang Cancer Hospital), Hangzhou, China, [2]Institute of Basic Medicine and Cancer (IBMC), Chinese Academy of Sciences, Hangzhou, China, [3]Department of Radiology, Affiliated Hangzhou First People's Hospital, Zhejiang University School of Medicine, Hangzhou, China, [4]Department of Pathology, The Cancer Hospital of the University of Chinese Academy of Sciences (Zhejiang Cancer Hospital), Hangzhou, China, [5]Research Center for Cancer Intelligent Diagnosis and Molecular Technology, The Cancer Hospital of the University of Chinese Academy of Sciences (Zhejiang Cancer Hospital), Hangzhou, China, [6]Key Laboratory of Head & Neck Cancer Translational Research of Zhejiang Province, The Cancer Hospital of the University of Chinese Academy of Sciences (Zhejiang Cancer Hospital), Hangzhou, China

Objective: The value of ultrasound grayscale ratio (UGSR) in the diagnosis of papillary thyroid microcarcinomas (PTMCs) and benign micronodules (BMNs) has been recognized by some authors, but studies have not examined these aspects in patients with Hashimoto's thyroiditis (HT). This retrospective study investigated the value of UGSR in the diagnosis of PTMCs and BMNs in patients with HT using data from two medical centers.

Methods: Ultrasound images of 428 PTMCs in 368 patients with HT and 225 BMNs in 181 patients with HT in center A were retrospectively analyzed and compared to the ultrasound images of 412 PTMCs in 324 patients with HT and 315 BMNs in 229 patients with HT in medical center B. All of the cases were surgically confirmed. The UGSR was calculated as the ratio of the grayscale value of lesions to the surrounding normal thyroid tissues. The optimal UGSR thresholds for the PTMCs and BMNs in patients with HT from the two medical centers were determined using a receiver operating characteristic (ROC) curve. Furthermore, other statistics, including the area under the curve (AUC), the optimal UGSR threshold, sensitivity, specificity, positive predictive value (PPV), negative predictive value (NPV), and diagnostic accuracy of the two medical centers, were pair analyzed in this study.

Results: The UGSR of PTMCs and BMNs in patients with HT from medical center A were 0.513 (0.442, 0.592) and 0.857 (0.677, 0.977) (Z = –15.564, p = 0), and those from medical center B were 0.514 (0.431, 0.625) and 0.917 (0.705, 1.131) (Z = –15.564, p = 0). For both medical centers A and B, the AUC, optimal UGSR threshold, sensitivity, specificity, PPV, NPV, and diagnostic accuracy of the UGSR in differentiating between PTMCs and BMNs in patients with HT were 0.870 and 0.889, 0.68 and 0.70, 0.921 and 0.898, 0.747 and 0.759, 0.874 and 0.829, 0.832 and 0.848, and 0.861 and 0.836, respectively. There were no significant differences in the UGSR for the PTMCs between patients from the two medical centers (Z = –0.815, p = 0.415), while there was a significant difference in the UGSR of the BMNs between patients from the two medical centers (Z = –3.637, p = 0).

Conclusion: In the context of HT, UGSR still has high sensitivity, accuracy, and stability in differentiating between PTMCs and BMNs, making it a complementary differentiator of thyroid imaging reporting and data systems. However, due to its low specificity, a comprehensive analysis of other ultrasound signs is required.

KEYWORDS

ultrasound grayscale ratio, papillary thyroid microcarcinomas, nodular goiters, diagnosis, echogenicity, Hashimoto's thyroiditis

Introduction

Hashimoto's thyroiditis (HT), also known as chronic lymphocytic or autoimmune thyroiditis, is the most common inflammatory thyroid disease. Its pathological basis is as follows: The thyroid is infiltrated by lymphocytes and plasma cells, and a lymphoid follicle with germinal centers appears, resulting in the gland undergoing parenchymal atrophy and fibrosing (1, 2). Ultrasound echo intensity reflects the internal pathological basis of HT. For example, lymphocyte and plasma cell infiltration decreases the echo intensity, and fibrosis causes heterogeneous echo intensity. Therefore, ultrasound has become the most important imaging method for evaluating and monitoring HT. Papillary thyroid carcinoma is the most common pathological subtype of thyroid carcinoma, usually coexisting with HT. HT is even considered an independent risk factor for papillary carcinoma (3, 4). Hypoechoic imaging is an important component in the diagnosis of papillary thyroid carcinoma, especially for papillary thyroid microcarcinoma (PTMC). According to the traditional ultrasound echo intensity grading scale, most authors (5–8) believe that ultrasound echo intensity has almost the same importance in differentiating between benign and malignant thyroid nodules regardless of the existence of HT. The proportions of hypoechoic imaging in malignant nodules in patients both with and without HT are 63.6%–78.5% (5, 6) vs. 65.9%–87.5% (5, 9), respectively. However, for benign and malignant nodules in patients with HT, due to lymphocytes' and plasma cells' different infiltration degrees, the echo intensity of the nodules and the surrounding normal thyroid tissue may vary. The results of echo intensity classification may not change as observers do not notice these minor differences with the naked eye. Therefore, the quantification of ultrasound echo intensity can identify these minor differences, thus providing a more objective basis for the classification of thyroid nodules.

Studies on the quantification of ultrasound echo intensity in terms of thyroid nodules include the directly quantified gray-scale histogram (10) and the indirectly quantified ultrasound grayscale ratio (UGSR), the latter of which is well recognized by the majority of scholars (11–16). Compared to the parameters of directly quantified gray-scale histograms, UGSR can effectively eliminate the unstable factors in gray-scale values that are caused by different ultrasound systems, operators, gains, and dynamics settings, and it uses a relatively stable ratio to indirectly quantify the echo intensity of nodules. In our previous studies (13–16), there are only six articles discussing UGSR (11–16), all of which suggest that the rates at which UGSR is used for malignant nodules are lower than those for solid benign nodules (11–15) but higher than those for cystic benign nodules (16). The diagnostic efficiency of UGSR is significantly higher than the traditional echo intensity grading scale. However, the current six articles have common deficiencies in that all of the samples comprised patients that did not have HT. Therefore, there is no

relevant study on whether UGSR is effective in differentiating between benign and malignant thyroid nodules in patients with HT.

Through pair-analyzing UGSR and its diagnostic accuracy in two medical centers, this study's objective is to evaluate the value and reproductivity of UGSR in differentiating between PTMCs and benign micronodules (BMNs) in patients with HT to provide a potential reference for improving thyroid imaging reporting and data systems (TI-RADS).

Materials and methods

Participants

The study was performed in accordance with the ethical guidelines of the Helsinki Declaration. It was approved by the Ethics Committee of Affiliated Hangzhou First People's Hospital (IRB-2019-200) and the Ethics Committee of Zhejiang Cancer Hospital (IRB-2020-287). Due to the retrospective nature of the study and the use of anonymized patient data, written informed consent for participation was waived. We identified a total of 4,343 consecutive patients with thyroid nodules who were treated in medical center A (the Affiliated Hangzhou First People's Hospital, Zhejiang University School of Medicine) and 5,414 consecutive patients with thyroid nodules who were treated in medical center B (the Cancer Hospital of the University of Chinese Academy of Sciences, Zhejiang Cancer Hospital) from January 2018 to February 2022. The inclusion criteria were as follows: (1) patients had to have thyroid nodules complicated with HT, confirmed by both surgery and pathology; (2) all cases had to include a preoperative ultrasound examination. The following types of nodules were excluded: (1) nodules with a maximum diameter of >1.0 or<0.4 cm; (2) cystic-dominated nodules in which the cystic component was greater than 50% of the nodule volume (9); (3) calcification-dominated nodules in which the nodules could not be measured due to obvious calcification (12, 13); (4) nodules without thyroid peroxidase antibodies (TPO-Ab) and antithyroglobulin antibodies (TG-Ab) upon examination; (5) unqualified images, including a heterogeneous echo of the thyroid or nodules due to operators' technical factors, diffuse hypoechoic nodules, and insufficient residual thyroid for grayscale values measurement, and more. This resulted in 1,102 patients with 1,380 thyroid nodules who met the inclusion criteria being included in the study. Figure 1 shows the characteristics of the study participants in a flow chart.

Ultrasonic examination

The following six models of ultrasonic diagnostic scanners were used in medical center A: MyLab 70 XVG (Genova, Italy), Esaote MyLab Classic C (Genova, Italy), Esaote MyLab 90 (Genova, Italy), Mindray (Shenzhen, China), Hitachi (Tokyo, Japan), and Philips EPIQ 5 (Washington, USA). The following four models of ultrasonic diagnostic scanners were used in medical center B: Toshiba Aplio 400 (Tochigi, Japan), GE Logiq E9 (Wauwatosa, USA), Siemens Acuson Sequoia (Auburn Hills, USA), and SonoScape S60 VO (Shenzhen, China). In this study, 5–10 MHz broadband linear array probes were used, with the central frequency being 7.5 MHz.

All patients were in the supine position, with their necks fully extended to the far back so that the anterior cervical area was fully exposed. Ultrasonic scanning of lesions was performed

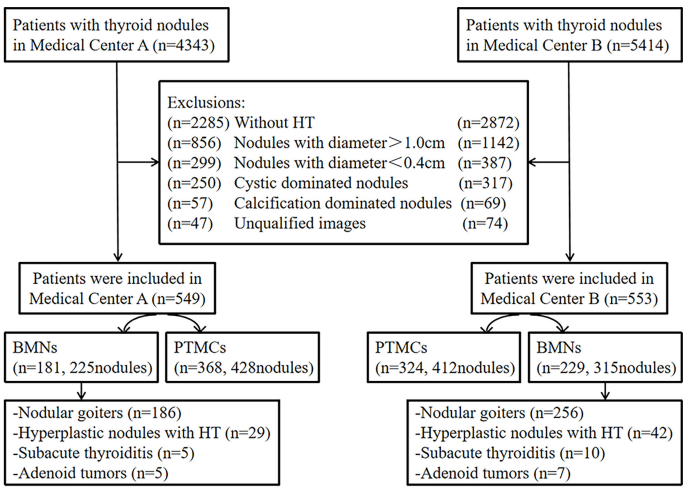

FIGURE 1
Flow chart of the study participants.

in transverse sections, longitudinal sections, and other sections. The number of nodules and their size, shape, boundary, surrounding acoustic halo, internal echo, calcification, and internal and peripheral blood supply as well as the bilateral neck lymph nodes were recorded.

TPO-Ab and TG-Ab tests

Thyroid function tests were performed in all cases before obtaining pathological tissues, and the TPO-Ab and TG-Ab values were recorded. Chemiluminescence immunoassays through the Siemens ADVIA Centaur XP System (Siemens Medical Diagnostics Inc., USA) were used in both medical centers.

Pathology

Tissue specimens were made into 5 μm sections with 10% neutral buffered formalin fixative and hematoxylin–eosin stains in both medical centers. Finally, these sections were examined under a light microscope, and all thyroid nodules were pathologically confirmed.

Image analysis

A radiologist with more than 10 years of experience in both medical centers, who was unaware of the pathological results, independently analyzed the selected cases of picture archiving and communication systems in order to determine the region of interest (ROI) location and the size of the thyroid nodules and their surrounding tissue. This was completed using gray-scale histogram software from RADinfo Systems (Zhejiang Rad Information Technology Co. Ltd., Hangzhou, China). The grayscale value of the nodules and their surrounding tissues were measured in ultrasound transverse or longitudinal section scanning. The ROI was as large as possible (Figures 2, 3) when the echo intensity of the measured nodule was homogeneous. When the echo intensity of the measured nodule was heterogeneous and dominated by a certain echo intensity area, the largest ROI was selected in this echo intensity area (Figures 4, 5). The largest ROI possible was taken when the echo intensity of the measured nodule was heterogeneous without a dominant echo intensity area (Figure 6). Calcification, cystic degeneration, and halo were avoided during all of these measurements (Figure 4). When measuring the surrounding thyroid tissues, the nonnodular echo areas with the largest proportion of the scanned sections and relatively consistent background echoes were selected, and the ROI that was greater than or equal to that of the nodule was adopted (Figures 4–7). Nodules and thyroid tissues that had the same gain levels at the ROI centers were selected. Abnormal echo areas caused by operators' technical factors were avoided. All nodules were measured twice, and the final UGSR of the nodule was derived from the means of two measurements, which were calculated as follows:

$$UGSR_1 = \frac{nodule\ grayscale\ values\ of\ measurement\ 1}{surrounding\ normal\ thyroid\ tissue\ grayscale\ value\ of\ measurement\ 1}$$

$$UGSR_2 = \frac{nodule\ grayscale\ values\ of\ measurement\ 2}{surrounding\ normal\ thyroid\ tissue\ grayscale\ value\ of\ measurement\ 2}$$

FIGURE 2
Female patient, 32 years old, 8-year case history of a thyroid nodule, pathology confirmed as PTMC with HT. TPO-Ab = 90.2 kU/L, TG-Ab>500 kU/L, UGSR = 43.18/95.61 = 0.4516 (medical center A).

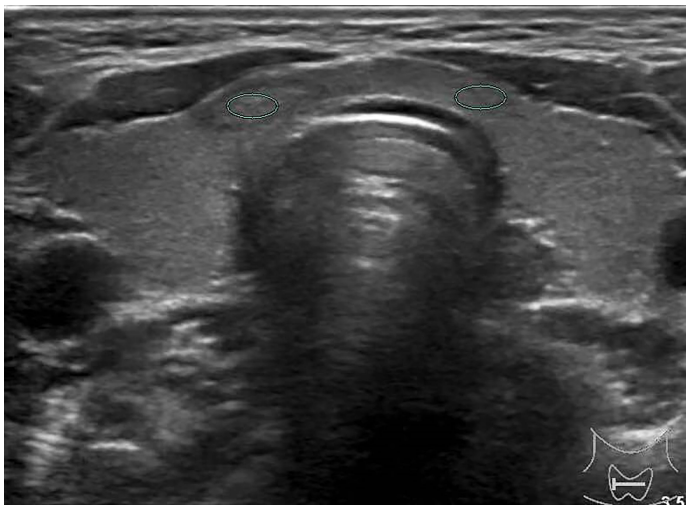

FIGURE 3
Female patient, 37 years old, 1-year case history of a thyroid nodule, pathology confirmed as nodular goiter with HT. TG-Ab = 1005.2 kU/L, TPO-Ab = 109.5kU/L, UGSR = 84.76/77.1 = 1.09945 (medical center B).

FIGURE 4
Female patient, 60 years old, 5-year case history of a thyroid nodule, pathology confirmed as adenomatous goiter with HT. TPO-Ab = 28.3 kU/L, TG-Ab>500 kU/L, UGSR = 78.73/105.3 = 0.7477 (medical center A).

$$UGSR = \frac{UGSR_1 + UGSR_2}{2}$$

Statistical analysis

Statistical analyses were performed using SPSS 26.0 (IBM Corporation, Armonk, NY, USA) and MedCalc 16.8 (MedCalc, Ostend, Belgium). Data are expressed as mean ± standard deviation or median with interquartile range (IR) depending on whether the data fit the normal distribution. Categorical data are reported as numbers. Continuous variables were analyzed using an independent samples *t*-test or a Mann–Whitney *U* test, while categorical variables were compared using a Pearson's Chi-squared test or Fisher's exact test. Receiver operating characteristic (ROC) curves were used to analyze the diagnostic efficiency of UGSR in differentiating between PTMCs and BMNs in patients with HT in medical

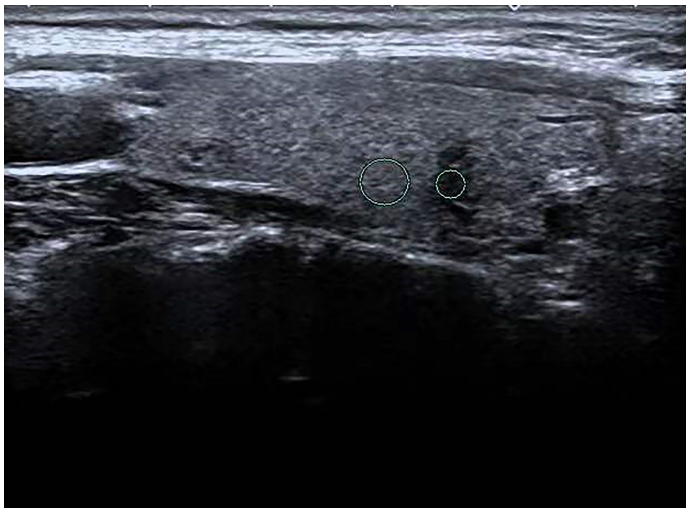

FIGURE 5
Female patient, 45 years old, 1-week case history of a thyroid nodule, pathology confirmed as a hyperplastic nodule with HT. TG-Ab = 115 kU/L, TPO-Ab< 28 kU/L, UGSR = 22.96/73.95 = 0.3105 (medical center B).

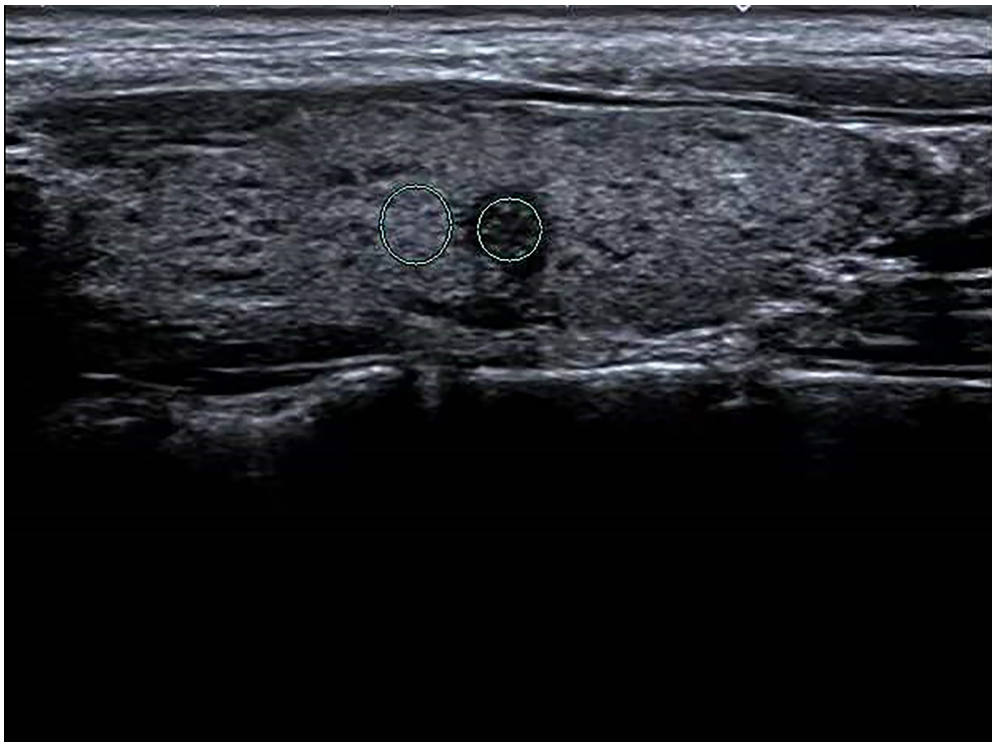

FIGURE 6
Female patient, 33 years old, half-month case history of a thyroid nodule, pathology confirmed as PTMC with HT. TG-Ab = 278 kU/L, TPO-Ab = 600 kU/L, UGSR = 30.04/85.33 = 0.352 (medical center B).

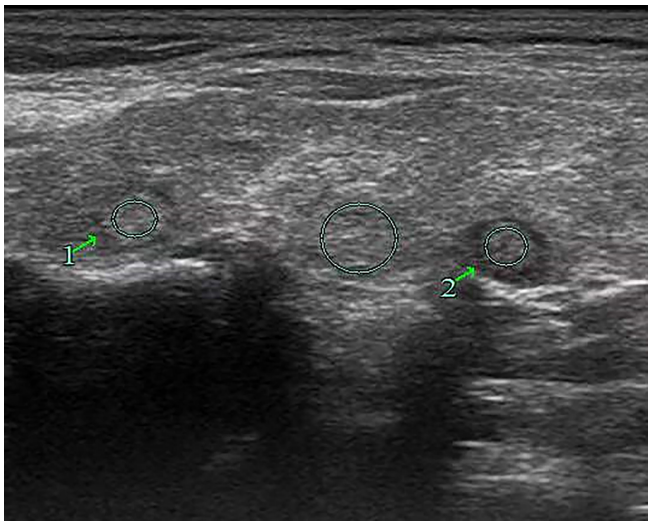

FIGURE 7
Female patient, 63 years old, 1-week case history of a right-side thyroid nodule, pathology confirmed as nodular goiter with HT. TPO-Ab > 1,300 kU/L, TG-Ab = 46.7 kU/L, UGSR 1 = 100.77/98.43 = 1.024, UGSR 2 = 84.82/98.43 = 0.8617 (medical center A).

centers A and B. Differences were considered significant at $p \leq 0.05$.

Results

Distribution of gender, age, size of nodules, TPO-Ab, and TG-Ab levels in PTMCs and BMNs in patients with HT in both medical centers

In both medical centers A and B, the proportion of female patients was significantly higher than that of male patients. The age of the PTMC patients was younger than that of the BMN patients, and the size of the PTMCs was smaller than that of the BMNs. There were no significant differences between the PTMC and BMN patients' TPO-Ab and TG-Ab levels (Table 1).

Distribution of UGSR for PTMC and BMN in patients with HT in both medical centers

In both medical centers, the UGSR of PTMC in patients with HT was significantly lower than that of BMN. There were no significant differences in the UGSR of PTMCs in the two medical centers, while there were significant differences in the UGSR of BMNs in the two medical centers. The UGSR of medical center A was lower than that of medical center B (Table 2).

The ultrasound images of PTMCs are shown in Figures 2, 6, and the ultrasound images of BMNs are shown in Figures 3–5, 7.

Diagnostic efficacy of UGSR in differentiating between PTMCs and BMNs in patients with HT

The AUC (Figure 8), optimal UGSR threshold, sensitivity, specificity, positive predictive value, negative predictive value, and diagnostic accuracy of UGSR in differentiating between PTMCs and BMNs in patients with HT were 0.870 and 0.889, 0.68 and 0.70, 0.921 and 0.898, 0.747 and 0.759, 0.874 and 0.829, 0.832 and 0.848, and 0.861 and 0.836 for medical centers A and B, respectively (Table 3).

Discussion

Ultrasound signs such as hypoechoic regions, irregular shapes, microcalcification, and an aspect ratio greater than 1 are important criteria for diagnosing malignant thyroid nodules (5–10). However, these signs are often judged subjectively by observers, especially in the hypoechoic regions (17). Regarding interobserver variability in thyroid nodule echo intensity, Park et al. (18) had a kappa value of 0.57 when analyzing the differences between three radiologists (with 7 to 10 years of training in thyroid imaging). Persichetti et al. (19) used a kappa value of 0.47 when analyzing the differences between seven thyroid imaging specialists (two radiologists and five endocrinologists

TABLE 1 Distribution of gender, age, size of nodules, TPO-Ab, and TG-Ab levels in PTMCs and BMNs in patients with HT in both medical centers.

Characteristics	Medical center A		Z/χ^2	*p*	Medical center B		Z/χ^2	*p*
	PTMCs	BMNs			PTMCs	BMNs		
Gender (*N*)								
Female	342	166	0.368	0.544	298	210	2.251	0.134
Male	27	16			26	19		
Age (years)								
Range	21~76	26~72			13~78	23~72		
Median (IR)	45 (36.5, 53.5)	53 (44.5, 58.0)	−5.963	<0.001	44 (36.0, 52.0)	50 (43.0, 56.0)	−5.839	<0.001
Size of nodule (mm)								
Range	4~10	4~10			4~10	4~10		
Median (IR)	6 (5, 7)	7 (5, 9)	−4.606	<0.001	6 (5, 8)	7 (6, 8)	−2.944	0.003
TPO-Ab (kU/L)								
Range	28~1300	28~1,300			28~1,300	28~1,300		
Median (IR)	165.5 (42.3, 1,300.0)	134.4 (28.0, 1,300.0)	−1.384	0.166	186.8 (43.5, 1,300.0)	137.0 (28.0, 654.0)	−1.92	0.055
TG-Ab (kU/L)								
Range	15~500	15~500			15~500	15~500		
Median (IR)	112.8 (47.7, 244.6)	132.8 (55.3, 245.6)	−1.074	0.283	156.1 (49.1, 334.4)	143 (45.2, 341.3)	−0.594	0.552

PTMCs, papillary thyroid microcarcinomas; BMNs, benign micronodules; IR, interquartile range.

TABLE 2 Distribution of UGSR in both medical centers.

UGSR	Medical center A	Medical center B	Z	*p*
PTMCs	0.513 (0.442, 0.592)	0.514 (0.431, 0.625)	−0.815	0.415
BMNs	0.857 (0.677, 0.977)	0.917 (0.705, 1.131)	−3.637	<0.001
Z	−15.564	−17.998		
p	<0.001	<0.001		

UGSR, ultrasound grayscale ratio; PTMCs, papillary thyroid microcarcinomas; BMNs, benign micronodules.

with more than 15 years of thyroid imaging training). Itani et al. (17) had a kappa value of 0.141–0.355 when analyzing the differences between four radiologists (none with American College of Radiology TI-RADS training, one radiologist with less than 5 years of experience, and three radiologists with more than 15 years of experience). Kim et al. (20) used a kappa value of 0.57 when analyzing five professionals (with 2–8 years of thyroid imaging training) and a kappa value of 0.23 when analyzing four residents (2 second-year residents with 2 months of thyroid imaging training, and 2 fourth-year residents with 6 months of thyroid imaging training). Additionally, a kappa value of 0.12 was used by Kim et al. for the analysis of two second-year residents. It can be seen that there are large differences in the classification of the echo intensity of thyroid nodules by different observers, especially by the junior doctors who have less experience in imaging diagnosis. Quantifying the echo intensity can greatly reduce observers' subjectivity.

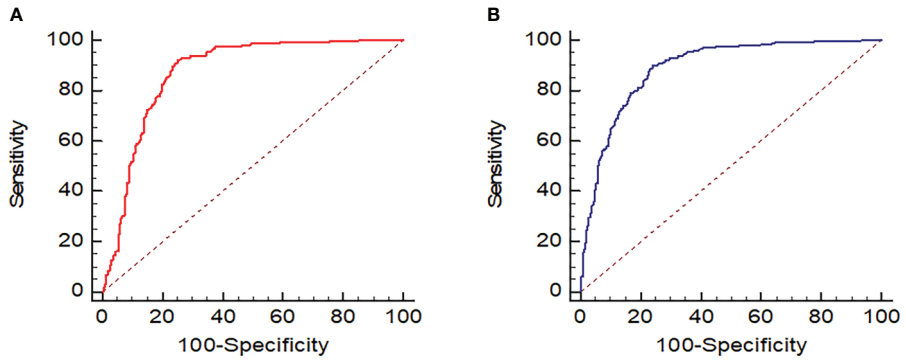

FIGURE 8
ROC of UGSR in differentiating between PTMCs and BMNs in patients with HT. **(A)** ROC of medical center A; **(B)** ROC of medical center B.

TABLE 3 The AUC, the optimal UGSR threshold, and diagnostic efficiency in both medical centers.

Center	AUC	Optimal threshold	Sensitivity	Specificity	PPV	NPV	Accuracy
Center A	0.870	0.68	0.921	0.747	0.874	0.832	0.861
Center B	0.889	0.70	0.898	0.759	0.829	0.8348	0.836

AUC, area under the curve; PPV, positive predictive value; NPV, negative predictive value.

In a quantification study of ultrasound echo intensity of thyroid nodules in 2015, Grani et al. (11) first proposed using UGSR as a method for quantifying the echo intensity of thyroid nodules. However, due to many limitations of their study, including the small sample of malignant nodules, the lack of pathological subtype classification, nodule ungrouping by size, and all nodules being derived from fine needle aspiration cytology rather than pathology, the sensitivity and specificity rates for diagnosing malignant nodules were only 56.7% and 72.0%, respectively. In 2016, Nam et al. (10) proposed using five parameters of the grayscale histogram, including means, skewness, kurtosis, standard deviation, and entropy, as a method for quantifying the echo intensity of thyroid nodules, and this approach's sensitivity and specificity rates in diagnosing malignant nodules were 56.2%–74.4% and 50.0%–61.8%, respectively, which were values that were far from that of the subjective classification by radiologists, which is 94.5% and 77.6%, respectively. The study of Nam et al. was innovative in that the nodule echo intensity was directly quantified by the five parameters of the histogram. However, these parameters were closely related to factors such as ultrasound model, operator, gain, and dynamics, and any changes in those factors would have resulted in a different parameter value. So, the method by Nam et al. has limitations in the quantification of the value of UGSR. In 2018 (13) and 2021 (14), we conducted a controlled study on using UGSR for PTMC and micronodular goiter (MNG) in a single medical center as well as in two medical centers. The AUC, optimal UGSR threshold, sensitivity, and specificity rates were highly consistent between the two studies, with values of 0.895–0.918, 0.691–0.721, 86.8%–88.1%, and 80.4%–83.3%, respectively. These two studies indicate that UGSR has high diagnostic efficiency and good reproducibility. In 2019, Chen et al. (12) used UGSR to differentiate between PTMC and MNG, and the results had an AUC and optimal UGSR threshold that were highly consistent with our previous studies (13, 14), with values of 0.919 and 0.692, respectively. The comparison of the use of UGSR on the same patient during different examination periods can also support UGSR's high diagnostic efficiency and reproducibility. We pair analyzed two sets of ultrasonic images from outpatient examinations and preoperative positioning of the same group of patients with PTMC and MNG in 2022. The results show that the AUC and optimal UGSR thresholds of the two sets were highly consistent at 0.860 and 0.856 as well as 0.649 and 0.646, respectively. It was slightly lower than that of our previous studies, which is due to the difference in the participants.

Grani et al. (11), Chen et al. (12) and our previous studies (13, 14) all show that the diagnostic efficiency of UGSR in differentiating between PTMC and MNG was significantly higher than that of a traditional echo intensity grading method (19–22), the latter of which had a sensitivity value of 62%–93.8% and a specificity value of 21.8%–49.7%. These studies were all based on normal thyroid tissues, while this study pair analyzed the UGSR of PTMCs and BMNs in patients with HT in two medical centers, and the results showed that the AUC, optimal UGSR threshold, sensitivity, and specificity values between the two medical centers were highly consistent, and the AUC and optimal UGSR threshold were almost the same as the previous studies. The results indicate that UGSR can still effectively differentiate between PTMCs and BMNs in patients with HT, and the diagnostic efficiency is also relatively stable (13, 14). Compared to previous studies, this study has a lower specificity of 0.747–0.759 but a higher sensitivity of 0.898–0.921. This suggests that UGSR can identify more PTMCs, thereby lowering the rate of missed diagnoses. However, BMNs can be misdiagnosed as PTMCs more often, especially in terms of hypoechoic hyperplastic nodules and subacute thyroiditis in patients with HT. Therefore, when differentiating between PTMCs and BMNs in patients with HT, in addition to UGSR, a comprehensive analysis of other ultrasonic imaging features, such as morphology, aspect ratio, microcalcification, elastography, and the like, is required. Unexpectedly, in this study, there were differences in the UGSR of BMNs between the two medical centers, which was related to the selected samples. We will further expand the medical centers to conduct a controlled study.

There were certain limitations to this study. Firstly, there were some uncertainties in the selection and measurement of ROI in cases with a heterogeneous echo of thyroid tissue due to ultrasound scanning technology or HT factors. Experienced radiologists in both medical centers conducting ROI measurements and adopting the means of two measurements can reduce the deviation as much as possible. Secondly, in this study, nodular goiter accounts for the majority of BMNs, while nodular HT, adenoma, and subacute thyroiditis account for a smaller proportion. However, this is in line with the objective distribution of BMNs. Thirdly, this study did not further analyze the diagnostic efficiency according to different ultrasound models since the models used for thyroid examination in the

two medical centers were quite different. Fourthly, this study's flaw was the lack of QA in checking the consistency/deviation of all ultrasound systems in both hospitals. At present, an ultrasound phantom imaged by all these systems cannot be realized, which is one of the significances of this study, that is, to explore and popularize the value of UGSR, so that the grayscale value can be directly measured on an ultrasound phantom imaged by all these systems in the near future. Furthermore, though some models are the same, the sample sizes are quite different, which does not allow for an accurate analysis. Fifthly, this study is a retrospective analysis, and there may be some selection bias. A prospective, multicenter controlled study would better verify the value and stability of UGSR.

In conclusion, UGSR still has high sensitivity and diagnostic accuracy in differentiating between PTMCs and BMNs in patients with HT, and the diagnostic efficiency of the two medical centers is highly consistent, which provides an important reference for improving TI-RADS. However, due to the low specificity, other ultrasound signs must be considered when analyzing thyroid nodules.

Data availability statement

The raw data supporting the conclusions of this article will be made available by the authors, without undue reservation.

Author contributions

NF: writing of original draft, acquisition of data, analysis of data, and substantive translation. PW: writing of original draft, acquisition of data, and analysis of data. XK: acquisition of data and preparation, creation, and presentation of the published work. JX: image processing and analysis of data. JY: writing, reviewing, and editing. FC: revising the manuscript. DO: revising the manuscript. LW: data curation, resources, and visualization. DX: providing oversight, leadership, and mentorship external to the core team. ZH: conception and design of the study, critically reviewing the manuscript for important intellectual content, management, and coordinating the execution of the research activity. All authors listed have made a substantial, direct, and intellectual contribution to the work and approved it for publication.

Funding

The study was supported in part by the National Natural Science Foundation of China (82071946), the Zhejiang Provincial Natural Science Foundation of China (LSD19H180001, LY20H180001, and LZY21F030001), and the Zhejiang Provincial Medical and Health Technology Project (2022KY110, 2021RC024, and 2020RC091).

Conflict of interest

The authors declare that the research was conducted in the absence of any commercial or financial relationships that could be construed as a potential conflict of interest.

Publisher's note

All claims expressed in this article are solely those of the authors and do not necessarily represent those of their affiliated organizations, or those of the publisher, the editors and the reviewers. Any product that may be evaluated in this article, or claim that may be made by its manufacturer, is not guaranteed or endorsed by the publisher.

References

1. Ragusa F, Fallahi P, Elia G, Gonnella D, Paparo SR, Giusti C, et al. Hashimotos' thyroiditis: Epidemiology, pathogenesis, clinic and therapy. *Best Pract Res Clin Endocrinol Metab* (2019) 33(6):101367. doi: 10.1016/j.beem.2019.101367

2. Guan H, de Morais NS, Stuart J, Ahmadi S, Marqusee E, Kim MI, et al. Discordance of serological and sonographic markers for hashimoto's thyroiditis with gold standard histopathology. *Eur J Endocrinol* (2019) 181(5):539–44. doi: 10.1530/EJE-19-0424

3. Uhliarova B, Hajtman A. Hashimoto's thyroiditis - an independent risk factor for papillary carcinoma. *Braz J Otorhinolaryngol* (2018) 84(6):729–35. doi: 10.1016/j.bjorl.2017.08.012

4. Liu YJ, Li CQ, Zhao WJ, Wang YG. Hashimoto's thyroiditis is an important risk factor of papillary thyroid microcarcinoma in younger adults. *Horm Metab Res* (2017) 49(10):732–8. doi: 10.1055/s-0043-117892

5. Gul K, Dirikoc A, Kiyak G, Ersoy PE, Ugras NS, Ersoy R, et al. The association between thyroid carcinoma and hashimoto's thyroiditis: the ultrasonographic and histopathologic characteristics of malignant nodules. *Thyroid* (2010) 20(8):873–8. doi: 10.1089/thy.2009.0118

6. Anderson L, Middleton WD, Teefey SA, Reading CC, Langer JE, Desser T, et al. Hashimoto thyroiditis: Part 2, sonographic analysis of benign and malignant nodules in patients with diffuse hashimoto thyroiditis. *AJR Am J Roentgenol* (2010) 195(1):216–22. doi: 10.2214/AJR.09.3680

7. Baser H, Ozdemir D, Cuhaci N, Aydin C, Ersoy R, Kilicarslan A, et al. Hashimoto's thyroiditis does not affect ultrasonographical, cytological, and histopathological features in patients with papillary thyroid carcinoma. *Endocr Pathol* (2015) 26(4):356–64. doi: 10.1007/s12022-015-9401-8

8. Durfee SM, Benson CB, Arthaud DM, Alexander EK, Frates MC. Sonographic appearance of thyroid cancer in patients with hashimoto thyroiditis. *J Ultrasound Med* (2015) 34(4):697–04. doi: 10.7863/ultra.34.4.697

9. Moon WJ, Jung SL, Lee JH, Na DG, Baek JH, Lee YH, et al. Benign and malignant thyroid nodules: US differentiation–multicenter retrospective study. *Radiology* (2008) 247(3):762–70. doi: 10.1148/radiol.2473070944

10. Nam SJ, Yoo J, Lee HS, Kim EK, Moon HJ, Yoon JH, et al. Quantitative evaluation for differentiating malignant and benign thyroid nodules using histogram analysis of grayscale sonograms. *J Ultrasound Med* (2016) 35(4):775–82. doi: 10.7863/ultra.15.05055

11. Grani G, Alessandri M, Carbotta G, Nesca A, Del Sordo M, Alessandrini S, et al. Grey-scale analysis improves the ultrasonographic evaluation of thyroid nodules. *Med (Baltimore)* (2015) 94(27):e1129. doi: 10.1097/MD.0000000000001129

12. Chen XY, Gao M, Hu LF, Zhu JL, Zhang S, Wei X. The diagnostic value of the ultrasound gray scale ratio for different sizes of thyroid nodules. *Cancer Med* (2019) 8(18):7644–9. doi: 10.1002/cam4.2653

13. Han ZJ, Lei ZK, Li MK, Zhu J, Zhang S, Wei X. Differential diagnosis value of the ultrasound gray scale ratio for papillary thyroid microcarcinomas and micronodular goiters. *Quant Imaging Med Surg* (2018) 8(5):507–13. doi: 10.21037/qims.2018.06.04

14. Han ZJ, Feng N, Lu YD, Li MK, Wei PY, Yao JC, et al. A control study on the value of the ultrasound gray scale ratio for the differential diagnosis of thyroid micropapillary carcinoma and micronodular goiter in two medical centers. *Front Oncol* (2021) 10:625238. doi: 10.3389/fonc.2020.625238

15. Gong Y, Yao XZ, Yu LF, Wei P, Han Z, Fang J, et al. Ultrasound gray scale ratio: a reliable parameter for differentiating between papillary thyroid microcarcinoma and micronodular goiter. *BMC Endocr Disord* (2022) 22(1):75. doi: 10.1186/s12902-022-00994-9

16. Lei ZK, Li MK, Luo DC, Wei P, Han Z, Fang J, et al. The clinical significance of ultrasound gray scale ratio (USGR) to differentiate markedly hypoechoic and anechoic minimal thyroid nodules. *J Cancer Res Ther* (2018) 14(7):1567–71. doi: 10.4103/jcrt.JCRT_1031_17

17. Itani M, Assaker R, Moshiri M, Dubinsky TJ, Dighe MK. Inter-observer variability in the American college of radiology thyroid imaging reporting and data system: In-depth analysis and areas for improvement. *Ultrasound Med Biol* (2019) 45(2):461–70. doi: 10.1016/j.ultrasmedbio.2018.09.026

18. Park SJ, Park SH, Choi YJ, Kim DW, Son EJ, Lee HS, et al. Interobserver variability and diagnostic performance in US assessment of thyroid nodule according to size. *Ultraschall Med* (2012) 33(7):E186–90. doi: 10.1055/s-0032-1325404

19. Persichetti A, Stasio ED, Coccaro C, Graziano F, Bianchini A, Donna VD, et al. Inter-and intraobserver agreement in the assessment of thyroid nodule ultrasound features and classificatio nSystems:A blinded multicenter study. *Thyroid* (2020) 30(2):237–42. doi: 10.1089/thy.2019.0360

20. Kim SH, Park CS, Jung SL, Kang BJ, Kim JY, Choi JJ, et al. Observer variability and the performance between faculties and residents: US criteria for benign and malignant thyroid nodules. *Korean J Radiol* (2010) 11(2):149–55. doi: 10.3348/kjr.2010.11.2.149

21. Sharma A, Gabriel H, Nemcek A, Nayar R, Du H, Nikolaidis P. Subcentimeter thyroid nodules: utility of sonographic characterization and ultrasound-guided needle biopsy. *AJR Am J Roentgenol* (2011) 197(6):W1123–8. doi: 10.2214/AJR.10.5684

22. Kim GR, Kim MH, Moon HJ, Chung WY, Kwak JY, Kim EK, et al. Sonographic characteristics suggesting papillary thyroid carcinoma according to nodule size. *Ann Surg Oncol* (2013) 20(3):906–13. doi: 10.1245/s10434-012-2830-4

frontiers | Frontiers in Endocrinology

TYPE Original Research
PUBLISHED 25 August 2022
DOI 10.3389/fendo.2022.955387

OPEN ACCESS

EDITED BY
Terry Francis Davies,
Icahn School of Medicine at Mount Sinai, United States

REVIEWED BY
Xiaowei Ma,
Central South University, China
Yue Chen,
Southwest Medical University, China
Hongcheng Shi,
Fudan University, China

*CORRESPONDENCE
Hua Pang
ph1973@126.com
Zhengjie Wang
bkzg1234@163.com

SPECIALTY SECTION
This article was submitted to Thyroid Endocrinology, a section of the journal Frontiers in Endocrinology

RECEIVED 28 May 2022
ACCEPTED 05 August 2022
PUBLISHED 25 August 2022

CITATION
Liu S, Zuo R, Yang T, Pang H and Wang Z (2022) A semiquantitative study of the optimal whole-body imaging time after ^{131}I therapy for differentiated thyroid cancer. *Front. Endocrinol.* 13:955387. doi: 10.3389/fendo.2022.955387

A semiquantitative study of the optimal whole-body imaging time after ^{131}I therapy for differentiated thyroid cancer

Shuang Liu, Rui Zuo, Tianyu Yang, Hua Pang* and Zhengjie Wang*

Department of Nuclear Medicine, The First Affiliated Hospital of Chongqing Medical University, Chongqing, China

Objective: We compared the efficacy of post-therapy whole-body scintigraphy (Tx-WBS) in terms of detecting lesions in patients with differentiated thyroid cancer (DTC) on days 3, 7, and 10 after ^{131}I treatment, and we determined the optimal imaging time.

Methods: Clinical data from 161 DTC patients treated with ^{131}I were collected. All patients underwent day 3 imaging, but only 98 patients underwent day 3 and day 7 imaging, and 63 patients underwent day 3 and day 10 imaging at the same time. And the thyroid bed uptake was visually graded. The radioactivity ratios of the thyroid bed, neck lymph nodes, lungs, and liver (to the background) were calculated to allow a semiquantitative analysis.

Results: Visual analysis showed that delayed imaging revealed more lymph node and lung radioactivity, early imaging showed more residual thyroid tissue, and significant differences in uptake were apparent at days 3, 7, and 10 ($P < 0.001$). Semiquantitative analysis revealed significant differences in the target-to-background ratios of the residual thyroid bed, lungs, and liver at days 3, 7, and 10. On these days, the imaging sensitivities in terms of detecting metastatic lymph nodes were 29.58%, 39.02%, and 19.35%, and the specificities were 75.56%, 75.86%, and 75% ($P = 0.465$, 0.154, and 0.763, respectively). In terms of lung metastasis detection, the sensitivities were 29.58%, 38.46%, and 13.33% respectively, and the specificities were 98.33%, 100%, and 95.83% ($P < 0.001$, < 0.001, and $P=0.238$).

Conclusion: More residual thyroid tissue can be detected by imaging on day 3; imaging on day 7 more effectively detects lung metastases than does imaging on day 3 or 10.

KEYWORDS

differentiated thyroid carcinoma, post-therapy ^{131}I whole-body scan, semiquantitative study, visual analysis, optimal imaging time

Introduction

A thyroid carcinoma is a malignant tumor originating from the thyroid follicular epithelium or parafollicular epithelial cells. In 2022, thyroid cancer was the seventh most common female tumor, with an incidence of 3% (1), and one of the most common malignant tumors of the head-and-neck endocrine system. Differentiated thyroid cancer (DTC) accounts for more than 95% of all thyroid carcinomas (2). The overall mortality of DTC patients is increasing; some cancer subtypes are prone to extrathyroidal and vascular invasion, high-level recurrence, and metastasis. The prognosis is thus poor (3). Early detection of recurrence and metastasis is important. The 2015 American Thyroid Association (ATA) Management Guidelines for Adult Patients with Thyroid Nodules and Differentiated Thyroid Cancer (4) state that radionuclide ^{131}I therapy can be performed after DTC surgery to remove residual thyroid tissue, reduce the risks of tumor recurrence and death, facilitate follow-up monitoring and timely clinical restaging, and guide follow-up treatment decisions. A post-therapy ^{131}I whole-body scan (Tx-WBS) after ^{131}I treatment evaluates whether residual thyroid tissue has been ablated and detects recurrent or metastatic lesions. The ATA guidelines and those of other societies suggest that Tx-WBS should be performed 2–10 days after ^{131}I treatment (4–7). However, the optimal time remains unknown. Currently, DTC patients undergo multiple examinations; this increases the radiation dose, hospitalization time, and cost. Therefore, it is very necessary for DTC patients to find an optimal imaging time.

Qiu et al. (8) found that the detection capacity of Tx-WBS varied significantly over the 3 consecutive days after ^{131}I treatment for metastatic thyroid cancer; ^{131}I uptake increased linearly, suggesting that lesional detection capacity was related to imaging time. However, no study has compared lesional detection in a large patient sample over 2–10 days; no consensus on the optimal imaging time has emerged. Here, we compared the efficacies of imaging at different times; we provide a theoretical basis for DTC follow-up and treatment.

Material and methods

Study population

This was a retrospective review. A total of 161 patients with DTC treated with ^{131}I in our department from December 2019 to March 2021 were enrolled; 94.4% had papillary cancer. Overall, 68 patients were male, 93 were female, and the mean age was 44.75 ± 14.43 (12–79) years. All stopped taking thyroxine and consumed a low-iodine diet for 4 weeks prior to therapy [to increase the level of thyroid stimulating hormone (TSH) to ≥ 30 μIU/mL]. All patients received oral ^{131}I (100–200 mCi) after formulating personalized treatment plan according to the preoperative evaluation of thyroglobulin (Tg) and antithyroglobulin antibody (TgAb) levels, and neck ultrasound. Tg was measured using a chemiluminescence method (Beckman Coulter Co. Ltd., USA) (range 0–50.03 ng/mL) and thyroid function was analysed *via* radioimmunoassay (Beijing North Institute of Biotechnology Co. Ltd., China). The TSH range was 0.3–5.0 mIU/mL, the TgAb range was 0–4 IU/mL, and the anti-thyroid peroxidase antibody range was 0–9 IU/mL.

^{131}I whole-body imaging

A total of 161 patients underwent whole-body imaging on the 3rd day after ^{131}I treatment, of which 98 patients underwent both 3rd and 7th day imaging, and 63 patients underwent both 3rd and 10th day imaging using a Siemens Symbia T2 single-photon emission computed tomography/computed tomography (SPECT/CT) instrument equipped with a high-energy, parallel hole universal collimator (energy peak 364 keV, window width 20%, magnification 1.0, matrix 256 × 1,024, and scanning speed 15 cm/min). The early imaging was the whole-body imaging on the 3rd day after 131 iodine treatment, and the delayed imaging was the whole body imaging on the 7th and 10th days after 131 iodine treatment. The same two senior nuclear medicine specialists, who were unware of reconstruction protocol, independently and randomly evaluated all Whole-body images. ^{131}I uptake by the oral and nasal cavities, gastrointestinal tract, and salivary glands were physiological; uptake by the residual thyroid and other foci was pathological. Thyroid bed uptake was visually graded: I = not visible; II = suspicious; or III = clearly visible. Circular regions of interest (ROIs) were manually drawn on the forehead, thyroid bed, lungs, and liver of frontal whole-body images and the target-to-background ratios (TBRs) calculated (the forehead served as the background). Recurrence or metastasis was examined *via* puncture biopsy, SPECT/CT imaging, cervical ultrasound, cervical-thoracic CT, and assay of serum Tg levels.

Statistics analysis

SPSS ver. 26.0 statistical analysis software was used. The paired test or χ^2 test was employed to compare groups. The Fisher test was used to compare detection efficiencies. A single-factor analysis of variance was employed to derive correlations among groups. The interobserver agreement for subjective analyses was assessed using kappa coefficients, with a k value of ≤0.20 indicating poor agreement, 0.21-0.40 fair, 0.41-0.60

moderate, 0.61-0.80 good, and ≥ 0.81 excellent agreement. *P* value of < 0.05 was considered statistically significant.

Results

General characteristics

Overall, 86.3% of patients had tumors of diameter ≤ 4 cm; 147 were pathologically diagnosed with lymph node metastases, 49.1% had multiple lesions, 56 evidenced thyroid capsule invasion, and 26.7% showed extra-glandular invasion. The clinical stages were I and II (67.1% and 24.2%, respectively), and There are 14 persons in phase III and IV; 86 people were classified as low risk, 22 as medium risk and 53 as high risk. A total of 105 patients were treated with ^{131}I once and 56 patients several times (Table 1).

Imaging of the residual thyroid, lymph nodes, and lung metastases

We compared the number of thyroid, lymph node, and lung lesions on the imaging of day 3, day 7 and day 10 by visual analysis, respectively. The results showed that imaging of the day 3 showed more residual thyroid tissue (59 vs. 57, 47 vs. 46) (P<0.001) than day 7 and day 10 , while the imaging of day 7 and day 10 showed more lymph node (36 vs. 29, 19 vs. 14) and lung (18 vs. 10, 6 vs. 4) uptake than day 3 imaging (P<0.001). The numbers of Thyroid, lymph node, and lung uptake were statistically different between imaging of day 3 and day 7 and imaging of between day 3 and day 10 (Table 2). The results showed that early imaging was easier to find residual thyroid tissue, and delayed imaging was easier to find lymph nodes and lung metastasis.

TABLE 1 General clinical characteristics of all included patient.

Characters		Patients (N)	(%)
Age	44.75 ± 14.43 (12-79)	161	100
Gender	male	68	42.2
	female	93	57.8
Pathological type	Papillary carcinoma	152	5.6
	Follicular carcinoma	9	94.4
TNM staging	T0	2	1.2
	T1	73	45.3
	T2	43	26.7
	T3	13	8.1
	T4	30	18.6
Clinical stages	I	108	67.1
	II	39	24.2
	III	4	2.5
	IV	10	6.2
Hazard stratification	Low risk	86	53.4
	Moderate risk	22	13.7
	High risk	53	32.9
Maximum diameter of tumor	<2	81	50.3
	2-4	58	36.0
	>4	22	13.7
Lymph node metastasis	Yes	147	91.3
	No	14	8.7
Lesion	Single	82	50.9
	Multiple	79	49.1
Tumor invading capsule	Yes	56	34.8
	No	105	65.2
Extra-glandular invasion	Yes	43	26.7
	No	118	73.3
^{131}I course of treatment	1	105	65.2
	2	34	21.1
	>2	22	13.7

TABLE 2 Comparison the numbers of lesions on day 3, day 7 and day 10 images.

Time	N	Thyroid bed	Statistics	*P*	lymph nodes	Statistics	*P*	Lung	Statistics	*P*
Day 3	98	59	77.57	0.000	29	27.13	0.000	10	28.21	0.000
Day 7	98	57			36			18		
Day 3	63	47	45.67	0.000	14	9.95	0.000	4	21.25	0.000
Day 10	63	46			19			6		
Day 7	98	57	3.67	0.055	36	0.74	0.391	18	2.36	0.124
Day 10	63	46			17			6		

Comparison of early and delayed imaging in terms of thyroid uptake grade

Through visual analysis, we can see that on the third day of imaging, there were 60 patients (60/161) with thyroid uptake grade I, 22 patients (22/161) with II grade and 79 patients (79/161) with III grade. On the 7th day, thyroid uptake was grade I in 33 patients (33/98), grade II in 28 patients (28/98) and grade III in 37 patients (37/98). In the 10th day imaging, thyroid uptake was grade I in 15 patients (15/63), II in 22 patients (22/63), and III in 26 patients (26/63). There was moderate to good interobserver agreement for all images at Whole-body images (kappa=0.60-0.80).The χ^2 test revealed significant differences in uptake grade between 3rd and 7th day imaging and 3rd and 10th day imaging (both $P < 0.001$) (Table 3). Day 3 imaging revealed more grade III uptakes, but on day 7 imaging more grade I and grade II uptakes. For example, the thyroid gland of 8 patients was not shown in the imaging on the 3rd day (the uptake grade was grade I), but it was clearly shown in the imaging on the 7th day. The day 3, day 7, and day 10 images differed in terms of thyroid uptake. Day 3 imaging detected obvious residual thyroid tissue; only minimal residual tissue was apparent on day 7.

The thyroid, lung, and liver TBRs

Semiquantitatively, the TBR of residual thyroid tissue decreased over time. The lung TBR was highest on 7th imaging; that of the liver increased with time. The thyroid TBR differed significantly between the day 3 and day 7 images (x ± S: 7.50 ± 14.27 vs. 4.70 ± 6.54, $P = 0.025$) but not between the day 3 and day 10 or day 7 and day 10 images (x ± S: 8.99 ± 24.887 vs. 5.73 ± 12.36; 4.70 ± 6.54 vs. 5.73 ± 12.37, P = 0.298 and 0.493, respectively). The left lung, right lung and liver TBRs differed significantly between days 3 and 7 and 3 and 10 (Left lung TBR x ± S: 1.79 ± 0.73 vs. 2.85 ± 4.20, 1.89 ± 0.86 vs. 2.31 ± 1.32, P=0.010, 0.020; Right lung TBR x ± S: 1.77 ± 0.72 vs. 2.64 ± 2.34; 1.84 ± 0.77 vs. 2.25 ± 1.26, P<0.001, P =0.019; Liver TBR x ± S: 1.93 ± 1.53 vs. 3.79 ± 3.43, 1.85 ± 0.88 vs. 3.24 ± 0.88, P<0.001, P=0.004) but not between days 7 and 10(Left lung TBR x ± S: 2.85 ± 4.20 vs. 2.31 ± 1.32, P=0.318; Right lung TBR x ± S: 2.64 ± 2.34 vs. 2.25 ± 1.26, P=0.171; Liver TBR x ± S: 3.79 ± 3.44 vs. 3.24 ± 0.88, P=0.330) (Figure 1). A residual thyroid is most obvious early; lung metastasis is most obvious at day 7.

Detection of metastases

Cervical ultrasound, partial lymph node biopsy, cervical-thoracic CT before ^{131}I treatment, and the injection of serum irritant Tg before treatment, revealed 71 patients with cervical lymph node metastases and 41 with lung metastases. Day 3 images revealed 43 cervical lymph node, and 14 lung uptakes; the figures for days 7 and 10 were 36, and 18; and 19, and 6, respectively. The data were evaluated using the Fisher test. The sensitivities of day 3, day 7, and day 10 images in terms of metastatic lymph node detection were 29.58%, 39.02%, and 19.35%; and the specificities were 75.56%, 75.86%, and 75%, respectively. The three imaging modalities similarly detected metastatic lymph nodes (P = 0.465, 0.763, and 0.154, respectively). In terms of lung metastases, the sensitivities of

TABLE 3 Comparison of day 3, day 7 and day 10 imaging in terms of thyroid uptake grade.

	grades of thyroid gland	Day 3			χ^2	*P*
		Grade I	Grade II	Grade III		
Day 7 (n = 98)	Grade I	30	2	1	73.630	0.000
	Grade II	7	8	13		
	Grade III	1	2	34		
Day 10 (n = 63)	Grade I	14	1	0	42.967	0.000
	Grade II	5	8	9		
	Grade III	3	1	22		

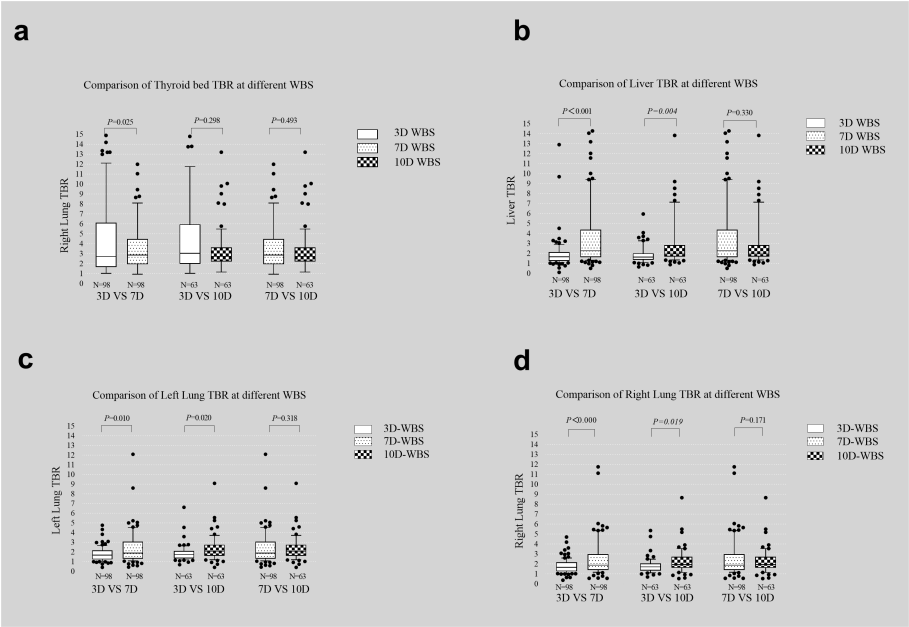

FIGURE 1
Comparison of thyroid bed **(A)**, liver **(B)**, left lung **(C)**, and right lung **(D)** TBR on day 3, day 7 and day 10 images.

day 3, day 7, and day 10 images were 29.58%, 38.46%, and 13.33%, and the specificities were 98.33%, 100%, and 95.83%, respectively ($P < 0.001$, < 0.001, and 0.238); day 7 imaging most effectively detected such metastases.

Here are two typical cases. One is a 31-year-old male with no 131 iodine uptake was found in the lungs on the 3rd day, but diffuse radioactive iodine uptake in both lungs was found on the 7th day (Figure 2). The other is a 71-year-old female, whose right neck was no obvious 131 iodine uptake on the 3rd day, but obvious radioactive iodine uptake in the right cervical lymph nodes on the 7th day (Figure 3).

Discussion

Tx-WBS sensitively detects metastatic lesions that take up iodine and locates lesions that are not evident on cervical ultrasound, CT, or magnetic resonance imaging. Tx-WBS reveals new lesions in 6–13% of patients; 8.3% are restaged (in terms of the tumor) and follow-up treatment and management adjusted accordingly (9). Tx-WBS is used to restage DTC and plan follow-up ^{131}I treatment. However, few studies have explored the optimal imaging time; a small number of retrospective studies on limited numbers of patients have shown that imaging detection efficiency varies with time.

Our larger study allowed us to draw certain conclusions. The number of residual thyroid uptakes on day 3 was twice those on days 7 and 10. In terms of lung metastasis, the sensitivity and specificity of day 7 images were significantly higher than those of day 3 and day 10 images, and the number of lymph node metastases evident on day 7 was 25–30% higher than on days 3 and 10.

Hung et al. (10) and Salvatoria et al. (11) reported that days 3–4 and 5–7 images did not differ significantly in terms of lesion numbers; day 10 images revealed fewer lesions. Lee (12) found that early imaging better detected thyroid residues and ^{131}I-positive metastatic lesions than delayed imaging (the uptake rates were higher early), and that diffuse liver uptake was more common in delayed than early images (86 vs. 6%). However, Khan, Chong, and Kodani et al. (13–15) concluded that day 7 imaging was more sensitive (all tissues) than day 3 imaging. The cited authors compared only day 3 and day 7 images. We imaged on days 3, 7, and 10; early imaging revealed more residual thyroid tissue but delayed imaging more lymph node and lung lesions, unlike what was reported by Hung (10) and Salvatoria et al. (11). The cited authors performed visual analyses only. However, most cervical uptakes evident on whole-body images cannot be visually assigned to residual thyroid tissue or cervical lymph node metastases. We subjected SPECT/CT scans to visual analysis but also performed cervical and thoracic CT to evaluate the neck. This revealed that many lesions that were suspect cervical lymph nodes on whole-body scans were in fact residual thyroid lesions. Also, we derived semiquantitative lesion uptakes.

We found that the TBR of the residual thyroid bed decreased gradually with time; the lung TBR was highest on day 7, and the

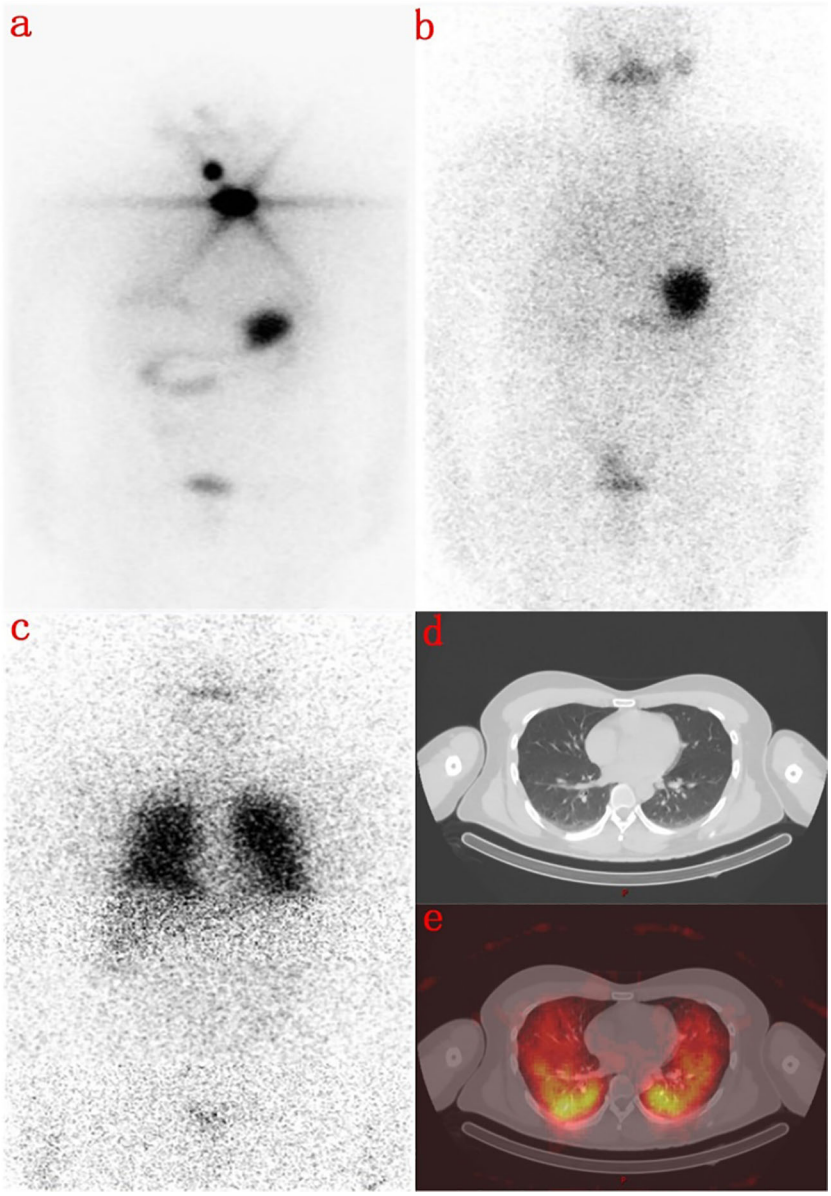

FIGURE 2
A 31-year-old male with total thyroidectomy one year ago. **(A)** shows a radioactive concentration in the residual thyroid on the first ^{131}I WBS imaging performed 8 months ago. **(B)** shows that there was no abnormal concentration of radioactivity on the day 3 imaging after second ^{131}I therapy. **(C)** shows that there was no display in the residual thyroid but a diffuse abnormal radioactive concentration in both lungs in the day 7 imaging. **(D)** is the Chest CT image, and **(E)** shows that lung metastasis of thyroid cancer on the day 7 with SPECT/CT fusion image.

liver TBR increased gradually. The early high uptake by residual thyroid tissue may be followed by a gradual decrease (clearance of the initial uptake) over time from metastatic cells, reducing the TBR. The pulmonary TBR on day 7 imaging was higher than on days 3 and 10, perhaps because ^{131}I uptake and excretion by pulmonary metastatic lesions are slower than those of residual tumor cells or because further acquisition of ^{131}I by malignant cells increased the TBR (16). The peak ^{131}I uptake (at approximately 6–7 days) decreased gradually over time; the day 10 uptake was lower than that on day 7. Some studies have suggested that on days 6–8 after ^{131}I-labelled thyroid hormone is released into the blood, the physiological uptake by the liver begins to increase (17–19). It is also possible that the Na^+/I^- symporter, a nonspecific iodine protein, and polyiodide

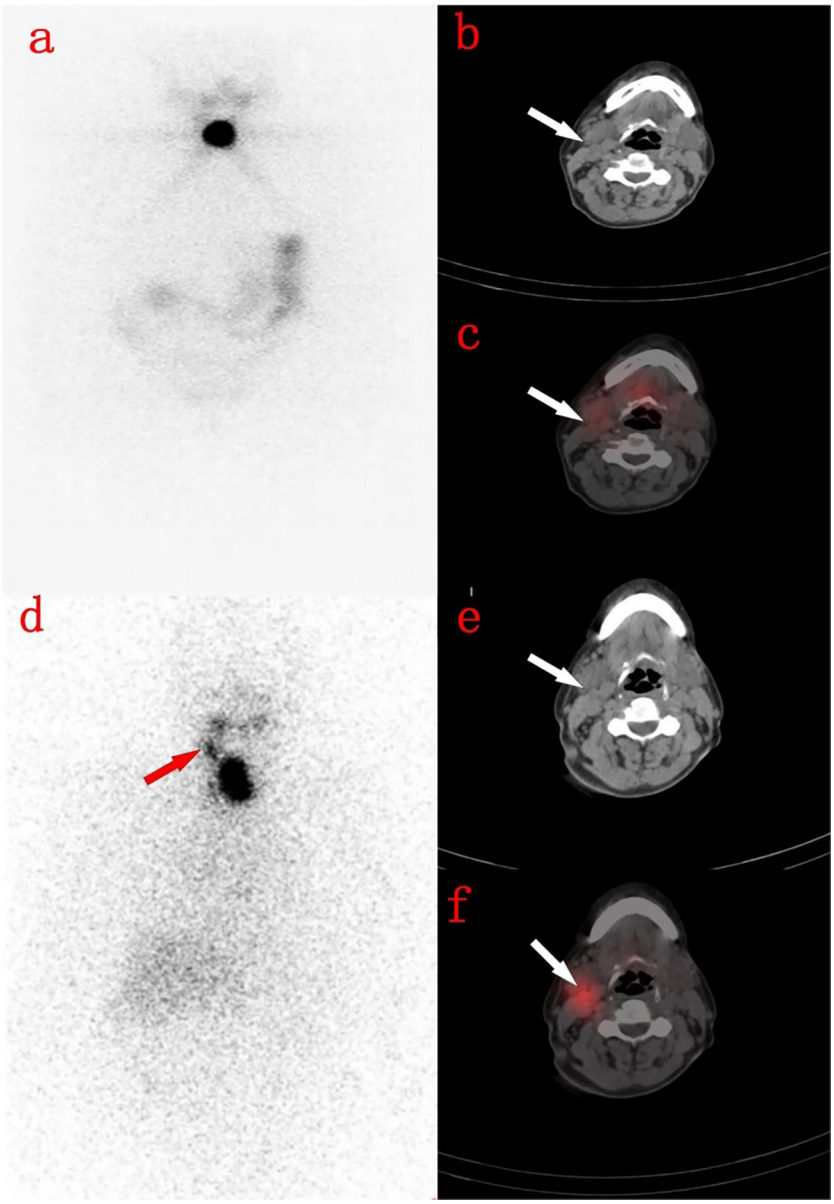

FIGURE 3
A 71-year-old woman with thyroidectomy 4 months ago. **(A)** shows the residual thyroid on the day 3 imaging. **(B)** shows the right cervical lymph nodes on the neck CT image. **(C)** shows the right cervical lymph nodes without radioactive uptake on the 3rd day SPECT/CT fusion image. **(D)** shows residual thyroid on the 7th day WBS, with radioactive accumulation in the right neck. **(E)** shows the right neck lymph nodes on the neck CT image. **(F)** shows the right neck lymph nodes showed radioactive accumulation on the 7th day SPECT/CT fusion image.

peroxidase in hepatocytes absorb iodine (20), but that the iodine uptake capacity is lower than that in thyroid tissue. Thus, the liver TBR increases gradually with time.

Besides, we found that the number of lymph nodes evident on day 7 images was greater than on day 3 and day 10 images, but the sensitivity and specificity of metastatic lymph node detection did not change over time. In terms of lung metastases, the sensitivities on days 3, 7, and 10 were 29.58, 38.46, and 13.33%, respectively, and the specificities were 98.33, 100, and 95.83%. Day 7 images optimally revealed lung metastases (with statistical significance). A high TBR aids the detection of metastases; the TBR probably rises over time. The ^{131}I clearance rates by physiological and pathological lesions differ, explaining the different detection rates of early and delayed scans. ^{131}I absorption and excretion by lung and bone metastases are slower than those of thyroid residues; delayed

scans better detect metastatic lesions. Our semiquantitative data and our comparisons of sensitivity and specificity confirmed that day 7 imaging better detected pulmonary metastases than day 3 and day 10 imaging. In summary, on visual analysis, day 3 imaging optimally detects residual thyroid tissue, but day 7 and day 10 imaging better detects cervical lymph node and lung metastases. Our semiquantitative analysis revealed that day 7 imaging better detected lung metastases than day 3 imaging.

Our work has certain limitations. Not all metastatic lesions were confirmed *via* pathological biopsy; we relied principally on SPECT/CT, cervical-thoracic CT, and laboratory indicators. Also, the ROIs were manually outlined, albeit by very experienced professionals. There is a possibility of bias.

Conclusion

We suggest that residual thyroid tissue in patients at low risk of metastasis should be screened on day 3 only; there is no need for delayed imaging. This reduces the radiation dose and costs, and the hospital stay. For patients at high risk of metastasis, additional imaging on day 7 optimally detects metastatic lesions and thus facilitates follow-up treatment.

Data availability statement

The raw data supporting the conclusions of this article will be made available by the authors, without undue reservation.

Ethics statement

The studies involving human participants were reviewed and approved by The ethics committee of the First affiliated Hospital of Chongqing Medical University. Written informed consent for participation was not required for this study in accordance with the national legislation and the institutional requirements. Written informed consent was obtained from the individual(s) for the publication of any potentially identifiable images or data included in this article.

Author contributions

ZW and HP contributed to conception and design of the study. RZ organized the database. SL and TY performed the statistical analysis. SL and RZ have been involved in drafting the manuscript and revising it critically for important intellectual content. All authors contributed to the article and approved the submitted version.

Funding

This work is supported by Chongqing medical scientific research project (2021MSXM042)、General program of Chongqing Nature Science Foundation (cstc2020jcyj-maxmX0713, 0301020499QC-W0117).

Conflict of interest

The authors declare that the research was conducted in the absence of any commercial or financial relationships that could be construed as a potential conflict of interest.

Publisher's note

All claims expressed in this article are solely those of the authors and do not necessarily represent those of their affiliated organizations, or those of the publisher, the editors and the reviewers. Any product that may be evaluated in this article, or claim that may be made by its manufacturer, is not guaranteed or endorsed by the publisher.

References

1. Siegel RL, Miller KD, Fuchs HE, Jemal A. Cancer statistics, 2022. *CA Cancer J Clin* (2022) 72(1):7–33. doi: 10.3322/caac.21708

2. Seib CD, Sosa JA. Evolving understanding of the epidemiology of thyroid cancer. *Endocrinol Metab Clin North Am* (2019) 48(1):23–35. doi: 10.1016/j.ecl.2018.10.002

3. Kazaure HS, Roman SA, Sosa JA. Aggressive variants of papillary thyroid cancer: incidence, characteristics and predictors of survival among 43,738 patients. *Ann Surg Oncol* (2012) 19(6):1874–80. doi: 10.1245/s10434-011-2129-x

4. Haugen BR, Alexander EK, Bible KC, Doherty GM, Mandel SJ, Nikiforov YE, et al. 2015 American Thyroid association management guidelines for adult patients with thyroid nodules and differentiated thyroid cancer: The American thyroid association guidelines task force on thyroid nodules and differentiated thyroid cancer. *Thyroid* (2016) 26(1):1–133. doi: 10.1089/thy.2015.0020

5. Luster M, Clarke SE, Dietlein M, Lassmann M, Lind P, Oyen WJ, et al. Guidelines for radioiodine therapy of differentiated thyroid cancer. *Eur J Nucl Med Mol Imaging* (2008) 35(10):1941–59. doi: 10.1007/s00259-008-0883-1

6. Iwano S, Kato K, Nihashi T, Ito S, Tachi Y, Naganawa S. Comparisons of I-123 diagnostic and I-131 post-treatment scans for detecting residual thyroid tissue and metastases of differentiated thyroid cancer. *Ann Nucl Med* (2009) 23(9):777–82. doi: 10.1007/s12149-009-0303-z

7. Cooper DS, Doherty GM, Haugen BR, Kloos RT, Lee SL, Mandel SJ, et al. Revised American thyroid association management guidelines for patients with thyroid nodules and differentiated thyroid cancer. *Thyroid* (2009) 19(11):1167–214. doi: 10.1089/thy.2009.0110

8. Qiu L, Tan H, Yin H, Zhou J, Cheng D, Shi H. Comparison of post-therapeutic sequential 131I whole-body scans in the detection of metastatic

thyroid cancer. *Q J Nucl Med Mol Imaging* (2020) 64(3):313–20. doi: 10.23736/S1824-4785.18.03074-1

9. Souza RP, Barroso AL, Rezende LL, Padrão EL, Fagundes TA, Penna GC, et al. Post I-131 therapy scanning in patients with thyroid carcinoma metastases: An unnecessary cost or a relevant contribution? *Clin Nucl Med* (2004) 29(12):795–8. doi: 10.1097/00003072-200412000-00005

10. Hung BT, Huang SH, Huang YE, Wang PW. Appropriate time for post-therapeutic I-131 whole body scan. *Clin Nucl Med* (2009) 34(6):339–42. doi: 10.1097/RLU.0b013e3181a345be

11. Salvatori M, Perotti G, Villani MF, Mazza R, Maussier ML, Indovina L, et al. Determining the appropriate time of execution of an I-131 post-therapy whole-body scan: Comparison between early and late imaging. *Nucl Med Commun* (2013) 34(9):900–8. doi: 10.1097/MNM.0b013e328363cc5c

12. Lee JW, Lee SM, Koh GP, Lee DH. The comparison of (131)I whole-body scans on the third and tenth day after (131)I therapy in patients with well-differentiated thyroid cancer: preliminary report. *Ann Nucl Med* (2011) 25(6):439–46. doi: 10.1007/s12149-011-0486-y

13. Khfan S, Waxman A, Nagaraj N. Optimization of post ablative I-131 scintigraphy: Comparison of 2 day vs. 7 day post therapy study in patients with differentiated thyroid cancer (DTC). *J Nucl Med* (1994) 35(5):15.

14. Kodani N, Okuyama C, Aibe N, Matsushima S, Yamazaki H. Utility of additional delayed post-therapeutic (1)(3)(1)I whole-body scanning in patients with thyroid cancer. *Clin Nucl Med* (2012) 37(3):264–7. doi: 10.1097/RLU.0b013e3182444286

15. Chong A, Song HC, Min JJ, Jeong SY, Ha JM, Kim J, et al. Improved detection of lung or bone metastases with an I-131 whole body scan on the 7th day after high-dose I-131 therapy in patients with thyroid cancer. *Nucl Med Mol Imaging* (2010) 44(4):273–81. doi: 10.1007/s13139-010-0051-y

16. Coakley AJ, Page CJ, Croft D. Scanning dose and detection of thyroid metastases. *J Nucl Med* (1980) 21(8):803–4.

17. Chung JK, Lee YJ, Jeong JM, Lee DS, Lee MC, Cho BY, et al. Clinical significance of hepatic visualization on iodine-131 whole-body scan in patients with thyroid carcinoma. *J Nucl Med* (1997) 38(8):1191–5.

18. Ziessman HA, Bahar H, Fahey FH, Dubiansky V. Hepatic visualization on iodine-131 whole-body thyroid cancer scans. *J Nucl Med* (1987) 28 (9):1408–11.

19. Nakayama M, Okizaki A, Sakaguchi M, Ishitoya S, Uno T, Sato J, et al. A quantitative evaluation of hepatic uptake on I-131 whole-body scintigraphy for postablative therapy of thyroid carcinoma. *Med (Baltimore)* (2015) 94(28):e1191. doi: 10.1097/MD.0000000000001191

20. Omur O, Akgun A, Ozcan Z, Sen C, OzkiliÇ H. Clinical implications of diffuse hepatic uptake observed in postablative and post-therapeutic I-131 scans. *Clin Nucl Med* (2009) 34(1):11–4. doi: 10.1097/RLU.0b013e31818f433c

frontiers | Frontiers in Endocrinology

TYPE Original Research
PUBLISHED 05 September 2022
DOI 10.3389/fendo.2022.938008

OPEN ACCESS

EDITED BY
Emerita Andres Barrenechea,
Veterans Memorial Medical Center,
Philippines

REVIEWED BY
Weiping Teng,
The First Affiliated Hospital of China Medical University, China
Jincao Yao,
University of Chinese Academy of Sciences, China

*CORRESPONDENCE
Xinlin Zhang
xinlzhang0807@163.com
Dalong Zhu
zhudalong@nju.edu.cn

†These authors have contributed equally to this work

SPECIALTY SECTION
This article was submitted to Thyroid Endocrinology, a section of the journal Frontiers in Endocrinology

RECEIVED 06 May 2022
ACCEPTED 15 August 2022
PUBLISHED 05 September 2022

CITATION
Zhang X, Ze Y, Sang J, Shi X, Bi Y, Shen S, Zhang X and Zhu D (2022) Risk factors and diagnostic prediction models for papillary thyroid carcinoma.
Front. Endocrinol. 13:938008.
doi: 10.3389/fendo.2022.938008

Risk factors and diagnostic prediction models for papillary thyroid carcinoma

Xiaowen Zhang[1†], Yuyang Ze[2†], Jianfeng Sang[3], Xianbiao Shi[3], Yan Bi[1], Shanmei Shen[1], Xinlin Zhang[4*] and Dalong Zhu[1*]

[1]Department of Endocrinology and Metabolism, Endocrine and Metabolic Disease Medical Center, Nanjing University Medical School Affiliated Drum Tower Hospital, Nanjing, China, [2]Department of Endocrinology and Metabolism, The Fifth People's Hospital of Suzhou Wujiang, Suzhou, China, [3]Department of Thyroid Surgery, Nanjing University Medical School Affiliated Drum Tower Hospital, Nanjing, China, [4]Department of Cardiology, Nanjing University Medical School Affiliated Drum Tower Hospital, Nanjing, China

Thyroid nodules (TNs) represent a common scenario. More accurate pre-operative diagnosis of malignancy has become an overriding concern. This study incorporated demographic, serological, ultrasound, and biopsy data and aimed to compare a new diagnostic prediction model based on Back Propagation Neural Network (BPNN) with multivariate logistic regression model, to guide the decision of surgery. Records of 2,090 patients with TNs who underwent thyroid surgery were retrospectively reviewed. Multivariate logistic regression analysis indicated that Bethesda category (OR=1.90, P<0.001), TIRADS (OR=2.55, P<0.001), age (OR=0.97, P=0.002), nodule size (OR=0.53, P<0.001), and serum levels of Tg (OR=0.994, P=0.004) and HDL-C (OR=0.23, P=0.001) were statistically significant independent differentiators for patients with PTC and benign nodules. Both BPNN and regression models showed good accuracy in differentiating PTC from benign nodules (area under the curve [AUC], 0.948 and 0.924, respectively). Notably, the BPNN model showed a higher specificity (88.3% vs. 73.9%) and negative predictive value (83.7% vs. 45.8%) than the regression model, while the sensitivity (93.1% vs. 93.9%) was similar between two models. Stratified analysis based on Bethesda indeterminate cytology categories showed similar findings. Therefore, BPNN and regression models based on a combination of demographic, serological, ultrasound, and biopsy data, all of which were readily available in routine clinical practice, might help guide the decision of surgery for TNs.

KEYWORDS

papillary thyroid carcinoma, logistic regression analysis, back propagation neural network, diagnostic prediction, Bethesda category

1 Introduction

The incidence of thyroid cancer has increased remarkably worldwide in recent years (1), with a more than 3-fold increase from 1974 to 2013 in the United States (2, 3). Thyroid cancer has also become the fastest-growing cancer among women at the beginning of this century in China (4). The sharp increase in the incidence of thyroid nodules (TNs) (5), although most of which are benign, adds to the burden of health system (6). Accurate pre-operative diagnosis of potentially malignant tumors is warranted.

Most guidelines recommend ultrasound as the first diagnostic approach for TNs. Thyroid Imaging Reporting and Data Systems (TI-RADS) are widely used to guide clinical practice. Recommendations for diagnostic fine-needle aspiration biopsy (FNAB) of TNs are based on sonographic features combined with nodule sizes. Following biopsy, the Bethesda System for Reporting Thyroid Cytopathology is used worldwide to classify FNAB cytology findings and determine whether surgery is needed. However, there are limitations with the categorical Bethesda system. Bethesda III and IV cytology diagnoses, known as indeterminate, comprise approximately 30% of FNAB results (7); and management of this group of patients varies widely from clinical observation, ultrasound follow up, repeat FNAB, molecular test to thyroid surgery. Overdiagnosis and surgery of thyroid cancer are common in clinical practice. Therefore, developing a systematic method to differentiate patients with papillary thyroid carcinomas (PTC) from benign nodules is important to guide surgery decision.

A back propagation neural network (BPNN) model is a kind of classical nonlinear artificial neural network (ANN) model based on the Deepest-Descent technique. When provided with sufficient hidden units, it will repeatedly adjust the weights of connections in the network and minimize the error of nonlinear functions between the actual and expected output values. First proposed in 1986 (8), BPNN has been applied to help clinical diagnosis, imaging, and prognosis prediction (9). Multiple studies have focused on using ultrasound images of TNs in deep convolutional neural networks (10, 11). However, to our knowledge, no study has yet combined demographic, serological, ultrasound, and biopsy data into one model. In this study, we aimed to construct a new diagnostic prediction model of PTC based on BPNN and compare it with conventional multivariate logistic regression model.

2 Materials and methods

2.1 Human subjects

This study protocol was approved by the Ethics Committee of Nanjing Drum Tower Hospital Institutional Review Board, and consent was waived for this retrospective study. We conducted a retrospective analysis of consecutive patients who underwent thyroid surgery due to TNs in the Department of Thyroid Surgery of Nanjing Drum Tower Hospital from January 2018 to January 2021. The inclusion criteria were as follows (1): aged 18 years or older (2), undergoing thyroidectomy (total thyroidectomy, unilateral and isthmic excision, double-lobed subtotal excision, etc.) (3), post-operative pathologic diagnosis was PTC or benign TNs. The exclusion criteria were as follows (1): history of other malignancies (2), previous thyroid surgery (3), incomplete clinical data (4), liver failure, renal failure, or severe infection in the last 3 months.

2.2 Demographic data, serum hormone and biochemical analysis

Baseline demographic characteristics including age, gender, family history of thyroid tumor, history of radiation, blood pressure, and body mass index (BMI) were collected. Serum thyroid-stimulating hormone (TSH), free triiodothyronine (FT3), free thyroxine (FT4), thyroid autoantibodies [TAb; thyroid peroxidase antibody (TPOAb) and thyroglobulin antibody (TgAb)], and thyroglobulin (Tg) concentrations were detected by electrochemical luminescence assays with Cobas Eless 601 (Roche Diagnostics, Basel, Switzerland). The reference ranges of TSH, TPOAb, and TgAb were 0.27–4.2 mIU/L, 0–34 IU/ml, and 0–115 IU/ml, respectively, as provided by the manufacturer. Serum high-density lipoprotein cholesterol (HDL-C) levels were tested with standard enzymatic methods (Kyowa Medex Co., Ltd. Tokyo, Japan), and serum low-density lipoprotein cholesterol (LDL-C) levels were measured with selective melt method (Kyowa Medex Co., Ltd. Tokyo, Japan).

2.3 Thyroid ultrasonography

All patients underwent two rounds of thyroid ultrasound examinations before surgery. They first received one in the out-patient department, by a sonologist randomly determined by the clinic appointment system. When they were hospitalized in the Thyroid Surgery Department, they received their second ultrasound test, performed by two specified sonologists with over 10-year experience. The sonologists were unaware of the cytopathology and histopathology, as well as of laboratory results of the patients. Kwak-TIRADS criteria were applied to each nodule for categorization. When more than one nodule was present in the thyroid, the nodule with the highest TIRADS score was chosen for analysis. The radiology reports were extracted from clinical records.

2.4 Thyroid nodule pathology

The ultrasound-guided FNAB was conducted by a senior sonologist, and the FNAB cytology slides were examined

according to the Bethesda System for Reporting Thyroid Cytopathology (7). The pathologists were blinded to the sonographic diagnosis of TNs. The FNAB results were classified into six categories, and Bethesda III to V cytopathology were categorized as indeterminate cytology (12).

2.5 Statistical analyses

Continuous variables were presented as means ± standard deviation and categorical variables as numbers with percentages. Differences between patients with benign nodules and PTC were analyzed using the independent sample t test for continuous variables, and $\chi 2$ test for categorical variables. Logistic regression analysis was performed to identify differentiating variables for patients with benign nodules from PTC. To account for the risk of type 1 error due to multiple comparison, Bonferroni correction was applied with an adjusted P value threshold of 0.003 (0.05/16). Variables with statistical significance (P<0.003) in univariate analysis and those with a high clinical relevance were included in multivariable logistic regression analysis with a backward stepwise selection mode.

Ten patients receiving first-round ultrasound examinations by one sonologist were assigned to receive the second-round ultrasound test by the other one. Interobserver variability of ultrasound features obtained from two sonologists was investigated by using intraclass correlation coefficients. Intraclass correlation coefficients less than 0.40 indicate poor agreement; 0.41–0.75, moderate agreement; and 0.75 or greater, good agreement. SPSS v26.0 software (IBM Corp., Armonk, NY, United States) was used for these statistical analyses.

2.6 BPNN model

2.6.1 Basic principles and parameter selection

ANN models are statistical models that simulate the cognitive processes of human brain, consisting of mess of neuron nodes. Compared with the traditional statistical methods or computer algorithms, it has good fault tolerance, highly non-linear, self-learning, self-organization, and self-adaptability (13). BPNN is one of the most widely used classical types of ANN. It includes an input layer, an output layer, and several hidden layers. Information propagates forward from the input layer to the hidden layer and the output layer. In each neuron, the information input from the previous layer is processed by the activation function and then inputted to the next layer. In each iteration, the weight coefficients of the nodes are modified using new data from the training data set, and the error is minimized after several iterations, as shown in Figure S1. A sigmoid function was used as the activation function to map the range of input values from (-∞, +∞) to the interval (0, 1). The number of iterations was 1,000 and the learning rate was 0.01 after several runs and adjustments.

2.6.2 Input and output variables

Input variables were selected in the BPNN model according to the results of the univariate logistic regression analyses and the notable clinical relevance of family history of thyroid tumor and history of radiation exposure. The output variable was pathological results (benign TN was assigned to 1 and PTC to 2).

2.6.3 Software implementation

The BPNN toolbox of MATLAB R2016b software (MathWorks Inc., Natick, Massachusetts, United States) was used to construct the BPNN model. The specific code is shown in supplemental file. The neural analysis was run with 70% of the cases (1,463 cases), randomly selected as the training set, and the remaining 30% (627 cases) as the prediction set, as previously reported (14). Our study conducted a conventional 3-layer BPNN, with an input layer, a hidden layer, and an output layer. The optimal number of nodes in the hidden layer of the BPNN was determined by repetitious data simulation, and 15 hidden neurons were adopted as the optimal case (Table S1). The differentiating performance of the BPNN model was assessed with parametric receiver operating characteristic curve (ROC) analysis.

2.6.4 Evaluation of diagnostic performance

GraphPad Prism 8.2.1 software (GraphPad Software Inc., San Diego, California, United States) was used to plot ROC curves. We calculated the true positive (TP), false positive (FP), true negative (TN), false negative (FN) values, as well as sensitivity, specificity, Youden index, negative predictive value (NPV), and positive predictive value (PPV) for each model.

3 Results

3.1 Baseline characteristics of patients with PTC compared with benign nodules

A total of 2,090 patients (546 males and 1,544 females) with TNs were included in the analysis, among whom 571 were with benign TNs (thyroid cystic adenoma, hyperplastic nodular goiter, etc.) and 1,519 were with PTC (Figure 1). Baseline characteristics are shown in Table 1. Patients with PTC tended to be younger (43.2 ± 12.4 vs. 50.8 ± 13.1 years, P<0.001), and were more likely to have family history of thyroid tumor (4.9% vs. 2.8%; P=0.038) and radiation exposure (2.7% vs. 0.1%; P=0.011), as compared with those with benign nodules. Patients with PTC also showed a higher Bethesda category (4.96 ± 1.44 vs. 2.66 ± 1.53, P<0.001) and Kwak TIRADS score (5.11 ± 1.15 vs. 3.31 ± 0.66, P<0.001), but a lower nodule diameter (1.2 ± 0.89 vs. 3.24 ± 1.6, P<0.001).

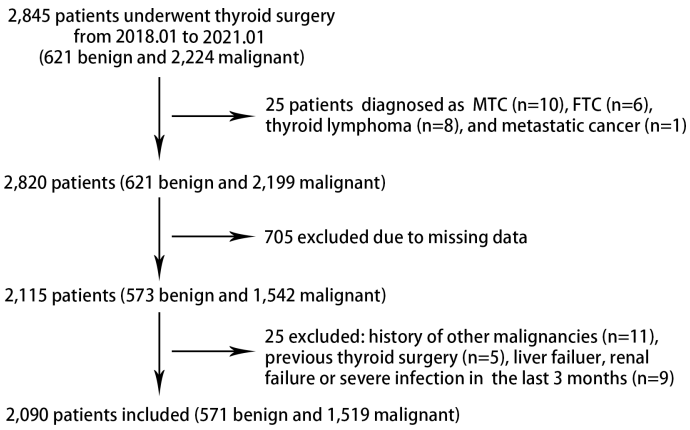

FIGURE 1
Flowchart of patient selection in the study. FTC, follicular thyroid carcinoma; MTC, medullary thyroid cancer.

3.2 Logistic regression analysis

Multivariate logistic regression analysis indicated that Bethesda category (OR=1.90, 95% CI 1.62–2.24, P<0.001), TIRADS score (OR=2.55, 95% CI 1.82–3.56, P<0.001), age (OR=0.97, 95% CI 0.94–0.99, P=0.002), nodule size (OR=0.53, 95% CI 0.41–0.69, P<0.001), serum levels of Tg (OR=0.994, 95% CI 0.991–0.998, P=0.004), and HDL-C (OR=0.23, 95% CI 0.10–0.53, P=0.001) were statistically significant independent differentiators for patients with PTC and benign nodules (Table 2, Table S2).

TABLE 1 Baseline characteristics of TN patients based on nodule types.

Indicator	Total (N=2090)	Benign TN (N=571)	PTC (N=1519)	*P*
Gender				0.042
Male	546 (26.1)	131(22.9)	415 (27.3)	
Female	1544 (73.9)	440 (77.1)	1104 (77.7)	
Age (years)	45.28 ± 13.01	50.77 ± 13.09	43.22 ± 12.38	<0.001
BMI (kg/m^2)	23.83 ± 3.45	23.85 ± 3.30	23.80 ± 3.51	0.892
History of Radiation				0.011
No	2044 (97.8)	566 (99.9)	1478 (97.3)	
Yes	46 (2.2)	5 (0.1)	41 (2.7)	
Family History				0.038
No	2000 (95.7)	555 (97.2)	1445 (95.1)	
Yes	90 (4.3)	16 (2.8)	74 (4.9)	
Bethesda Category	4.80 ± 1.56	2.66 ± 1.53	4.96 ± 1.44	<0.001
Kwak TIRADS	4.62 ± 1.32	3.31 ± 0.66	5.11 ± 1.15	<0.001
Nodule diameter (cm)	1.8 ± 1.4	3.24 ± 1.6	1.2 ± 0.89	<0.001
TSH (mIU/L)	2.32 ± 1.97	1.95 ± 1.93	2.45 ± 2.02	<0.001
FT3 (pmol/L)	4.94 ± 0.77	4.95 ± 0.74	4.93 ± 0.79	0.629
FT4 (pmol/L)	16.78 ± 3.38	16.82 ± 3.65	16.7 ± 3.30	0.681
TgAb (IU/ml)	11.51 ± 24.08	10.71 ± 6.34	11.9 ± 47.5	<0.001
TPOAb (IU/ml)	17.00 ± 15.00	16.77 ± 11.76	17.1 ± 17.25	0.090
Tg (ng/ml)	20.60 ± 47.30	52.1 ± 178.85	15.7 ± 30.06	<0.001
HDL-C (mmol/L)	1.16 ± 0.43	1.20 ± 0.44	1.15 ± 0.43	0.002
LDL-C (mmol/L)	2.42 ± 0.90	2.45 ± 0.91	2.40 ± 0.90	0.546

Data are expressed as mean ± standard deviation or frequency (%). Kwak TIRADS assignment: 3 assigned to 3, 4a assigned to 4, 4b assigned to 5, 4c assigned to 6, 5 assigned to 7. TIRADS: Thyroid Imaging Reporting and Data Systems. TN, thyroid nodules; PTC, papillary thyroid carcinoma; BMI, body mass index (weight/height2). TSH, thyroid-stimulating hormone; FT3, free triiodothyronine; FT4, free thyroxine; TgAb, antithyroglobulin antibody; TPOAb, anti-thyroid peroxidase antibody; TAb, thyroid autoantibody (positive if TgAb and/or TPOAb are positive); Tg, thyroglobulin; HDL-C, high-density lipoprotein cholesterol; LDL-C, low-density lipoprotein cholesterol.

A multivariate logistic regression model was constructed with the above variables, as well as family history of thyroid tumor and history of radiation exposure, used as the independent variables and the pathological finding as the dependent variable. The corresponding ROC curve is shown in Figure 2, and the AUC was 0.924 (95% CI 0.896–0.952, SE=0.014, P<0.001). The Hosmer-Lemeshow goodness-of-fit value was 0.434. The predicted probability (P) value (0.8607) at the highest Youden index (sensitivity+specificity-1) value was selected as the diagnostic cutoff, based on the ROC curve coordinates (sensitivity and 1-specificity) outputted by SPSS. The multivariate logistic regression model had a sensitivity of 93.9%, a specificity of 73.9%, an NPV of 45.8%, and a PPV of 98.1% (Table 3).

3.3 BPNN model

Baseline characteristics of the training set and the prediction set are shown in Table 4. No significant difference was found between these two groups. Ten indicators, including age, family history of thyroid tumor, history of radiation exposure, nodule size, Bethesda category, TIRADS, serum levels of TSH, TPOAb, Tg, and HDL-C, were selected as the input variables in the BPNN model, i.e., variables with statistical significance in the univariate logistic regression analyses, as well as family history of thyroid tumor and history of radiation exposure, which have notable clinical relevance. The pathological results were set as the output variables. A structural diagram of the model is shown in Figure S2.

After training, the model based on the training set (1463 cases), the results predicted by the BPNN model, and actual results for the 627 patients in the prediction set were compared. The specific values are shown in supplementary file. The AUC was 0.948 (95% CI 0.928–0.969, SE=0.010, P<0.001). A diagnostic cutoff value of 1.5168 (at the highest Youden index value) was selected, with a sensitivity of 93.1%, a specificity of 88.3%, an NPV of 83.7%, and a PPV of 95.2% (Figure 2).

As compared with the multivariate logistic regression model, BPNN model showed a comparable but numerically higher AUC (0.948 vs. 0.924; Table 3). BPNN model showed a much higher specificity (88.3% vs. 73.9%) than logistic regression model, while their sensitivity (93.1% vs. 93.9%) was similar. BPNN also showed a higher NPV value (83.7% vs. 45.8%) but the PPV value (95.2% vs. 98.1%) was lower.

We also performed stratified analysis based on Bethesda indeterminate cytology categories III to V, and the findings were similar. BPNN model showed a higher specificity (82.3% vs. 77.1%) than logistic regression model, although the AUC was smaller than the overall analysis for both models (Table S3).

Inter-operator variability between two sonologists proved to be small by using intraclass correlation coefficients, as provided in Table S4.

4 Discussion

The assessment of TNs, particularly the risk stratification assessment of TNs by using single features, is not an easy task. A number of studies have applied computer-aided diagnosis (CAD) methodologic analysis to assist the evaluation of TNs. For example, Lee and colleagues developed a CAD system to identify and differentiate metastatic lymph nodes of thyroid cancer. This system proved to be highly sensitive and but relatively less specific for predicting lymph node malignancy (15). A retrospective, multicohort study from China analyzed over 300,000 ultrasound images from patients with thyroid cancer and negative controls, and found that these AI-guided models showed similar sensitivity and improved specificity in identifying thyroid cancer compared with skilled radiologists

TABLE 2 Multivariate logistic regression analysis of PTC in TN patients.

Indicator	*B*	*SE*	*Wald*	*df*	*P*	*OR*	95% *CI*	
							Lower limit	Upper limit
Age	-0.036	0.012	9.483	1	0.002	0.965	0.943	0.987
Bethesda Classification	0.643	0.083	59.537	1	<0.001	1.902	1.616	2.240
Family history	1.231	1.248	0.973	1	0.324	3.425	0.297	39.538
History of Radiation	-0.344	1.068	0.104	1	0.747	0.709	0.087	5.753
Maximum diameter	-0.642	0.131	24.091	1	<0.001	0.526	0.407	0.680
Kwak TIRADS	0.935	0.171	29.762	1	<0.001	2.547	1.820	3.564
HDL-C	-1.465	0.425	11.902	1	0.001	0.231	0.101	0.531
Tg	-0.006	0.002	8.457	1	0.004	0.994	0.991	0.998

PTC, papillary thyroid carcinoma; TN, thyroid nodules; Tg, thyroglobulin; HDL-C, high-density lipoprotein cholesterol. TIRADS, Thyroid Imaging Reporting and Data Systems; HDL-C, high-density lipoprotein cholesterol; Tg, thyroglobulin.

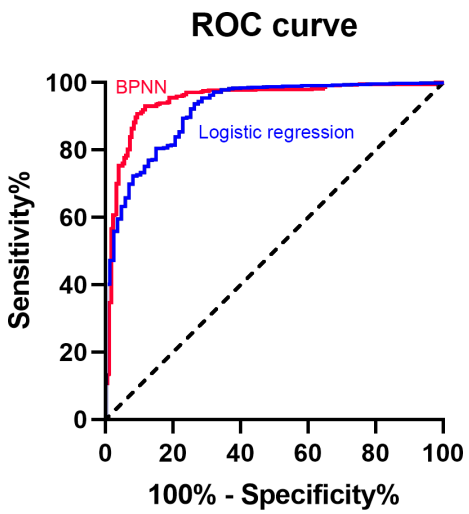

FIGURE 2
ROC curve of BPNN and multivariate logistic regression model. BPNN, back propagation neural network; ROC, receiver operating characteristic curve.

(10). However, Choi et al. reported that CAD system had a similar sensitivity as experienced radiologist (90.7% vs. 88.4%) but with lower specificity (74.6% vs. 94.9%) (16). Machine learning based on sonographic or pathological images is still under-development and far from mature. For example, the sonographic features may not be adequately captured, or may look differently between axial and transverse images, which might decrease the performance of deep learning (17). Notably, the vast majority of these studies focused on the comparison of radiologists and deep-learning models by reading only ultrasound images. They relied on handcrafted features or deep features extracted from images after processing, where detailed raw information may be distorted or even lost. Besides, these studies inevitably brought intensive labor work to extract features from ultrasound images. In contrast, our study, which was based on a combination of relevant demographic, serological, ultrasound, and biopsy data (all were readily available from a routine clinical practice), showed promising performance in differentiating patients with PTC from benign nodules, and thus might help guide the decision of surgery. To the best of our knowledge, this is the first study that attempted to incorporate different lines of variables, rather than only ultrasound images as used in other studies, into machine-learning model and aimed to aid the diagnosis of PTC.

Results from multivariate logistic regression analysis indicated that Bethesda category and TIRADS were positively associated with PTC, which were in agreement with previous literature, whereas age, nodule size, and serum levels of Tg and HDL-C were negatively associated with PTC. In consistent with our findings, a large prospective study including 6,391 patients showed that the incidence of TNs increased but thyroid malignancy decreased with age (18). Another study involving over 30,000 TN patients undergoing FNAB found that younger age was an independent risk factor for PTC (19). All patients included in our study were all age 18 years or older since the proportion of patients under the age of 18 years, who underwent thyroid surgery in our hospital, were small (most might have received therapy in children's hospital). Excluding adolescent patients could also prevent the analysis from confounding due to the heterogeneity between adults and adolescents; however, whether our conclusions could be generalized to other age groups needs further investigation.

We included HDL-C and LDL-C in our analysis because some previous studies suggested potential associations between these cholesterol parameters and endocrine-related cancer, including thyroid cancer, although these association was not consistently reported (20). A recent study from China demonstrated that patients with PTC had a higher monocyte to HDL-C ratio (MHR), and MHR was an independent risk factor for PTC (21). It is interesting that in our large study, HDL-C might act as a protective factor for thyroid cancer. Very recently, two studies from South Korea confirmed that a low level of HDL-C was associated with a higher risk of thyroid cancer, especially in a metabolically unhealthy population (22, 23). The mechanism underlying the association between HDL-C and thyroid cancer remains unclear and warrants further investigation. Insulin resistance has been suggested as one of the contributing factors. A decrease of HDL-C often accompanies insulin resistance (24),

TABLE 3 Comparison of diagnostic performance of BPNN with multivariate logistic regression model.

Indicator	Multivariate logistic regression	BPNN
AUC	0.924 (0.896-0.952)	0.948 (0.928-0.969)
Sensitivity	93.9% (92.3%-95.1%)	93.1% (90.2%-95.2%)
Specificity	73.9% (63.2%-82.4%)	88.3% (82.5%-92.5%)
Youden index	0.677 (0.555-0.775)	0.814 (0.727-0.877)
NPV	45.8% (37.5%-54.3%)	83.7% (77.5%-88.5%)
PPV	98.1% (97.1%-98.7%)	95.2% (92.6%-96.9%)

AUC, area under receiver operating characteristic curve (95% CI is shown in parentheses); BPNN, back propagation neural network; NPV, negative predictive value; PPV, positive predictive value. Youden index=sensitivity+specificity-1.

10.3389/fendo.2022.938008

TABLE 4 Baseline characteristics of TN patients in the training and prediction cohorts.

Indicator	All patients (N=2090)	Training cohort (N=1463)	Prediction cohort (N=627)	*P*
Gender (%)				0.501
Male	546	376 (68.9%)	170 (31.1%)	
Female	1544	1087 (70.4%)	457 (29.6%)	
Age (years)	45.28 ± 13.01	45.98 ± 13.35	44.98 ± 12.86	0.110
BMI (kg/m^2)	23.83 ± 3.45	23.78 ± 3.42	23.86 ± 3.46	0.615
Nodule type (%)				0.351
Benign	571	391 (68.5%)	180 (31.5%)	
Malignant	1519	1072 (70.6%)	447 (29.4%)	
History of Radiation				0.216
No	2044	1427 (69.8%)	617 (30.2%)	
Yes	46	36 (78.3%)	10 (21.7%)	
Family History				1.000
No	2000	1400 (70.0%)	600 (30.0%)	
Yes	90	63 (70.0%)	27 (30.0%)	
Bethesda Category	4.80 ± 1.56	4.77 ± 1.56	4.81 ± 1.56	0.693
Kwak TIRADS	4.62 ± 1.32	4.67 ± 1.36	4.60 ± 1.30	0.224
Nodule diameter (cm)	1.80 ± 1.40	1.84 ± 1.40	1.79 ± 1.42	0.852
TSH (mIU/L)	2.32 ± 1.97	2.38 ± 2.01	2.24 ± 1.85	0.123
FT3 (pmol/L)	4.94 ± 0.77	4.94 ± 0.78	4.92 ± 0.78	0.904
FT4 (pmol/L)	16.78 ± 3.38	16.74 ± 3.33	16.80 ± 3.40	0.123
TgAb (IU/mL)	11.51 ± 24.08	11.67 ± 25.80	11.30 ± 20.60	0.904
TPOAb (IU/ml)	17.00 ± 15.00	17.00 ± 15.10	17.00 ± 14.75	0.074
Tg (ng/ml)	20.60 ± 47.30	20.60 ± 46.05	20.30 ± 51.32	0.723
HDL-C (mmol/L)	1.16 ± 0.43	1.18 ± 0.43	1.13 ± 0.42	0.630
LDL-C (mmol/L)	2.42 ± 0.90	2.43 ± 0.90	2.41 ± 0.91	0.799

Data are expressed as mean ± standard deviation or frequency (%). Kwak TIRADS assignment: 3 assigned to 3, 4a assigned to 4, 4b assigned to 5, 4c assigned to 6, 5 assigned to 7. TIRADS, Thyroid Imaging Reporting and Data Systems; TN, thyroid nodules; PTC, papillary thyroid carcinoma; BMI, body mass index (weight/height2); TSH, thyroid-stimulating hormone; FT3, free triiodothyronine; FT4, free thyroxine; TgAb, antithyroglobulin antibody; TPOAb, anti-thyroid peroxidase antibody; TAb, thyroid autoantibody (positive if TgAb and/or TPOAb are positive); Tg, thyroglobulin; HDL-C, high-density lipoprotein cholesterol; LDL-C, low-density lipoprotein cholesterol.

and diabetes, another condition with insulin resistance, is associated with an increased risk of thyroid cancer (25). It is unclear whether the antioxidant and anti-inflammatory effect of HDL-C was involved (20).

In this study, we found that both BPNN and multivariate logistic regression model had an AUC >0.92, showing a promising performance in differentiating patients with PTC from those with benign nodules. Both models included a variety of variables from different aspects. All of these variables were readily to be obtained from routine clinical practice and were almost noninvasive. It is intriguing that the BPNN model showed a higher diagnostic specificity than the logistic regression model, while the sensitivity was maintained. These specific advantages of BPNN over logistic model make BPNN a more clinically useful approach (26).

FNAB is a routinely recommended pre-operative cytological examination. With the dramatic development of molecular diagnostic technologies in recent years, researchers have discovered *BRAF*, *RAS*, and telomerase reverse transcriptase (*TERT*) promoter mutations, *RET/PTC* rearrangement, and other genetic mutations to be associated with thyroid cancers (27, 28). Several key characteristic molecules such as long noncoding RNAs and microRNAs also show an association (29–31). These genetic technologies may improve the diagnosis for some patients who failed to be diagnosed with cytopathology. We did not include molecular information in our analysis due to limited data, but future studies incorporating molecular data might further increase the accuracy and specificity for prediction of PTC.

With the advance of TNs screening technology and increased detection demand, we can anticipate a dramatic increase of thyroid nodules (32). Thus, the development of a systematic method to differentiate patients with PTC from those with benign nodules is critical, given that there is concern regarding the overdiagnosis and surgery of thyroid cancer. Our study suggests the advantages of combing demographic, serological, and nodule characteristics for the differentiation of

PTC from benign nodules. Further prospective studies are warranted to confirm these findings and determine whether similar effect could be generalized to other thyroid tumors. Overtreatment of thyroid tumors is commonly seen in real-world practice in China. If validated, our model might improve the accuracy of defining surgical necessity.

Several limitations should also be acknowledged in our study. First, the retrospective nature of the study made it impossible to avoid potential confounding, although the sonologists and researchers were all well-trained and experienced, and the inter-operator variability between two sonologists was small. Second, all the study subjects were inpatients who underwent thyroid surgery, which might induce selection bias that may favor more complex or malignant cases. We are performing a prospective study to assess the performance of the BPNN and logistic regression models among all FNAB cases with and without surgery to address this bias; and those without surgery will be followed up with ultrasonography. Third, follicular carcinomas were rare in China due to a high iodine supply. Thus, whether our predictive system can be applied to other populations with different iodine supply or to tumors of different histotypes remains to be determined. Fourth, although we utilized a randomly set 30% of patients for validation, an independent validation population is still needed to further validate the performance of our BPNN model. Finally, the BPNN model was divided into two sets, whereas the regression model was evaluated only in one combined set; the difference of patients being compared, although not big, might affect the findings. However, we aimed not to compete with logistic regression model, but to provide a tool with excellent performance in aiding PTC risk stratification.

5 Conclusions

Bethesda category, TIRADS, nodule size, and serum levels of HDL-C were most significant differentiators for patients with PTC and those with benign nodules. Based on demographic, serological, ultrasound, and biopsy data, both BPNN and multivariate logistic regression model showed excellent performance in differentiating patients with PTC from those with benign nodules, but the BPNN model provided more specific prediction for PTC than conventional regression analysis, and thus might help guide the decision of surgery. Future studies are needed to validate our findings.

Data availability statement

The original contributions presented in the study are included in the article/Supplementary Material. Further inquiries can be directed to the corresponding authors.

Ethics statement

The studies involving human participants were reviewed and approved by the Ethics Committee of Nanjing Drum Tower Hospital Institutional Review Board. Written informed consent for participation was not required for this study in accordance with the national legislation and the institutional requirements.

Author contributions

Conceptualization, XWZ, YB, and DZ; Methodology, XWZ, YZ, and XLZ; Investigation, XWZ, YZ, JS, XS, SS, and XLZ; Writing—original draft preparation, XWZ, YZ, SS, and XLZ; Funding acquisition, XWZ. All authors have read and agreed to the published version of the manuscript.

Funding

This project was supported by the National Nature Science Funds of China (Grant No. 81800752), and Fundings for Clinical Trials from the Affiliated Drum Tower Hospital, Medical School of Nanjing University (2022-YXZX-NFM-02).

Conflict of interest

The authors declare that the research was conducted in the absence of any commercial or financial relationships that could be construed as a potential conflict of interest.

Publisher's note

Supplementary material

The Supplementary Material for this article can be found online at: https://www.frontiersin.org/articles/10.3389/fendo.2022.938008/full#supplementary-material

References

1. Li M, Maso LD, Vaccarella S. Global trends in thyroid cancer incidence and the impact of overdiagnosis. *Lancet Diabetes Endo* (2020) 8:468–70. doi: 10.1016/S2213-8587(20)30115-7

2. Ahn H, Kim H, Welch H. Korea's thyroid-cancer "epidemic"–screening and overdiagnosis. *N Engl J Med* (2014) 371:1765–7. doi: 10.1056/NEJMp1409841

3. Lim H, Devesa S, Sosa J, Check D, Kitahara C. Trends in thyroid cancer incidence and mortality in the united states, 1974-2013. *JAMA* (2017) 317:1338–48. doi: 10.1001/jama.2017.2719

4. Chen W, Zheng R, Baade P, Zhang S, Zeng H, Bray F, et al. Cancer statistics in China, 2015. *CA-Cancer J Clin* (2016) 66:115–32. doi: 10.3322/caac.21338

5. Li Y, Teng D, Ba J, Chen B, Du J, He L, et al. Efficacy and safety of long-term universal salt iodization on thyroid disorders: epidemiological evidence from 31 provinces of mainland China. *Thyroid* (2020) 30:568–79. doi: 10.1089/thy.2019.0067

6. Miyauchi A, Ito Y, Oda H. Insights into the management of papillary microcarcinoma of the thyroid. *Thyroid* (2018) 28:23–31. doi: 10.1089/thy.2017.0227

7. Kobaly K, Kim CS, Mandel SJ. Contemporary management of thyroid nodules. *Annu Rev Med* (2022) 73:517–28. doi: 10.1146/annurev-med-042220-015032

8. Rumelhart DE, Hintont GE, Williams RJ. Learning representations by back-propagating errors. *Nature* (1986) 323:533–6. doi: 10.1038/323533a0

9. Baxt WG. Application of artificial neural networks to clinical medicine. *Lancet* (1995) 346:1135–8. doi: 10.1016/S0140-6736(95)91804-3

10. Li X, Zhang S, Zhang Q, Wei X, Pan Y, Zhao J, et al. Diagnosis of thyroid cancer using deep convolutional neural network models applied to sonographic images: a retrospective, multicohort, diagnostic study. *Lancet Onco* (2019) 20:193–201. doi: 10.1016/S1470-2045(18)30762-9

11. Zhao C, Ren T, Yin Y, Shi H, Wang H, Zhou B, et al. A comparative analysis of two machine learning-based diagnostic patterns with thyroid imaging reporting and data system for thyroid nodules: diagnostic performance and unnecessary biopsy rate. *Thyroid* (2021) 31:470–81. doi: 10.1089/thy.2020.0305

12. Radebe L, van der Kaay DCM, Wasserman JD, Goldenberg A. Predicting malignancy in pediatric thyroid nodules: early experience with machine learning for clinical decision support. *J Clin Endocrinol Metab* (2021) 106:e5236–46. doi: 10.1210/clinem/dgab435

13. Lyu J, Zhang J. BP Neural network prediction model for suicide attempt among Chinese rural residents. *J Affect Disord* (2019) 246:465–73. doi: 10.1016/j.jad.2018.12.111

14. Ke B, Nguyen H, Bui XN, Bui HB, Nguyen-Thoi T. Prediction of the sorption efficiency of heavy metal onto biochar using a robust combination of fuzzy c-means clustering and back-propagation neural network. *J Environ Manage* (2021) 293:112808. doi: 10.1016/j.jenvman.2021.112808

15. Lee JH, Baek JH, Kim JH, Shim WH, Chung SR, Choi YJ, et al. Deep learning-based computer-aided diagnosis system for localization and diagnosis of metastatic lymph nodes on ultrasound: a pilot study. *Thyroid* (2018) 28:1332–8. doi: 10.1089/thy.2018.0082

16. Choi YJ, Baek JH, Park HS, Shim WH, Kim TY, Shong YK, et al. A computer-aided diagnosis system using artificial intelligence for the diagnosis and characterization of thyroid nodules on ultrasound: initial clinical assessment. *Thyroid* (2017) 27:546–52. doi: 10.1089/thy.2016.0372

17. Chai YJ, Song J, Shaear M, Yi KH. Artificial intelligence for thyroid nodule ultrasound image analysis. *Ann Thyroid* (2020) 5. doi: 10.21037/AOT.2020.04.01

18. Kwong N, Medici M, Angell TE, Liu X, Marqusee E, Cibas ES, et al. The influence of patient age on thyroid nodule formation, multinodularity, and thyroid cancer risk. *J Clin Endocrinol Metab* (2015) 100:4434–40. doi: 10.1210/jc.2015-3100

19. Rago T, Fiore E, Scutari M, Santini F, Di Coscio G, Romani R, et al. Male Sex, single nodularity, and young age are associated with the risk of finding a papillary thyroid cancer on fine-needle aspiration cytology in a large series of patients with nodular thyroid disease. *Eur J Endocrinol* (2010) 162:763–70. doi: 10.1530/EJE-09-0895

20. Revilla G, Cedo L, Tondo M, Moral A, Perez JI, Corcoy R, et al. LDL, HDL and endocrine-related cancer:from pathogenic mechanisms to therapies. *Semin Cancer Biol* (2021) 73:134–57. doi: 10.1016/j.semcancer.2020.11.012

21. Xu H, Pang Y, Li X, Zha B, He T, Ding H. Monocyte to high-density lipoprotein. *Lab Anal* (2021) 35:e24014. doi: 10.1002/jcla.24014

22. Kim J, Kim M, Baek K, Song K, Han K, Kwon H. Repeated low high-density lipoprotein cholesterol and the risk of thyroid cancer: a nationwide population-based study in Korea. *Endocrinol Metab (Seoul)* (2022) 37:303–11. doi: 10.3803/EnM.2021.1332

23. Nguyen D, Kim J, Kim M. Association of metabolic health and central obesity with the risk of thyroid cancer: data from the Korean genome and epidemiology study. *Cancer Epidemiol Biomarkers Prev* (2022) 31:543–53. doi: 10.1158/1055-9965.EPI-21-0255

24. Rashhid S, Uffelman K, Lewis G. The mechanism of HDL lowering in hypertriglyceridemic, insulin-resistant states. *J Diabetes Complications* (2002) 16:24–8. doi: 10.1016/S1056-8727(01)00191-X

25. Aschebrook-Kilfoy B, Sabra M, Brenner A, Moore S, Ron E, Schatzkin A, et al. Diabetes and thyroid cancer risk in the national institutes of health-AARP diet and health study. *Thyroid* (2011) 21:957–63. doi: 10.1089/thy.2010.0396

26. Haugen BR, Alexander EK, Bible KC, Doherty GM, Mandel SJ, Nikiforov YE, et al. 2015 American thyroid association management guidelines for adult patients with thyroid nodules and differentiated thyroid cancer: The American thyroid association guidelines task force on thyroid nodules and differentiated thyroid cancer. *Thyroid* (2016) 26:1–133. doi: 10.1089/thy.2015.0020

27. Zou M, Baitei EY, Alzahrani AS, BinHumaid FS, Alkhafaji D, Al-Rijjal RA, et al. RET/PTC, or BRAF mutations in advanced stage of papillary thyroid carcinoma. *Thyroid* (2014) 24:1256–66. doi: 10.1089/thy.2013.0610

28. Huang Y, Qu S, Zhu G, Wang F, Liu R, Shen X, et al. BRAF V600E mutation-assisted risk stratification of solitary intrathyroidal papillary thyroid cancer for precision treatment. *J Natl Cancer Inst* (2018) 110:362–70. doi: 10.1093/jnci/djx227

29. Chou CK, Liu RT, Kang HY. MicroRNA-146b: a novel biomarker and therapeutic target for human papillary thyroid cancer. *Int J Mol Sci* (2017) 18:636. doi: 10.3390/ijms18030636

30. Jendrzejewski J, He H, Radomska HS, Li W, Tomsic J, Liyanarachchi S, et al. The polymorphism rs944289 predisposes to papillary thyroid carcinoma through a large intergenic noncoding RNA gene of tumor suppressor type. *Proc Natl Acad Sci U.S.A.* (2012) 109:8646–51. doi: 10.1073/pnas.1205654109

31. Nikiforova MN, Tseng GC, Steward D, Diorio D, Nikiforov YE. MicroRNA expression profiling of thyroid tumors: biological significance and diagnostic utility. *J Clin Endocrinol Metab* (2008) 93:1600–8. doi: 10.1210/jc.2007-2696

32. Fisher SB, Perrier ND. The incidental thyroid nodule. *CA-Cancer J Clin* (2018) 68:97–105. doi: 10.3322/caac.21447

frontiers | Frontiers in Endocrinology

TYPE Original Research
PUBLISHED 23 September 2022
DOI 10.3389/fendo.2022.965241

OPEN ACCESS

EDITED BY
Emerita Andres Barrenechea,
Veterans Memorial
Medical Center, Philippines

REVIEWED BY
Fenglin Dong,
The First Affiliated Hospital of
Soochow University, China
Jiang Lixin,
Shanghai Jiao Tong University, China

*CORRESPONDENCE
Liping Wang
wanglp@zjcc.org.cn
Dong Xu
xudong@zjcc.org.cn

†These authors have contributed equally to this work

SPECIALTY SECTION
This article was submitted to Thyroid Endocrinology, a section of the journal Frontiers in Endocrinology

RECEIVED 09 June 2022
ACCEPTED 12 September 2022
PUBLISHED 23 September 2022

CITATION
Zhou L, Yao J, Ou D, Li M, Lei Z, Wang L and Xu D (2022) A multi-institutional study of association of sonographic characteristics with cervical lymph node metastasis in unifocal papillary thyroid carcinoma. *Front. Endocrinol.* 13:965241. doi: 10.3389/fendo.2022.965241

A multi-institutional study of association of sonographic characteristics with cervical lymph node metastasis in unifocal papillary thyroid carcinoma

Liuhua Zhou[1†], Jincao Yao[2,3†], Di Ou[2,3], Mingkui Li[4], Zhikai Lei[5], Liping Wang[2,3*] and Dong Xu[2,3,6,7*]

[1]Zhejiang Chinese Medical University, Hangzhou, China, [2]Cancer Hospital of the University of Chinese Academy of Sciences (Zhejiang Cancer Hospital), Hangzhou, China, [3]Institue of Basic Medicine and Cancer (IBMC), Chinese Academy of Sciences, Hangzhou, China, [4]Zhejiang Xiaoshan Hospital, Hangzhou, China, [5]Hangzhou Cancer Hospital, Hangzhou, China, [6]Key Laboratory of Head & Neck Cancer Translational Research of Zhejiang Province, Hangzhou, China, [7]Zhejiang Provincial Research Center for Cancer Intelligent Diagnosis and Molecular Technology, Hangzhou, China

Objective: Papillary thyroid carcinoma (PTC) is the most common pathological type of thyroid carcinoma, and is prone to cervical lymph node metastases (CLNM). We aim to evaluate the association between sonographic characteristics of PTC and CLNM before the initial surgery.

Methods: Clinical information as well as ultrasonographic measurements and characteristics for 2376 patients from three hospitals were acquired in this retrospective cohort study. Univariate and multivariate logistic analysis were performed to predict CLNM in unifocal PTC patients. Receiver operating characteristic (ROC) curve was created to evaluate diagnostic performance.

Results: Univariate analysis showed that gender, age, maximum tumor diameter and volume, cross-sectional and longitudinal aspect ratio, location, echogenicity, margin, and echogenic foci were independently associated with CLNM metastatic status ($P < 0.05$). Multivariate logistic analysis showed that gender, age, maximum tumor diameter and volume, cross-sectional aspect ratio (CSAR), location, echogenicity, margin, and echogenic foci were independent correlative factors; CSAR showed a significant difference for PTC2 to predict CLNM. The area under the curve (AUC) of the maximum tumor diameter, tumor volume, margin, and echogenic foci was 0.70, 0.69, 0.65, and 0.70, respectively. The multiple-variable linear regression model was constructed with an AUC of 0.77, a specificity of 73.4%, and a sensitivity of 72.3%. Kruskal-Wallis analysis for positive subgroups, maximum tumor diameter and volume, cross-sectional and longitudinal aspect ratio, margin, and echogenic foci showed statistical significance ($P < 0.05$).

10.3389/fendo.2022.965241

Conclusions: Younger age (< 55 years), male, larger tumor, and echogenic foci were high risk factors for CLNM in patients with unifocal PTC. CSAR had a more effective predictive value for CLNM in patients with larger thyroid tumors. A larger tumor with irregular and punctate echogenic foci was also more prone to the lateral neck, and both central and lateral neck metastasis.

KEYWORDS

ultrasonography, thyroid cancer, papillary, lymphatic metastases, imaging, TI-RADS category

Background

As a noninvasive imaging examination method, ultrasonography is widely used in clinical settings. The thyroid imaging report and data system (TI-RADS) white paper, which was proposed by the American College of Radiology in 2017, has been internationally recognized and used recently (1). This paper presented the characteristics of thyroid nodules based on sonographic characteristics such as composition, echogenicity, shape, margin, and echogenic foci. TI-RADS regulates the classification diagnostic criteria, which provides better guidance in judgement of thyroid nodules.

Papillary thyroid carcinoma (PTC) is the most common pathological type of thyroid carcinoma, among which unifocal tumors often occur. The incidence of multifocal PTC is about 30% (2). CLNM is prone to occur early, and there is a risk of postoperative recurrence as well as distant metastasis (3). However, there are many limitations in ultrasonography of cervical lymph nodes, especially for CLNM, and ultrasonography has a detection rate of 18.8%–31.0%. This technique is limited because of interference from the trachea, esophagus, osseous tissue, and thyroid underlying diseases, as well as the experience of the examiner (4, 5). In recent years, preventive central lymph node dissection has been executed for PTC patients (6–8); however, according to the 2015 American Thyroid Association Management Guidelines (9), thyroidectomy without prophylactic central neck dissection is appropriate for small (T1 or T2), noninvasive, clinically node-negative PTC (cN0). We hope that high risk factors of PTC nodules with CLNM will be stratified in routine ultrasound examination, such that head and neck surgeons as well as radiologists can better assess and complete preoperative surgical planning. Then, prophylactic neck dissection (central/lateral) can be offered accordingly. This will be useful to guide treatment protocols prior to operating.

Ultrasonography is the primary inspection method for the thyroid gland, and nodular sonographic characteristics are easy to access through basic training. In this study, unifocal PTC was selected for analysis in combination with clinical information, ultrasonographic measurements, and characteristics. There is an urgent need to identify metrics for predicting the risk of lymph node metastasis before surgery when performing routine thyroid and cervical lymph node ultrasonic screening.

Abbreviations: PTC, Papillary thyroid carcinoma; CLNM, Cervical lymph node metastasis; PTMC, Papillary thyroid microcarcinoma; ROC, Receiver operating characteristic; CSAR, Cross-sectional aspect ratio; AUC, Area under the curve; TI-RADS, Thyroid imaging report and data system; CT, Computed tomography; SD, Standard deviation; OR, Odds ratio; CI, Confidence interval.

Materials and methods

Patients

The enrolled participants were symptomatic with palpable or incidental thyroid lumps, and all ultimately underwent thyroidectomy in Cancer Hospital of the University of Chinese Academy of Sciences (Zhejiang Cancer Hospital, Hangzhou, China), Zhejiang Xiaoshan Hospital and Hangzhou Cancer Hospital from July 2017 to September 2020. The inclusion criteria were as follows: 1) patients were undergoing first-time thyroidectomy; 2) patients received enhanced computed tomography (CT) scan of neck and thorax to assess cervical lymph node and pulmonary metastasis, as well as thyroid and neck ultrasonography before operation; and 3) PTC was confirmed by biopsy before surgery. The exclusion criteria were as follows: 1) identification of lung or other distant metastasis; and 2) postoperative pathology diagnosis of multifocal PTC. Unilateral thyroid lobe plus isthmus excision or total thyroidectomy were performed for each patient. If lateral lymph node metastasis was suspected by preoperative comprehensive evaluation and confirmed by biopsy, lateral lymph node dissection was performed (6). All patients underwent preventive central lymph node dissection (6–8) and

metastatic lymph nodes were confirmed by pathology. This study was approved by the Ethics Committee of Cancer Hospital of the University of Chinese Academy of Sciences (Zhejiang Cancer Hospital), Zhejiang Xiaoshan Hospital and Hangzhou Cancer Hospital. Informed consent was obtained from all enrolled patients.

A total of 3065 patients undergoing thyroidectomy were enrolled. Of the 689 cases excluded from the study, 357 were multifocal PTC, 225 had no pathological results in cervical lymph nodes, and 107 had incomplete imaging data. Ultimately, we analyzed 2376 patients with unifocal PTC in the study. Patients were divided into the following two groups: (1) 949 patients with CLNM were placed in the positive group and (2) 1427 patients with no CLNM were placed in the negative group. For the positive group, subgroups of central lymph node metastasis, lateral lymph node metastasis, and both central and lateral lymph node metastasis were created. We also assigned papillary thyroid microcarcinoma (PTMC) as group PTC1 and PTC above pT1a as group PTC2 (Figure 1).

Instruments

For examinations, we used the GE Logiq E9 ultrasonographic instrument (General Electric Healthcare, Milwaukee, WI, USA) with a high-resolution linear probe (ML6-15) and the Philips iU22 ultrasonographic instrument (Royal Dutch Philips Electronics, Amsterdam, Noord-Holland, Netherlands) with a high frequency linear probe (L12-5).

Protocol

Patients were maintained in a supine position with the neck hyperextended while the thyroid and both sides of the neck were scanned in multi-section. The three diameters (length, width, and height), lesion location, composition, echogenicity, shape, margin, and echogenic foci of the tumor were recorded and evaluated from workstations. The patients were followed up until they underwent thyroidectomy and pathological results were obtained. The duration of follow-up ranged from 1 week to 2 months.

The ultrasonographic images were obtained by the same three professional physicians, each with more than 10 years of experience, board-certification, and training in thyroid ultrasound. The ultrasonographic images and reports were independently analyzed in a blinded fashion by another two ultrasound specialists (each with more than 10 years of experience). All imaging data were compared to the pathological results from neck dissections. For measurements, if the error was less than 2 mm between the two ultrasound specialists, the average value was applied. When the measurement error exceeded 2 mm, or if any other discordance occurred for ultrasonographic characteristics, a separate experienced sonographer (with more than 20 years of experience in thyroid ultrasound) reviewed the images and a final decision was reached.

Clinical information as well as ultrasonographic measurements and characteristics were used for data collection. Clinical information included gender and age. An age threshold of 55

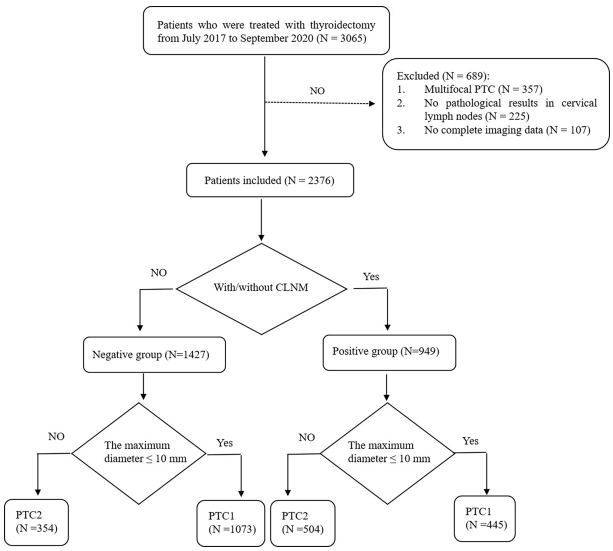

FIGURE 1
Flow diagram of the study selection procedure.

years was used for analysis according to the 8th edition of the United States Joint Committee on Cancer, as the diagnostic age of the TNM staging system for thyroid cancer was 55 years (9). US measurements included the maximum tumor diameter, tumor volume, cross-sectional aspect ratio, and longitudinal aspect ratio.

The three diameters of the tumor were determined by: 1) completing a longitudinal scan of the thyroid, selecting the maximum section of the nodule, and measuring the maximum long diameter as the length; 2) measuring the vertical diameter of long diameter as the height; and 3) performing a transversal scan of the thyroid, selecting the maximum section of the nodule, and recording the maximum diameter from left to right as the width. The maximum diameter was the maximum of length, width and height, volume = 0.523 × length × width × height, cross-sectional aspect ratio = height/width and longitudinal aspect ratio = height/length.

Sonographic characteristics according to ACR TI-RADS were carried out as follows: composition (cystic, mixed cystic and solid, solid/almost completely solid); echogenicity (anechoic, hyperechoic or isoechoic, hypoechoic and very hypoechoic); shape (aspect ratio < 1 or ≥ 1); margin (smooth or ill-defined, lobulated or irregular, extra-thyroid extension); and echogenic foci (none or large comet-tail artifacts, macro, peripheral and punctate echogenic foci).

Statistical analysis

The obtained data were statistically analyzed by IBM SPSS Statistics version 23 (IBM SPSS INC., Chicago, USA). Continuous quantitative data were expressed as the mean± standard deviation (SD). Data-counting were described statistically by the number of cases and rates. Chi-square test and independent-sample T test were used for univariate analysis. A multivariate analysis using binary logistic regression analysis was adopted if analysis index $P < 0.05$ in the univariate analysis.

Odds ratios (ORs) with 95% confidence intervals (CIs) were calculated and ROC curves were analyzed for factors with significance on binary linear regression analysis, AUC curves, sensitivity and specificity of each significant independent variable were acquired. Multiple linear regression equations reflect the relationship between independent variables and covariates; covariates are originated from binary linear regression analysis that conform to $P < 0.05$. Kruskal-Wallis analysis was used for the positive subgroups to find out the significance. $P < 0.05$ was considered statistically significant.

Results

A total of 2376 patients with 2376 lesions were included (1518 PTC1 and 858 PTC2), and the clinical data and sonographic characteristics were retrospectively analyzed. There were 569 males and 1807 females, aged 12 to 84 years, with an average age of 44.5 ± 11.8 years; the maximum tumor diameter was 3.5 to 64.7 mm, with an average diameter of 10.4 ± 7.5 mm. A total of 949 cases were in the positive group (39.9% of total); 445 were PTC1 and 504 were PTC2. In the positive group, 669 (70.5%) patients had only central lymph node metastasis, 70 (7.4%) had only lateral lymph node metastasis, and 210 (22.1%) had metastasis in both central and lateral lymph nodes. There were 1427 cases included in negative group (60.1% of total); 1073 were PTC1 and 354 were PTC2. Of these, 227 patients underwent lateral lymph node dissection due to a positive preoperative biopsy. Lateral neck lymph node dissection was performed in seven cases with high imaging suspicion but negative puncture results. Four of these cases were found to have lateral neck lymph node metastasis and three were confirmed negative during operation.

For the positive and negative groups, the results showed that male ($x2 = 37.914$, $P < 0.001$), age ($t = 13.342$, $P < 0.001$), age < 55 years ($x2 = 33.608$, $P < 0.001$), maximum tumor diameter ($t = -17.431$, $P < 0.001$) and volume ($t = -9.051$, $P < 0.001$), cross-sectional aspect ratio ($t = 6.926$, $P < 0.001$), and longitudinal aspect ratio ($t = 9.343$, $P < 0.001$) were all significantly related to CLNM (Table 1).

By comparing sonographic characteristics of patients in the positive and negative groups using the Chi-square test and the independent-sample T test, our results showed that location, echogenicity, aspect ratio, margin, and echogenic foci showed significant differences (Table 2).

We further divided the positive group into two subgroups, PTC1 and PTC2. In comparing these two subgroups, CSAR ≥ 1

TABLE 1 Univariate analysis of nodular parameters with CLNM in PTC.

Variable	Positive group (n=949)	Negative group (n=1427)	Statistics	P
Gender (male/female)	290/659	279/1148	$x^2 = 37.914$	P < 0.001
Age	41.1 ± 12.0	46.6 ± 11.3	t=13.342	P < 0.001
Age (≥ 55 years/< 55 year)	139/810	349/1078	$x^2 = 33.608$	P < 0.001
Tumor maximum diameter (mm)	13.3 ± 9.1	8.5 ± 5.6	t=-17.431	P < 0.001
Tumor volume (ml)	1.6 ± 4.0	0.5 ± 2.1	t=-9.051	P < 0.001
Cross-sectional aspect ratio	1.0 ± 0.3	1.1 ± 0.3	t=6.926	P < 0.001
Longitudinal aspect ratio	0.9 ± 0.3	1.0 ± 0.3	t=9.343	P < 0.001

10.3389/fendo.2022.965241

TABLE 2 Univariate analysis of sonographic features with CLNM in PTC.

Variable	Positive group (n=949)	Negative group (n=1427)	Statistics	P
Location			x^2 = 34.052	P<0.001
Left upper	117 (12.3)	196 (13.7)		
Left middle	195 (20.6)	364 (25.5)		
Left lower	88 (9.3)	119 (8.4)		
Right upper	175 (18.4)	223 (15.6)		
Right middle	203 (21.4)	366 (25.7)		
Right lower	112 (11.8)	100 (7.0)		
Isthmus	59 (6.2)	59 (4.1)		
Composition			x^2 = 0.281	P=0.596
Mixed cystic and solid	10 (1.1)	12 (0.8)		
Solid or almost completely solid	939 (98.9)	1415 (99.2)		
Echogenicity			x^2 = 18.186	P<0.001
Hyperechoic or isoechoic	16 (1.7)	26 (1.8)		
Hypoechoic	856 (90.2)	1344 (94.2)		
Very hypoechoic	77 (8.1)	57 (4.0)		
Aspect ratio			x^2 = 28.974	P<0.001
<1	451 (47.5)	520 (36.4)		
≥1	498 (52.3)	907 (63.6)		
Margin			x^2 = 255.392	P<0.001
smooth or ill-defined	533 (56.2)	1221 (85.6)		
lobulated or irregular	359 (37.8)	182 (12.7)		
extra-thyroid extension	57 (6.0)	24 (1.7)		
Echogenic foci			x^2 = 368.018	P<0.001
none or large comet-tail artifacts	328 (34.6)	1049 (73.5)		
macro	52 (5.5)	55 (3.8)		
peripheral	48 (5.0)	41 (2.9)		
punctate echogenic foci	521 (54.9)	282 (19.8)		

showed a significant difference to predict CLNM in the PTC2 subgroup (Table 3).

Clinical information as well as ultrasonographic measurements and characteristics were included in the binary linear regression analysis. Aspect ratio was included in cross-sectional and longitudinal section aspect ratio. The results showed that gender, age, maximum tumor diameter and volume, CSAR, location, echogenicity, margin, and echogenic foci were independent risk factors for CLNM (Table 4).

Binary linear regression analysis and the ROC curves were used to obtain the independent correlative factors for CLNM. The AUC, specificity, and sensitivity of maximum tumor diameter were 0.70, 64.5%, and 65.7%, respectively. For tumor volume, the AUC, specificity, and sensitivity were 0.69, 66.4%, and 63.8%, respectively. For margin, the AUC, specificity, and sensitivity were 0.65, 85.6%, and 43.5%, respectively. For echogenic foci, the AUC, specificity, and sensitivity were 0.70, 74.0%, and 64.8%, respectively. To consider CLNM in PTC patients as a dependent variable and independent risk factors as covariates, a regression equation of CLNM was deduced from the parameters: Y = −3.657+0.063*X1-0.061*X2+0.519*X3+0.444*X4. In this equation, Y = CLNM, X1 = maximum tumor diameter, X2 = tumor volume, X3 = margin, and X4 = echogenic foci. The ROC curve was used to evaluate the regression model constructed by combining four independent correlative factors (maximum tumor diameter and volume, margin, and echogenic foci), in which the

TABLE 3 Univariate analysis of PTC1 and PTC2 in the positive group.

Variable	Cross-sectionalaspect ratio≥1	longitudinal section aspect ratio≥1	Statistics	P
			x^2 = 14.455	P<0.001
PTC1+CLNM (445)	281	205		
PTC2+CLNM (504)	181	70		

TABLE 4 Logistic regression analysis of correlative factors with CLNM in PTC.

Variable Overall (N=949, n=1427)	OR	95% CIs	P
Gender	1.69	1.45~1.97	P < 0.001
Age	0.97	0.96~0.97	P < 0.001
Maximum tumor diameter	1.07	1.05~1.09	P < 0.001
Tumor volume	0.94	0.91~0.98	P = 0.002
Cross-sectional aspect ratio	1.52	1.08~2.12	P = 0.016
Longitudinal section aspect ratio	1.04	0.74~1.46	P = 0.836
Location	1.07	1.03~1.11	P=0.001
Echogenicity	2.68	2.14~3.36	P < 0.001
Margin	1.68	1.56~1.81	P < 0.001
Echogenic foci	1.56	1.48~1.64	P < 0.001

N, The number of patients for the positive group; n, The number of patients for the negative group.

value of AUC, specificity, and sensitivity was 0.77, 73.4%, and 72.3%, respectively (Table 5, Figure 2). The AUC differences among the prediction model and the dependent variables have statistical significance (P < 0.001).

According to the differences in clinical and ultrasonic characteristics using Kruskal-Wallis analysis, maximum tumor diameter and volume, cross-sectional and longitudinal aspect ratio, margin, and echogenic foci were statistically significant (P. < 0.05). The comparisons between the positive subgroups are shown in Table 6.

Discussion

With the application of high frequency ultrasound, the incidence of thyroid lesions in adults can be up to 60%–70% (10). PTC is the most common malignant thyroid tumor, and lymph node metastasis of PTC is associated with the diameter, location, number, and invasive growth of the primary tumor (9, 11). The sensitivity of ultrasound for the evaluation of central and lateral compartment lymph nodes is around 60% (9) In this study, compared with cN1 and pN1, the detection rate of cervical lymph node metastases was 62.2% (590/949). CLNM in PTC generally first occurs in the central region and then progresses to the lateral region (12), which is most common in area VI, followed by areas III and IV (13). However, not all PTC lymph node metastases follow this pattern and instead skip, where lymph node metastasis occurs in the lateral neck region and no metastasis is identified in the ipsilateral central region (14). Some studies have reported that the rate of lymph node skip metastasis is 3.0%–21.8% (15). Only unifocal PTC was included in this study and the lymph node skip metastasis rate was 7.4% (70/949).

Heaton et al. (16) reported that women and elderly patients were at higher risk of PTC, while men and younger patients were at higher risk of CLNM. In this study, CLNM occurred in 51.0% (290/569) of male patients, and occurred in only 36.5% (659/1807) of female patients, which also suggests that male patients have a higher risk of lymph node metastasis. We used 55 years as the threshold in this study according to the TNM staging system

TABLE 5 ROC analysis of the independent variables in identifying CLNM in PTC.

Variable Overall (N=949, n=1427)	AUC	95% CIs	Specificity	Sensitivity
Gender	0.55	0.54~0.57	80.5%	30.1%
Age	0.37	0.35~0.38	99.9%	0.2%
Tumor maximum diameter	0.70	0.68~0.71	64.5%	65.7%
Tumor volume	0.69	0.68~0.71	66.4%	63.8%
Cross-sectional aspect ratio	0.43	0.41~0.45	99.6%	0.2%
Location	0.54	0.52~0.55	88.8%	18.0%
Echogenicity	0.53	0.51~0.55	94.1%	11.8%
Margin	0.65	0.63~0.66	85.6%	43.5%
Echogenic foci	0.70	0.69~0.72	74.0%	64.8%
Equation	0.77	0.75~0.78	73.4%	72.3%

N, The number of patients for the positive group; n, The number of patients for the negative group.

10.3389/fendo.2022.965241

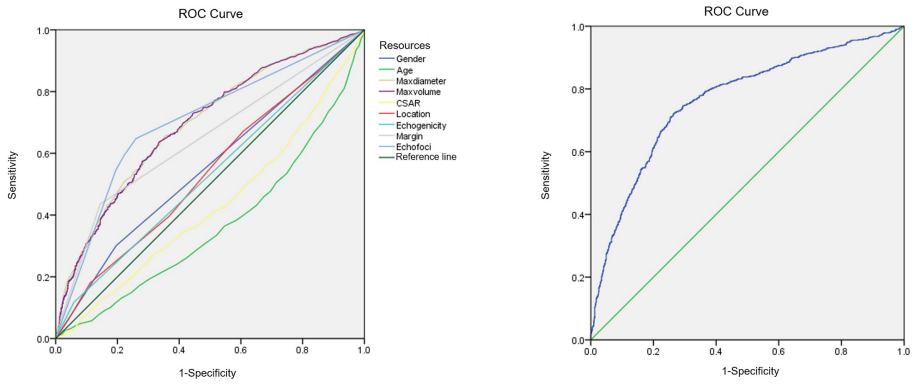

FIGURE 2
ROC curves for independent correlative factors and equation with CLNM in PTC.

for thyroid cancer (17), and 42.4% (827/1952) of patients who were younger than 55 years had CLNM. Among those who were 55 years or older, lymph node metastases occurred in only 28.8% (122/424) of patients in this study.

Maximum tumor diameter is an important reference index for PTC treatment protocols and for range of surgery (18). The results of this study demonstrated that the average maximum tumor diameter in the positive group was about 1.6 times that in the negative group (13.3 mm vs. 8.5 mm, respectively). The tumors appeared to be ellipsoid, and therefore volume as the evaluation parameter made the result more objective and scientific. The average tumor volume in the positive group was about 3.2 times that in the negative group (1.6 ml vs. 0.5 ml, respectively). For larger tumors, cervical lymph nodes should be examined in order to improve the detection rate of CLNM. In particular, in patients with large tumors, the presence of central and lateral lymph node metastasis should be determined in advance.

TI-RADS was mainly adopted for the differential diagnosis of benign and malignant thyroid neoplasms. The consistent conclusion of the association between lymph node metastasis and gender, age, and sonographic characteristics was difficult to achieve (19–21). This study only included unifocal PTC and was conducted as a stratified study to comprehensively evaluate the

TABLE 6 Kruskal-Wallis analysis of the positive subgroups with CLNM in PTC.

Variable	Central (n=669)	Lateral (n=70)	Both (n=210)	Statistics	P
Gender (male/female)	197/472	17/53	76/134	x^2 = 4.821	P = 0.090
Age	41.1 ± 11.5	44.2 ± 13.5	40.1 ± 13.0	x^2 = 5.654	P = 0.059
Tumor maximum diameter	11.2 ± 7.3	15.9 ± 9.5	19.0 ± 11.4	x^2 = 130.278	P < 0.001
Tumor volume	0.9 ± 2.2	2.8 ± 6.2	3.2 ± 6.2	x^2 = 132.410	P < 0.001
Cross-sectional aspect ratio	1.0 ± 0.3	1.0 ± 0.3	0.9 ± 0.2	x^2 = 16.378	P < 0.001
Longitudinal aspect ratio	0.9 ± 0.3	0.9 ± 0.2	0.8 ± 0.3	x^2 = 41.625	P < 0.001
Echogenicity				x^2 = 0.474	P = 0.789
Hyperechoic or isoechoic	10 (1.5)	0 (0)	6 (2.9)		
Hypoechoic	603 (90.1)	66 (94.3)	187 (89.0)		
Very hypoechoic	56 (8.4)	4 (5.7)	17 (8.1)		
Margin				x^2 = 69.606	P < 0.001
smooth or ill-defined	436 (65.2)	23 (32.9)	74 (35.2)		
lobulated or irregular	199 (29.7)	43 (61.4)	117 (55.7)		
extra-thyroid extension	34 (5.1)	4 (5.7)	19 (9.1)		
Echogenic foci				x^2 = 35.508	P < 0.001
none or large comet-tail artifacts	274 (41.0)	17 (24.3)	37 (17.6)		
macro	36 (5.4)	1 (1.4)	15 (7.1)		
peripheral	27 (4.0)	7 (10.0)	14 (6.7)		
punctate echogenic foci	332 (49.6)	45 (64.3)	144 (68.6)		

risks of CLNM in PTC. This was combined with clinical information, ultrasonographic measurements, and TI-RADS to obtain a more complete and effective result.

PTC can occur in any part of the thyroid, including bilateral lobes and the isthmus. For the isthmus, the incidence of thyroid cancer is 2.5%–9.2% (22). Studies have found that PTC of the isthmus is more likely to invade the thyroid capsule and surrounding tissues, compared to lateral lobe PTC (18, 23). This is mainly because the area of the isthmus tumor in contact with thyroid capsule is relatively large, and can therefore easily invade the capsule or break through the capsule to invade surrounding tissues, leading to CLNM. Previous studies (24) have suggested that tumors located in the middle or lower pole of thyroid have increased risk of CLNM. In this study, the incidence of PTC lymph node metastasis was higher in the middle pole than in the upper pole, lower pole, or isthmus (middle, 42%; upper, 30.7%; lower, 21.1%; isthmus, 6.2%).

An aspect ratio ≥ 1 is a highly specific index for the diagnosis of malignant thyroid nodules (25, 26). According to previous literature, the results of association between aspect ratio and CLNM in PTC were not consistent. Some studies (27, 28) have suggested that CLNM was prone to occur with an aspect ratio > 1 and that CLNM was the risk factor. One study (29) reported that no statistical significance could be seen in the prediction of lateral CLNM with an aspect ratio ≥ 1. According to the morphology of a thyroid lesion, we divided the aspect ratio into cross-sectional and longitudinal section aspect ratios. Aspect ratio had statistical significance in univariate analysis, and while we used the binary logistical analysis, there was no significant difference for longitudinal section aspect ratio. The main reason was that PTMC patients comprised 63.9% (1518/2376) of the study participants, and just 29.3% (445/1518) were in the positive group. We compared CSAR and longitudinal section aspect ratio for PTC1 and PTC2 groups, and it could be concluded that the CSAR had a better predictive value for CLNM in PTC2. There was less relevant literature with the association between cross-sectional and longitudinal section aspect ratio in predicting CLNM, especially for PTC2. Additional studies are needed in the future for clarification.

When malignant tumors grow rapidly, the cancer cells continue to invade outward and the incidence of lymph node metastasis is increased (16, 30). Margin is traditionally used to analyze the invasiveness of a tumor. Nodules with high invasiveness show irregular and lobulated boundaries, while smooth boundaries generally indicate low invasiveness and slow growth (31). In this study, univariate analysis and logistic regression analysis both showed a good association between margin and CLNM in PTC. This is consistent with previous literature reports (20, 24). Lesions with lobulated or irregular shape occurred more often in the lateral metastasis and both metastasis groups than the central metastasis group by Kruskal-Wallis analysis.

Echogenic foci are classified as micro-calcification, macro-calcification, or ring calcification around the nodules on the basis of 1 mm (32). Micro-calcification can reflect the psammoma bodies in pathology, which results from calcification and necrosis of cancer cells and is a specific indicator for the diagnosis of PTC (33); it is also significantly related to lymph node metastasis. Continuous follow-up studies found that CLNM was more likely to occur in PTC with micro-calcification (31, 34). In this study, 54.9% (521/949) of lesions with CLNM had punctate echogenic foci. Among the negative group, punctate echogenic foci occurred in only 19.8% (282/1427) of lesions. For the positive subgroups, echogenic foci also showed a significant difference ($P < 0.001$). Therefore, ultrasonography can better predict the risk of CLNM in PTC using the different types of calcifications.

TI-RADS comprehensively evaluated tumors according to sonographic characteristics of thyroid nodules. Its scoring and grading system were used for the differential diagnosis of benign and malignant nodules, and it would be of great value for further determination of diagnosis and treatment protocols. In this study, ultrasonographic measurements and characteristics were included for logistic regression analysis to establish a prediction model for CLNM with the AUC of 0.77, a specificity of 73.4% and a sensitivity of 72.3%. Sun et al. (35) reported that they used gender, age, max tumor diameter, number of nodules, and cervical lymph node detected by ultrasound as covariates; CLNM was a dependent variable, and a prediction model was acquired with a specificity of 80.8% and a sensitivity of 59.8%. Zou et al. (36) reported that the area under the ROC curve was 0.758 for the preoperative prediction of lymph nodes posterior to the right recurrent laryngeal nerve metastasis, and used five independent correlative factors (age, male, tumor diameter, US-detected lateral compartment lymph node metastasis, and microcalcifications) for evaluation. Liang et al. (37) found that central lymph node metastasis was associated with male gender, younger age (< 45 years), extrathyroidal invasion, multifocality, and lateral lymph node metastasis in PTMC. In our study, central neck metastasis, lateral neck metastasis, and both central and lateral neck metastasis were analyzed and compared for PTC, including PTMC. We also divided the aspect ratio into cross-sectional and longitudinal section aspect ratios, and CSAR had a more effective predictive value for larger thyroid tumors. The result has reference value and also demonstrates the importance of comprehensive evaluation of ultrasound in clinical practice.

This study has some limitations. First, this was a retrospective study including unifocal PTC and lymph node dissection performed in the central area, which may cause selection bias. Second, cases with metastases in lateral locations were not adequate, and large samples are required to study cervical metastases in different locations. For skip lateral lymph node metastases, more effective preoperative assessment

should be adopted. Finally, this is our preliminary study for a larger future study of PTC patients. In future research, we will add detailed clinical and pathological staging, subdivided pathological types, and machine learning models.

Conclusions

In conclusion, based on PTC pathology, the correlations between gender and age, as well as ultrasonographic measurements and characteristics were analyzed in order to assess a good clinical value for preoperative evaluation of the risk of lymph node metastasis. For PTC patients with high-risk factors such as age < 55 years, male, larger tumor and punctate echogenic foci, preoperative lymph node examination should be conducted in detail. This examination should include a cervical lymph node sonographic scan by an experienced sonographer (with experience of more than 10 years) and CT scan of the neck, which will cover a wide range of thyroid cancer population and help develop the most reasonable clinical treatment protocol.

Data availability statement

The original contributions presented in the study are included in the article/Supplementary Material. Further inquiries can be directed to the corresponding authors.

Ethics statement

The studies involving human participants were reviewed and approved by the Ethics Committee of Cancer Hospital of the University of Chinese Academy of Sciences (Zhejiang Cancer Hospital), Zhejiang Xiaoshan Hospital and Hangzhou Cancer Hospital. The patients/participants provided their written informed consent to participate in this study.

Author contributions

DX had full access to all data and took responsibility for the integrity and accuracy of the data analysis. LZ and JY were major contributors in writing the manuscript. DO participated in collection and management of the data. LW, ML and ZL contributed to analyze and interpret the data. All authors contributed to the article and approved the submitted version.

Funding

This study was supported by National Natural Science Foundation of China (NO. 82071946) and Zhejiang Provincial Natural Science Foundation of China (NO. LSD19H180001). DX is responsible for these two funds.

Acknowledgments

The authors thank Chen Cui, PhD for reviewing the manuscript and providing support with data analysis. This manuscript has been released as a pre-print at Research Square, DOI:10.21203/rs.3.rs-839643/v1.

Conflict of interest

The authors declare that the research was conducted in the absence of any commercial or financial relationships that could be construed as a potential conflict of interest.

Publisher's note

Supplementary material

The Supplementary Material for this article can be found online at: https://www.frontiersin.org/articles/10.3389/fendo.2022.965241/full#supplementary-material

References

1. Tessler FN, Middleton WD, Grant EG, Hoang JK, Berland LL, Teefey SA, et al. ACR thyroid imaging, reporting and data system (TI-RADS): white paper of the ACR TI-RADS committee. *J Am Coll Radiol* (2017) 14(5):587–95. doi: 10.1016/j.jacr.2017.01.046

2. Lim H, Devesa SS, Sosa JA, Check D, Kitahara CM. Trends in thyroid cancer incidence and mortality in the united states, 1974-2013. *JAMA* (2017) 317 (13):1338–48. doi: 10.1001/jama.2017.2719

3. Kim SY, Kwak JY, Kim EK, Yoon JH, Moon HJ. Association of preoperative US features and recurrence in patients with classic papillary thyroid carcinoma. *Radiology* (2015) 277(2):574–83. doi: 10.1148/radiol.2015142470

4. Li JW, Chang C, Chen M, Fan YW, Zeng W, Gao Y, et al. Identification of calcifications in thyroid nodules: comparison between ultrasonography and CT. *Chin J Ultrasonogr* (2016) 25(5):384–7. doi: 10.3760/cma.j.issn.1004-4477.2016.05.006

5. Zhu Q, Li JW, Zhou SC, Chang C, Chen M, Fan YW. Diagnostic value of ultrasonography in predicting neck lymph node metastasis in hashimoto's thyroiditis with papillary thyroid carcinoma. *Chin J Ultrasonogr* (2016) 25 (11):962–5. doi: 10.3760/cma.j.issn.1004-4477.2016.11.011

6. Chinese Association of Thyroid Oncology (CATO). Chinese experts' consensus on diagnosis and treatment of thyroid micropapillary carcinoma. *Chin J Clin Oncol* (2016) 43(10):405–11. doi: 10.3969/j.issn.1000-8179.2016.10.001

7. Chinese Thyroid association (CTA), thyroid committee of Chinese research hospital association. expert consensus on lymph node dissection in cervical region of differentiated thyroid cancer. *Chin J Pract Surg* (2017) 37(9):985–91. doi: 10.19538/j.cjps.issn1005-2208.2017.09.13

8. Wang TS, Evans DB. Commentary on: Occult lymph node metastasis and risk of regional recurrence in papillary thyroid cancer after bilateral prophylactic central neck dissection: A multi-institutional study. *Surgery* (2017) 161(2):472–4. doi: 10.1016/j.surg.2016.09.019

9. Haugen BR, Alexander EK, Bible KC, Doherty GM, Mandel SJ, Nikiforov YE, et al. 2015 American Thyroid association management guidelines for adult patients with thyroid nodules and differentiated thyroid cancer. *Thyroid* (2016) 26(1):1–133. doi: 10.1089/thy.2015.0020

10. Guth S, Theune U, Aberle J, Galach A, Bamberger CM. Very high prevalence of thyroid nodules detected by high frequency (13MHz) ultrasound examination. *Eur J Clin Invest* (2009) 39:699–706. doi: 10.1111/j.1365-2362.2009.02162.x

11. Park JP, Roh JL, Lee JH, Baek JH, Gong G, Cho KJ, et al. Risk factors for central neck lymph node metastasis of clinically noninvasive, node-negative papillary thyroid microcarcinoma[J]. *Am J Surg* (2014) 208(3):412–8. doi: 10.1016/j.amjsurg.2013.10.032

12. Zeng RC, Zhang W, Gao EL, Cheng P, Huang GL, Zhang XH, et al. Number of central lymph node metastasis for predicting lateral lymph node metastasis in papillary thyroid microcarcinoma. *Head Neck* (2014) 36(1):101–6. doi: 10.1002/hed.23270

13. Kim KE, Kim EK, Yoon JH, Han KH, Moon HJ, Kwak JY. Preoperative prediction of central lymph node metastasis in thyroid papillary microcarcinoma using clinicopathologic and sonographic features. *Word J Surg* (2013) 37(2):385–91. doi: 10.1007/s00268-012-1826-3

14. Lee YS, Shin SC, Lim YS, Lee JC, Wang SG, Son SM, et al. Tumor location-dependent skip lateral cervical lymph node metastasis in papillary thyroid cancer. *Head Nek* (2014) 36(6):887–91. doi: 10.1002/hed.23391

15. Lei J, Zhong J, Jiang K, Li Z, Gong R, Zhu J. Skip lateral lymph node metastasis leaping over the central neck compartment in papillary thyroid carcinoma. *Oncotarget* (2017) 8(16):27022–33. doi: 10.18632/oncotarget.15388

16. Heaton CM, Chang JL, Orloff LA. Prognostic implications of lymph node yield in central and lateral neck dissections for well-differentiated papillary thyroid carcinoma. *Thyroid* (2016) 26(3):434–40. doi: 10.1089/thy.2015.0318

17. Zheng G, Zhang H, Hao S, Liu C, Xu J, Ning J, et al. Patterns and clinical significance of cervical lymph node metastasis in papillary thyroid cancer patients with delphian lymph node metastasis. *Oncotarget* (2017) 8(34):57089–98. doi: 10.18632/oncotarget.19047

18. Xiang D, Xie L, Xu Y, Li Z, Hong Y, Wang P. Papillary thyroid microcarcinomas located at the middle part of the middle thyroid of the thyroid gland correlates with the presence of neck metastasis. *Surgery* (2015) 157(3):526–33. doi: 10.1016/j.surg.2014.10.020

19. Afif A AI, Williams BA, Rigby MH, Bullock MJ, Taylor SM, Trites J, et al. Multifocal papillary thyroid cancer increases the risk of central lymph node metastasis. *Thyroid* (2015) 25(9):1008–12. doi: 10.1089/thy.2015.0130

20. Lin DZ, Qu N, Shi RL, Lu ZW, Ji QH, Wu WL. Risk prediction and clinical model building for lymph node metastasis in papillary thyroid microcarcinoma. *Onco Targets Ther* (2016) 9:5307–16. doi: 10.2147/OTT.S107913

21. Qu N, Zhang L, Lin DZ, Ji QH, Zhu YX, Wang Y. The impact of coexistent hashimoto's thyroiditis on lymph node metastasis and prognosis in papillary thyroid microcarcinoma. *Tumor Biol* (2016) 37(6):7685–92. doi: 10.1007/s13277-015-4534-4

22. Lee YS, Jeong JJ, Nam KH, Chung WY, Chang HS, Park CS. Papillary carcinoma located in the thyroid isthmus. *World J Surg* (2010) 34(1):36–9. doi: 10.1007/s00268-009-0298-6

23. Fan FJ, Qin L, Ding HY, Liu DQ, Jia JY, Tan Z. Study on ultrasound image features of papillary thyroid carcinoma originating in the isthmus. *Chin J Clin* (2015) 9(20):3720–3. doi: 10.3877//cma.j.issn.1674-0785.2015.20.012

24. Sun W, Lan X, Zhang H, Dong W, Wang Z, He L, et al. Risk factors for central lymph node metastasis in CN0 papillary thyroid carcinoma: a systematic review and meta-analysis. *PloS One* (2015) 10(10):e0139021. doi: 10.1371/journal.pone.0139021

25. Kwak JY, Han KH, Yoon JH, Moon HJ, Son EJ, Park SH, et al. Thyroid imaging reporting and data system for US features of nodules: a step in establishing better stratification of cancer risk. *Radiology* (2011) 260(3):892–9. doi: 10.1148/radiol.11110206

26. Na DG, Baek JH, Sung JY, Kim JH, Kim JK, Choi YJ, et al. Thyroid imaging reporting and data system risk stratification of thyroid nodules: categorization based on solidity and echogenicity. *Thyroid* (2016) 26(4):562–72. doi: 10.1089/thy.2015.0460

27. Nam SY, Shin JH, Han BK, Ko EY, Ko ES, Hahn SY, et al. Preoperative ultrasonographic features of papillary thyroid carcinoma predict biological behavior. *J Clin Endocrinol Metab* (2013) 98(4):1476–82. doi: 10.1210/jc.2012-4072

28. Zhou J, Zhou SC, Li JW, Wang Y, Chen YL, Wang F, et al. Risk factors of central neck lymph node metastasis following solitary papillary thyroid carcinoma. *Chin J Ultrasonogr* (2019) 28(3):235–40. doi: 10.3760/cma.j.issn.1004-4477.2019.03.009

29. Deng SP, Xiong HH, Li QS, Chen SH, Guo GQ, Wang J, et al. Ultrasonographic characteristics of papillary thyroid cancer: predicting factors of lateral lymph node metastasis. *Chin J Ultrasound Med* (2017) 33(3):196–8. doi: 10.3969/j.issn.1002-0101.2017.03.002

30. Lan Y, Song Q, Jin Z, Zhang Y, Lin L, Luo YK. Correction of routine ultrasound features and BRAFV600E gene to the cervical lymph node metastasis of thyroid papillary carcinoma. *Med J Chin PLA* (2019) 44(9):747–52. doi: 10.11855/j.issn.0577-7402.2019.09.06

31. Bai Y, Zhou G, Nakamura M, Ozaki T, Mori I, Taniguchi E, et al. Survival impact of psammoma body, stromal calcification and bone formation in papillary thyroid carcinoma. *Mod Pathol* (2009) 22(7):887–94. doi: 10.1038/modpathol.2009.38

32. Oh EM, Chung YS, Song WJ, Lee YD. The pattern and significance of the calcifications of papillary thyroid microcarcinoma presented in preoperative neck ultrasonography. *Ann Surg Treat Res* (2014) 86(3):115–21. doi: 10.4174/astr.2014.86.3.115

33. Shi C, Li S, Shi T, Liu B, Ding C, Qin H. Correlation between thyroid nodule calcification morphology on ultrasound and thyroid carcinoma. *J Int Med Res* (2012) 40(1):350–7. doi: 10.1177/147323001204000136

34. Deng SP, Li QS, Chen SH, Guo GQ, Wang J, Luo CR, et al. Analysis of related factors on cervical lymph node metastasis and ultrasonographic characteristics of papillary thyroid microcarcinoma. *J Clin Ultrasound Med* (2017) 19(6):424–6. doi: 10.3969/j.issn.1008-6978.2017.06.025

35. Sun YS, HJ LV, Zhao YR, Shi BY. Risk factors for central neck lymph node metastases of papillary thyroid carcinoma. *Chin J Otorhinolaryngol Head Neck Surg* (2017) 52(6):421–5. doi: 10.3760/cma.j.issn.1673-0860.2017.06.005

36. Zou M, Wang YH, Dong YF, Lai XJ, Li JC. Clinical and sonographic features for the preoperative prediction of lymph nodes posterior to the right recurrent laryngeal nerve metastasis in patients with papillary thyroid carcinoma. *J Endocrinol Invest* (2020) 43(10):1511–7. doi: 10.1007/s40618-020-01238-0

37. Liang JW, Luo YH, Liang K, Huang B, Zhao YJ, Wang HT, et al. Clinicopathologic factors and preoperative ultrasonographic characteristics for predicting central lymph node metastasis in papillary thyroid microcarcinoma: a single center retrospective study. *Braz J Otorhinolaryngol* (2020) 88(1):36–45. doi: 10.1016/j.bjorl.2020.05.004

frontiers | Frontiers in Endocrinology

TYPE Original Research
PUBLISHED 21 February 2023
DOI 10.3389/fendo.2023.964074

OPEN ACCESS

EDITED BY
Terry Francis Davies,
Icahn School of Medicine at Mount Sinai, United States

REVIEWED BY
Erivelto Martinho Volpi,
Centro de Referência no Ensino do Diagnóstico por Imagem, Brazil
Zeyu Wu,
Guangdong Provincial People's Hospital, China

*CORRESPONDENCE
Xi Wei
weixi@tmu.edu.cn

†These authors have contributed equally to this work and share first authorship

SPECIALTY SECTION
This article was submitted to Thyroid Endocrinology, a section of the journal Frontiers in Endocrinology

RECEIVED 08 June 2022
ACCEPTED 10 February 2023
PUBLISHED 21 February 2023

CITATION
Chang L, Zhang Y, Zhu J, Hu L, Wang X, Zhang H, Gu Q, Chen X, Zhang S, Gao M and Wei X (2023) An integrated nomogram combining deep learning, clinical characteristics and ultrasound features for predicting central lymph node metastasis in papillary thyroid cancer: A multicenter study.
Front. Endocrinol. 14:964074.
doi: 10.3389/fendo.2023.964074

An integrated nomogram combining deep learning, clinical characteristics and ultrasound features for predicting central lymph node metastasis in papillary thyroid cancer: A multicenter study

Luchen Chang[1†], Yanqiu Zhang[1†], Jialin Zhu[1†], Linfei Hu[2], Xiaoqing Wang[1], Haozhi Zhang[2], Qing Gu[3], Xiaoyu Chen[1], Sheng Zhang[1], Ming Gao[2,4] and Xi Wei[1*]

[1]Department of Diagnostic and Therapeutic Ultrasonography, Tianjin Medical University Cancer Institute and Hospital, National Clinical Research Center for Cancer, Key Laboratory of Cancer Prevention and Therapy, Tianjin's Clinical Research Center for Cancer, Tianjin, China, [2]Department of Thyroid and Neck Cancer, Tianjin Medical University Cancer Institute and Hospital, National Clinical Research Center of Cancer, Key Laboratory of Cancer Prevention and Therapy, Tianjin's Clinical Research Center for Cancer, Tianjin, China, [3]Department of Ultrasonography, Cangzhou Hospital of Integrated Traditional Chinese and Western Medicine of Hebei Province, Cangzhou, Hebei, China, [4]Department of Breast and Thyroid Surgery, Tianjin Union Medical Center, Tianjin, China

Objective: Central lymph node metastasis (CLNM) is a predictor of poor prognosis for papillary thyroid carcinoma (PTC) patients. The options for surgeon operation or follow-up depend on the state of CLNM while accurate prediction is a challenge for radiologists. The present study aimed to develop and validate an effective preoperative nomogram combining deep learning, clinical characteristics and ultrasound features for predicting CLNM.

Materials and methods: In this study, 3359 PTC patients who had undergone total thyroidectomy or thyroid lobectomy from two medical centers were enrolled. The patients were divided into three datasets for training, internal validation and external validation. We constructed an integrated nomogram combining deep learning, clinical characteristics and ultrasound features using multivariable logistic regression to predict CLNM in PTC patients.

Results: Multivariate analysis indicated that the AI model-predicted value, multiple, position, microcalcification, abutment/perimeter ratio and US-reported LN status were independent risk factors predicting CLNM. The area under the curve (AUC) for the nomogram to predict CLNM was 0.812 (95% CI, 0.794-0.830) in the training cohort, 0.809 (95% CI, 0.780-0.837) in the internal validation cohort and 0.829(95%CI, 0.785-0.872) in the external validation

cohort. Based on the analysis of the decision curve, our integrated nomogram was superior to other models in terms of clinical predictive ability.

Conclusion: Our proposed thyroid cancer lymph node metastasis nomogram shows favorable predictive value to assist surgeons in making appropriate surgical decisions in PTC treatment.

KEYWORDS

deep learning, papillary thyroid carcinoma, central lymph node metastasis, nomogram, ultrasound

Introduction

The global prevalence of thyroid cancer has sharply increased in the past few decades, and it is also increasing in China. Papillary thyroid carcinoma (PTC) is the most common type of thyroid cancer, which accounts for approximately 80% of all thyroid carcinomas (1–3). PTC is usually an indolent cancer, and the 10-year survival rate of PTC can reach 93% if standardized treatment is accepted (4). However, PTC easily metastasizes to cervical lymph nodes, and the prevalence of central lymph node metastasis (CLNM) can reach as high as 40% to 60% (5, 6). CLNM status is an important risk factor for high recurrence rates and low patient survival (7, 8). A key and controversial problem in thyroid cancer management is if prophylactic central lymph node dissection (CLND) is necessary. CLND is recommended for patients who are suspected of CLNM in preoperative assessment. Some researchers demonstrated that prophylactic CNLD can more accurately stage tumors and reduce recurrence rates in patients with intermediate and high-risk thyroid cancer, while others argue that patients may gain no benefit or some temporary morbidity (such as hypocalcemia and spinal accessory nerve dysfunction), and endoscopic lymphadenopathy (9, 10). Therefore, most studies do not recommend the routine use of prophylactic CLND in PTC (11, 12).

According to the American Thyroid Association guidelines, preoperative neck ultrasound (US) is recommended to evaluate cervical lymph nodes, but the diagnosis rate is not accurate; although it has high diagnostic value for accessing lateral lymph node metastasis(LLNM), it has relatively low sensitivity in the diagnosis of CLNM (13–15).Thus, an effective and non-invasive way to predict CLNM before surgery is urgently needed to provide optimal surgical treatments.

Thyroid cancer nomograms are widely used as a prognostic tool to understand the nature of thyroid cancer lesions, assess the unknown risk of disease and predict the possible outcome of treatment. Several established models based on the clinical and ultrasound characteristics to predict CLNM, but their performance is not satisfactory and not adaptable to actual clinical work (16–19). Currently, the use of artificial intelligence (AI) in medicine has gained interest, particularly in analyzing and diagnosing medical images (20, 21). AI models provide another opinion to assist radiologists in interpreting the images by improving the accuracy and consistency of disease diagnosis and by reducing the time to output results. Several studies have investigated deep learning to diagnose thyroid malignancy and have achieved better performance than human readers (22–25). Therefore, the prospect of deep learning in predicting lymph node metastasis is worth exploring. To our knowledge, deep learning has not yet been integrated with clinical and ultrasound factors to construct a combined nomogram to predict CLNM in PTC patients.

Recently, we developed a thyroid cancer lymph node metastasis AI system-based deep learning model to predict the status of cervical lymph nodes. The purpose of the present study was to (1) evaluate the value of this system to predict CLNM and to (2) combine it with additional clinical and ultrasound characteristics to establish a more robust and generalizable model for the prediction of CLNM in PTC patients. The flowchart of our model development is shown in Figure 1.

Materials and methods

Patients

In this study, a total of 3359 PTC patients who had undergone first-time thyroidectomy to treat thyroid carcinoma at two centers (center#1: Tianjin Medical University Cancer Institute and Hospital; center#2: Binzhou Medical University Hospital) were enrolled from March 2011 to June 2018. Data from center#1 were randomly divided into two groups as follows: 70% for a training cohort (n=2114) and 30% for an internal validation cohort(n=906), respectively. Data from center#2 (n = 339) were used for an external validation cohort. This study was approved by the Ethics Committee of Tianjin Medical University Cancer Institute and Hospital(No. bc2020190), and the requirements for informed consent were waived.

Total thyroidectomy or thyroid lobectomy with therapeutic or prophylactic lymph node dissection was performed for patients. Ipsilateral central neck lymph node dissection (CLND) was routinely performed, total thyroidectomy with bilateral CLND was performed for patients with bilateral PTC or patients with clinical evidence of contralateral CLNM. At the center#1, the

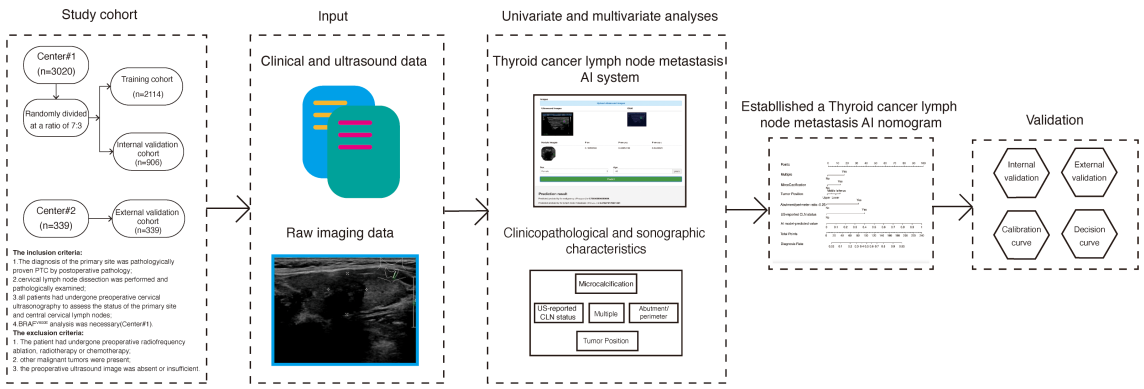

FIGURE 1
Flow diagram of the thyroid cancer lymph node metastasis nomogram.

inclusion criteria were as follows: (1) the diagnosis of the primary site was pathologically proven PTC by postoperative pathology; (2) cervical lymph node dissection was performed and pathologically examined; (3) all patients had undergone preoperative cervical ultrasonography to assess the status of the primary site and central cervical lymph nodes; and (4) $BRAF^{V600E}$ analysis was necessary. The exclusion criteria were as follows: (1) the patient had undergone preoperative radiofrequency ablation, radiotherapy or chemotherapy; (2) other malignant tumors were present; and (3) the preoperative ultrasound image was absent or insufficient. All pathology specimens were reviewed retrospectively by two or more experienced pathologists. At the center#2, we have the same inclusion criteria, but the $BRAF^{V600E}$ analysis is not within the scope of the record.

Ultrasonography and image analysis

All patients had undergone ultrasound examination before surgery to assess the characteristics of the nodules and status of the central lymph node (CLN). All ultrasound images were reviewed and interpreted by two experienced radiologists (Dr. Wei X and Dr. Zhang S with 15 and 30 years of experience in thyroid cancer US diagnosis, respectively).

All ultrasound examinations used a Phillips EPIQ 5, IU 22, HD11 (Philips Healthcare, Eindhoven, The Netherlands) equipped with a high-frequency linear array probe (5–12 MHz) to perform thyroid cross-section, longitudinal section and cervical lymph node scan. We reviewed the size, number, location and sonographic features of the thyroid lesions in the longitudinal and transverse axes. The size of the tumor was the largest diameter of the tumor and was divided into the following groups: ≤0.5 cm, 0.5~1.0 cm, 1.0~2.0 cm and ≥2.0 cm. If there was more than one nodule that was suspected as malignant, we defined it as multiple. In multiple cases, the size of the tumor was classified according to the diameter of the largest tumor. The position of the lesion was evaluated from the following four aspects: upper, middle, lower and isthmus. We further divided several typical ultrasound features of nodules according to the American College of Radiology Thyroid Imaging Reporting and Data System (ACR TI-RADS) (26), including the composition (mixed cystic and solid or solid), echogenicity (isoechoic or hyperechoic, hypoechoic or very hypoechoic), shape (taller-than-wide<1 or taller-than-wide≥1), margin (clear or unclear) and microcalcifications (yes or no). In addition, Hashimoto's thyroiditis and the abutment of the thyroid capsule were evaluated on the basis of ultrasound images. Hashimoto's thyroiditis manifests as uneven echogenicity of the thyroid parenchyma on ultrasonography, with a few or multiple lamellar hypoechoic areas showing grid-like changes. The measurement of abutment or the perimeter in a thyroid lesion was calculated by the average ratio (1/2) on the transverse + longitudinal section of a nodule. Based on our previous study (27), we selected the 1/4 (25%) perimeter of the thyroid lesion as the cutoff value.

The ultrasound features of the involved lymph nodes were based on various criteria. Lymph nodes showing one or more suspicious US features (internal microcalcifications, cystic changes, hyperechogenicity, round shape, loss of hilar echogenicity or the presence of peripheral flow) on ultrasound images were regarded as US-reported metastatic CLN according to ACR TI-RADS (26).

$BRAF^{V600E}$ mutation analysis

Fine needle aspiration biopsies were repeated at least three times per aspiration using a 22-gauge needle for $BRAF^{V600E}$ mutation assessment in cytology. Immediately after aspiration, the needle and syringe were washed with 1 ml of normal saline, and samples with sufficient numbers of tumor cells were used for real-time PCR analysis (28).

Thyroid cancer lymph node metastasis AI system

The fully automated deep learning model used in this research was developed by the author, ZHZ, and a cloud-based artificial intelligence diagnosis platform, named the thyroid cancer lymph

node metastasis AI system, was established based on this model. This model uses the Mask R-CNN framework as a computer vision framework for nodules segmentation and has the following capabilities: uses a convolutional neural network as a backbone; automatically learns and trains according to the range of artificially labeled nodules; recognizes the relevant features of the nodule; and uses the relevant features as quantifiable parameters (29). The nodule image was then enlarged to 1.5 times the pixel size, and the SE-ResNeXt-50 model was used as the classification model (30). We used mirrored, rotated, folded and normalized data augmentation during the training process and applied random dropout to prevent the model from overfitting. ResNeXt improves the accuracy without increasing the complexity of the parameters while also reducing the number of hyperparameters. After predicting each image of the patient's nodule by the SE-ResNeXt-50 neural network, we obtained the corresponding labels [benign nodules (BN), malignant nodules without cervical lymph node metastasis (MN-LN(-)), and malignant nodules with cervical lymph node metastasis (MN-LN(+))] of the patient. A logistic regression model was then established based on the relationships among cervical lymph node status, sex, age and model prediction results. Finally, we obtained the final AI model-predicted value of the patient's probability of cervical lymph node metastasis. The cloud-based AI diagnosis platform can be accessed on the following website: http://thyai.zzinf.com/.

Our proposed model was implemented using Python (version 3.7.6; https://www.python.org/), DL toolkit Pytorch (version 1.5.1; https://pytorch.org/) and OpenCV (version 4.4.0; https://opencv.org). All experiments were conducted on a workstation equipped with a NVDIA 2080Ti GPU.

Development of a thyroid cancer lymph node metastasis nomogram

We used data in the training cohort to construct the nomogram, which included the AI-predicted value, clinical characteristics and ultrasound features. Pearson's chi-squared test and t-test were applied for univariate analysis. Statistically significant factors in univariate analysis were incorporated into multivariate logistic regression analysis to construct the predictive model. Statistical significance was decided by a criterion of two-sided P<0.05. A nomogram was then developed based on the multivariate analysis in the training cohort.

Model evaluation and comparison

To fully evaluate our thyroid cancer lymph node metastasis nomogram, we compared the model with the following other methods: (1) the thyroid cancer lymph node metastasis AI system; (2) a clinical model based on the age, sex and remaining ultrasound features of the primary site in the multiple logistic regression analysis; and (3) the US-reported CLN status based on the involved lymph nodes.

Statistical analysis

The Mann-Whitney U test and chi-square test were separately used to compare the differences in continuous variables and categorical variables. The model predictions were assessed by sensitivity, specificity, positive predictive value, negative predictive value, the area under the curve (AUC) of the receiver operating characteristic (ROC) curve and 95% confidence interval (CI) as well as calibration curves in both the training and validation cohorts. Delong test was used to compare different AUC. Calibration plot analysis was performed by bootstrapping with 1,000 replications. Decision curve analysis was used to evaluate clinical usefulness and net benefits. All analyses were performed using R statistical software (version 3.3.3; www.R-project.org). P<0.05 was considered statistically significant.

Results

Clinical characteristics and ultrasound features of the patients

The clinical and ultrasound characteristics of the patient are summarized in Table 1.

Univariate and multivariate analyses of CLNM risk factors

Table 1 shows the association between CLNM and several risk factors in PTC patients. According to univariate analysis, gender (P<0.001), age (P<0.001), tumor size (P<0.001), tumor position (P<0.001), multiple (P<0.001), taller-than-wide (P=0.012), echo (P<0.001), microcalcification (P<0.001), abutment/perimeter ratio>0.25 (P<0.001), US-reported CLN status (P<0.001) and AI model-predicted value (P<0.001) were closely related to CLNM. Multivariate regression analysis showed that AI model-predicted value (P<0.001), tumor position (P<0.001), multifocality (P<0.001), microcalcification (P=0.001), abutment/perimeter ratio>0.25 (P<0.001) and US-reported CLN status (P<0.001) were significantly associated with a high risk of CLNM (Table 2).

Construction and validation of the thyroid cancer lymph node metastasis nomogram

Multivariable analysis demonstrated that the AI model-predicted value, multifocality, tumor position, microcalcification, abutment/perimeter ratio and US-reported CLN status remained important predictors of CLNM metastasis in PTC patients. Thus, a thyroid cancer lymph node metastasis nomogram incorporating these six predictors was constructed (Figure 2). The nomogram showed that the AI model-predicted value was the largest contributor to the scores followed by US-reported CLN status

10.3389/fendo.2023.964074

TABLE 1 Clinicopathological and sonographic characteristics of patients in PTC by central lymph node status.

	Training cohort n=2114			Internal Validation cohort n=906			External Validation cohort n=339		
Characteristic	CLNM (+)	CLNM (-)	P value	CLNM (+)	CLNM (-)	P value	CLNM (+)	CLNM (-)	P value
Gender			**<0.001**			**0.04**			0.06
Female	746(70.2%)	851(81%)		340(73.9%)	356(79.8%)		116(71.6%)	143(80.8%)	
Male	317(29.8%)	200(19%)		120(26.1%)	90(20.2%)		46(28.4%)	34(19.2%)	
Age (years)			**<0.001**			**<0.001**			0.116
>55	114(10.7%)	234(22.3%)		36(7.8%)	106(23.8%)		28(17.3%)	44(24.9%)	
≤55	949(89.3%)	817(77.7%)		424(92.2%)	340(76.2%)		134(82.7%)	133(75.1%)	
Braf ^{V600E} mutation			0.250			0.743			–
No	212(19.9%)	188(17.9%)		100(21.7%)	92(20.6%)		/	/	
Yes	851(80.1%)	863(82.1%)		360(78.3%)	354(79.4%)		/	/	
Position			**<0.001**			0.337			0.133
Upper	281(26.4%)	365(34.7%)		145(31.5%)	156(35%)		20(12.3%)	21(11.9%)	
Middle	288(27.1%)	251(23.9%)		98(21.3%)	105(23.5%)		87(53.7%)	84(47.5%)	
Lower	454(42.7%)	399(38.0%)		198(43%)	172(38.6%)		46(28.4%)	68(38.4%)	
Isthmus	40(3.8%)	36(3.4%)		19(4.2%)	13(2.9%)		9(5.6%)	4(2.3%)	
Diameter			**<0.001**			**<0.001**			**<0.001**
≤0.5	7(0.6%)	24(2.3%)		5(1.1%)	11(2.5%)		13(8%)	42(23.7%)	
0.5-1	244(23.0%)	424(40.3%)		110(23.9%)	167(37.4%)		57(35.2%)	104(58.8%)	
1-2	555(52.2%)	495(47.1%)		246(53.5%)	219(49.1%)		62(38.3%)	22(12.4%)	
≥2	257(24.2%)	108(10.3%)		99(21.5%)	49(11%)		30(18.5%)	9(5.1%)	
Microcalcification			**<0.001**			**<0.001**			**0.001**
No	118(11.1%)	282(26.8%)		66(14.3%)	119(26.7%)		31(19.1%)	63(35.6%)	
Yes	945(80.9%)	769(73.2%)		394(85.7%)	327(73.3%)		131(80.9%)	114(64.4%)	
Margin			0.791			0.633			1
Clear	78(7.3%)	73(6.9%)		39(8.5%)	33(7.4%)		11(6.8%)	13(7.3%)	
unclear	985(92.7%)	978(93.1%)		421(91.5%)	413(92.6%)		151(93.2%)	164(92.7%)	
Shape			**0.012**			0.249			0.095
Taller-than-wide < 1	350(32.9%)	292(27.8%)		145(31.5%)	124(27.8%)		34(21%)	24(13.6%)	
Taller-than-wide≥1	713(67.1%)	759(72.2%)		315(68.5%)	322(72.2%)		128(79%)	153(86.4%)	
Composition			0.68			0.579			1
Mixed cystic and solid	12(1.1%)	9(0.9%)		7(1.5%)	4(0.9%)		4(2.5%)	5(2.8%)	
Solid	1051(98.9%)	1042(99.1%)		453(98.5%)	442(99.1%)		158(97.5%)	172(97.2%)	
Echo			**<0.001**			**0.026**			0.340
Hyper or isoechoic	20(1.8%)	18(1.7%)		9(2%)	7(1.6%)		14(8.6%)	9(5.1%)	
Hypo-echoic	818(77.0%)	729(69.4%)		347(75.4%)	303(67.9%)		120(74.1%)	131(74%)	
Very Hypo-echoic	225(21.2%)	304(28.9%)		104(22.6%)	136(30.5%)		28(17.3%)	37(20.9%)	
Abutment/perimeter			**<0.001**			**<0.001**			**<0.001**

(Continued)

10.3389/fendo.2023.964074

TABLE 1 Continued

	Training cohort n=2114			Internal Validation cohort n=906			External Validation cohort n=339		
Characteristic	CLNM (+)	CLNM (-)	P value	CLNM (+)	CLNM (-)	P value	CLNM (+)	CLNM (-)	P value
≤ 0.25	295(27.8%)	665(63.3%)		119(25.9%)	270(60.5%)		53(32.7%)	143(80.8%)	
>0.25	768(72.2%)	386(36.7%)		341(74.1%)	176(39.5%)		109(67.3%)	34(19.2%)	
Hashimoto thyroiditis			0.257			0.329			**<0.001**
Negative	845(79.5%)	857(81.5%)		371(80.7%)	347(77.8%)		103(63.6%)	162(91.5%)	
Positive	218(20.5%)	194(18.5%)		89(19.3%)	99(22.2%)		59(36.4%)	15(8.5%)	
Multiple			**<0.001**			**<0.001**			0.533
Negative	595(56%)	719(68.4%)		239(52%)	315(70.6%)		99(61.1%)	115(65%)	
Positive	468(44%)	332(31.6%)		221(48%)	141(29.4%)		63(38.9%)	62(35%)	
US-reported CLN status			**<0.001**			**<0.001**			**<0.001**
Negative	642(60.4%)	956(91%)		291(63.3%)	412(92.4%)		103(63.6%)	162(91.5%)	
Positive	421(39.6%)	95(9%)		169(36.7%)	34(7.6%)		59(36.4%)	15(8.5%)	
AI model predicted value			**<0.001**			**<0.001**			**<0.001**
median(interquartile range)	0.58(0.45-0.76)	0.42(0.29-0.53)		0.58(0.45-0.74)	0.42(0.29-0.54)		0.38(0.26-0.56)	0.27(0.17-0.39)	

Bold values indicate statistical significance ($p < 0.05$).

TABLE 2 Risk factors for central lymph node metastasis in the training cohort.

Clinical variable	Multivariate analysis			
	Estimate	Std. Error	95%CI	P value
Diameter				
≤0.5	–	–	–	–
0.5-1	0.162	0.463	0.497-3.125	0.726
1-2	0.071	0.463	0.453-2.855	0.878
≥2	0.240	0.482	0.515-3.490	0.619
Position				
Upper	–	–	–	–
Middle	0.648	0.142	1.449-2.527	**<0.001**
Lower	0.506	0.127	1.293-2.130	**<0.001**
Isthmus	-0.141	0.295	0.487-1.550	0.633
Microcalcification				
No	–	–	–	–
Yes	0.457	0.141	1.201-2.085	**0.001**
Shape				
Taller-than-wide < 1	–	–	–	–
Taller-than-wide≥1	0.520	0.122	0.829-1.340	0.671
Echo				

(Continued)

TABLE 2 Continued

Clinical variable	Multivariate analysis			
	Estimate	Std. Error	95%CI	P value
Hyper or isoechoic	–	–	–	–
Hypo-echoic	0.351	0.385	0.667-3.041	0.363
Very Hypo-echoic	0.252	0.396	0.592-2.813	0.524
Abutment/perimeter				
≤ 0.25	–	–	–	–
>0.25	1.166	0.111	2.582-3.995	**<0.001**
Multiple				
Negative	–	–	–	–
Positive	0.638	0.109	1.530-2.345	**<0.001**
US-reported CLN status				
Negative	–			
Positive	1.311	0.140	2.828-4.898	**<0.001**
AI model predicted value	3.397	0.283	17.264-52.341	**<0.001**

Bold values indicate statistical significance ($p < 0.05$).

and abutment/perimeter ratio>0.25. Microcalcification, tumor position and multifocality showed a modest impact on the model. The AUC for the nomogram to predict CLNM was 0.812 (95% CI, 0.794-0.830) in the training cohort, 0.809 (95% CI, 0.780-0.837) in the internal validation cohort, and 0.829 (95%CI, 0.785-0.872) in the external validation cohort (Figure 3A–C). The calibration curve of this nomogram presented good agreement between the bias-corrected prediction and ideal reference line with an additional 1000 bootstraps in the training and two validation cohorts (Figure 4A–C).

Performance of the thyroid cancer lymph node metastasis nomogram

We also compared the thyroid cancer lymph node metastasis nomogram with the thyroid cancer lymph node metastasis AI system, clinical model and US-reported CLN status. In the training cohort, the nomogram yielded remarkable performance (sensitivity = 72.4%, specificity = 76.5% and AUC = 0.812; 95% CI: 0.794-0.830) and was superior to the thyroid cancer lymph node metastasis AI system (sensitivity = 67.3%, specificity = 68.9% and AUC = 0.725; 95% CI: 0.703-0.746), clinical model (sensitivity =68.9%, specificity = 72.1% and AUC = 0.764; 95% CI: 0.744-0.784) and US-reported CLN status (sensitivity =39.6%, specificity = 91.0% and AUC = 0.653; 95% CI: 0.636-0.670). In the internal validation cohort, the performance of the nomogram also achieved reasonable performance (sensitivity = 73.9%, specificity = 76.7% and AUC = 0.809; 95% CI: 0.780-0.837) and was better than that of the thyroid cancer lymph node metastasis AI system (sensitivity =50.9%, specificity = 83.2% and AUC = 0.713; 95% CI: 0.679-0.746), clinical model (sensitivity =78.1%, specificity = 60.5%, and AUC = 0.765; 95% CI: 0.734-0.795) and US-reported CLN status (sensitivity =36.7%, specificity = 92.4%, and AUC = 0.646; 95% CI: 0.620-0.671). In the external validation cohort, the thyroid cancer lymph node metastasis nomogram still shows the most outstanding performance, compared with several other models. (Table 3)

We also performed decision curve analysis (DCA) to compare the clinical usability and benefits of predicting the risk of CLNM of this model with those of the traditional ultrasound methods. The DCA curves of the new nomogram showed greater net benefits across a range of CLNMs risks in the three cohorts than the other models (Figure 5A–C).

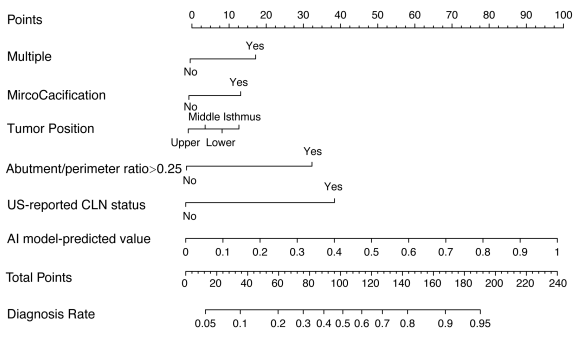

FIGURE 2
Thyroid cancer lymph node metastasis nomogram for predicting CLNM in PTC patients.

Discussion

Lymph node metastasis is common among PTC patients. Thyroidectomy combined with therapeutic lymph node dissection

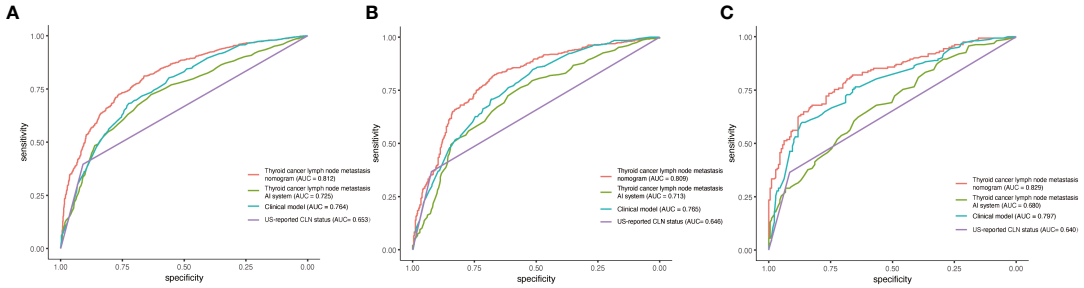

FIGURE 3
Performance of the thyroid cancer lymph node metastasis nomogram, thyroid cancer lymph node metastasis AI system, clinical model and US-reported CLN status in PTC patients. **(A)** ROC curve for predicting CLNM in the training cohort. **(B)** ROC curve for predicting CLNM in the internal validation cohort. **(C)** ROC curve for predicting CLNM in the external validation cohort.

has become a preferred initial surgical strategy for PTC patients with clinically positive lymph nodes, but disagreement persists regarding whether patients with negative lymph node metastasis on ultrasound should undergo preventive central neck dissection. Total thyroidectomy plus prophylactic CLND and total thyroidectomy alone did not differ significantly in local recurrence rates or postoperative complication rates between PTC patients with clinically node-negative. Therefore, prophylactic CLND may not be required if total thyroidectomy is planned (31, 32).

Ultrasonography is one of the most commonly used non-invasive tools applied to the examination of thyroid nodules, but it still has some limitations. For example, ultrasonography relies greatly on the radiologists' work experience, and less experienced radiologists may show less accuracy in the identification of CLNM. Therefore, it is necessary to develop a reliable and noninvasive preoperative tool to predict CLNM in PTC.

In the present study, we performed a systematic and comprehensive analysis of the clinical and ultrasound characteristics of 3359 patients from two medical centers with PTC and incorporated our established thyroid cancer lymph node metastasis AI system. We then developed and validated a thyroid cancer lymph node metastasis nomogram to predict CLNM. The AUC value of our model was exceeded 80% in both the training and two validation cohorts. Additionally, the calibration plot showed that the predicted and observed metastasis risks of CLNM were in good agreement. Thus, our model has good practical effects in clinical applications.

Nomograms are widely used for the prediction of cancer prognosis, mainly for their ability to simplify statistical prediction models to estimate the probability of occurrence of an event (e.g., death or recurrence) and to make predictions based on the actual situation of individual patients (33). In general, one of the most conventional methods for predicting lymph node metastasis in PTC is to establish a clinical model that integrates the statistical analysis information of ultrasound and clinicopathological factors. For instance, Wang et al. established a nomogram to predict CLNM in PTMC patients and considered that age < 55 years, male sex, tumor size 0.5-1.0 cm, multifocal lesions, extrathyroidal extension and lateral lymph node metastasis are independent risk factors for CLNM (34). Lu et al. screened six variables for demographic and clinicopathological characteristics as potential risk factors and further constructed a model for lymph node involvement based on the Surveillance, Epidemiology, and End Results (SEER)

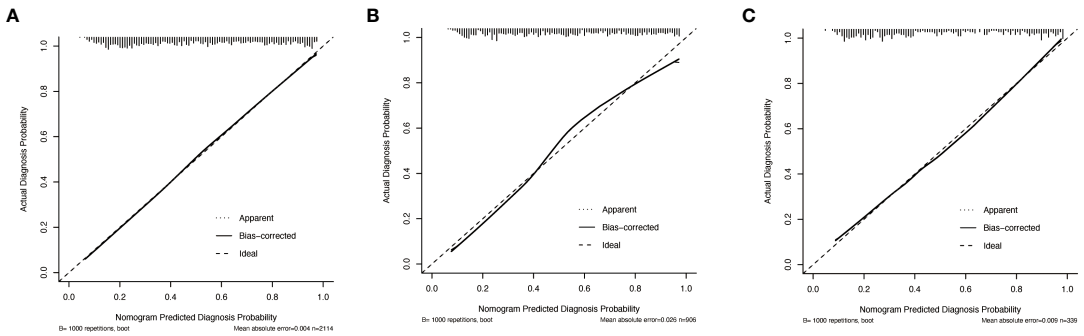

FIGURE 4
Calibration curves of the thyroid cancer lymph node metastasis nomogram, thyroid cancer lymph node metastasis AI system, clinical model and US-reported CLN status in PTC patients. **(A)** Calibration curves for predicting CLNM in the training cohort. **(B)** Calibration curves for predicting CLNM in the internal validation cohort. **(C)** Calibration curves for predicting CLNM in the external validation cohort.

TABLE 3 Identification performance of thyroid cancer lymph node metastasis nomogram, thyroid cancer lymph node metastasis AI system, clinical model and US-reported CLN status in the training cohort, internal validation cohort and external validation cohort.

	Training cohort				Internal Validation cohort				External Validation cohort			
Model	Thyroid cancer lymph node metastasis nomogram	Thyroid cancer lymph node metastasis AI system	Clinical model	US-reported CLN status	Thyroid cancer lymph node metastasis nomogram	Thyroid cancer lymph node metastasis AI system	Clinical model	US-reported CLN status	Thyroid cancer lymph node metastasis nomogram	Thyroid cancer lymph node metastasis AI system	Clinical model	US-reported CLN status
AUC (95% CI)	0.812 (0.794-0.830)	0.725 (0.703-0.746)	0.764 (0.744-0.784)	0.653 (0.636-0.670)	0.809 (0.780-0.837)	0.713 (0.679-0.746)	0.765 (0.734-0.795)	0.646 (0.620-0.671)	0.829 (0.785-0.872)	0.680 (0.624-0.737)	0.797 (0.749-0.845)	0.640 (0.597-0.682)
	Sensitivity	0.724	0.673	0.689	0.396	0.739	0.509	0.781	0.367	0.759	0.630	0.654
0.364												
Specificity	0.765	0.689	0.721	0.910	0.767	0.832	0.605	0.924	0.768	0.638	0.859	0.915
Positive predictive value	0.757	0.686	0.714	0.816	0.766	0.757	0.656	0.833	0.750	0.614	0.809	0.797
Negative predictive value	0.733	0.675	0.696	0.598	0.740	0.621	0.742	0.586	0.777	0.653	0.731	0.611
P value	-	**<0.001**	**<0.001**	**<0.001**	-	**<0.001**	**<0.001**	**<0.001**	-	**<0.001**	**<0.001**	**<0.001**

Significant differences between Thyroid cancer lymph node metastasis nomogram and other models. The DeLong test method was used to compare AUCs. Bold values indicate statistical significance ($p < 0.05$).

Program (35). Although a large amount of data was included in the above studies, the performance of these models was not satisfactory and lacked detailed analysis of several clinical features, such as the absence of $BRAF^{V600E}$ mutation testing.

Deep learning consists of a neural network including many layers and features extracted from the original input image. Currently, deep learning is widely used in medical imaging to achieve computer-aided diagnosis, providing assisted diagnostic suggestions in clinical settings and obtaining more accurate results faster than radiologists. In our previous research, we performed a series of studies on artificial intelligence diagnosis of the thyroid in the area of ultrasound. We applied a large dataset of over 300,000 images to build a DCNN model, which had ameliorative accuracy, sensitivity and specificity in the classification of thyroid nodules. The area under the curve exceeded 90% for both the internal test set and the external test set (36). In addition, we constructed a deep CNN model, named the Brief Efficient Thyroid Network (BETNET), for the localization and classification of thyroid nodules, which precisely and intuitively shows the nodular characteristic area with a higher weight within the neural network (22). The abovementioned studies demonstrate the feasibility of applying a deep convolutional neural network in patients with PTC. Thus, we aimed to establish a deep learning platform for the prediction of lymph node status in patients with PTC before surgery.

There have been a few studies applying deep learning models to predict CLNM from ultrasound images. However, these previous studies are based on traditional machine learning-based radiomics

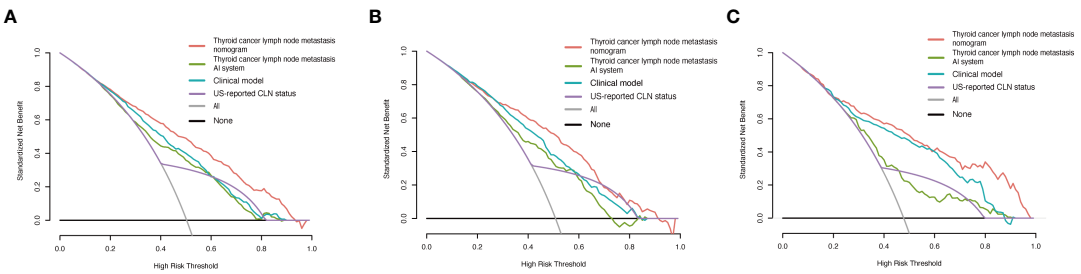

FIGURE 5
Decision curve analysis of the thyroid cancer lymph node metastasis nomogram, thyroid cancer lymph node metastasis AI system, clinical model and US-reported CLN status in PTC patients. **(A)** Decision curve analysis for predicting CLNM in the training cohort. **(B)** Decision curve analysis for predicting CLNM in the internal validation cohort. **(C)** Decision curve analysis for predicting CLNM in the external validation cohort.

methods that extract intensity, boundary, texture and wavelet features from ultrasound images and establish the relationship between these high-throughput features and lymph node status (37). Jiang et al. established a radiomics nomogram based on the SWE radiomics signature and achieved an area under the curve of nearly 85% (37). Although this model achieved better results, the sample size of the patients was only 237, suggesting that the diagnostic value of the shear-wave elastography images in thyroid ultrasound is debatable (38). Additionally, due to the imbalance of medical development in different regions, this model based on SWE radiomics it is not universal to each hospital.

In our preliminary work, we successfully established a cloud-based artificial intelligence diagnosis platform called the thyroid cancer lymph node metastasis AI system based on deep learning to accurately localize thyroid nodules on ultrasound and automatically distinguish the nature of nodules and lymph node status, which included age and sex as independent risk factors affecting cervical lymph node metastasis. Due to the different scanning angles and positions, the object area may pan, and its shape may change, causing differences between images of the same category. Unlike previous deep learning models that predict classification results from a single image, our system simultaneously inputs multiple images of different sections of a patient's lesion and precisely visualizes and locates the nodes to determine the status of the lymph nodes in a comprehensive manner, which is highly interpretable and can be better implemented for clinical applications. In this study, we further evaluated the diagnostic performance of this system in assessing the risk of CLNM.

We then performed detailed statistical analysis of the other clinical and ultrasound characteristics of the patients. Ultrasound parameters are descriptive and distinguishable, and they can be used as a reference for ACR classification. Certain independent risk factors in the clinical features also assist in the determination of lymph node metastasis. The results of the present suggested that multifocality, tumor position, microcalcification, abutment/perimeter>0.25, AI-predicted value and US-reported CLN status were significantly associated with CLNM. These independent risk factors were incorporated to form a new combined model, and a nomogram called the thyroid cancer lymph node metastasis nomogram was developed at the same time. In addition, the external validation further proves the universality of our model. Although the diagnostic performance of the thyroid cancer lymph node metastasis AI system is slightly lower than that of clinical model, AI-predicted value as the largest contributor to scores in the nomogram.

According to ACR TI-RADS guidelines, calcifications within thyroid cancer are classified into four types as follows: microcalcifications, macrocalcifications, marginal calcifications and noncalcifications. Many studies have reported that the formation of microcalcifications is caused by the rapid proliferation of cancer cells and is significantly associated with the incidence of CLNM (39). In our previous studies, we evaluated cervical lymph node metastases based on the tumor abutment/perimeter ratio of the primary site, providing a relatively high reference value to assess the risk of papillary thyroid microcarcinoma metastasis (27). As expected, the 1/4 (25%) perimeter of the thyroid lesion was closely related to CLNM in PTC patients. Moreover, in the present study of Chinese patients, we identified a cohort of more than 3000 patients with classic PTC to explore the relationship between $BRAF^{V600E}$ mutation and CLNM. To our knowledge, this is the largest cohort of samples included in relevant research, and we conclude that $BRAF^{V600E}$ has limited value as an indicator of the risk of CLNM in PTC.

The present study had several limitations. First, regardless of training, internal validation or external validation cohort, our model performed well. These results need to be validated with a larger prospective cohort to test the application value of our model in clinical practice. Second, the immunohistochemical staining patterns and results of fine-needle aspiration may affect the prediction of lymph node status. Thus, we should incorporate these factors into a future study. Finally, our model was only applied to PTC and not to other thyroid cancer subtypes. Future research will focus on other thyroid cancer subtypes, including medullary thyroid carcinoma and follicular thyroid carcinoma.

Conclusion

In the present study, we developed a thyroid cancer lymph node metastasis nomogram combining deep learning, clinical characteristics and ultrasound features. This nomogram will serve as a noninvasive tool to predict CLNM in patients with PTC that will assist inexperienced radiologists in diagnosing the status of lymph nodes and provide effective guidance to surgeons in preoperative diagnosis.

Data availability statement

The raw data supporting the conclusions of this article will be made available by the authors, without undue reservation.

Ethics statement

This study was approved by the Ethics Committee of Tianjin Medical University Cancer Institute and Hospital (No. bc2020190), and the requirements for informed consent were waived.

Author contributions

LC, SZ, MG, and XW designed this study. YZ, JZ, XQW and XC conducted the experiment and interpreted the data. HZ, XC, QG and LH analyzed the data. All authors contributed to the article and approved the submitted version.

Funding

This study has received funding by National Natural Science Foundation of China (#81771852), Tianjin Major Science and Technology Project of Artificial Intelligence (#18ZXZNSY00300), Tianjin Health Research Project (#ZD20018, #QN20018), Tianjin Research Innovation Project for Postgraduate Students

(#2020YJSS178) and the Science and Technology Development Fund of Tianjin Education Commission for Higher Education(#2021KJ194).

Acknowledgments

We thank Guanghe Cui for his help in providing external validation cohort from Binzhou Medical University Hospital.

Conflict of interest

The authors declare that the research was conducted in the absence of any commercial or financial relationships that could be construed as a potential conflict of interest.

Publisher's note

Supplementary material

The Supplementary Material for this article can be found online at: https://www.frontiersin.org/articles/10.3389/fendo.2023.964074/full#supplementary-material

References

1. Byrd JK, Yawn RJ, Wilhoit CST, Sora ND, Meyers L, Fernandes J, et al. Well differentiated thyroid carcinoma: current treatment. *Curr Treat options Oncol* (2012) 13 (1):47–57. doi: 10.1007/s11864-011-0173-1

2. Lim H, Devesa SS, Sosa JA, Check D, Kitahara CM. Trends in thyroid cancer incidence and mortality in the united states, 1974-2013. *JAMA* (2017) 317(13):1338–48. doi: 10.1001/jama.2017.2719

3. Morris LGT, Sikora AG, Tosteson TD, Davies L. The increasing incidence of thyroid cancer: The influence of access to care. *Thyroid: Off J Am Thyroid Assoc* (2013) 23(7):885–91. doi: 10.1089/thy.2013.0045

4. Yu QA, Ma DK, Liu KP, Wang P, Xie CM, Wu YH, et al. Clinicopathologic risk factors for right paraesophageal lymph node metastasis in patients with papillary thyroid carcinoma. *J endocrinol Invest* (2018) 41(11):1333–8. doi: 10.1007/s40618-018-0874-4

5. Pereira JA, Jimeno J, Miquel J, Iglesias M, Munné A, Sancho JJ, et al. Nodal yield, morbidity, and recurrence after central neck dissection for papillary thyroid carcinoma. *Surgery* (2005) 138(6):1095–100, discussion 1100-1. doi: 10.1016/j.surg.2005.09.013

6. Roh JL, Kim JM, Park CI. Central lymph node metastasis of unilateral papillary thyroid carcinoma: Patterns and factors predictive of nodal metastasis, morbidity, and recurrence. *Ann Surg Oncol* (2011) 18(8):2245–50. doi: 10.1245/s10434-011-1600-z

7. Suh YJ, Kwon H, Kim SJ, Choi JY, Lee KE, Park YJ, et al. Factors affecting the locoregional recurrence of conventional papillary thyroid carcinoma after surgery: A retrospective analysis of 3381 patients. *Ann Surg Oncol* (2015) 22(11):3543–9. doi: 10.1245/s10434-015-4448-9

8. Grogan RH, Kaplan SP, Cao H, Weiss RE, Degroot LJ, Simon CA, et al. A study of recurrence and death from papillary thyroid cancer with 27 years of median follow-up. *Surgery* (2013) 154(6):1436–46; discussion 1446-7. doi: 10.1016/j.surg.2013.07.008

9. Medas F, Canu GL, Cappellacci F, Anedda G, Conzo G, Erdas E, et al. Prophylactic central lymph node dissection improves disease-free survival in patients with intermediate and high risk differentiated thyroid carcinoma: A retrospective analysis on 399 patients. *Cancers (Basel)* (2020) 12(6):1658. doi: 10.3390/cancers12061658

10. Polistena A, Monacelli M, Lucchini R, Triola R, Conti C, Avenia S, et al. Surgical morbidity of cervical lymphadenectomy for thyroid cancer: A retrospective cohort study over 25 years. *Int J Surg* (2015) 21:128–34. doi: 10.1016/j.ijsu.2015.07.698

11. Kim SK, Woo JW, Lee JH, Park I, Choe JH, Kim JH, et al. Prophylactic central neck dissection might not be necessary in papillary thyroid carcinoma: Analysis of 11,569 cases from a single institution. *J Am Coll Surg* (2016) 222(5):853–64. doi: 10.1016/j.jamcollsurg.2016.02.001

12. Sippel RS, Robbins SE, Poehls JL, Pitt SC, Chen H, Leverson G, et al. A randomized controlled clinical trial: No clear benefit to prophylactic central neck dissection in patients with clinically node negative papillary thyroid cancer. *Ann Surg* (2020) 272(3):496–503. doi: 10.1097/sla.0000000000004345

13. Kim E, Park JS, Son K-R, Kim J-H, Jeon SJ, Na DG. Preoperative diagnosis of cervical metastatic lymph nodes in papillary thyroid carcinoma: Comparison of ultrasound, computed tomography, and combined ultrasound with computed tomography. *Thyroid* (2008) 18(4):411–8. doi: 10.1089/thy.2007.0269

14. Roh JL, Park JY, Kim JM, Song CJ. Use of preoperative ultrasonography as guidance for neck dissection in patients with papillary thyroid carcinoma. *J Surg Oncol* (2009) 99(1):28–31. doi: 10.1002/jso.21164

15. Jeong HS, Baek CH, Son YI, Choi JY, Kim HJ, Ko YH, et al. Integrated 18F-FDG PET/CT for the initial evaluation of cervical node level of patients with papillary thyroid carcinoma: Comparison with ultrasound and contrast-enhanced CT. *Clin Endocrinol (Oxf)* (2006) 65(3):402–7. doi: 10.1111/j.1365-2265.2006.02612.x

16. Wang Y, Guan Q, Xiang J. Nomogram for predicting central lymph node metastasis in papillary thyroid microcarcinoma: A retrospective cohort study of 8668 patients. *Int J Surg* (2018) 55:98–102. doi: 10.1016/j.ijsu.2018.05.023

17. Feng JW, Hong LZ, Wang F, Wu WX, Hu J, Liu SY, et al. A nomogram based on clinical and ultrasound characteristics to predict central lymph node metastasis of papillary thyroid carcinoma. *Front Endocrinol (Lausanne)* (2021) 12:666315. doi: 10.3389/fendo.2021.666315

18. Zou Y, Shi Y, Liu J, Cui G, Yang Z, Liu M, et al. A comparative analysis of six machine learning models based on ultrasound to distinguish the possibility of central cervical lymph node metastasis in patients with papillary thyroid carcinoma. *Front Oncol* (2021) 11:656127. doi: 10.3389/fonc.2021.656127

19. Wu Y, Rao K, Liu J, Han C, Gong L, Chong Y, et al. Machine learning algorithms for the prediction of central lymph node metastasis in patients with papillary thyroid cancer. *Front Endocrinol (Lausanne)* (2020) 11:577537. doi: 10.3389/fendo.2020.577537

20. Zhou W, Yang Y, Yu C, Liu J, Duan X, Weng Z, et al. Ensembled deep learning model outperforms human experts in diagnosing biliary atresia from sonographic gallbladder images. *Nat Commun* (2021) 12(1):1259. doi: 10.1038/s41467-021-21466-z

21. Penzkofer T, Padhani AR, Turkbey B, Haider MA, Huisman H, Walz J, et al. ESUR/ESUI position paper: Developing artificial intelligence for precision diagnosis of prostate cancer using magnetic resonance imaging. *Eur Radiol* (2021) 31(12):9567–9578. doi: 10.1007/s00330-021-08021-6

22. Zhu J, Zhang S, Yu R, Liu Z, Gao H, Yue B, et al. An efficient deep convolutional neural network model for visual localization and automatic diagnosis of thyroid nodules on ultrasound images. *Quant Imaging Med Surg* (2021) 11(4):1368–80. doi: 10.21037/qims-20-538

23. Wei X, Gao M, Yu R, Liu Z, Gu Q, Liu X, et al. Ensemble deep learning model for multicenter classification of thyroid nodules on ultrasound images. *Med Sci monit* (2020) 26:e926096. doi: 10.12659/MSM.926096

24. Chen Y, Li D, Zhang X, Jin J, Shen Y. Computer aided diagnosis of thyroid nodules based on the devised small-datasets multi-view ensemble learning. *Med Image Anal* (2021) 67:101819. doi: 10.1016/j.media.2020.101819

25. Liu T, Guo Q, Lian C, Ren X, Liang S, Yu J, et al. Automated detection and classification of thyroid nodules in ultrasound images using clinical-knowledge-guided convolutional neural networks. *Med Image Anal* (2019) 58:101555. doi: 10.1016/j.media.2019.101555

26. Tessler FN, Middleton WD, Grant EG, Hoang JK, Berland LL, Teefey SA, et al. Reporting and data system (TI-RADS): White paper of the ACR TI-RADS committee. *J Am Coll Radiol* (2017) 14(5):587–95. doi: 10.1016/j.jacr.2017.01.046

27. Wei X, Wang M, Wang X, Zheng X, Li Y, Pan Y, et al. Prediction of cervical lymph node metastases in papillary thyroid microcarcinoma by sonographic features of the primary site. *Cancer Biol Med* (2019) 16(3):587–94. doi: 10.20892/j.issn.2095-3941.2018.0310

28. Zarkesh M, Zadeh-Vakili A, Akbarzadeh M, Nozhat Z, Fanaei SA, Hedayati M, et al. BRAF V600E mutation and microRNAs are helpful in distinguishing papillary

thyroid malignant lesions: Tissues and fine needle aspiration cytology cases. *Life Sci* (2019) 223:166–73. doi: 10.1016/j.lfs.2019.03.034

29. He K, Gkioxari G, Dollar P, Girshick R. Mask R-CNN. *IEEE Trans Pattern Anal Mach Intell* (2020) 42(2):386–97. doi: 10.1109/tpami.2018.2844175

30. Hu J, Shen L, Sun G. (2018). Squeeze-and-excitation networks, in: *Proceedings of the IEEE conference on computer vision and pattern recognition*. doi: 10.48550/arXiv.1709.01507

31. Alsubaie KM, Alsubaie HM, Alzahrani FR, Alessa MA, Abdulmonem SK, Merdad MA, et al. Prophylactic central neck dissection for clinically node-negative papillary thyroid carcinoma. *Laryngoscope* (2022) 132(6):1320–8. doi: 10.1002/lary.29912

32. Ahn JH, Kwak JH, Yoon SG, Yi JW, Yu HW, Kwon H, et al. A prospective randomized controlled trial to assess the efficacy and safety of prophylactic central compartment lymph node dissection in papillary thyroid carcinoma. *Surgery* (2022) 171(1):182–9. doi: 10.1016/j.surg.2021.03.071

33. Iasonos A, Schrag D, Raj GV, Panageas KS. How to build and interpret a nomogram for cancer prognosis. *J Clin Oncol* (2008) 26(8):1364–70. doi: 10.1200/jco.2007.12.9791

34. Yang Z, Heng Y, Lin J, Lu C, Yu D, Tao L, et al. Nomogram for predicting central lymph node metastasis in papillary thyroid cancer: A retrospective cohort study of two clinical centers. *Cancer Res Treat* (2020) 52(4):1010–8. doi: 10.4143/crt.2020.254

35. Lu S, Zhao R, Ni Y, Ding J, Qiu F, Peng Y, et al. Development and validation of a nomogram for preoperative prediction of cervical lymph node involvement in thyroid microcarcinoma. *Aging (Albany NY)* (2020) 12(6):4896–906. doi: 10.18632/aging.102915

36. Li X, Zhang S, Zhang Q, Wei X, Pan Y, Zhao J, et al. Diagnosis of thyroid cancer using deep convolutional neural network models applied to sonographic images: A retrospective, multicohort, diagnostic study. *Lancet Oncol* (2019) 20(2):193–201. doi: 10.1016/s1470-2045(18)30762-9

37. Jiang M, Li C, Tang S, Lv W, Yi A, Wang B, et al. Nomogram based on shear-wave elastography radiomics can improve preoperative cervical lymph node staging for papillary thyroid carcinoma. *Thyroid* (2020) 30(6):885–97. doi: 10.1089/thy.2019.0780

38. Han DY, Sohn YM, Seo M, Yun SJ, Park WS, Jeon SH, et al. Shear-wave elastography in thyroid ultrasound: Can be a predictor of extrathyroidal extension and cervical lymph node metastasis in papillary thyroid carcinoma? *Med (Baltimore)* (2020) 99(52):e23654. doi: 10.1097/md.0000000000023654

39. Liu J, Jia X, Gu Y, Chen X, Guan L, Yan J, et al. Thyroid parenchyma microcalcifications on ultrasound for predicting lymph node metastasis in papillary thyroid carcinoma: A prospective multicenter study in China. *Front Oncol* (2021) 11:609075. doi: 10.3389/fonc.2021.609075

Frontiers in Endocrinology

Explores the endocrine system to find new therapies for key health issues

The second most-cited endocrinology and metabolism journal, which advances our understanding of the endocrine system. It uncovers new therapies for prevalent health issues such as obesity, diabetes, reproduction, and aging.

Discover the latest Research Topics

See more →

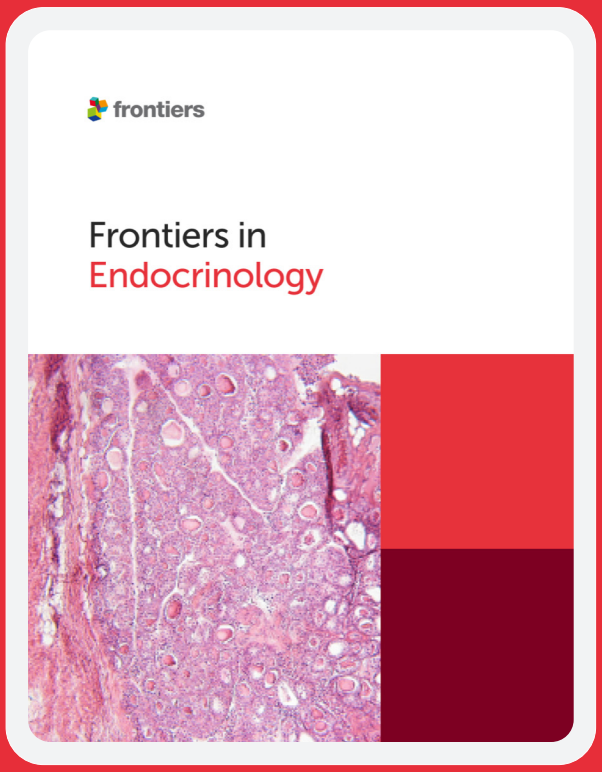

Frontiers

Avenue du Tribunal-Fédéral 34
1005 Lausanne, Switzerland
frontiersin.org

Contact us

+41 (0)21 510 17 00
frontiersin.org/about/contact